Algal Biomass as Adsorbents for Heavy Metal Sorption from Aqueous Solutions

by

Danish J. Malik

A Doctoral Thesis submitted in partial fulfilment of the requirements for the award of Doctor of Philosophy of Loughborough University

June 1999

Abstract

This thesis evaluates the performance of marine algal-based biosorbents in treating trace metal bearing aqueous solutions. Native seaweed varieties (*Ascophyllum nodosum*, *Lessonia flavicans*, *Durvillea potatorum* and *Laminaria hyperborea*) were selected on the basis of their varying algin composition as well as their characteristic mannuronic/guluronic acid content. Dealginated seaweed residues, i.e. waste materials arising during algin extraction from brown marine algae were also evaluated as potential metal biosorbent materials. The biosorbents showed significant metal sorption capacity for copper, cadmium, nickel and zinc from synthetic single metal and multi-metal bearing aqueous solutions. The equilibrium biosorption process may be described using a surface complex formation model. Copper biosorption involved chelation-type surface reactions as well as ion exchange whereas nickel and zinc biosorption may be described by simple ion exchange and electrostatic interactions between metal ions and the negatively charged algal surface. Evidence of stoichiometric release of protons upon metal biosorption has been found. Metal biosorption was found to be dependent upon transport limitations due to intraparticle diffusion.

Surface functional groups within algal biosorbents that are responsible for metal-ion binding were identified in an attempt to understand the mechanisms of metal biosorption. Physical and chemical characterization techniques such as potentiometric titrations and esterification were used for surface acidity measurements, nitrogen sorption porosimetry for surface area and pore size distribution analysis and FT-IR spectroscopy to identify carboxyl groups attached to structural polysaccharides in algae.

Performance of native and dealginate algal fixed-bed mini-columns provided optimum operating conditions for dynamic exchange between metal ions in solution and the algal biomass. Selected biosorbents were successfully employed to treat real industrial metal-plating rinse waters. The most efficient eluants for regeneration of metal-laden biosorbent columns were also identified.

Acknowledgments

In the three years that it has taken me to complete this thesis, the continued support, advice and good humour of my supervisor, Michael Streat is greatly appreciated and duly acknowledged.

I would like to thank Jim Grieg, of Monsanto plc, for the numerous interesting discussions, related and sometimes delightfully unrelated to the subject matter of this thesis. I also acknowledge the financial support of Brite-Euram Contract BRPR-CT96-0158 and an ORS award from the British Government.

Thanks to my colleagues in the adsorption and ion exchange group who have made my studies an enjoyable experience. Thanks also to all the Brite-Euram project partners working with whom was most rewarding.

I would like to acknowledge the following people

- David Drott of the Chemical Engineering Department for his advice during biosorption kinetics studies.
- Ian Sutherland and David Maton of the Chemistry Department for the use of their infra-red spectrophotometer.
- Arto Yli-Pentti and Tuomo Karppinen of Finnair for allowing me to spend two weeks at the Finnair plating shop in Helsinki.
- The academic and technical staff in the Chemical Engineering Department.

I would also like to mention my family, especially my parents Izzat and Javed and my sister Natasha for their invaluable support during the entire duration of my studies.

Finally, I salute the memory of my dearest Nano, a woman of outstanding character whom I will never forget.

Contents

List of Figures

List of Tables

Literature Review and Scope of Current Work

***Macrocystis Pyrifera*-Giant Kelp Beds off the coast of California.**

Chapter 1

Literature Review and Scope of Current Work

This chapter provides an overview of the field of biosorption as it currently stands. The role of cellular polysaccharides in metal sequestration by bacteria, fungi and algae is discussed. In particular, metal sorption by brown marine algae is reviewed in detail and pertinent literature cited. Processed dealginated seaweed, sourced from the algin extraction industry is introduced as a possible biosorbent. Finally, the scope of the current work and selection of biosorbents and metal solutions used in the present study are justified.

Section 1.1. An Introduction to Biosorption and Biosorbents

Biosorption is a term used to describe the passive uptake of solutes by inactivated non-living organisms. It is therefore not to be confused with the active removal of metallic ions as a consequence of the metabolic activities of living organisms. This latter phenomenon is termed bioaccumulation. Biosorption is therefore independent of the metabolic activities of the organism and occurs due to interactions between solute and external components constituting the cellular structure of the organism. As a general observation, the cell wall has been found to play a key role in the sequestration of metallic species from solution. Since the sorption phenomenon is independent of the metabolic activities of the cell, biosorption is responsible for binding and accumulating metallic ions even when the cell is dead. Once the cell has died, the cellular debris left constitutes a potent biosorbent.

This distinction between biosorption and bioaccumulation is important from a process design view point. Utilizing living microbial organisms where the cells are actively metabolizing in what is usually a special culture environment (high toxic metal content) represents a clear problem of process optimization. Decoupling the growth and propagation of the biomass from its function as a biosorbent would be desirable.

This would allow an independent and well optimized propagation of the microbial culture in a separate fermentation system which would be geared to produce biosorbents possessing high metal sorption properties. In other cases, biosorbents may arise as by-products of well established processes employing microbial cultures (pharmaceutical or brewing industries). Harvesting biomass directly from its natural environment is also being looked at; fresh water algae and marine algae are abundantly found in their natural habitat.

One of the features that distinguishes the microbial cells of bacteria, fungi and algae from animal cells is the presence of a protective envelope "the cell wall". A detailed account of the structure of the cell wall of bacteria and fungi is to be found in a monograph on biosorption of heavy metals to which the reader should refer[1].

Section 1.2. Bacteria as Biosorbents for Metal Sorption

In gram-positive bacteria, the cell wall is 50-150nm thick. It is mainly composed of peptidoglycan (40-90% of cell wall material) which is a rigid, porous, amorphous material and consists of linear chains of the disaccharide N-acetylglucosamine-β-1,4-N-acetylmuramic acid. The peptidoglycan consists of several layers bearing anionic groups and is highly permeable to molecules of molecular weight between 1200 and 70,000 Daltons because of its network structure. Three mechanisms account for the sequestration of the metallic ions by the microbial cell wall: adsorption, micro-precipitation and nucleation. Metal ion sorption is dependent not only on the type, number and accessibility of the functional sites but also the mesh diameter of the cell wall framework[2]. Labischinski et al.,[3] employed X-ray diffraction, infrared (IR) spectroscopy and conformation energy data to conceive the following atomic model of peptidoglycan. The disaccharide strands are represented as a tubular helix with peptide cross-linkages which are attached along a helicoidal line. The cell wall of the gram-positive bacteria consists of several layers bearing anionic functional groups. Attention is drawn to two main wall constituents; teichuronic acids and teichoic acids which are covalently attached to the peptidoglycan. The teichoic acids are made of 30-40 molecules of ribitol or glycerol phosphate residues. Ester groups (glycosyl and

D-alanine) are attached to the techoic acid linear chain which is linked to N-acetylmuramic acid of the peptidoglycan by a phosphate group. In comparison, the teichuronic acids are free from phosphate and are made up of hexuronic acid linear chains. Teichoic acids and teichuronic acids were proven to participate in metal sorption.

In Gram-negative bacteria the cell wall is 30-80nm thick (somewhat thinner than the cell wall of Gram-positive bacteria). The peptidoglycan differs from the cell wall of Gram-positive bacterial peptidoglycan in several features. The thickness of the peptidoglycan layer is only between 15-20nm thick and accounts for only 10% of the cell wall material. It is not as heavily cross-linked as in Gram-positive bacteria. The outer membrane is composed of an outer layer of lipopolysaccharides (LPS) and of phospholipids and proteins. Hancock[4] suggests that the heavy negative surface charge on Gram-negative bacteria arises due to LPS.

The archaebacteria are composed of groups of bacteria sharing the ability to grow in harsh environments as well as some common physiological and biochemical features. Muramic acid, which is a typical constituent of the eubacterial cell wall is absent[5]. A Gram-positive archaebacteria cell is surrounded by a cell wall containing either pseudo-murein, methanochondroitin or heteropolysaccharides[6]. Several types of cell walls have been described in Gram-negative archaebacteria.

Several articles have shown that bacterial cell walls are capable of sorbing significant quantities of heavy metal[7,8,9,10,11,12,13]. Reviews discussing various bacterial interactions with heavy metals, both with living cells and cell walls, have recently been published[1,11]. *Bacillus subtillis* and *E. Coli* are two bacterial species that have been studied extensively. Sorption studies with dead cells indicate that most of the interaction occurs on or within the outer cell membrane. It has been reported[7] that, for *E. Coli*, the phosphoryl groups in the lipopolysaccharides are mainly responsible for the high divalent ion capacity, however, other studies seem to indicate that metals accumulate along the peptidoglycan layer in the cell membrane[14].

Extracellular polymers produced by bacteria can also bind metal ions[11]. These polymers can exist either in soluble form or as solid colloidal particles. The selectivity order may be different for the two forms particularly in a multicomponent mixture. Rudd[15] found that the soluble form of an extracted *Klebsiella aerogenes* polymer sorbed nickel preferentially to copper, cadmium and cobalt whereas copper and cadmium were mostly found on the colloidal form. Sorption isotherms indicated multiple binding sites for this material. *Saccharomyces cerevisiae* cells have been found to accumulate uranium on their surface while in *Pseudomonas aeruginosa*[16] the metal is accumulated more in the interior. *Saccharomyces cerevisae* system could be regenerated.

Section 1.3. Fungi as Biosorbents for Metal Sorption

Fungi possess a true cell wall which, as in the case of bacteria, is rigid. The chemical and structural characteristics of the fungal cell wall is rather different from those of bacterial cells. Various polysaccharides are the primary constituents of the fungal cell wall (up to 90%) and are often complexed with proteins, lipids and other substances (e.g. pigments). The fungal cell wall has a microfibrillar structure and consists of several layers; (1) an outer layer of glucans, mannans or galactans and (2) an inner microfibrillar layer which is made of parallel chains of chitin, in some cases these may be replaced by cellulose chains, or in certain yeast, of non-cellulosic glucan[17]. Chitin is a polymer of N-acetyl-D-glucosamine; cellulose consists of chains of D-glucopyranose, mostly linked by β-1,4-glucosidic bonds. These chains are strengthened by proteins, lipids and polysaccharides. Kihn et al.,[18] suggest that phosphodiester and carboxyl groups present within the fungal cell wall confer the electrical surface potential. Microfungi feature enormous variations in their cell wall composition and this may be used as a criterion in the fungal classification[19].

Fungal systems have been shown to compare favorably with ion exchange resins, activated carbons and metal oxides[20] for binding divalent metal species, e.g. UO_2, Zn, Fe, Cu, Cd, Pb and others[1,11,21]. *Rhizopus arrhizus* has been studied extensively to elucidate the metal binding sites[22,23,24]. The economics of some systems may not,

however, be competitive[25]. The major functional groups present in the fungal cell wall are depicted in Figure 1.1. The illustration shows only the major polysaccharides present, proteins, lipids and melanin are not shown. The simplified illustration shows that there is a wide variation in the composition of the cell walls for the different species which contributes to the variation in capacities reported for these non-living organisms[1].

Competition between divalent metal cations reduces the capacity for particular metal species. Tobin[26] found that the uptake capacity of *Rhizopus arrhizus* for cadmium decreased by as much as 70% in the presence of UO_2^{2+}. No competitive effects were observed with sodium. Carboxylate and phosphate functional groups were thought to be responsible for the uptake. Tsezos[27] suggested that chitin in the cell wall plays an important role in the uptake of uranium and thorium. Competition in the presence of iron (Fe^{2+}) strongly affected the sorption isotherms for uranium, reducing the maximum capacity (0.76 mmol g^{-1}) by 78% in the presence of 1.8 M Fe^{2+} at pH4 and ambient temperature.

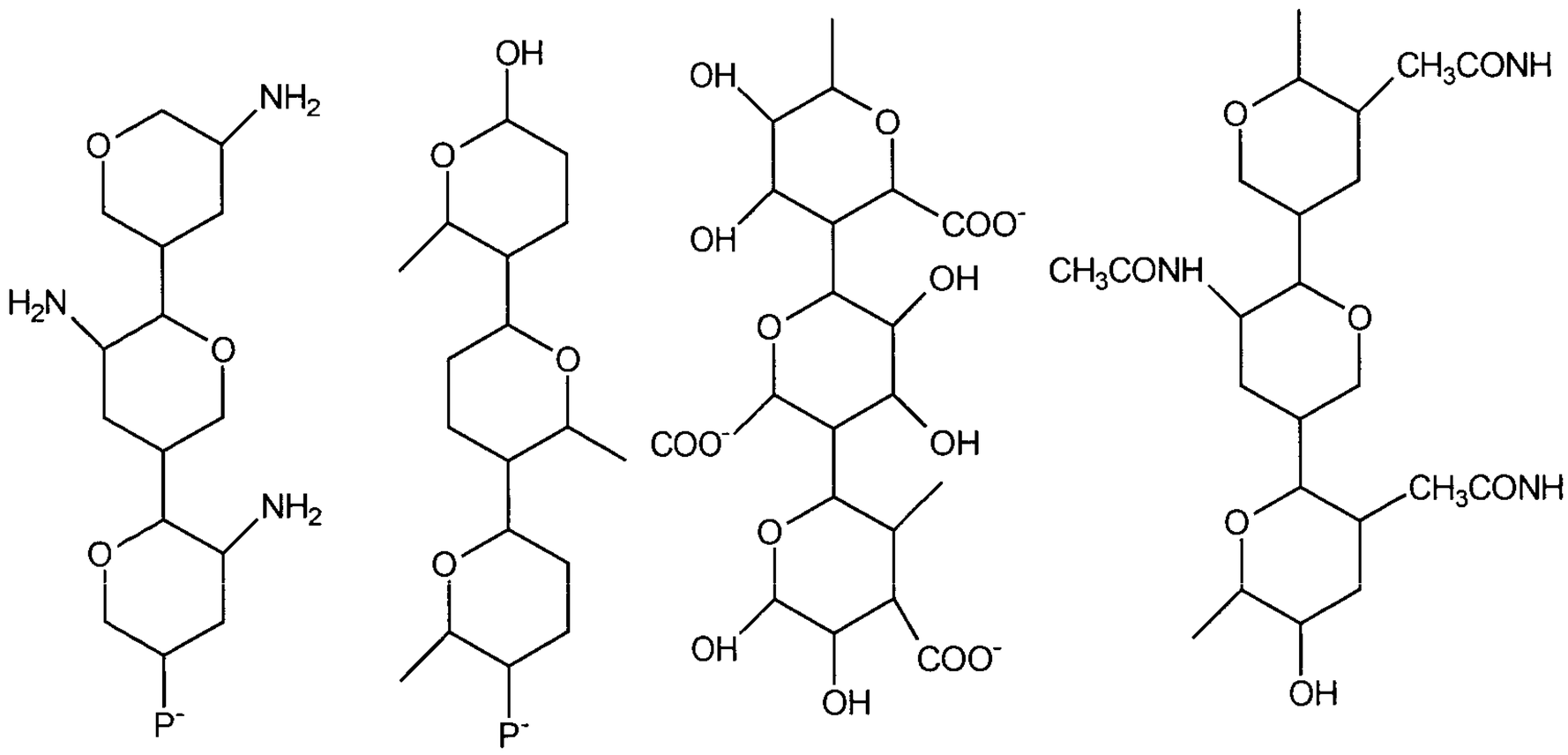

Chitosan Glucan Polyuronide Chitin

Figure 1.1. Major functional groups present in the fungal cell wall.

Melanins (polyquinones) were evidently responsible for metal uptake by the fungus *Cladosprium cladosporoides*[20,28]. *Penicillium* has also been studied[29] but usually has

a capacity somewhat less than *Rhizopus arrhizus*, particularly for the uranium radionuclide. Chemical pre-treatment of *Penicillium* with 80% methanol or ethanol enhanced the capacity for uranium by as much as 50%[30].

Muraleedharan et al.[31,32] studied the sorption of copper on wood rotting fungus *Ganoderma lucidum* and found that only 5% of the biosorption was due to chitin and none to associated proteins. They were not able to identify the nature of the active sites within the cell matrix but concluded that a free radical was indirectly involved.

Section 1.4. Algae as Biosorbents in Metal Sorption

The main constituents of the cell walls of algae are carbohydrates. They may be divided into materials soluble in boiling water such as mucilaginous or pectic substances and constituents that are insoluble in water[33]. There are two fractions within the cell wall: a fibrillar part that gives the wall its strength and an amorphous part in which the fibrils are embedded. The fibrillar fraction of the brown algal wall consists of cellulose[33,36] and the structural component is probably stiffened by insoluble alginate[34,35]. The amorphous embedding matrix is composed of glycoproteins.

Seaweeds, the algal plants, are classified into four principal groups: Chlorophyceae, the green algae; Phaeophyceae, the brown algae; Rhodophyceae, the red algae; and Cyanophyceae, the blue green algae. The Chlorophyceae and the Cyanophyceae occur in the sea and in the fresh water, in soil and on tree trunks. The Phaeophyceae and Rhodophyceae are primarily salt-water plants. They are important commercially because of their polysaccharide content and because they are available in quantities sufficient to support a sizable industry. Agar and carrageenan are extracted from various types of the red algae and algin is derived from the brown seaweeds. These polysaccharides are specific to seaweeds and are not found in land plants. The giant kelp, *Macrocystis pyrifera*, which grows in abundance along the coasts of North and South America, New Zealand, Australia and Africa, is one of the principal sources of

the world algin supply. Other varieties including *Laminaria*, *Ecklonia* and *Ascophyllum nodosum* are also utilized. The map in Figure 1.2. shows the locations of various varieties which are extensive enough to support commercial use.

The botanical classification of the seaweeds is based primarily on their morphology, particularly with respect to their reproductive systems, but the division into classes has been aided by the nature of pigments present. Though all marine algae have been found to contain chlorophyll, the colour of chlorophyll in some classes is masked by strongly coloured pigments. Rhodophyceae owe their red colour to the presence of biliproteins whereas fucoxanthin and xanthophyll are responsible for the brown colour of Phaeopyceae.

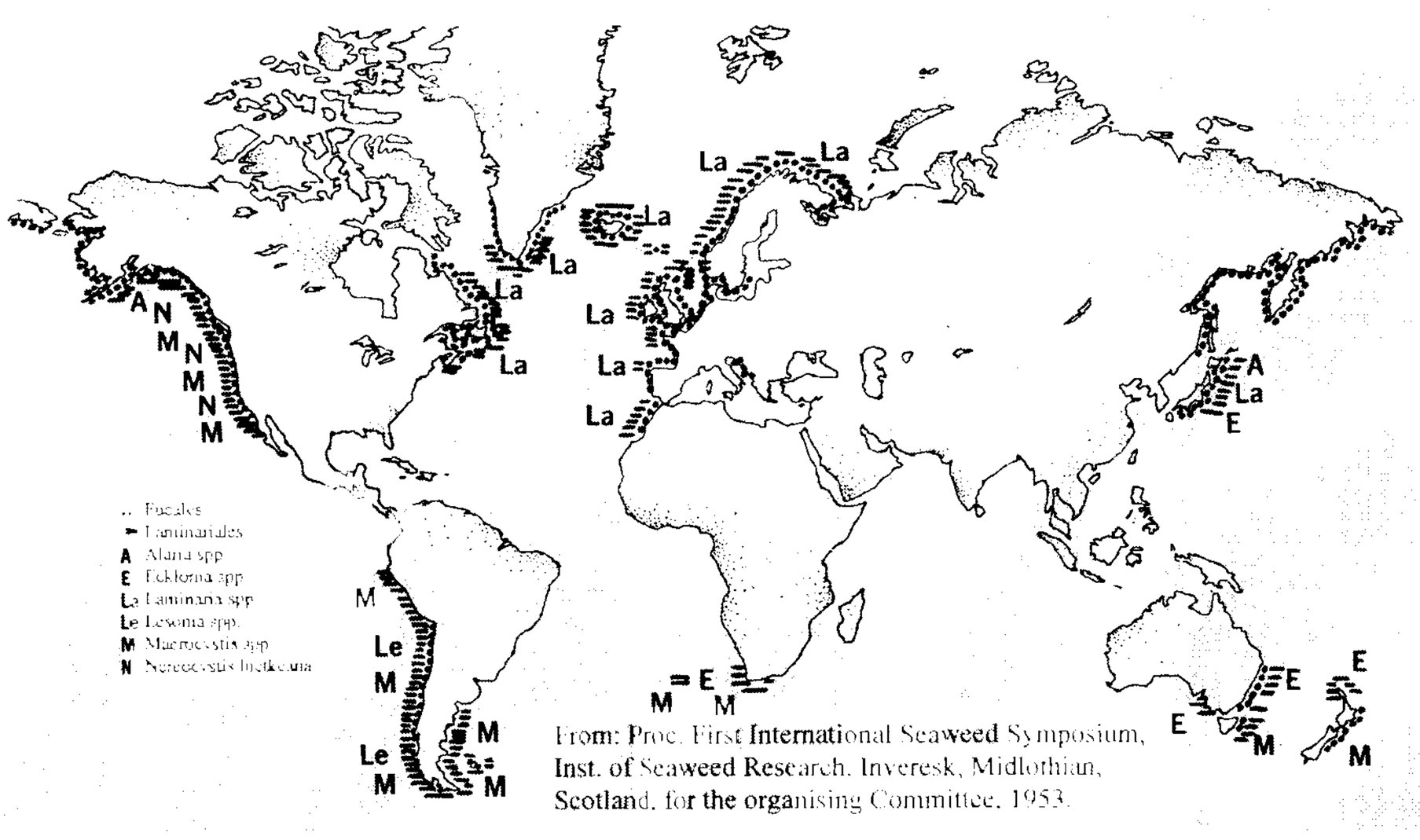

Figure 1.2. Areas known to support brown seaweed[42].

The subject matter of this thesis is concerned primarily with brown marine algae. Polysaccharides occurring in Phaeophyceae have been found to play an important role in algal/metal interactions. The discussion below provides a brief introduction to the various polysaccharides found in Phaeophyceae. An excellent account of the structure of algal polysaccharides including a thorough treatment of their identification and

extraction procedures is provided in the text by Percival and McDowell[36] to which the reader is referred for further details.

It is well known that for many species, the polysaccharide composition depends on the season of the year, the habitat, depth of immersion and state of development. An interesting point worth noting concerns the variation of polysaccharide content along the length of a mature frond. Black[37] reported that in a mature frond about seven months old, near the stipe (i.e. actively growing region) there was about 3% mannitol, and little or no alginic acid or laminaran. About a third of the way along the frond, mannitol was at a maximum 6%, with laminaran 2% and alginic acid 2.5%. Two thirds of the way up, the mannitol content had fallen to 2% with laminaran at 6% and alginic acid 4%. Variations in the polysaccharide composition within the same variety is therefore quite normal and hence any quantification of polysaccharides must be treated with caution as there will be some degree of variability depending on the factors discussed above.

Polysaccharides constituting the cellular make-up of algae have been studied by carrying out successive extractions with conditions so arranged that different groups of compounds are dissolved at various stages. Preliminary separation of polysaccharides can be made by successive extraction with solvents of increasing power. The sequence cold water, hot water, cold dilute alkali, and hot dilute alkali will yield fractions of differing composition and properties[36]. The use of water, acids and alkali are common. Fractional precipitation of mixtures of polysaccharides has been accomplished by the use of metallic salts[38], precipitation in organic solvents and the use of other selective complexing agents. The optical microscope has played an important role in the study of plant tissues. The use of staining techniques alone or in parallel with polarized light has yielded useful insights into the location of the various polysaccharides within the algal cells. Scanning electron micrographs of algae have demonstrated distinct microfibrils however, due to the complex chemical constitution of the tissue, X-ray studies have yielded less information.

Laminaran, a water soluble β-glucan, is the food reserve material of the Phaeophyceae (for structure see Fig. 1.3.). Laminaran occurs in two forms, distinguished by thier solubility in cold water. It is therefore referred to as "soluble" and "insoluble" laminaran, although both forms readily dissolve in hot water. This polysaccharide is particularly prone to attack by moulds and bacteria[39]. Early methylation studies[40], together with the low negative rotation, indicated that laminaran is an essentially linear β-1,3-linked glucan, since 2,4,6-tri-O-methyl-D-glucose was the major methylated sugar obtained on hydrolysis of the methylated material. M-chains of laminaran are terminated by a mannitol residue. The G-chains of laminaran are terminated by reducing glucose residues linked through C-3.

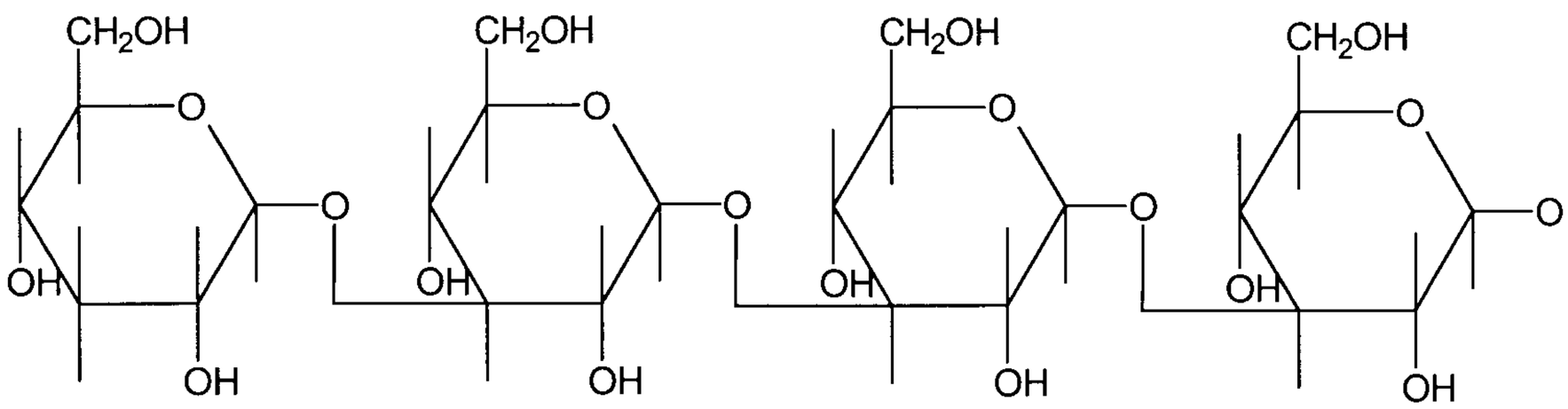

Figure 1.3. Chain of β-D-Glucopyranose units in Laminaran.

As a result of microscopic and X-ray examination of the cell walls, cellulose has been reported to be present in all the major classes of marine algae however, few chemical investigations into the structure of these materials have been carried out. The percentage of cellulose[41] in different species of the Phaeophyceae is given in Table 1.1.

Species	Frond	Stipe
Laminaria digitata	3-5	6-8
Laminaria hyperborea	4-5	8.5-10
Fucus serratus	2.0-3.5	
Fucus vesiculosus	1.25-2.75	
Ascophyllum nodosum	2	

Table 1.1. The cellulose content of a number of brown algae expressed as percentage of dry weight (adapted from reference 36).

Alginic acid, a polyuronide found in Phaeophyceae has been extensively studied[42]. It is composed of D-mannuronic acid and L-guluronic acid segments[43,44,45,46]. Accurate determinations of the composition of alginic acid extracted from different sources has been made (see Table 1.2.). It is widely agreed that alginic acid from various sources is composed of three polymer segments[47,48,49]. One segment consists essentially of D-mannuronic acid units; a second segment consists of essentially L-guluronic acid units and the third segment consists of alternating D-mannuronic acid and L-guluronic acid residues (see Fig. 1.4.).

Species	Algin (%)	MA (%)	GA (%)	M/G	M/G Range
Macrocystis pyrifera	-	61	39	1.56	-
Ascophyllum nodosum	24.5	65	35	1.85	1.4-1.95
Laminaria digitata	-	59	41	1.45	1.4-1.6
Laminaria hyperborea (stipes)	~20	31	69	0.45	0.4-1.0
Ecklonia cava	33	62	38	1.6	-
Durvillea potatorum	50	-	-	-	-
Lessonia flavicans	31	-	-	-	-

Note: MA: mannuronic acid, GA: Guluronic acid

Table 1.2. Mannuronic acid (M) and Guluronic acid (G) composition of alginic acid obtained from commercial brown marine algae (adapted from reference 42).

The proportions of the three polymer segments in alginic acid samples varies from species to species[50] (see Table 1.3.). The variations in the composition of the uronic acid segments, as highlighted in Tables 1.2. and 1.3., account for the differences in properties and functionality of alginates isolated from different species of brown algae. The dissociation constant for alginic acid depends on the relative amounts of mannuronic acid to guluronic acid. Reported values[42] for pK_a are: mannuronic acid 3.38 and guluronic acid 3.65.

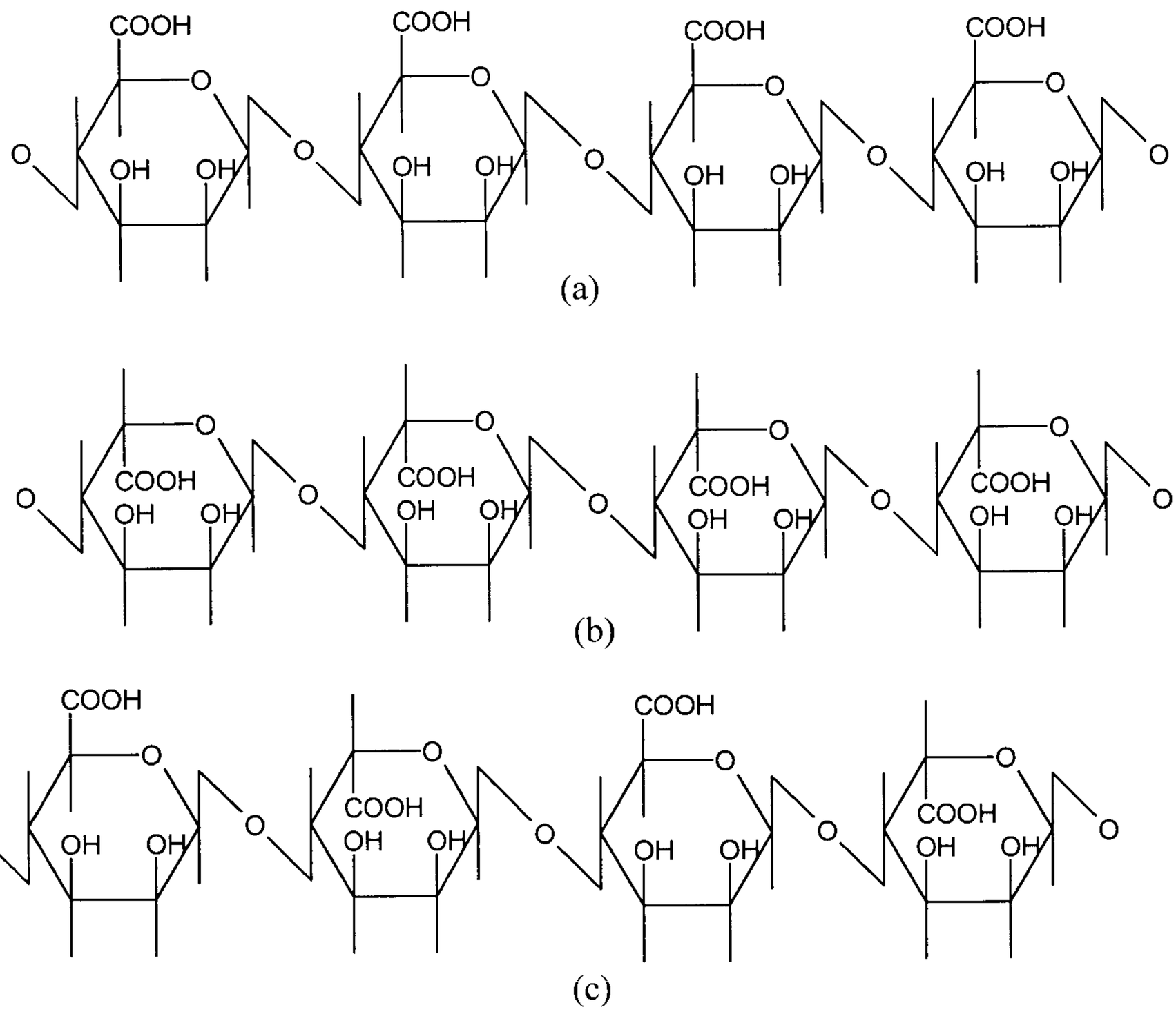

Figure 1.4. Structure of the polymer segments contained in alginic acid; a: -M-M-, b: -G-G-G-, c: -M-G-M-G-.

Species	MA segment (%)	GA segment (%)	Alternating segment (%)
Macrocystis pyrifera	40.6	17.7	41.7
Ascophyllum nodosum	38.4	20.7	41.0
Laminaria hyperborea	12.7	60.5	26.8

Table 1.3. Proportions of polymannuronic acid, polyguluronic acid and alternating segments in alginic acid isolated from brown algae (adapted from reference 42).

Information on the crystalline structure of polymannuronic acid and polyguluronic acid has been obtained by X-ray diffraction studies on fibres of alginic acid and polarised infrared spectroscopy of oriented films. Elucidation of the conformational structure of polymannuronic acid and polyguluronic acid chains is due to the work of Atkins et al[51].

The shape of the polymannuronic acid chain is quite similar to β1→4 linked hexosans such as cellulose. The mannuronic acid is di-equatorially linked and has a C1 conformation (see Fig. 1.5.). The conformation is stabilised by the formation of an intra-molecular hydrogen bond between the hydroxyl group on C3 of one unit and the oxygen atom of the next sugar unit in the chain. The chains themselves are bonded into sheets by means of hydrogen bonds formed between the hydroxyl of the carboxyl group and the oxygen atom on C3 in sugar units in parallel chains and between the axial hydroxyl group on C2 and the oxygen atom of the carboxyl group in antiparallel chains.

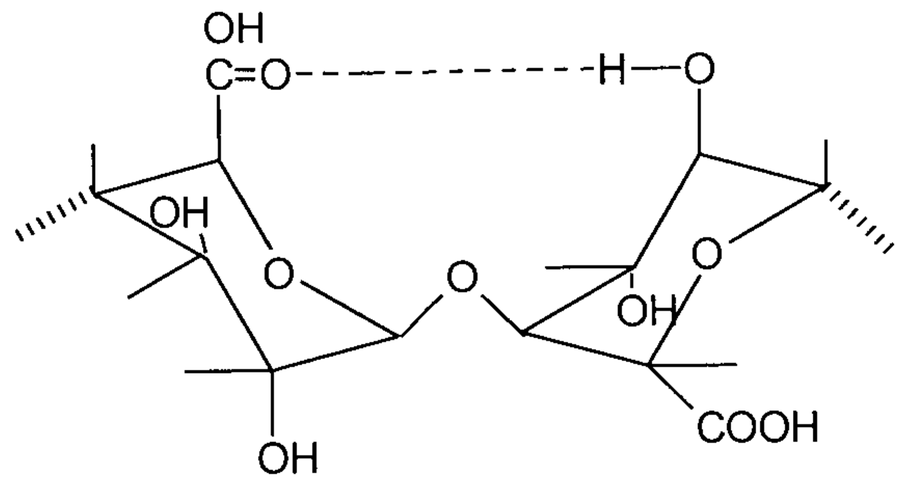

(a)

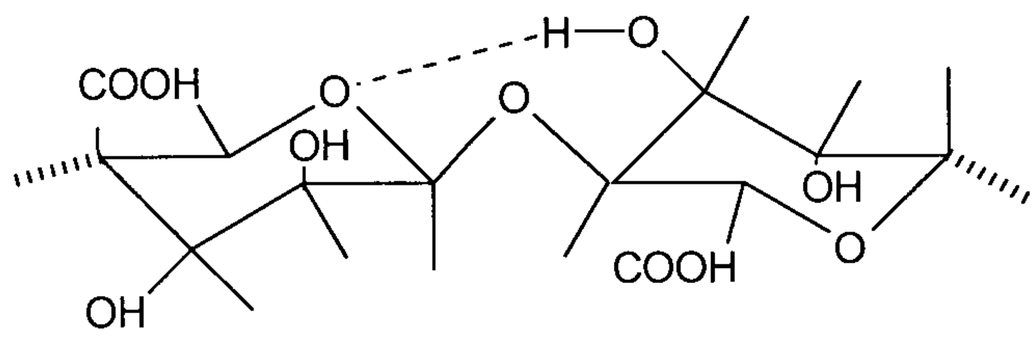

(b)

Figure 1.5. Conformation of uronic acid residues; a: guluronic acid, b: mannuronic acid.

In comparison, the shape of the polyguluronic acid chain is rather different from that of polymannuronic acid. Polyguluronic acid is a buckled, ribbon-like molecule in which the guluronic acid is in the 1C conformation and therefore, diaxially linked. Intramolecular hydrogen bonds between the hydroxyl group on C2 and the oxygen atom of the carboxyl group in adjacent units stabilize the ribbon-like conformation. The inter-chain bonds are more complicated than in the case of mannuronic acid and involve water molecules. The hydrogen molecule plays a dual role in acting as a hydrogen donor and a hydrogen acceptor, the hydrogen bonds so formed are in the range of $2.7\,\mathring{A}$ -$2.9\,\mathring{A}$. From density measurements and or symmetry preservation, four molecules of water are required in the unit cell[51]. The two types of alginic acid in fibre form were examined by X-ray crystallography[52] and the fibre spacing was found to be $8.7\,\mathring{A}$ for the G blocks and $10.3\,\mathring{A}$ for the M blocks. Evidence from other sources agrees well with the conformations described above. The NMR spectra of the two block types in solution have been shown[50] to agree well with this X-ray crystal structure and the difference in conformation could explain the difference in the ultraviolet circular dichroism[53] which have shown that calcium ions interact preferentially with the polyguluronic acid segments.

The nature of the interaction between the polyguluronate segments and calcium ions has been further refined using both the known coordination geometries of model compounds and the requirements for cooperative association. The proposed interaction of the polyguluronate segments and calcium ions is such that the polyguluronate segments associate into aggregates with interstices into which the calcium ions fit, the so called 'egg-box model'[54] (see Fig. 1.6.).

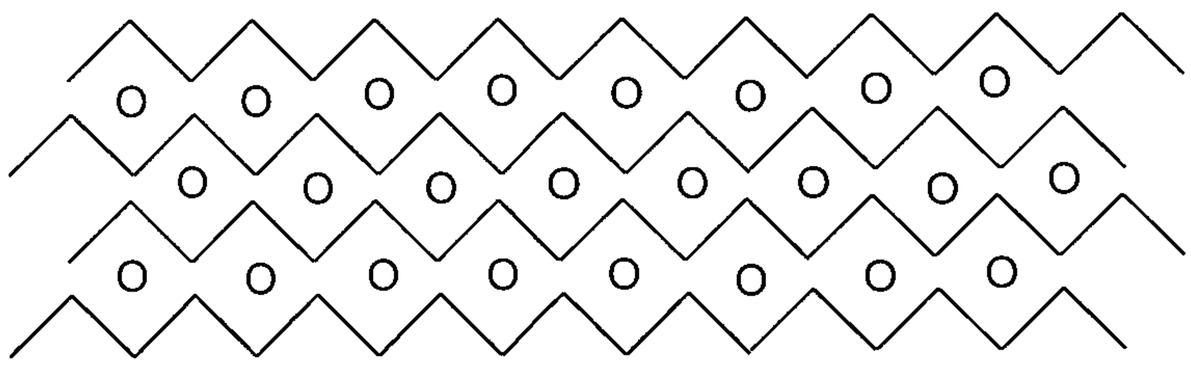

Figure 1.6. Egg-box structure of calcium-polyguluronate[54].

Polysaccharides with sulphate hemi-ester groups attached to sugar units are found in the form of fucoidan in the Phaeophyceae (see Fig. 1.7.). It is thought to occur in the intercellular tissues or mucilaginous matrix. It is very hygroscopic and may therefore serve to prevent dehydration of the plant upon long exposures. Plants occurring at intertidal level have been found to contain a higher fucoidan content[36].

Fucoidan probably exists as a galactofucan and xylogalactofucan. Fractionation of a sample of fucoidan from *F. vesiculosus* on DEAE-cellulose gave a small quantity of a xylan together with several fractions which contained fucose and small proportions of galactose. Evidence for more than a single molecular species in fucoidan has also been revealed by free-boundary electrophoresis[55] on material extracted from *A. nodosum* and from *F. vesiculosus*. Three boundaries were observed for the *A. nodosum* extract and only two boundaries with electrophoretic mobilities of 2.3 and 2.5×10^{-4} cm^2 s^{-1} V^{-1} for the *F. vesiculosus* sample.

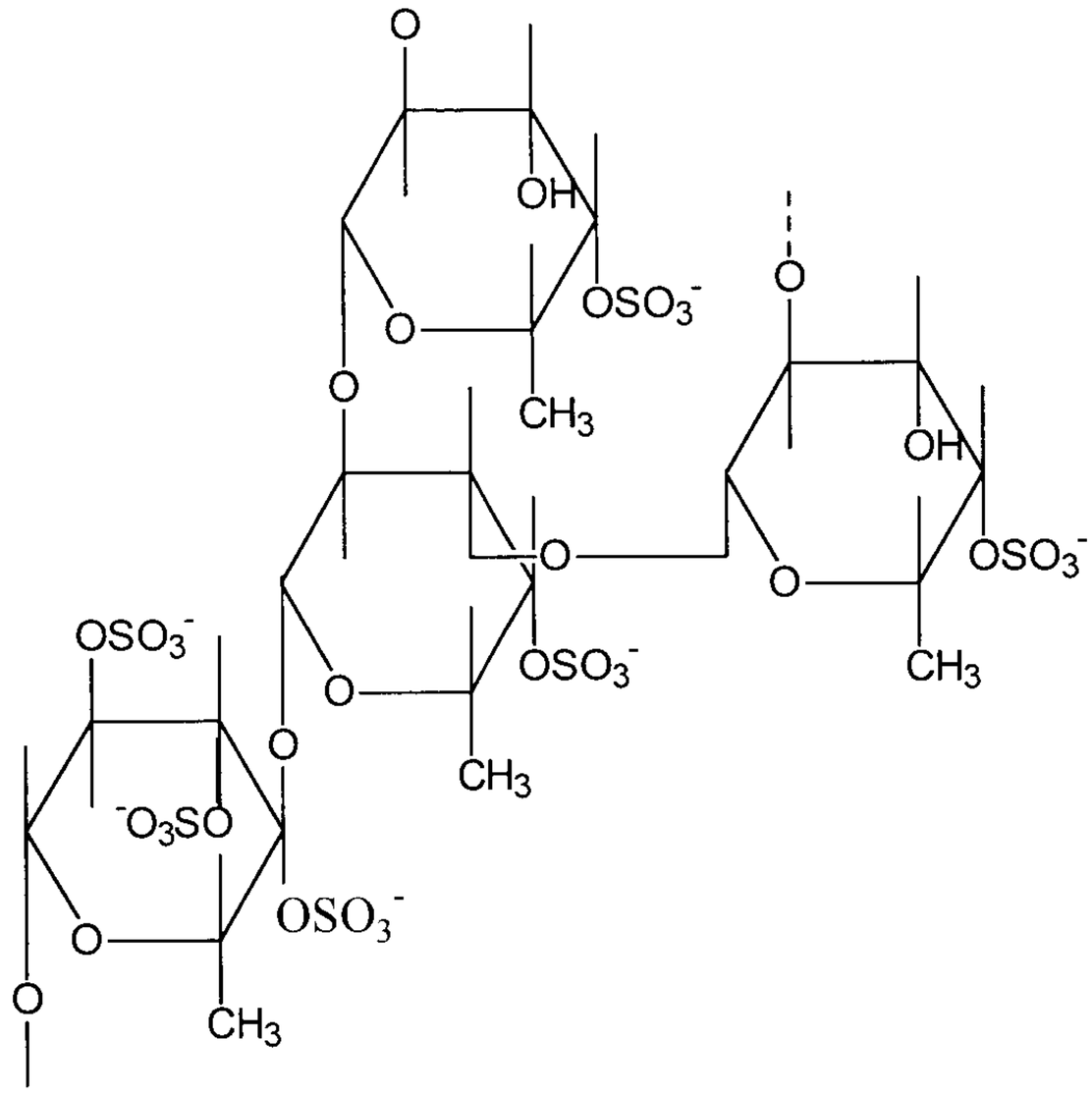

Figure 1.7. All possible linkages between L-fucose units in fucoidan polysaccharides.

Although fucoidan isolated from different genera of brown seaweeds appear to have somewhat different compositions, they all comprise mainly fucose and ester sulphate. In salt solution, the fucan molecule is considered to be a highly charged, branched, random coil. Its electrophoretic mobility has been reported[36] as $27x10^{-5}$ cm^2 s^{-1} V^{-1} at pH5.

The type and variety of fucose containing polysaccharides has been found to be extensive. Whereas fucoidan refers to polysaccharides consisting almost entirely of fucose and ester sulphate, complex polymers containing fucose, xylose, protein and glucuronic acid have been termed glucuronoxylofucan sulphates. In some cases, glucuronic acid comprises the backbone of the macromolecule to which are attached glycosidically, relatively long, side-chains of sulphated fucose and xylose.

The literature is rich in reports on investigations concerning the interactions of heavy metals and algae. The following section concerns itself with summarising results of these studies and highlighting areas which require further investigations.

Trace metals have a vital role to play as constituents of enzymatic systems in biological processes[56]. Interactions of metallic species with proteins and polysaccharides found constituting the cellular structure of algae have been proposed[57]. Amino-carboxyl groups from polysaccharides as well as nitrogen and oxygen of the peptide bond have counter ions which could be available for replacement by metal ions[58]. Heavy metals have been found to show strong affinity for protein[59]. Metal sorption was found to be reversible with bound metal released by different counter ions. Strontium was able to displace zinc in the alga *Vaucheria* even though the zinc was bound to the cell wall[58] suggesting that electrostatic attraction plays an important role in the metal uptake process. The strength of sequestering of various divalent ions to *Vaucheria* cell walls was proportional to formation of ions or stability constants, suggesting that covalent bonding is also important in the uptake process.

Copper sorption by algae

Copper is one of the most common of the industrial metals. Absorption of excess copper by man results in "Wilson's disease" in which excess copper is deposited in the brain, skin, liver, pancreas and myocardium. Copper is a nutrient necessary for algal growth but at high concentrations, it finds use as an algicide.

Crist[60] demonstrated that copper was adsorbed not only by ion exchange but also by additional covalent binding with the carboxyl groups of *Vaucheria pectins*. A comparison of the uptake of copper by living and previously scalded (treated with boiling water) algal cells showed that copper removal was faster for scalded cells in comparison with living cells[61]. McKnight and Morel[62] investigated the copper complexing properties of twenty one species of algae. Experimental data was found to be in good agreement to theoretical predictions calculated by MINEQL computer program. Low concentrations of mercury resulted in redistribution of intracellular copper and zinc in algae[63]. A low molecular weight protein (metallothionein) was thought to play a role in storage or binding of heavy metal in the marine alga *Skeletonema costatum*.

In *Nitzschia palea*, the major portion of the copper was found in the cell wall and slime envelope which constituted 6% of the total carbon of the cell[58]. Polysaccharides extracted from *Chlorella stigmatophora*[64] were shown to bind copper in solution. Various algal species within the same genus, although producing polysaccharides did not however show similar metal sorption characteristics. Free carboxylic groups (contributed by uronic acids) and their relatively homogenous distribution in the polysaccharide of *C. stigmatophora* were found to play a major role in metal sequestration. Matheickal et al.,[65] studied the copper sorption phenomenon on *Ecklonia radiata*. Table 1.4. summarises some of the metal sorption data encountered during the literature review.

Lead sorption by algae

Lead has been found to have a high affinity to algal cells[66] and polysaccharides of algae[67]. Prolonged exposure to lead in the environment resulted in entrapment of lead ions within the cell wall. Eventually, the lead diffused through the cell wall to the plasma and eventually to the cytoplasm[66]. In laboratory experiments, algae specimen (*Cladophora*) packed in columns removed 85% of lead from the feed solution at near neutral pH. Regeneration of the lead laden column was achieved by washing the algal biomass with small quantities of (0.01-0.1)M EDTA in 0.1M sodium acetate at pH7.5. During lead sorption, release of calcium, magnesium and potassium along with small amounts of sodium were observed, indicating a cation exchange type phenomenon was responsible for metal sorption. Holan[73] screened 45 algal biomass samples (native and cross-linked) for the uptake of lead. Lead uptake was found to be highest among the Phaeophyta order of algae. Among the Phaeophyta, lead biosorption decreased as follows: *Fucus>Ascophyllum>Sargassum>Padina*. These trends in lead uptake for the various species are to be viewed with caution since no material pre-treatment (e.g. washing with dilute HCl) was carried out.

Metal	Species	Metal uptake mmol g^{-1}	Reference	Comments
Copper	*Ascophyllum nodosum*	1.2	Leusch et al.[68]	
	Sargassum fluitans	1.4	Leusch et al.[68]	
	Ecklonia radiata	1.2	Matheickal et al.[65]	
	Scenedesmus Obliquus	0.16	Mattuschka et al.[69]	fresh water algae
Cadmium	*Ascophyllum nodosum*	1.9	Holan et al.[70]	
	Sargassum fluitans	0.81	Leusch et al.[68]	
Gold	*Ascophyllum nodosum*	0.12	Kuyucak et al.[71]	
	Palmaria tevera	0.83	Kuyucak et al.[71]	
	Palmaria palmata	0.63	Kuyucak et al.[71]	
	Sargassum natans	2.0	Volesky et al.[72]	
	Chlorella pyrenoidosa	0.5	Darnall et al.[71]	fresh water algae
	Cyanidium caldarium	0.43	Darnall et al.[71]	
	Chlorella vulgaris	0.41	Gee et al.[71]	
	Chondrus crispus	0.39	Kuyucak et al.[71]	
	Spirulina platensis	0.36	Darnall et al.[71]	
	Rhodymenia palmata	0.2	Darnall et al.[71]	
Lead	*Sargassum fluitans*	0.69	Leusch et al.[68]	
	Ascophyllum nodosum	1.1	Leusch et al.[68]	
	Ecklonia radiata	1.36	Matheickal et al.[65]	
	Palmaria tevera	(1.3-1.7)	Holan et al.[73]	
	Sargassum natans	(1.1-1.3)	Holan et al.[73]	
Nickel	*Sargassum fluitans*	0.78	Leusch et al.[68]	
	Ascophyllum nodosum	0.9	Leusch et al.[68]	
	Fucus vesiculosus	0.7	Kuyucak et al.[71]	

Metal	Species	Metal uptake mmol g^{-1}	Reference	Comments
Zinc	*Sargassum natans*	(0.4-0.75)	Holan et al.[73]	
	Sargassum fluitans	1.4	Leusch et al.[68]	
	Ascophyllum nodosum	0.61	Leusch et al.[68]	
Chromium	*Sargassum fluitans*	0.77	Kratochvil et al.[74]	
Cobalt	*Ascophyllum nodosum*	1.7	Kuyucak et al.[75]	

Table 1.4. Summary of various metal sorption results of algal biomass.

The uptake of lead by *F. vesiculosus* and *A. nodosum* was found to be very pH dependent, increasing with increasing solution pH. Sorption isotherms tend to show a sudden rise in uptake values at high residual metal concentrations. Holan[73] attributed this to distortion effects by metal complexes formed as colloids occurring in the solution due to the leaching of water soluble biopolymers (alginates) from the biomass.

Zinc sorption by algae

Zinc has been widely studied in its relationship with algae and alginates. Polikarpov[76] found that concentration factors for zinc were among the highest of the metals reported. Equilibrium calculations on the speciation of zinc in sea water reveal zinc is most likely present in the form of a chlorocomplex[77]. From chemical equilibrium considerations, in freshwater, zinc was found to be present predominantly as the hydrated cation, while carbonate, sulphate and hydroxyl species were also present to some extent[78].

Nitzchia closterium accumulated considerable amounts of zinc[79]; far in excess of the metabolic needs of the organism. The rate of zinc uptake was rapid with 80% removal in the first hour. Addition of complexing agents such as EDTA prevented the uptake of zinc which was particularly dependent on solution pH. In *Chlorella vulgaris*, zinc was postulated to be bound in the free spaces of the cell walls[80]. In a

comparative study of three algal species: *Chlorella vulgaris*, *Euglena viridis* and *Pediastrum tetras*, *E. viridis* concentrated the greatest amount of zinc[81].

Mercury sorption by algae

Mercury is one of the "big three" pollutants (lead and cadmium being the other two), in terms of its toxicity and potential hazard to humans and the environment. In sea water, inorganic mercury is predominantly in the form $HgCl_4^{2-}$ ions. In fresh water, mercury can exist in the Hg_{aq} state and also as the Hg^{2+} ion. Under various conditions of redox potential (E_h) and pH, mercury may exist as HgS_2^{2-}, HgOH, Hg, HgCl(OH) and $HgCl_2$. The chemistry of mercury is further complicated by its metal affinity for sulfhydryl groups as well as its ability to be methylated.

In a comparative study of the degree of toxicity of various metals, mercury was found to be more toxic than copper, cadmium, lead and silver when tested with one freshwater *Chlorella pyrenoidosa* and three marine organisms, *Phaeodactyleum tricornutum*, *Cyclotella nana* and *Chaetoceros galves tonensis*[82]. Glooschenco[83] concluded that the most important process for mercury uptake was surface adsorption by studying mercury sorption by the marine diatom *Chaetoceros costatum*. Suggestions that a metallothionien-like substance might be responsible for sequestering heavy metals in the diatom were proposed. The blue-green algae C*hlorella pyrenoidosa* was found to have high mercury sorption capacity at low solution pH.

Cadmium sorption by algae

Cadmium has joined lead and mercury in forming the "big three" of heavy metals with the greatest potential hazard to humans and the environment due to its acute toxicity. In sea water, it is probably present in the form $CdCl^+$ ions. Cadmium uptake by the herbivorous marine copepod *Pseudodiaptomus coronatus* has been studied by Sick[84]. Evidence of protein-metal interaction has been proposed. The protein which is known to complex with cadmium is rich in cysteine (one out of every four amino acids) indicating a possible interaction between cadmium and sulfhydryl groups[85].

Dialysed solutions of carageenan were prepared and interaction of cadmium with polysaccharides indicated that binding occurred mainly due to the electrostatic interactions between the sulphate ester groups and the metal cation.

In another study, a cadmium binding component with a molecular weight of 12,800 Daltons was detected in lysates of *Chlorella pyrenoidosa*. Evidence that the metal binding component was a metallothionein-like protein[86] was based on the molecular size, heat stability, and the ability to incorporate ^{35}S along with ^{115}Cd.

Holan[70] has looked at the biosorption of cadmium by several seaweed biomass types. Both native and crosslinked biomass were investigated and compared with commercial ion exchange resins. The biomass *A. nodosum* demonstrated high equilibrium uptake of cadmium from aqueous solutions. The native biomass was found to be rather soft, with the tendency to disintegrate. In order to improve the stability and mechanical properties of the biomass, crosslinking of *A. nodosum* biomass proved to be promising. The influence of drying procedures on subsequent metal sorption indicated that drying temperatures below 100°C did not affect the biosorbent performance. Solution pH was found to be very important in cadmium biosorption by *A. nodosum*. Cadmium uptake fell from 1.8 mmol g^{-1} at pH 4.9 to less than 0.3 mmol g^{-1} at pH 2. Cadmium sorption was influenced by the type of anionic species in solution. Cadmium uptake[70] from cadmium sulphate solution (0.9 mmol g^{-1}) was less in comparison with cadmium sorption from cadmium acetate solution (1.1 mmol g^{-1}).

While cadmium uptake by native biomass of *A. nodosum* and *S. natans* was found to be rather encouraging, the dried biomass was found to swell upon rewetting. In order to overcome this problem, an attempt to establish a simple cost effective granulation of *A. nodosum* biomass by crosslinking was investigated by Holan[70]. The most promising results were obtained using divinylsulfone and formaldehyde under acidic conditions. *A. nodosum* crosslinked with divinylsulfone resulted in slightly decreased metal uptake than the native biomass. This could be attributed to the release of valuable polysaccharides that may have played an important part in metal

sequestration. Crosslinking with divinylsulfone or with formaldehyde-urea mixtures may not be considered as pure crosslinking due to the tendency of resin formation that could stabilize the biomass. While the formaldehyde-urea mixture was found to improve the mechanical stability of the material, resin formation blocked or masked the functional groups responsible for the sequestration of the metal.

Aldor[87] investigated the desorption performance of cadmium laden *Sargassum fluitans*. In addition to various inorganic acids, the complexing agent Na_2EDTA proved a successful eluant capable of regenerating the cadmium laden biomass. NaCl, $CaCl_2$ and NH_4Cl showed good cadmium elution properties. An exchange equilibrium between protons in solution and cadmium on the biomass was found to exist. Aldor[87] demonstrated an almost stoichiometric exchange between cadmium and protons during metal desorption.

Nickel sorption by algae

Nickel-containing industrial effluents are common in a large number of industrial applications ranging from electroplating to long life batteries. There is evidence of nickel carcinogenity at elevated levels. In sea water, nickel was found to be principally in an ionic state, while in fresh water the carbonate species was the most important, followed by the free ion and then the hydroxide.

Alginates extracted from the brown seaweed *Laminaria digitata*, were found to have a low affinity for nickel; this affinity was lower than for any other divalent ion except magnesium[88]. Holan[73] compared the performance of several algal varieties which had shown promise as lead biosorbents and found the uptake for nickel was almost an order of magnitude lower. The biomass types tested exhibited decreasing affinity for nickel in the sequence: Phaeophyta>Rhodophyta>Chlorophyta. For several varieties of Phaeophyta, nickel sorption followed the order: *A. nodosum* > *S.fluitans* > *S.natans* > *F.vesiculosus*. The sorption of nickel was found to be pH dependent. In comparison with an ion exchange resin Amberlite IR 120 (2.2 mmol g^{-1}), *A. nodosum* displayed a comparatively lower nickel sorption capacity of 0.8 mmol g^{-1} under similar conditions. Nickel uptake was thought to occur by interaction with carboxyl

ligands, present abundantly as polyuronides in the algal cell walls. Differences in metal sorption capacity was attributed to morphologically different architecture of algal tissues: *F. vesiculosus* consists of parenchymatous cells with apical meristems[89] instead of the predominantly filamentous architecture of *A. nodosum*.

Cobalt sorption by algae

Cobalt is not a particularly hazardous metal however, its use in industry as an essential element in super alloys and specialty chemicals combined with limited stocks has resulted in it becoming a valuable metal ($18/lb.)[90].

Kuyucak and Volesky[75] examined the cobalt biosorbent properties of several marine algae (species of brown, red and green algae). The brown algae, *A. nodosum* showed promise with cobalt sorption capacity (2.65 mmol g^{-1}) almost twice as much as a commercially used ion exchange resin Duolite C-20. Cobalt sorption was found to be pH dependent with optimum pH in the range 4 to 5. The effect of temperature was not significant on the equilibrium sorption of cobalt. Competition with other cations (except Ca^{2+} and Fe^{2+}) resulted in reduced cobalt uptake. Fast biosorption kinetics were displayed by *A. nodosum* with the relationship between initial rates of cobalt sorption and initial cobalt concentration found to follow first order kinetics. Kuyucak[91] studied the desorption of cobalt from metal laden biomass. The effect of various eluants including inorganic acids, complexing agents (EDTA and KSCN) and competing cations (NH_4OH, $KHCO_3$, KCl and $CaCl_2$) were looked at. $CaCl_2$/HCl appeared to be the best eluant for the cobalt - *A. nodosum* system with more than 96% elution efficiency at pH 2.5. Exposure to this eluant left the granular biomass unchanged in its structure and texture as revealed by transmission electron micrographs. The elution rate was also rapid and the re-sorption capacity of the alga remained unchanged, permitting the reuse of the biomass in several sorption-desorption cycles[91]. Alginates of the algal cell wall were found to play a dominant role in sequestering cobalt from solution[92]. Ion exchange was proposed as the prevailing mechanism for cobalt biosorption.

Arsenic sorption by algae

Arsenic and its compounds have been widely used in pigments, as insecticides and herbicides, as an alloy in metals and arsenic compounds were developed as chemical warfare agents. The toxicity of arsenic increases greatly when arsenic is reduced from a +5 to a +3 oxidation state. Ferguson et al.,[93] discuss the interesting chemistry of arsenic with oxidation-reduction, ligand exchange, precipitation and adsorption reactions all taking place. Arsenic forms kinetically stable bonds with sulfur and carbon in organic compounds. Like mercury, arsenic (+3) reacts with sulfhydryl groups of cysteine in proteins. Arsenate, the stable form in aerobic water, may be removed by several mechanisms. Hydrous iron oxides have been shown to effectively co-precipitate arsenate species. Marine organisms are known to accumulate arsenic. In sea water containing arsenic ranging from (0.05-5)μg l^{-1}, marine plants are reported to have arsenic concentrations ranging between (1-12)mg kg^{-1} (dry weight)[93]. Hassett et al.[94] studied five species of marine algae and found that inorganic arsenic from the culture media was incorporated predominantly in the lipid phase and was organically bound. *P. tricornutum* had the highest concentrations of arsenic.

Codium taylori (a green alga), showed higher arsenic (+3) uptake (90 mg g^{-1}) at acidic pH(2-4) values[95]. In contrast, dried yeast *Saccharomyces cerevisiae* removed up to 75 mg g^{-1} of As^{3+} at pH 8.

Chromium sorption by algae

The green algae *Halimeda opuntia*[95] showed excellent potential as a chromium biosorbent concentrating up to 380 mg g^{-1} of Cr^{3+}. The uptake of chromium was shown to be highly selective and independent of the presence of other cations or anions in solution. The kinetics of chromium sorption was fast while the optimum pH for metal biosorption was between pH 4 to 6. Algal bound chromium was sequestered using sulfuric acid and the algae could be reused several times for multiple metal sorption/desorption cycles.

Kratochvil et al.[74] studied the removal of Cr^{3+} by the marine algae *Sargassum fluitans/natans*. The seaweed bound up to 40 mg g^{-1} of Cr^{3+}. The mechanism of

chromium removal was thought to be ion exchange between $Cr(OH)^{2+}$ and H^+ of the carboxylate groups supplied by alginic acid within the algal matrix.

Calcium, actinides and radioactive metal sorption by algae

Volesky[1] discusses the interactions between calcium carbonate contained in marine algae and presence of ^{226}Ra, ^{232}Th and ^{238}U in green, brown and red algal species. Two mechanisms for the binding of actinides in algae were proposed: (1) ion exchange or co-precipitation of the metal ions with the calcium carbonate matrix, and (2) complex formation with either the protein nitrogen or other organic fraction.

Horikoshi[96] found that uranium uptake by *Synechococcus elongatus* from sea water was strongly pH dependent. The maximum uranium uptake was found to take place at pH5. Carbonate ions strongly inhibited uranium uptake. Greene et al.[97] found that decarbonation of sea water greatly enhanced the uranium removal. Dead cells of S*ynechococcus* as a result of heat treatment were found to have twice the uranium sorption capacity compared to living cells. The uranium absorbed by *Synechococcus* was found located in the inner space of cells and only a small amount was present within the cell walls. On the other hand, in *Chlorella regularis,* most of the uranium absorbed was located in the cell wall[98].

Sakaguchi et al.[96] selectively extracted cellular material to determine which components of *Chlorella* cells were responsible for heavy metal ion binding. Cellulose was found to play a major role in metal ion binding. Protein-metal interactions were thought to be significant, although, the degree of interaction was metal ion specific.

The fungal biomass *Rhizopus arrhizus* has been evaluated[99] for the successful sequestration of uranyl ions from solution. The biosorbent was capable of removing between (150-250) mg g^{-1} of uranyl ions at equilibrium. The mechanism of uranyl ion uptake was found to be ion exchange or complexation. The sorbent material could be regenerated using inorganic acids with subsequent reuse possible. In another study[100] uranium coordination and adsorption in the cell wall chitin structure and precipitation

of uranyl hydroxide within the chitin microcrystalline cell wall structure was found to be the primary mechanisms for the removal of uranium (+6) from solution.

Inactive cells of *Rhizopus arrhizus* were found to exhibit a high thorium biosorptive capacity (170 mg g^{-1}) from aqueous solutions[101]. Thorium was found to coordinate with the nitrogen of the chitin wall network and in addition, more thorium was adsorbed by the external section of the fungal cell wall.

The activity and concentrations of plutonium and other nuclides in selected samples of brown, red and green algae as well as marine grasses were compared by Wong et al[102]. Hodge et al.,[103] found the giant brown alga, *Macrocystis pyrifera* could be used as an indicator for monitoring rapid changes in coastal sea water plutonium concentrations. Spies et al[104], postulated that plutonium was concentrated in the living tissue and the skeleton of the calcareous alga *Halimeda macrophysa*.

Rice[105] studied the simultaneous uptake of two or more radioactive elements of ^{89}Sr, ^{90}Sr and ^{90}Y by planktonic algae from an artificial sea water medium. Ten of the twelve species became more radioactive from the uptake of ^{90}Y which was present in very small amounts whereas the other two species showed selectivity towards ^{89}Sr. The instantaneous removal of yttrium from the medium by *Carteria* was shown to occur due to adsorption on the cell surface, whereas strontium was found to be located within the cells. Dead cells and non-dividing living cells did not remove any significant quantities of strontium from the medium. The concentration factor for *Carteria* was influenced by the rate of cell division, the age of the culture and the initial pH of the medium in which the cells were grown. Very little radioactive strontium was lost from radioactive *Carteria* cells suspended on a filter and washed with various eluant solutions[105].

Kalin[106] revealed that *Chara*, a macrophytic alga may be used *in situ* to improve the waste water quality of tailings from mining operations, thereby economizing on waste water treatment and on reclamation. *Chara*, in its metabolically dormant state was found to have attractive potential in removing metals such as aluminium, arsenic,

cadmium, cobalt, iron, nickel, lead, selenium and radionucleides such as uranium, radium and thorium as well as calcium and barium from alkaline mine effluents.

Algae as biosorbents for precious metals

Marine algae have been found to have a high affinity for precious metals such as gold[76]. The formation of certain gold deposits in South Africa have been attributed to the involvement of Precambrian algal blooms and bacteria[107,108]. Algal gels have been found to be effective in sequestering chromium, silver, mercury, platinum and gold[111]. *Chlorella vulgaris* immobilized gold with more than 90% gold removed from very dilute solutions with the metal concentration in the parts per billion range. Sites for the binding of $AuCl_4^-$ were found to be independent of pH whereas removal of other complexes of gold were strongly pH dependent. A brown marine alga, *Sargassum natans* in its non-living form was found to a potent biosorbent material for gold[72]. The alga showed higher gold uptake capacity than that of a commercial ion exchange resin when acidic gold chloride solution was employed. The sequestered gold could be successfully eluted using a mixture of thiourea and ammonium ferric sulphate[109]. The gold was reduced to its elemental form by the biosorbent. The cell wall of the alga was the major locale for gold deposition which was confirmed by transmission electron micrographs of the gold laden biomass. The alga-bound gold which could be eluted by thiourea from the cells was in the +1 oxidation state. This was confirmed by measuring 3 moles of chloride ions released for each mole of gold bound to the alga[110,111]. The gold binding ability of algae was attributed to the presence of nitrogen and sulfur containing ligands. Kuyucak and Volesky[112] provided some evidence that cellulosic materials of the algal cell wall provided carbonyl (C=O) groups that were functional in gold binding.

Non-living red marine algae *Chondris crispus* and *Palmaria palmata* successfully sequestered silver and platinum respectively[113]. The optimum pH range for silver sorption was pH(2-6) whereas pH(<3) was suitable for platinum biosorption.

Section 1.5. Dealginate Seaweed Residue

Brown marine algal plants (seaweeds) are commercially important because of their high algin content. Companies such as NutraSweet Kelco (part of Monsanto) process seaweed into free-flowing granular or fibrous powders known as alginates by harvesting from giant kelp beds off the coast of California and Mexico and collecting seaweed from the shores of Chile, Tasmania and Scotland. Alginates find use in a wide range of food products including puddings, milk shake mixes, dessert gels and ice cream. Salad dressings are emulsified and stabilised with alginates. In bakery products, texture is improved and moisture retained using algin, while in frozen foods, the stabilizing properties of alginates assure smooth texture and uniform thawing. Beer foam stabilization is another commercially important use for alginates. The primary industrial applications of alginate products are textile printing, dyeing and paper coating and sizing. Important uses in pharmaceutical and cosmetic products include tabletting, manufacture of dental impression compounds and antacid formulations.

Once the algin has been extracted, the algin stripped seaweed residue (dealginate residue) is disposed off back into the sea. Recently, some interest has surfaced regarding the use of this waste biomass as a biosorbent for removing metal ions from dilute metal bearing effluents[114]. No detailed evaluation of the surface characteristics, sorption properties nor the viability of employing this waste biomass for waste-water treatment has been conducted to any great extent. Even if dealginate seaweed materials were found to possess significant metal sorption properties, considerable research effort will be needed to evaluate the optimum process parameters for usage. The solids slurry arising after algin extraction contains only 2% solids (wet wt. basis). This slurry (see Fig. 1.8. for algin extraction process) needs to be dewatered to obtain a sufficiently dry solids material that can be transported in a manner similar to conventional ion exchange materials.

During the past three years the dewatering of the solids slurry to obtain (90-95)% solids has been successfully solved (this work was carried out by Monsanto plc.). The

favoured route involves the direct treatment of the solids slurry, after secondary solid/liquid separation, with acidified calcium chloride solution followed by centrifugation. Decanter discharge material is further de-watered by direct pressing using a screw process. Using this approach, dealginate seaweed residue with an average dry matter of 25-28% can be produced for trial evaluation as a biosorbent. For a considerably drier product, trials utilizing an air swept tubular (AST) dryer were carried out. This equipment was capable of drying 95% liquid slurries to fine powder, 90-95% solids (wet wt. basis) with a residence time of 3-5 seconds. The unit provides agitation that mixes hot air with the wet slurry entering the dryer inlet, reducing the drying time and breaking up lumps. The dryer is capable of reducing the slurry moisture content from 95% to 1% in a single pass. Adjustable paddles and air dams facilitate a change in retention time and allow for variations in the drying process.

The influence of dryer temperature and drying rate could have a deleterious effect on the subsequent metal sorption performance of dealginate materials. This and the impact of other process parameters have been considered in subsequent chapters of this thesis.

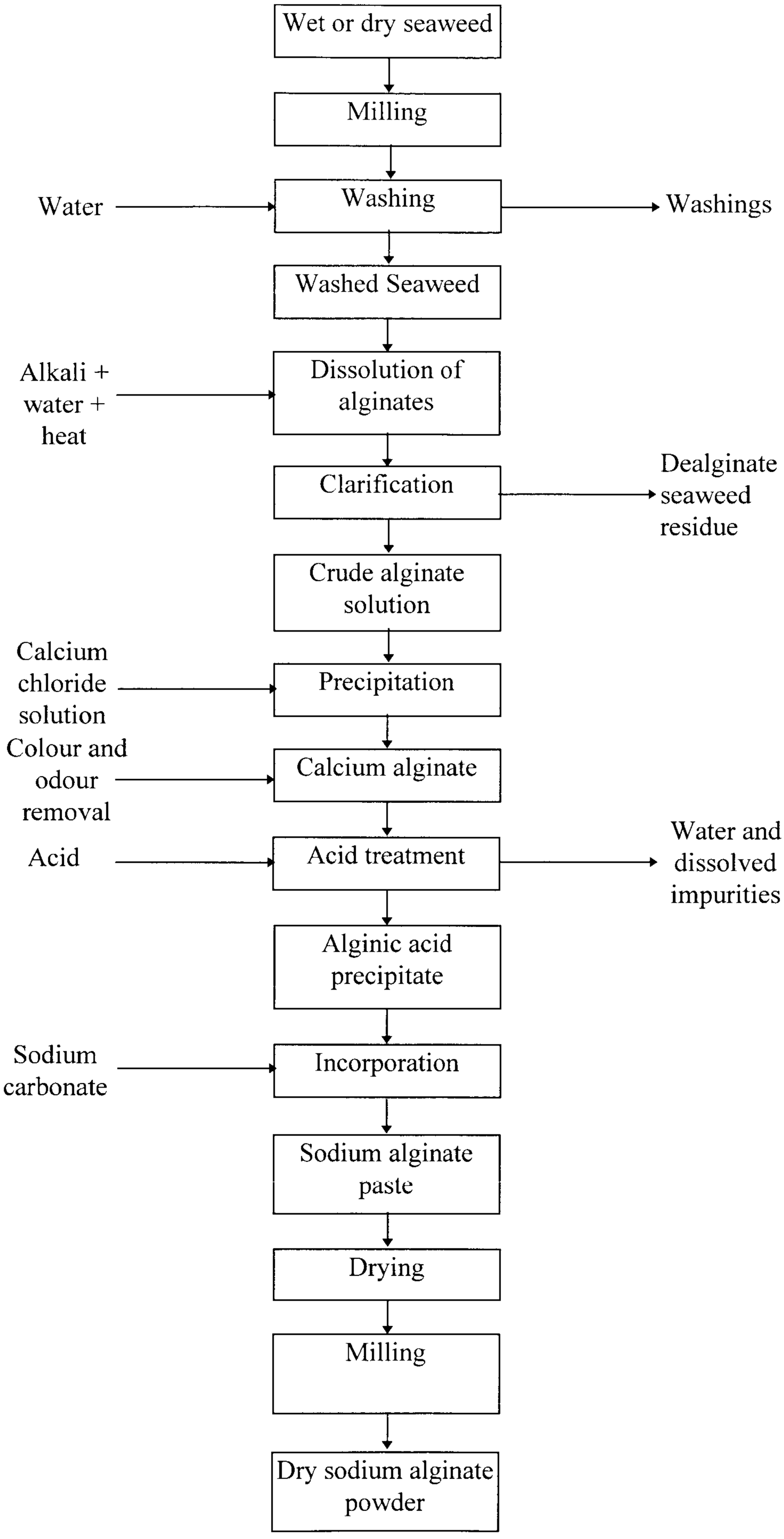

Figure 1.8. Sodium alginate manufacturing process.

Section 1.6. Selection of Biosorbent Materials and Target Metal Solutions

The discussion in the preceding sections and literature survey suggests that biosorption has development potential for metal removal/recovery from waste waters. In particular, marine algae possess interesting metal sorption properties which coupled with their relative abundance and low cost makes them suitable for detailed evaluation as potential biosorbents. The dealginate seaweed residue; a waste product of the algin extraction industry has not been studied to any great extent and clearly satisfies the criteria of being cheap and readily available. Both native and dealginate seaweed materials are potential sorbent materials for treating metal-bearing effluents. Four native brown marine algal varieties have been selected for evaluation as potential biosorbent materials. *Sargassum* and *Ascophyllum* are two seaweed varieties which have received some attention as metal biosorbents (see Table 1.4.). It was decided therefore, that one of these two varieties should be studied for comparison. *Ascophyllum nodosum* harvested from Ireland was selected on this basis.

Most marine algae used for algin extraction contain a ratio of mannuronic acid to guluronic acid segments of about 1.5 (see Table 1.2.). The exception is *Laminaria hyperborea* (M/G ~ 0.45). Metal sorption experiments with alginates derived from different algae with varying M/G ratios indicated higher selectivity coefficients for some metals depending on the G blocks in the alginate molecules[115]. By selecting *Laminaria hyperborea*, a comparison of the role of M/G ratios and the guluronic acid content of different algal varieties on metal removal selectivity can be investigated.

Durvillea potatorum (Bull Kelp) from Australia was selected due to the high algin content of this particular algal variety (50%) compared with the other algal varieties (see Table 1.2.). The fourth algal variety selected was *Lessonia flavicans* (from Chile). The choice was based on the fact that *Flavicans* are combined with *Ascophyllum* or *Durvillea* to obtain mixed algins possessing certain characteristic

properties (e.g. medium range viscosity, formation of brittle hydrogels etc.) which find use in many industrial processes. In addition, two dealginate seaweed residues derived from native *Ascophyllum nodosum* and *Lessonia flavicans* were selected for detailed study.

The choice of metal bearing solutions against which the biosorbents were tested was based on an assessment of the likely extension of results, such that the metals studied covered as broad a range of metal-effluent generating industries as possible. Comparison of algal biosorbents against conventional ion exchange sorbent materials would then be possible in order to ascertain whether the algae exhibit competitive performance. Some of the considerations taken into account in selecting the metal ions used in this study are discussed below.

The composition of waste waters originating from different or even relatively similar industrial processes may vary considerably from one operation to another as well as with time from the same source point. The manufacture of mineral colours and fillers is based on the use of pigments. These pigments usually consist of oxides, sulfides and chromates of metal or metal mixtures. Wide varieties of pigments exist, such as titanium oxides, brown irons, lemon chrome, molybdate red, chrome ochre, ferro prussiate, zinc chromates and cadmium selenites and mixed component pigments with nickel, antimony, cobalt, titanium, chromium, aluminium etc. exist. Thus, contaminated waste waters arising from rinsing and washing operations will require treatment. Typically, 150 m^3 of waste water is generated[1] for the production of 1 ton of the end product of lead or zinc pigments. Cadmium containing waters with a concentration greater than 1 mg l^{-1} of cadmium are of specific concern.

In the iron and steel industry, waste water with trace metal content is generated in the blast furnace sector during wet dust removal from the blast furnace gas and during slag granulation. Continuously operated metallurgical plants need around 60 m^3 of water per ton of pig iron produced[1]. Water treatment circuits are required since the throughput of water in such operations is high, e.g. 500 m^3 h^{-1}, depending on the size

of the plant. The waste water discharge limits are below approximately 20 mg l^{-1} for Fe, 4 mg l^{-1} for Zn and between 0.5-2 mg l^{-1} for Pb.

Water originating from ore mining and ore processing operations invariably contains traces of all soluble metal salts that have been contacted. The leaching of sulfide non-ferrous metal ores by microorganisms (*thiobacilli* and others) leads to acidic aqueous effluent streams containing metallic ions and sulphates of heavy metals.

The non-ferrous metal industry, which includes some mines and metallurgical plants for the production of light and heavy metals such as copper, zinc, lead and aluminium, remelt and "semi-finished products" plants, foundries and "special metals" plants, generate metal-bearing waste water.

Different methods are employed for the detoxification of cyanides (oxidation) and chromates as well as for the purification of industrial effluents containing sulfides or complexing agents. Mixing of individual wash streams under controlled conditions is often practiced. Acidic streams may be mixed with alkaline waters, Fe(II) can be mixed with Cr(VI) carrying streams. The precipitation at an optimum pH value followed by removal of the solids is often the most satisfactory and widely employed method practiced for removal of metals from large waste water streams.

The manufacture of lead accumulators results in waste waters containing dissolved and undissolved lead compounds (Pb, PbO, PbO_2, $PbSO_4$) and also dilute sulfuric acid. Nickel/cadmium batteries result in dissolved and undissolved nickel and cadmium as well as dilute caustic potassium and sodium hydroxide in the water.

The metal working industry includes a broad range of manufacturing and process industries. Some are listed below:

- machine and apparatus manufacturing
- steel and light metal construction
- railway industry and ship building

- building of aircraft and spacecraft
- electronics industry
- hardware, tin ware and metal products industry

The following processes are employed in the metal-working industry:

- mechanical metal finishing with aqueous media
- thermal (heat) treatment
- surface polishing processes using chemical and electrochemical methods
- surface pretreatment preceding enameling
- surface pretreatment preceding hot galvanizing

The waste waters with predominantly inorganic content include:

- concentrates
- exhausted long-lasting process baths (electrolytes)
- exhausted short-lasting process baths (pickles)
- concentrated rinse waters (e.g. from batch or cascading rinsing baths)
- waste waters from the exhaust air pollution control operations

Cadmium, nickel and zinc plating baths along with chromium and silver are most common. Aircraft parts have to be plated with cadmium for safety reasons. More and more car manufacturers are galvanizing vehicles to provide corrosion free guarantees of up to 10 years or more.

From the processes considered above, four metals; copper, cadmium, nickel and zinc have been selected as target metals for biosorption studies. In addition to synthetic single metal and multi-metal solutions, the most promising biosorbents were tested against real plating rinse waters arising from the metal-plating industry and compared with the performance of conventional ion exchangers designed for this specific application.

Section 1.7. Conclusions

Bacteria, fungi and algae possess significant metal accumulating properties which are assuming increasing importance due to problems arising from the levels of toxic metals in the environment. Bacteria have been found to possess significant capacity for biosorption of many elements or, alternatively, depending upon the species they may be element specific. In the future, it is likely that microorganisms will be tailored for a specific element or groups of elements by employing recombinant DNA technology. An organism tailored for fine-scale discrimination between elements, e.g. tantalum and niobium will find many areas of application in hydrometallurgy and other industrial processes. Other applications, such as the bulk treatment of metallic ores, *in situ* biological mining, mineral prospecting and the control of biosorption are all likely to experience revolutionary progress from future applications of biotechnology.

Filamentous fungi and yeasts have shown favorable metal ion-binding, however, most literature has considered the effects of metals on the metabolically active cultures of fungi, whereas reports analyzing the passive biosorption behavior of fungal biomass systems are relatively limited. A significant effort was focused on the common yeast *S. cerevisiae*, even though its metal biosorbent properties are not very impressive. Recently, the genus *Rhizopus* particularly *R. arrhizus* and *R. javanicus* have shown good metal binding properties and increased our current understanding of the metal biosorption phenomenon.

The availability of large quantities of biomass serving as a basis for formulation of suitable biosorbent products is essential for industrial exploitation. Fungal cultures currently employed in large-scale fermentation processes should be examined for their biosorbent capabilities.

Certain algal varieties possess high affinity for heavy metals. This property expressed as the "sorbent sorption capacity" may be employed in concentrating metals from

dilute solutions arising from industrial processes such as tailings, plating effluents, radioactive waste waters etc.

Differences in growth media produce different algal structures and different functional binding groups in terms of the relative amounts of various polysaccharides constituting the algal cellular matrix. These in turn influence the affinity of metal ions to the non-living algal biomass and this is eventually reflected in the amount of metal sorbed.

The rate of metal removal depends on the algal species as well as the metal ions to be removed. Sufficient exposure time needs to be allowed in order to achieve maximum metal removal by the biomass. In-active (dead cells) algae possess significantly higher metal sorption capacity than live algal culture. In the absence of active mass (ion) transport by the algal cell, the chemical structure of dead biomass is obviously responsible for metal ion removal. Competition between metal ions for metal binding sites on biosorbents makes the treatment of real waste solutions complicated and challenging.

Section 1.8. References

1. Volesky, B. 1990, Biosorption of heavy metals, CRC Press, Inc., Boca Raton, Florida.
2. Beveridge, T.J. and Murray, R.G.E. 1976, J. Bacteriol., vol. 127, 1502.
3. Labischinski, H., Barnickel, G., Naumann, D. and Keller, P. 1985, Ann. Inst. Pasteur Microbiol., 136A, 45.
4. Hancock, R.E.M. 1984, Annu. Rev. Microbiol., vol. 38, 237.
5. Kandler, D. and Konig, H. 1985, The bacteria, 8, Woese, C.R. and Wolfe, R.S., (eds.) Academic Press, NewYork.
6. Konig, H. 1988, Can. J. Microbiol., vol. 34, 407.
7. Ferris, F.G. and Beveridge, T.J. 1985, BioScience, vol. 35, 172.
8. Beveridge, T.J. and Fyfe, W.S. 1985, Can. J. Earth Sci., vol. 22, 1893.
9. Hoyle, B. and Beveridge, T.J. 1983, Appl. Environ. Microbiol., vol. 46, 749.
10. Beveridge, T.J. 1986, Biotech. Bioeng. Symp., vol. 16, 127.
11. Ehrlich, H.L. and Brierley, C.L., (eds.). 1990, In Environmental Biotechnology Series: Microbial Mineral Recovery, , McGraw-Hill Publishing Co., NewYork.
12. Churchill, S.A., Walters, J.V. and Churchill, P.F. 1995, J. Environ. Eng., vol. 121, no. 10, 706.
13. Hu, M.Z.L., Norman, J.M., Faison, B.D. and Reeves, M.E. 1996, Biotech. Bioeng., vol. 51, no. 2, 237.
14. Beveridge, T.J. and Koval, S.F. 1981, Appl. Environ. Microbiol., vol. 42, 325.
15. Rudd, T., Sterritt, R.M. and Lester, J.N. 1984, Wat. Res., vol. 18, 379.
16. Strandbery, G.W., Shumate, S.E. and Parrott, J.R. Jr. 1981, Appl. Environ. Microbiol., vol. 41, 237.
17. Reiskind, J.B. and Mullins, J.T. 1981, Can. J. Microbiol., vol. 27, 110.
18. Kihn, J.C., Masy, C.L and Mestdagh, M.M. 1988, Can. J. Microbiol., vol. 34, 773.
19. Bartnicki-Garcia, S. 1970, Phytochemical Phylogeny, Harborn, J.B., (ed.), Academic Press, New York.
20. Anderson, P. 1986, In proc. interim symp. on metal speciation, sparation and recovery, Illinois Institute of Technology and Italian National Research Council, Chicago, IL.
21. Siegel, S.M., Gahun, M. and Siegel, B.Z. 1990, Wat. Air and Soil Poll., vol. 53, 335.
22. Fourest, E., Serre, A. and Roux, J.C. 1996, Toxicol. Environ. Chem. vol. 54, no. 1-4, 1.
23. Brady, J.M. and Tobin, J.M. 1994, Enzyme and Microbial Tech., vol. 16, no. 8, 671.
24. Subudhi, E. and Kar, R.N. 1996, Int. J. Environ. Studies A&B, vol. 50, no. 2, 111.
25. McReady, R.C.L. and Lakshmanan, V.I. 1986, In immobilisation of ions by biosorption, Eccles, H. and Hunt, S. (eds.), Ellis Harwood, Chichester, UK.
26. Tobin, J.M., Cooper, D.G. and Neufield, R.J. 1988, Biotech. Bioeng., vol. 31, 282.
27. Tsezos, M. 1985, Can. Metall. Quart., vol. 24, 141.

28. Fogarty, R.V. and Tobin, J.M. 1996, Enzyme and Microbial Tech., vol. 19, no. 4, 311.
29. Niu, H., Xu, X.S. and Wang, J.H. 1993, Biotech. Bioeng., vol. 42, no. 6, 785.
30. Patterson, J.W. and Passino, R. (eds.). 1987, Fungal Biosorption, Lewis Publishers, Inc., Chelsea, MI.
31. Muraleedharan, T.R. and Venkobachar, C. 1990, Biotech. Bioeng., vol. 35, 320.
32. Muraleedharan, T.R., Venkobachar, C. and Leela, L. 1994, Sep. Sci. Tech., vol. 29, no.14, 1893.
33. Lewin, R.A. 1962, Physiology and biochemistry of algae, Acadmeic Press, New York.
34. Baardseth, E. 1966, Proc. 5th Int. Seaweed Symp., 19.
35. McCully, M.E., 1966, Protoplasma, vol. 42, 287.
36. Percival, E. and McDowell, R.H. 1967, Chemistry and enzymology of marine algal polysaccharides, Academic Press, London and New York.
37. Black, W.A.P. 1954, J. Mar. Biol. Ass., U.K., vol. 33, 49.
38. Haug, A. and Smidsrod, O. 1965, Acta. Chem. Scand., vol. 19, 1221.
39. Dillon, T. 1964, Proc. 4th int. Seaweed Symp., Biarritz, deViville, A.D., and Feldman, J. (eds.), Pergamon Press, London and NewYork.
40. Barr, V.C. 1939, Sci. Proc. R. Dubl. Soc., vol. 22, 59.
41. Black, W.A.P. 1950, J. Marine Biol. Ass. UK, vol. 29, 379
42. Commercial literature. 1987, Alginate products for scientific water control, Kelco NutraSweet Co., 3rd. edition.
43. Hirst, E.L., Jones, J.K.N. and Jones, W.O. 1939, Part 1, J. Chem. Soc. 1880.
44. Fischer, F.G. and Dorfel, H. 1955, Part 1, Z. Physiol. Chem. vol. 302, 186.
45. Vincent, D.L. 1960, Chem. Ind. 1109.
46. Hirst, E.L., Percival, E. and Wold, J.K. 1964, J. Chem. Soc., 1493.
47. Haug, A., Larsen, B. and Smidsrod, O. 1966, Acta. Chem. Scand., vol. 20, 183.
48. Haug, A., Larsen, B. and Smidsrod, O. 1967, Acta. Chem. Scand., vol. 21, 691.
49. Haug, A., Myklestad, S., Larsen, B. and Smidsrod, O. 1967, Acta. Chem. Scand., vol. 21, 768.
50. Penman, A. and Sanderson, G.R. 1972, Carbohyd. Res., vol. 25, 273.
51. Atkins, E.D.T., Mackie, W. and Smolko, E.E. 1970, Nature, vol. 225, 626.
52. Atkins, E.D.T., Mackie, W., Parker, W.D. and Smolko, E.E. 1971, J. Polymer Sci., vol. 9, 311.
53. Morris, E.R., Rees, D.A. and Thom, D. 1973, J.Chem.Soc., Chem. Comm., 245.
54. Grant, G.T., Morris, E.R., Rees, D.A., Smith, P.J.C. and Thom, D. 1973, Febs Letters, vol. 32, 195.
55. Larsen, B. and Haug, A. 1963, Acta. Chem. Scand., vol. 17, 1646.
56. Dodge, J.D. 1973, The fine structure of algal cells, Academic Press, New York.
57. Khummongkol, D., Canterford, G.S. and Fryer, C. 1982, Biotech. Bioeng., vol. 24, 2643.
58. Crist, R.H., Oberholser, K., Shank, N. and Nguyen, M. 1981, Environ. Sci. Tech., vol. 15, 1212.
59. Passow, H., Rothstein, A. and Clarkson, T.W. 1961, Pharm. Rev., vol. 13, 185.
60. Crist, R.H., Martin, J.R., Guptill, P.W., Eslinger, J.M. and Crist, D.R. 1990, Environ. Sci. Tech., vol. 24, 337.
61. Hassall, K.A. 1963, Physiol. Plant., vol. 16, 323.

62. McKnight, D.M. and Morel, F.M.M. 1979, Limnol. Ocean., vol. 24, 823.
63. Cloutier-Martha, L. and Brown, D.A. 1980, Botanica Marina, vol. 23, 53.
64. Kaplan, D., Christiaen, D. and Arad, S.M. 1987, Appl. Environ. Microb., vol. 53, no. 12, 2953.
65. Matheickal, J.T., Yu, Q. and Feltham, J. 1996, Environ. Technol., vol. 18, 25.
66. Schulz-Blades, M. and Lewin, R.A. 1976, Biol. Bull., vol. 150, 118.
67. Foster, P. 1976, Environ. Poll., vol. 10, 45.
68. Leusch, A., Holan, Z.R. and Volesky, B. 1995, J. Chem. Tech. Biotechnol., vol. 62, 279.
69. Mattuschka, B., Junghaus, K. and Straube, G. 1993, In Biohydrometallurgical technologies, Torma, A.E., Apel, M.L., Brierley, C.L., (eds.), The Minerals, Metals & Materials Society, Warrendale, PA, vol. 2.
70. Holan, Z.R., Volesky, B. and Prasetyo, I. 1993, Biotech. Bioeng., vol. 41, 819.
71. Norris, P.R. and Kelly, D.P.(eds.). 1988, In Biohydrometallurgy: Proceedings of the International Symposium, Sci. Technol. Lett., Kew, Surrey, UK.
72. Volesky, B. and Kuyucak, N. 1988, Biosorbents for Gold, US Patent 4-769,233.
73. Holan, Z.R. and Volesky, B. 1994, Biotech. Bioeng., vol. 43, 1001.
74. Kratochvil, D., Pimentel, P.F. and Volesky, B. 1998, Environ. Sci. Tech. vol. 32, no. 18, 2693.
75. Kuyucak, N. and Volesky, B. 1989, Biotech. Bioeng., vol. 33, 809.
76. Polikarpov, G.G. 1966, Radioecology of aquatic organisms, Reinhold Publishers, New York.
77. Zirino, A. and Yamamoto, S. 1972, Limnol. Ocean., vol. 17, 661.
78. Jackson, A.G. and Morgen, J.J. 1977, Limnol. Ocean., vol. 23, 268.
79. Chipman, W.A., Rice, T.R. and Price, T.J. 1958, U.S. Fish and Wildlife Service Fish. Bull., vol. 58, 279.
80. Defilippis, L.F. and Pallaghy, C.K. 1976, Z. Pflanzenphysiol. Bd., vol. 79, 323.
81. Coleman, R.D., Coleman, R.L. and Rice, E.L. 1971, Bot. Gaz., vol. 132, 102.
82. Hannan, P.J. and Patouillet, C. 1972, Biotech. Bioeng., vol. 14, 93.
83. Glooschenco, W.A. 1969, J. Phycol., vol. 5, 224.
84. Sick, L.V. 1979, Limnol. Ocean., vol. 24, 453.
85. Kagi, J.H. and Vallee, B.L. 1961, J. Biol. Chem., vol. 236, 2435.
86. Hart, B.A. and Bertram, P.E. 1979, Environ. Poll., vol. 14, 401.
87. Aldor, I., Fourest, E. and Volesky, B. 1995, Can. J. Chem. Eng., vol. 73, 516.
88. Bryan, G.W. 1971, Proc. Roy. Soc. Lond., vol. 177, 389.
89. Chapman, A.R.O. 1978, Phaeophyta, In CRC handbook of microbiology, vol. 2, 2nd edition, Laskin, A.I. and Lechevalier, H.A. (eds.), CRC Press, Boca Raton, Fl.
90. Solman, P. 1999, Commodities section, Financial Times, 12 February issue.
91. Kuyucak, N. and Volesky, B. 1989, Biotech. Bioeng. vol. 33, 815.
92. Kuyucak, N. and Volesky, B. 1989, Biotech. Bioeng. vol. 33, 823.
93. Ferguson, J. F. and Gavis, J. 1972, Water Res., vol. 6, no. 9, 989.
94. Hassett, J. M., Jennett, J. C. and Smith, J. E. 1979, Control of heavy metals in the environment using algae, in Management and Control of Heavy Metal Environments, Int. Conf., CEP Consultants Ltd., Edinburgh, Scotland, 210.
95. Kuyucak, N. and Volesky, B. 1989, Water Pollut. Res. J. Can., CAWPRC, 23, 425.

96. Horikoshi, T., Nakajima, A. and Sakaguchi, T. 1981, Eur. J. Appl. Microbiol. Biotechnol., vol. 12, 76.
97. Greene, B., Henzl, M. T., Hosea, J. M. and Darnall, D. W. 1986, Biotechnol. Bioeng., vol. 28, 764.
98. Horikoshi, T., Nakajima, A. and Sakaguchi, T. 1979, J. Ferment. Technol., vol. 57, 191.
99. Treen-Sears, M. E., Volesky, B. and Neufeld, R.J. 1984, Biotechnol. Bioeng., vol. 26, 1323.
100. Tsezos, M. and Volesky, B. 1982, Biotechnol. Bioeng., vol. 24, 385.
101. Tsezos, M. and Volesky, B. 1982, Biotechnol. Bioeng., vol. 24, 955.
102. Wong, K. M., Hodge, V. F. and Folsum, T. R. 1972, Nature (London), vol. 237, 460.
103. Hodge, V. F., Hoffman, F. L. and Folsum, T. R. 1974, Health Phys., vol. 27, no. 1, 29.
104. Spies, R. B., Marsh, K. V. and Kercher, J. R. 1981, Limnol. Oceanogr., 27(1), 29.
105. Rice, T. R. 1956, Limnol. Oceanogr., vol. 2, 123.
106. Kalin, M. N. 1985, The Chara Process, Contract No. 148Q.28440-4-9185, OSQ84-00260 for CANMET, Dept. of energy, mines and resources, Ottawa, Canada.
107. Zumberge, J. E., Sigleo, A. C. and Nagy, B. 1978, Miner. Sci. Eng., vol. 10, 223.
108. Hallbauer, D. K. 1975, Miner. Sci. Eng., vol. 7, 111.
109. Kuyucak, N. and Volesky, B. 1989, Biorecovery, vol. 1, 189.
110. Greene, B., Hosea, M., McPherson, R., Henzl, M., Alexander, M. D. and Darnall, D. W. 1986, Environ. Sci. Technol., vol. 20, no. 6, 627.
111. Darnall, D. W., Greene, B. and Gardea-Torresday, J. 1987, Biohydrometallurgy symp., Norris, P. R. and Kelly, D. P. (eds.), Warwick, England.
112. Kuyucak, N. and Volesky, B. 1989, Biorecovery, vol. 1, 219.
113. Kuyucak, N. and Volesky, B. 1989, Water Pollut. Res. J. Can., CAWPRC, vol. 23, 425.
114. Pawson, D., Bangert, N., Williams, C. J. and Edyvean, R. G. J. 1997, The 1997 Jubilee Research event, Nottingham, 8-9 April 1997, IChemE, 145.
115. McDowell, R. H. 1986, Properties of alginates, Commercial literature, Kelco International.

Characterisation of Algal Biosorbents

"Concepts without factual content are empty; sense data without concepts are blind....The understanding cannot see. The senses cannot think. By their union only can knowledge be produced"

(Immanuel Kant 1724-1804)

Chapter 2

Characterisation of Algal Biosorbents

This chapter discusses techniques employed for the characterisation and quantification of surface functional groups found in brown marine algae that are responsible for metal sorption from near neutral aqueous solutions. Physical characterisation of algal particles was performed using Nitrogen Sorption Porosimetry, Scanning Electron Microscopy and Fourier Transform Infra-Red Spectroscopy. Chemical characterisation methods employed were classical potentiometric titrations as well as esterification procedures.

Section 2.1. Theory and Literature Review

Potentiometric titrations and quantification of alginate

The cellular make-up of marine algae is not easy to characterise. The isolation of individual polysaccharides and the elucidation of their structure may be attributed to the efforts of many researchers[1]. The amount of each polysaccharide varies from species to species and even within the same variety due to seasonal variations. Differential extraction is often employed to separate components in different fractions. The ease of extraction depends on the location of the materials in the plant and also on their chemical nature. The different types of polysaccharides found in brown marine algae have already been discussed in chapter 1. In this chapter, techniques employed for the characterisation of algal functional groups that may be responsible for metal ion sorption will be discussed.

Traditionally, surface functional groups which are commonly found in cationic exchangers such as carboxylate, sulphonate, hydroxyl etc., have been quantified using potentiometric titrations. The reader is referred to the excellent treatise on this subject by Helfferich[2]. Fourest and Volesky[3] carried out potentiometric and conductometric titrations of native and modified *Sargassum fluitans* biomass as well as alginic acid

derived from algae. They were able to quantify the amount of weakly acidic surface functional groups in *S. fluitans* which are responsible for cadmium and lead sorption. Alginic acid was found to leach out of the algal particles during the course of the titration which resulted in an increase in the measured conductivity of the solution. The technique was unable to distinguish between strong and weak acid groups due to the small quantity of strong acid functional groups present within the biomass. The apparent dissociation constants, pK_a, were determined from the experimental titration curves; alginic acid ($pK_a = 4$) and *S. fluitans* ($pK_a = 5.2$). The effect of ionic strength on titrations of protonated *Sargassum* seaweed and of alginate was investigated in another study[4]. A combined potentiometric titration/electrophoretic mobility measurement of *Sargassum* showed that the biomass particles bear a significant negative charge[5] in the relative absence of protons or covalently bound divalent metal ions. The apparent proton-binding constant was found to change drastically with ionic strength; decreasing from 5 to 3 at high ionic strength, indicating a change in the value of the dissociation constants by a factor of 100. The reason for the change in dissociation constant values was attributed to electrostatic effects; the local proton concentration at the solid-solution interface is higher than the bulk concentration. Consequently reduced electrostatic effects at high ionic strength allows the apparent proton-binding constant value to approach the intrinsic proton-binding constant value. The pK_a values for alginate were found to be generally lower than for *Sargassum*. Also, electrostatic effects were less apparent in the case of alginates. Seki and Suzuki[6] determined the acid-dissociation characteristics of acidic sites in brown algae *Macrocystis pyreifera*, *Kjellmaniella crassiforia* and *Undaria pinnatifida*. The acid-dissociation constants of the three brown algae were almost the same; *Macrocystis pyrifera*: 3.19, *Kjellmaniella crassiforia*: 3.14 and *Undaria pinnatifida*: 3.2. The weakly-acidic properties of brown algae were attributed to carboxyl groups in alginic acid since the acid-dissociation constant values for brown algae were almost identical to the acid-dissociation constant values obtained for alginic acid (3.21). The influence of ionic strength on potentiometric titration curves of algae was not taken into account in this study[6].

Schiewer[4] found that the apparent pK_a approached the intrinsic pK_a value at high ionic strength values (100 mM or higher) for *Sargassum natans*. The proposed Donnan model that accounted for ionic strength effects was based on the premise that the sorbent particles behave essentially as mono-functional exchangers with carboxyl groups the predominant surface acidic groups between pH 2-6. Other functional groups such as 'phenolic-type', do not play a role in acid-base reactions since they are protonated and hence inactive between pH 2-6. A much simpler model proposed by Seki and Suzuki[6] may be used to fit potentiometric titration data and extract acid-dissociation constants of the acidic sites on brown algae between pH 2-6. Assuming that the major acidic sites on brown algae are the carboxyl groups associated with alginic acid, the acid-dissociation reaction can be written as:

$$B\text{-}COOH \leftrightarrow B\text{-}COO^- + H^+ \qquad (1)$$

The acid-dissociation constant K is defined as:

$$K = \frac{\alpha[H^+]}{1-\alpha} \qquad (2)$$

where α is the degree of dissociation of carboxyl groups. The number of deprotonated carboxylic groups on brown algae (dry wt. basis, g), X_o, can be expressed as:

$$X_o = N\alpha = \frac{NK}{K+[H^+]} \qquad (3)$$

where, N represents the number of carboxyl groups on brown algae. Equation (3) may be fitted to potentiometric data (deprotonated acidic groups, mmol g^{-1} vs. equilibrium pH) to extract values for the two unknown parameters, N and K.

The principal structural polysaccharide of brown algae, alginic acid, solubilises as sodium alginate during potentiometric titrations with alkali. A good review of

analytical methods to determine the alginate content of extracted liquors is provided by Percival and McDowell[1]. Most of the techniques encounter the problem of isolating a relatively pure alginate sample without degradation or interference from other materials. It is usual to precipitate the alginate as alginic acid by treatment with dilute acid. The extracted alginic acid is redissolved, followed by reprecipitation in alcohol in order to remove impurities that may coprecipitate. This frees the alginate from colouring matter. Acid or calcium precipitation is more effective in removing the protein and any fucoidan originally present in the extract. The precipitated alginic acid may be titrated with standard carbonate free sodium hydroxide. Problems due to formation of viscous sodium alginate solutions which prolong the time required for titration may be overcome by adding calcium acetate. The acetic acid liberated can then be titrated in the usual way.

The method discussed above works well when there is a substantial amount of alginic acid in solution. However, during potentiometric titrations of algae, relatively small amounts of sodium alginate may leach out into the supernatant liquors. In this instance, titration as discussed above may not be the best technique for alginic acid quantification and detection. Other methods such as carbazole in concentrated sulphuric acid provide a colorimetric method for algin quantification[7]. Gregory[8] reported a greatly enhanced absorption by glucuronic and iduronic acids with sodium tetraborate in sulphuric acid. Brown and Hayes[9] found orcinol in hydrochloric acid (Bial's reagent) successful in quantifying algin in solution. Absorption could be increased by addition of borate. Naptho-resorcinol adapted from the original method by Tollens[10] is another useful means of identifying alginic acid in solution. The values obtained by these methods depend to some extent on thc properties of the uronic acids present in the alginic acid. None of the tests is entirely specific. Another method involves decomposing the alginic acid into furfural and carbon dioxide when alginic acid is heated with hydrochloric acid under carefully controlled conditions. The amount of carbon dioxide evolved can be used as a measure of the alginate[11]. The technique still depends on the doubtful assumption that alginic acid is the only uronide present.

Many of the reagents employed for alginate determination react in an identical manner with impurities present after alginic acid extraction. Others do not show an identical response towards both D-mannuronic and L-guluronic acid[12,13]. Recently however, Kennedy and Bradshaw[14,15] reported that poly[hexamethylene biguanidinium chloride] can be employed for the rapid quantitative determination of alginates. The organic cation [$PHMBH^+Cl^-$; see Fig. 2.1.] complexes the alginate in solution and produces a white precipitate. The residual amount of organic cation unprecipitated following addition of a known excess of $PHMBH^+Cl^-$ is determined quantitatively by measuring UV absorption at 235nm. This wavelength was found to be characteristic of the absorption by $PHMBH^+Cl^-$.

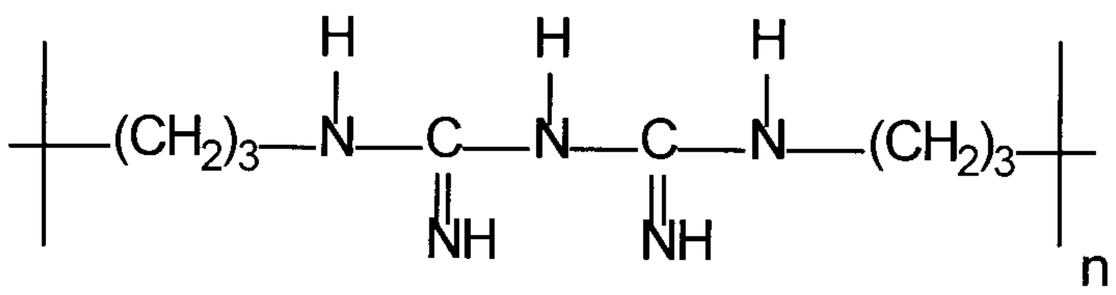

where n=12

Figure 2.1. Structure of poly(hexamethylene biguanidinium chloride).

The PHMBHCl-assay technique has several distinct advantages over the other methods mentioned above for alginate detection and quantification. The detection method is rapid, reproducible and has been shown to be insensitive to salt concentration and, within defined limits, to pH and temperature. The working range of the assay can be altered by simply adjusting the excess quantity of $PHMBH^+Cl^-$ added during the precipitation stage. Protein present in the cellular material of the brown seaweed as well as fucoidan may interfere with the quantitative determination of alginates in liquor samples. Kennedy et al[16]. showed that as the pH was below the isoelectric point for proteins there was little interference from protein precipitation at or below pH 7.

The presence of varying amounts of Ca^{2+} on the response of sodium alginate to $PHMBH^+Cl^-$-assay was investigated[15]. As Ca^{2+} ions show a higher affinity for

carboxylic acid groups in comparison with Na^+, variation of the alginate- $PHMBH^+Cl^-$ precipitate might occur giving rise to interference. Kennedy and Bradshaw et al.[15] added known amounts of Ca^{2+} to sodium alginate solutions to observe deviation in UV absorbance values. They concluded that low levels of Ca^{2+} (up to 1% w/w; weight basis relative to sodium alginate) did not cause interference to the $PHMBH^+Cl^-$ assay. However, if the Ca^{2+} is present in sufficient quantity to cause gelling of alginates, then this would interfere with the precipitation stage of the assay procedure.

Zeta potential measurement

Zeta potential measurement is based on the principle of determining the mobility or electrokinetic velocity of particles as they move through an electric field. The potentiometric titration method of Bernde et al.[17], Yates and Thomas[18], Cornell et al.[19], Bowden et al[20] and Marabini and Barbaro[21] was used to study the surface charge present on biosorbent particles in aqueous solution,. The method relates to the protonation or deprotonation of surface functional groups on carbons, but the technique easily lends itself for the study of biosorbent particles. Acidic groups such as carboxyl or hydroxyl may be protonated/deprotonated by reactions similar to those depicted below:

$$BH_{Surface} + OH^- \leftrightarrow B^-_{Surface} + H_2O \qquad (4)$$

$$BH_{Surface} + H_3O^+ \leftrightarrow BH^+_{2\,Surface} + H_2O \qquad (5)$$

where $BH_{Surface}$ represents the functional groups on the biosorbent surface. Titrations carried out at high ionic strengths result in a lower potential in the diffuse layer σ_d (the point of zero charge (pzc) naturally is not affected)[22]. At this point, the charge on the biosorbent surface (σ_o) is neutral (i.e. zero). The quantities of H^+ taken up or removed from the biosorbent surface are represented as a function of solution pH at different ionic strengths. These curves theoretically cross at the point of zero charge where $\sigma_o = \sigma_d = 0$. In theory, the charge on the surface can be computed for all values of pH (other than the pH at the point of zero charge) by the equation:

$$\sigma_o = F\left[\Gamma_{H^+} - \Gamma_{OH^-}\right] (\text{C m}^{-2}) \qquad (6)$$

At high ionic strength, the electric double layer is compressed[23,24].

Alkalimetric titration is a process involving the transfer of H^+ or OH^- ions between the bulk phase and the surface (both the internal and external surface) of the biosorbent particles; whereas electrophoretic mobility measurements detect the potential at the shear plane which is adjacent to the external surface. The pH at which the electrophoretic mobility of a particle is zero is defined as the isoelectric point (iep).

The surface concentration of protons is not directly measurable; it may be calculated from pH measurement in the bulk phase, i.e., $\left[H^+\right]_b$ by the Boltzmann equation:

$$\left\{H^+\right\} = \left[H^+\right]_b \exp\left(\frac{-F\psi_o}{RT}\right) \qquad (7)$$

The surface potential (ψ_o) is not a directly measured quantity. In a dilute inert electrolyte solution, the surface potential is close to the potential at the outer Helmoltz plane (OHP), or the diffuse layer potential, (ψ_d). Since H^+ and OH^- are considered the sole potential determining ions (indicated by the change of electrophoretic mobility at different pH values) therefore, in the absence of specific adsorption (such as in a dilute electrolyte solution), the surface charge σ_o, obtained from alkalimetric titration can be set equal to the charge in the diffuse layer σ_d[25]. The surface potential can therefore be calculated by Guoy-Chapman electrical double layer theory:

$$\psi_o \approx \psi_d \approx 2\frac{RT}{|z|F}\sinh^{-1}\left[\sqrt{\frac{\pi}{2RT\varepsilon I}}\right]\sigma_d \qquad (8)$$

When the pH<pH_{iep}, the surface is predominantly positively charged and when pH> pH_{iep}, the surface is negatively charged. Interestingly, there is some controversy in

literature regarding the difference between the point of zero charge and the isoelectric point.

Recently, Sposito[26] discussed the generic properties of surface charge which relate to certain macroscopic conditions imposed by electroneutrality and thermodynamic stability. The generic properties refer to the behaviour that derives solely from the existence of conservation laws and from the conditions of chemical stability, irrespective of any molecular mechanism used to describe adsorption.

Sposito[26] accounts for the surface charge as three discrete contributions due to structural substitutions (σ_o), adsorbed protons (σ_H) and finally due to adsorption of ions (other than H^+ and OH^-) due to reactions at the surface of the particle (Δq). An overall charge balance is written as:

$$\sigma_o + \sigma_H + \Delta q = 0 \qquad (9)$$

Plotting surface charge data Δq vs. σ_H (Chorover plot) was recommended to verify that the data are consistent with the surface charge balance equation (should lie on a straight line).

$$\Delta q = \sigma_S + \sigma_d \qquad (10)$$

Points of zero charge have been traditionally defined as pH values for which one of the categories of surface charge is equal to zero (see Table 2.1.).

IUPAC symbol	**name**	**definition**
pznpc	point of zero net proton charge	$\sigma_H=0$
pznc	point of zero net charge	$\sigma_{in}=0$
pzc	point of zero charge	$\sigma_p=0$

Table 2.1. Conventional points of zero charge[26].

where:

$$\sigma_{in} \equiv \sigma_o + \sigma_H \qquad (11)$$

$$\sigma_p \equiv \sigma_{in} + \sigma_S \qquad (12)$$

and σ_S denotes the Stern layer surface charge[27] representing all adsorbed ions not in the diffuse ion swarm. This latter conceptual distinction based largely on adsorbed ion mobility, is epitomised by defining the total particle charge, σ_p which is the net surface charge contributed by the adsorbent structure and by adsorbed ions that are immobilised in surface complexes (i.e. adsorbed ions that do not engage in translational motions relative to the adsorbent that may be likened to the diffusive motions of a free ion in aqueous solution).

Sposito[26] argued that pznpc values based on the use of potentiometric measurements to determine σ_H yield only changes in σ_H relative to the net proton surface charge at the beginning of a titration experiment. An additional independent measurement is needed to establish the true value of σ_H. Unfortunately, this renormalisation of σ_H obtained from titration cannot be done unambiguously by the common device of choosing $\sigma_H \equiv 0$ at the crossover point of two (or more) apparent σ_H vs pH curves that have been determined at different ionic strengths. Each such apparent σ_H curve is, in principle offset from the true σ_H curve by a different amount that corresponds to the particular initial state of the titrated system, thus making even the crossover point illusory.

The pznc (σ_{in}) is the pH value at which the intrinsic surface charge is equal to zero while the pzc ($\sigma_p=0$) is the pH value at which the net total particle charge is equal to zero. The term Δq may be written in terms of net charge of ion adsorbed in inner-sphere surface complexes (IS), in outer-sphere surface complexes (OS), or in the diffuse ion swarm (d). The net charge of ions adsorbed in inner-sphere and outer-sphere surface complexes may be combined and represented as σ_s. At the pzc, there is

no surface charge to be neutralised by ions in the diffuse swarm, and any adsorbed ions that exist are bound in surface complexes. Therefore, pzc can be measured by ascertaining the pH value at which a perfect charge balance exists among the ions in the aqueous solution and those within the particle. The pzc is inferred from the pH value at which suspension flocculates rapidly or when the particle electrophoretic mobility vanishes (commonly known as the iep). Equality between iep and pzc however, is problematic because it requires demonstrating experimentally, that none of the ions in the diffuse layer will be transported with the particle (by adhering to it) as it moves steadily in response to a uniform constant electric field.

In this thesis, the iep is taken as the pH value at which the measured zeta-potential value is zero[28,24]. The pzc however, is taken to be the pH value where no Na^+ uptake occurs within or on the biosorbent particle (obtained from potentiometric titration) or where the zeta-potential vs pH curves (calculated at two or more ionic strengths) crossover.

Chemical modification of metal-binding sites

A better understanding of the chemical nature of the metal-binding process in biomass is imperative in order to use algal biomass effectively in water purification and metal reclamation. It is necessary to identify the chemical functional groups on the algal cell wall that are responsible for binding different metal ions. One approach is the chemical modification of the metal-binding functional groups on the algal surface. As an example, consider the hypothesis that binding of copper(II) occurs through interaction with carboxyl groups. The contribution of these groups for metal sorption may be better understood by carrying out chemical modification specific for carboxyl groups in order to mask their availability for subsequent metal complexation. Conversion of free carboxyl groups to the corresponding methyl esters is one possible modification. The carboxyl oxygen atoms of esters are known to coordinate metal ions, however, the interaction is weak in comparison with carboxylate ions. Two common methods of esterifying carboxyl groups make use of water-soluble carbodiimides and esterification via acidic-methanol[29]. The technique employing water soluble carbodiimides is advantageous because of its high degree of specificity

and mild conditions. Unfortunately, the high cost, both of reagents and equipment required to complete the modification and the fact that the method does not lend itself to easy monitoring of the degree of modification made it unsuitable for use in the current study. Esterification of carboxyl groups using acidic methanol is relatively inexpensive. Base hydrolysis of the modified sample allows analysis of the methanol released as the quantification step on extent of modification[30,31]. Carboxyl groups in alginic acid may be esterified by reaction with 1,2-alkylene oxides under mild conditions causing little degradation[32]. The primary hydroxyl group of propylene glycol is likely to be the one involved in esterification. A possible structure of groups in the polymer chain is depicted in Figure 2.2.

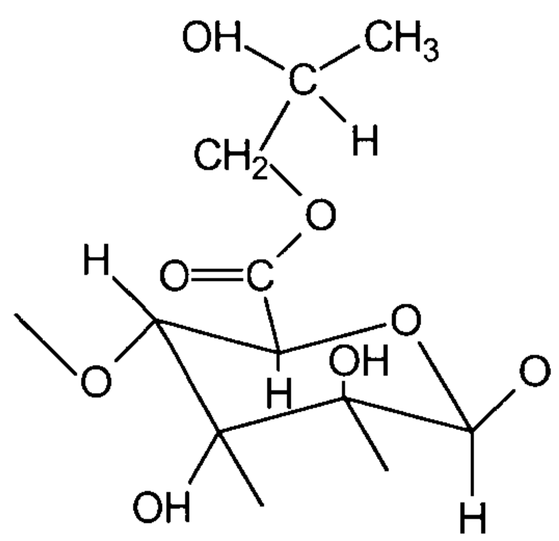

Figure 2.2. Propylene glycol alginate.

Propylene glycol ester is prepared by reacting moist alginic acid with propylene oxide. Up to 90% of the carboxyl groups can be esterified depending on the reaction conditions. Propylene glycol alginates are not easily precipitated by acids and can be used to thicken and stabilise acidic products. The extent to which acids can be tolerated depends mainly on the degree of esterification. A product with about 85% of the acid groups esterified can be used to thicken strong acids temporarily without precipitation, however, storage under these conditions will lead to depolymerisation of the alginate[33]. Propylene glycol ester is water soluble, probably due to the way in which the substituent propylene glycol groups hinder the aggregation of the polymer chains, while fewer carboxyl groups are available for interaction with cations.

McDowell[33], Haug et al.[34] and Ragan et al.[35] identified and characterised condensed or hydrolysable polyphenols as reducing compounds present in brown algae in

significant amounts. Slabbert[36] indicated interaction of metal ions with these polyphenolic compounds. Extraction of these reducing compounds using acetone/water was employed by Fourest and Volesky[3], who reported no subsequent reduction in cadmium or lead uptake by the biosorbent *Sargassum fluitans*.

Surface area and pore-size distribution

Phaeophyceae have pores between most of the algal cells. Kuyucak[48] reported that the brown marine algae *Sargassum natans* has a very porous, sponge-like surface. Fagerberg[37] observed that the membrane surface areas in the blades of *S. natans* were up to 65% larger than in its stipe, this was also found for other species of Phaeophyceae. Kuyucak[48] recorded the surface area of *S. natans* by observing CO_2 adsorption on dry algal biomass. The results of the CO_2 adsorption method showed that the surface area of *S. natans* was quantitatively 473 $m^2\ g^{-1}$ which was reported as 3.5 times higher than the surface area of *A. nodosum* (no data as actually reported for this algal variety). Holan[38] reported that the difference in metal sorption performance of *F. vesiculosus* and *A. nodosum* was linked to the morphologically different architecture of their algal tissues. The thallus of the former consists of parenchymatous cells with apical meristems[39] instead of predominantly filamentous architecture of the latter. The parenchymatous cells in *F. vesiculosus* were responsible for the increased surface area available for metal sorption.

Diffuse reflectance infra-red spectroscopy

Kuyucak and Volesky[40] recorded spectra of native *A. nodosum* after cobalt sorption and following desorption of the metal using various eluants. Peaks which relate to (-C=C-) bond stretching at 1033cm^{-1} and -COOH stretching at 1650cm^{-1} were noted. The accumulation of cobalt by *A. nodosum* was associated with these stretching vibrations with the help of hydrogen bonding. In another study[41], characteristic vibration bands of virgin *A. nodosum* were found at 1624, 1419, 1261 and 1036cm^{-1}. The 1650-1620cm^{-1} band was related to the existence of the amide I band due to the combined effect of double bond stretching vibrations (mainly C=O stretching) and hydrogen bonding[42]. The IR-spectra of virgin and cobalt-exposed biomass samples showed changes in intensity of peaks at 1033cm^{-1} and 1650cm^{-1} which were

interpreted as changes in concentrations rather than structural changes. These spectral studies were carried out with unprotonated algal samples. Alkali and alkali-earth metal ions such as Na^+, K^+, Ca^{2+} and Mg^{2+} etc,. may still be present in the algal samples studied. Interaction of surface functional groups with the metal ions may give rise to shifts in characteristic vibration-peaks. IR-spectral studies should be performed with protonated native seaweed as well as alginic acid derived from its native precursor in order to compare characteristic peaks which may indicate the functional groups responsible for algal-metal interactions during metal biosorption.

Section 2.2. Experimental Parameters

Biological materials

The seaweed varieties used in this study belong to the botanical classification of *Phaeophyceae* (brown seaweeds). Native seaweed varieties of *Ascophyllum nodosum* (AN), *Lessonia flavicans* (LF), *Durvillea potatorum* (BK; also called Bull Kelp) and *Laminaria hyperborea* (LH) were supplied by the NutraSweet Kelco Company (now Monsanto plc), Girvan, Ayrshire, Scotland, UK. In addition, algin extracted samples of AN and LF were prepared (see procedure below) and were designated dealginate samples, DAN and DLF, respectively. Alginic acid samples extracted from AN and LF were obtained and were labeled AA-AN and AA-LF respectively. After processing in a laboratory blender, all samples were washed with 100 bed volumes (BV) of HCl (0.1 mol l^{-1}) at 10 BV h^{-1} and then rinsed extensively with deionised distilled water (DDW) until the pH of the solution leaving the wash column was greater than pH4. The purpose of the pre-treatment was to convert acidic groups of the polysaccharides in seaweed to the hydrogen form and also to wash out salts (sodium, potassium, magnesium and calcium) present. 5g of each sorbent was centrifuged at 3000 rev. min^{-1} (~1400g) for 10 minutes using a Baird & Tatlock Auto Bench Centrifuge Mark IV. A weighed sample of the centrifuged material was dried in an oven at 105°C until constant weight for moisture determination. Thermal drying may cause degradation of the cellular structure of the algae and may adversely affect metal sorption. It was therefore decided to compare freeze drying with thermal drying

for moisture removal. The freeze dried algal material was pre-wetted for a minimum of 30 minutes before use in any sorption experiments. Comparison of metal sorption data for freeze dried and thermal dried material (maximum drying temperature 50°C) gave similar results. However, thermal drying above 50°C did result in some reduction of subsequent metal sorption capacity by native algal biosorbents. Consequently, freeze-dried algal particles were used in all subsequent metal-sorption studies.

Following washing and protonation of algal particles, the materials were dry sieved to achieve the desired size fraction (300-355μm). These particles were then characterised to obtain several parameters; particle size distribution of swollen particles, dry bulk density (ρ_d), wet bulk density (ρ_S), swollen volume of particles (V_s) etc. The dry bulk density of algal particles was calculated by measuring the volume occupied by 1g of algal particles in a measuring cylinder. The measuring cylinder was tapped gently as the particles were added, in order to ensure uniform packing of the particles. Following measurement of the dry bulk density, the particles were swollen in DDW and left to equilibrate overnight. After 12h of equilibration with DDW, the excess water was removed and the wet bulk volume of the swollen algal particles was determined.

In order to determine the particle size of swollen algal particles in aqueous solution, 100 mg of algal particles (dry size range: 300-355μm) were left equilibrating overnight in 100 ml of DDW (pH4; adjusted using HCl). Particle size measurement was carried out employing laser diffraction particle size analysis on a "Malvern-S" instrument. The seaweed slurry was circulated through the analysis cell using an automatic "small volume sample dispersion unit" set at a stirrer speed of 1000 min^{-1}. Each sample measurement was obtained using 2000 sweeps at 2 ms. The measurement data was analysed using a "Malvern Instruments 3 OHD presentation model". In the absence of specific information on seaweed particles certain assumptions regarding refractive index (1.5) as well as absorption by seaweed particles (0.1) had to be introduced in the presentation model. However, since the particle size range measured was greater than 10μm, the significance of these

assumptions is not crucial for particle size measurement[43]. Residuals of less than 3% indicated a fairly good fit to measured data. Background measurement was made with blank samples to account for any contamination, electrical noise etc.

Extraction of algin

Algin extracted samples of *Ascophyllum nodosum* and *Lessonia flavicans* were prepared according to a method used to extract algin by Kelco NutraSweet (carried out by R&D department, Monsanto plc). In order to extract algin from AN, 500 ml DDW (70°C) containing 3 ml of $CaCl_2$ (20% wt/wt) was put into a 1l nominal capacity stainless steel beaker. The beaker was placed in a water bath maintained at 70°C (±1°C). 30g of sun dried algal particles were added into this solution. The slurry was hand-stirred occasionally over a 15 minute period using a polypropylene rod. The suspension was then allowed to stand for 15 minutes in order to settle the algal particles. 350 ml of the supernatant solution was decanted. 20 ml of 1.8%(v/v) formaldehyde solution was added into the remaining seaweed slurry. The slurry was hand-stirred for 1 minute and then left in the water bath for a further 30 minutes. The beaker was then removed from the water bath and made up to a final reactant mass of 600g by addition of hot DDW water (70°C). 5.5g of sodium carbonate and 5.5 ml of sodium hydroxide (10% w/v) was thoroughly mixed with the seaweed slurry, and the beaker replaced in the water bath. The slurry was stirred occasionally (approximately every half hour) over a period of 2.5h.

Algin extraction from *L. flavicans* was carried out under slightly different conditions. 23.5g of dry seaweed meal was added to 200 ml of tap water (80°C) in a 1l nominal capacity stainless steel beaker. The beaker was placed in a temperature controlled water bath (80°C ± 1°C). The algal slurry was hand-stirred for 15 minutes using a polypropylene rod. 10 ml of 1.8% (v/v) formaldehyde solution was added to the mixture which was hand-stirred for a further 1 minute. The mixture was allowed to react for a further 30 minutes after which time the beaker was removed from the water bath. Hot tap water (80°C) was added to the algal mixture to obtain a final reactant mass of 400g. 4.7g of sodium carbonate and 4.8 ml of 10% sodium hydroxide solution were added to the algal mixture, hand-stirred thoroughly and then the beaker

was replaced into the water bath. The slurry was stirred occasionally (every 30 minutes) over a period of 4h.

Dilution and separation step

Following extraction of algin from the seaweeds, cold tap water was added to the extract mix (4 parts water for each part of algal slurry) in order to aid dissolution of the alginate. Phase separation was achieved via solids sedimentation over an 18h period. The beaker was removed from the water bath and the extract slurry transferred to a 4l container containing a nominal amount of cold water. A final mass of 3 kg was attained by addition of cold tap water. The diluted extract was mechanically stirred for 15 minutes after which time, 8 ml of formaldehyde (40% v/v) solution was added to the system. After 2h, 30 ml of bentonite bulking solution was added to the weed extract slurry. The mixture was stirred for a further 2h 25 min and then 60 ml of Magnafloc R140 polyacrylamide settling agent was added. The stirrer speed was reduced to a minimum rate such that the solids were kept 'just suspended' in solution. The stirring was continued for a further 2 min. The stirrer was then removed and the dilute (algin extract/seaweed) slurry was allowed to settle.

Recovery of dealginate seaweed solids

A distinct solid/liquid interface was evident after 18h (approx.) settling time. The supernatant solution (containing algin) was carefully siphoned off. The remaining seaweed solids were washed by adding cold tap water to make up a 3 kg mass. The slurry was stirred for 15 min and then allowed to settle until a good phase separation had been achieved. The supernatant liquid was again siphoned off. The remaining solids were termed "dealginate seaweed" and represented the residue waste material produced by algin extraction from marine algae.

Chemicals

$CuCl_2.2H_2O$, $NiCl_2.6H_2O$ and $ZnCl_2$ of analytical reagent quality were supplied by Fisons, Loughborough, England. $CdCl_2.2.5H_2O$ of analytical reagent quality was supplied by May & Baker Ltd., Dagenham, England. Volumetric standard HCl(0.0944mol l^{-1}), NaOH(0.098 mol l^{-1}) and methyl alcohol (99.8%) ACS reagent

quality were supplied by Aldrich Chemical Company, Milwaukee, USA. Propylene oxide(99%) and acetone (99+%) ACS reagent quality were supplied by Acros Organics, New Jersey, USA. A 20% (v/v) solution of poly[hexamethylene biguanidinium chloride] (PHMBHCl) was supplied by Zeneca Biocides, Manchester, UK (complimentary).

Potentiometric titrations, quantification of alginate and zeta-potential measurement

Potentiometric titrations of algal sorbents were carried out using the method described by Helfferich[2]. Typically, a number of samples (containing 100 mg each) of algal sorbent were weighed into separate dry flasks. Successively larger amounts of volumetric standard NaOH were added to the different samples using a calibrated burette. 50 ml of 0.1M NaCl solution was added to each flask to maintain a high background electrolyte concentration. A total batch volume of 100 ml was made up by adding deionised distilled water (DDW) in order to keep the solution volume to sorbent weight ratio constant. The batches were left to equilibrate for 10 days after which the pH of the supernatant solution was recorded using a Mettler-Toledo 340 pH meter.

Quantification of alginate in solution

10 ml of 0.3% PHMBHCl in 1% sodium acetate was added to duplicate aliquots (5 ml) of supernatant solutions arising from pH titration. The solution was stirred continuously using a magnetic stirrer in a 50 ml Erlenmeyer flask for five minutes. This allowed the formation of the alginate-PHMBHCl precipitate, which was separated from the supernatant solution by using 0.2μm Whatman PTFE filters. The filtrate was diluted by taking 100μl of filtrate and adding 10 ml of DDW before analysing for UV absorbance at 235nm using a Shimadzu UV-1201 UV-VIS Spectrophotometer.

In industry, alginate extraction is carried out at temperatures around 70°C using sodium carbonate instead of sodium hydroxide to prevent degradation of the polysaccharide structure. A β-elimination reaction with the formation of αβ-

unsaturated uronic acid derivatives is the principal degradation process at high pH values. The pH titrations however, were carried out at 25°C. Low viscosity alginates of lower molecular weights may be easier to leach out in comparison with high viscosity alginates. It was therefore thought important to compare the responses of alginates of varying viscosity and mannuronic/guluronic ratios in an effort to ensure identical response of the assay. A variety of commercial sodium alginate products of varying viscosity, possessing a range of calcium content as well as D-Mannuronic/L-Guluronic acid ratios were obtained from Monsanto (see Table 2.2.).

Sample	Viscosity (mPa.s)	Calcium (%)	Weed type[1]
Kelgin HV	750-875	0.6-1.5	M
Kelgin LV	55-70	0.2-1.5	M
Manucol DM	200-300	0.3 max	M
Manucol LF	20-40	0.4 max	M
Manugel DMB	250-375	0.25 max	G
Manugel SFB	200-250	0.2-0.5	G
Manugel GHB	60-90	0.3 max	Mixed M/G

[1] M: high mannuronic, G: high guluronic

Table 2.2. Product characteristics of commercial alginates.

Calibration samples were prepared using the algin samples tabulated above. The procedure described earlier for the determination of algin in potentiometric titres was followed. The concentration range studied was 1-5 mg ml^{-1}.

Zeta-potential measurement

The zeta-potential of native algal biomass *A. nodosum* and *D. potatorum* was determined using a zetamaster (Zetasizer-3000) from Malvern Instruments. The previously dry algal particles were crushed using a coffee grinder. The particles were then dry sieved to obtain a fraction (<45μm). Potentiometric titrations of algal samples was carried out as described earlier except, for zeta potential measurements, both acid and alkaline ranges were studied. Volumetric standard sodium hydroxide (0.1M) and hydrochloric acid (0.01M/0.1M) were used. In addition, the batch volume was 50 ml, with 30 ml of background electrolyte added (NaCl) and 20 mg of sorbent material. The effect of ionic strength on the zeta-potential curves (in particular pzc and iep) of AN was determined by carrying out potentiometric titrations at two different ionic strengths using 0.1M and 0.01M NaCl as background electrolyte. Comparison of the zeta-potential values obtained for algal particles against a weakly-acidic cation exchanger (predominantly carboxylate functionality) Purolite C104 was also carried out under identical conditions. Equilibration times in excess of 48h were allowed before measurement of pH and zeta potential. The colloidal solution was injected into a flow-through quartz cell positioned in an electrophoresis chamber for zeta-potential measurement following equilibration of titres. Electrophoretic measurements were based on an analysis of the frequency spectrum of laser light scattered by the particle suspension using a photon-counting detector and digital correlator. The instrument measures the electrophoretic mobilities of the samples in aqueous media as a function of pH and determines the isoelectric point pH. All measurements were made at 298K.

Chemical modification of metal binding sites

Partial modification of algal and dealginate seaweed samples was performed according to the method of Gardea-Torresdey et al[44]. 1g of sorbent particles was contacted with 50 ml of absolute methanol to which 1% (v/v) of concentrated HCl was added. Two batches of each material were prepared in order to investigate the influence of contact time (48 hours, 96 hours). Control samples contacted with methanol alone were used to compare the degree of esterification attained. Alginate-

free samples of algal biosorbent were prepared by contacting the biomass with an aqueous solution of propylene oxide according to the procedure of Fourest et al[3]. Algal particles were contacted with 37% (v/v) propylene oxide solution (20 ml g^{-1}) at room temperature. Two batches were used to investigate the influence of time (4 hours and 48 hours) on the degree of esterification. Following esterification, the modified algal sorbents were washed extensively with DDW and subsequently freeze dried for further use. The influence of acetone/water (1:1) treatment on algal samples was studied in order to determine whether extraction of polyphenolic type compounds had an effect on metal sorption[3]. Weight loss of samples was noted.

Methanolic-HCl treated samples were further investigated for degree of modification (methylation) by base hydrolysis of the modified biomass and subsequent analysis of the released methanol by gas chromatography (GC). 50 mg of modified biosorbent was contacted for seven days with 5 ml of 2 mol l^{-1} NaOH in glass vials with Teflon caps. After equilibration, 1 ml of supernatant solution was filtered using 0.2μm Whatman (PTFE) disposable filters. The samples were spiked with 2-propanol (0.2% v/v) as internal standard before 1μl of the resulting solution was injected in a Pye Unicam series 304 GC using a Hamilton 7101 1μl injection syringe. The GC was equipped with a flame ionisation detector and a 25m CP-Sil-5 CB (0.25 mm i.d.) column. Conditions for the GC analysis were as follows: injector temperature 110°C; detector temperature 120°C; column temperature 40°C; carrier gas helium. Methanol concentrations were determined by integration of peak areas on a Pye Unicam PU 4810 computing integrator.

Surface area and pore size distribution

Surface area and pore size distributions for native and dealginate algal samples were obtained using a Micromeritics ASAP 2010C automatic analyser fitted with an optimal high stability 1torr pressure transducer. Samples of the algal particles, in the particle size range 300-355 μm were freeze dried and then outgassed for a minimum of 24h at 30°C on the degas ports of the analyser. The sorbent mass was determined by subtracting the weight of the empty tube from the nitrogen back-filled degassed

sorbent containing sample tube. The sample tubes were sealed at the top using seal frits to prevent air leaking into the degassed samples.

Adsorption isotherms were recorded by dosing high purity nitrogen (>99.99%) onto the algal particles with the sample tube immersed in a bath of liquid nitrogen (at approximately 77K). The analysis and cold trap Dewars were filled using liquid nitrogen and an isothermal jacket was placed around the sample tube before connecting it to the analysis port of the analyser.

Data were recorded using "High resolution nitrogen adsorption/desorption" mode. The dose mode of "rate of adsorption" was selected to enable kinetic effects to be investigated prior to data collection which was defined in the high resolution adsorption/desorption pressure table. The equilibration interval was initially set at 45s in order to achieve adequate diffusion of nitrogen into any micropores present. Subsequently, the effect of equilibration interval was investigated by analysing samples at intervals of 5, 10 and 30 seconds. An interval of 5s was finally selected since longer times seemed to have no observable effect on the pore size distribution or sorption isotherm. The molecular drag pump was operated for all measurements.

Microscopy

Low magnification scanning electron micrograph pictures (SEM); magnification (100-20,000x), of native and dealginate algal biosorbents were obtained using a Cambridge Stereoscan 360, scanning electron microscope at an accelerating voltage of 10 kV (these SEM pictures were produced by a qualified technician).

All samples were freeze dried under a vacuum for 24h and stored in a desiccating jar over silica gel. The sorbent particles were glued to aluminium platforms prior to gold coating. SEMs of protonated and water-washed dealginate seaweed particles as well as protonated native algal particles and methanol/HCl and propylene oxide treated samples were obtained.

Infra-red spectroscopy

Direct transmission-IR spectroscopy of algal samples was compared with a relatively new diffuse reflectance FT-IR (DRIFT) spectroscopy technique. In transmission spectroscopy, samples of finely ground algal particles (<20μm) are dispersed in IR-grade potassium bromide (0.25% wt/wt seaweed in KBr) and then pressed with special dies (Pressure between 10,000-15,000 psi)[45] to obtain transparent disks. However, the drift technique overcomes some of the contamination and reflection problems experienced by the transmission technique and is a lot simpler, saving significant time in disk preparation. IR-spectra recorded for native AN and LF using both techniques indicated little difference in sensitivity. Direct transmission-IR spectroscopy was used for all subsequent spectra recorded.

The spectra were recorded on a Nicolet 20-DXC FT-IR spectrophotometer with a dry-air purge, liquid nitrogen cooled MCT (mercury-cadmium-telluride) detector and a Spectra-Tech diffuse reflectance accessory. The diffuse reflectance accessory consisted of a hemi-spherical mirror which split into two halves, with the sample mounted on the central platform. The accessory was aligned to provide maximum signal intensity using a stainless steel mirrored platform. The height of the sample on the platform was adjusted to minimise the gain of the detector.

Samples of AN, LF, BK, LH, DAN, DLF, AA-AN and AA-LF as well as reference materials laminarin, fucoidan, mannitol and glucuronic acid were crushed using an agate mortar and pestle to provide particles <20μm. Finely divided spectroscopic grade potassium bromide (Fisher scientific) was ground and stored in a desiccator jar over silica gel prior to use. The samples were mixed with KBr (0.1% wt/wt) to enable absorbance values less than 1 to be recorded.

Background spectra of KBr and water vapour were recorded every 100 minutes. Spectra were recorded at a resolution of 4 cm^{-1} using a minimum of 250 scans and an aperture setting of 15. Before recording spectra, the samples were left to equilibrate

in the sample compartment for 10 min with a continuously flowing purge stream of dry air.

Section 2.3. Results and Discussion

Biological materials

Analysis of ionic species in the effluent leaving the wash-column indicated significant concentrations of sodium, potassium, magnesium and calcium ions. Matheickal et al.[46] reported release Ca^{2+} and Mg^{2+} upon lead sorption by a brown marine alga *Ecklonia radiata*. During propagation in the marine environment, cationic exchange between the metabolically active algal cells and the surrounding medium occurs. These ions are present within the biomass once the seaweed is harvested. Washing of the algal particles with DDW did not wash out the ions indicating that the ions may be chemically bound within the algal matrix. Exchange of these cations with protons seems to result in displacement of Na^{+}, K^{+}, Ca^{2+} and Mg^{2+} due to interaction of protons with the metal-binding sites. Ashing of native biosorbents at 600°C resulted in an ash content of between 20-25 % indicating the presence of inorganic metal salts (see chapter 5).

Native algal particles (sun-dried) showed significant swelling upon rewetting in the wash-column. The extent of swelling followed the sequence BK>LF>AN≈LH which matches the amount of algin present in each algal variety. Upon contacting the algal-bed with hydrochloric acid (0.1M), shrinkage of the biomass particles was noted. The shrinkage of the BK algal-bed was striking, with the occupied volume reduced to less than half its original volume. LF showed around 30% shrinkage whereas AN and LH showed 10% reduction in swollen volume. Washing of the protonated algal-beds with DDW resulted in slight reswelling. The extent of this expansion varied for the different algal species studied. The BK sorbent bed expanded by 6% of its original swollen volume, resulting in an overall shrinkage of 46% (this native material showed the highest swelling and shrinkage during initial washing and protonation compared with all other native and processed materials that were studied).

Following washing and protonation, the freeze dried algal particles showed interesting swelling characteristics upon rewetting. Laser diffraction particle size analysis of swollen native algal particles ranged between 330-740 μm with the average size range 470-570 μm. LF showed the highest swollen volume (11.1 cm^3 g^{-1}) while the processed dealginate sorbents displayed lower swollen volumes with respect to their native precursors (see Table 2.3.). This reduction in swelling may be the result of reduced algin content in the processed dealginate material. It is well known that algin has a significant water retention capability (it finds many uses as a hydrocolloid[33]). LH shows the highest swollen volume (4.5 cm^3 g^{-1}) compared with the other native algae with the exception of LF. The higher proportion of guluronic acid segments in LH may be responsible for the higher swollen volume (see section 1.4.). There is evidence of four water molecules interacting with a single guluronic acid unit[1]. LF particles show a significantly low dry bulk density indicating loose packing arrangement of the particles. This high occupied volume was retained during wetting indicating very weak crosslinking within the algal matrix. No simple explanation is available to account for this phenomenon. Dealginate particles show significantly lower swollen volume compared with the native material. The distention index for DLF (see Table 2.3.) is still higher than for DAN but in comparison with native *L. flavicans* is an order of magnitude lower.

Species	AN	LF	BK	LH	DAN	DLF
Dry bulk density, ρ_D (g cm^{-3})	0.625	0.18	0.71	0.61	0.68	0.68
Wet bulk density, ρ_S (g cm^{-3})	0.25	0.09	0.28	0.22	0.33	0.28
Swollen volume, V_S (cm^3 g^{-1})	4	11.1	3.6	4.5	3	3.6
Dry volume, V_D (cm^3 g^{-1})	1.6	5.6	1.4	1.64	1.47	1.47
Distention index, DI $\left(\frac{V_S}{\rho_D}\right)$	16	123	12.9	20.5	9.1	12.9
Swelling ratio, Q$\left(\frac{\rho_S}{\rho_D}\right)$	0.4	0.5	0.4	0.36	0.49	0.41
Swelling index, SI $\left(\frac{V_S - V_D}{V_D}\right)$	1.5	1.0	1.6	1.7	1.1	1.45
Avg. swollen particle size, μm	559	473	553	571	499	563

Note: Dry particles sieved to obtain size fraction 300-355 μm

Table 2.3. Swelling characteristics of biosorbent materials.

Potentiometric titrations, quantification of alginate and zeta potential measurement

The pH titration curves are characteristically those of weak acid type sorbents, showing a gradual rise in solution pH with addition of small amounts of alkali (see Fig. 2.3.). Comparison of the native materials shows no significant variation in the shape of the curves except for LF; there is no inflection point in the pH range 6-8 as exhibited by the other native biosorbents. The sodium sorption capacity of the materials (see Fig. 2.4.) over the pH range 3-6 shows a marked difference between BK (4.2 mmol g^{-1}) and the rest of the sorbents (see Table 2.4.). BK displays a steep rise in sodium uptake between pH 3-4; the other native materials do not mirror this behaviour and their relatively shallower rise occurs over the pH range 3.5-4.5. This may be due to several phenomenon arising principally as a consequence of the higher number of acidic functional sites within BK. This shift towards the lower pH range at which Na^+ uptake begins to take place by BK is reflected in the lower pK_{a1} of the groups calculated from the titration curves (see Table 2.4.). It is clear from these

results that BK stands out amongst the native algae studied in having a pK_{a1} value which is very close to the value calculated for alginic acid samples AA-AN and AA-LF. It is, therefore, intuitively concluded that the principal contribution towards the acidity of biosorbent particles arises due to the presence of alginic acid within the algal matrix.

Species	AN	LF	BK	LH	DAN	AA-AN	AA-LF
pK_{a1}	4.2	4.1	3.4	4.15	4.34	3.6	3.7
pK_{a2}	6.3	5.0	6.7	7.0	6.2	11.3	11.9
$^{1}Na^{+}$ capacity mmol g^{-1}	2.2	3.4	4.2	2.2	1.0	4.8	5.3
$^{2}Na^{+}$ capacity mmol g^{-1}	4.5	3.9	6.2	4.5	2.2	9	>10

[1.] calculated over pH 2-6, [2.] calculated over pH 2-10

Table 2.4. Acid-dissociation constants and sodium capacity values for algal biosorbents.

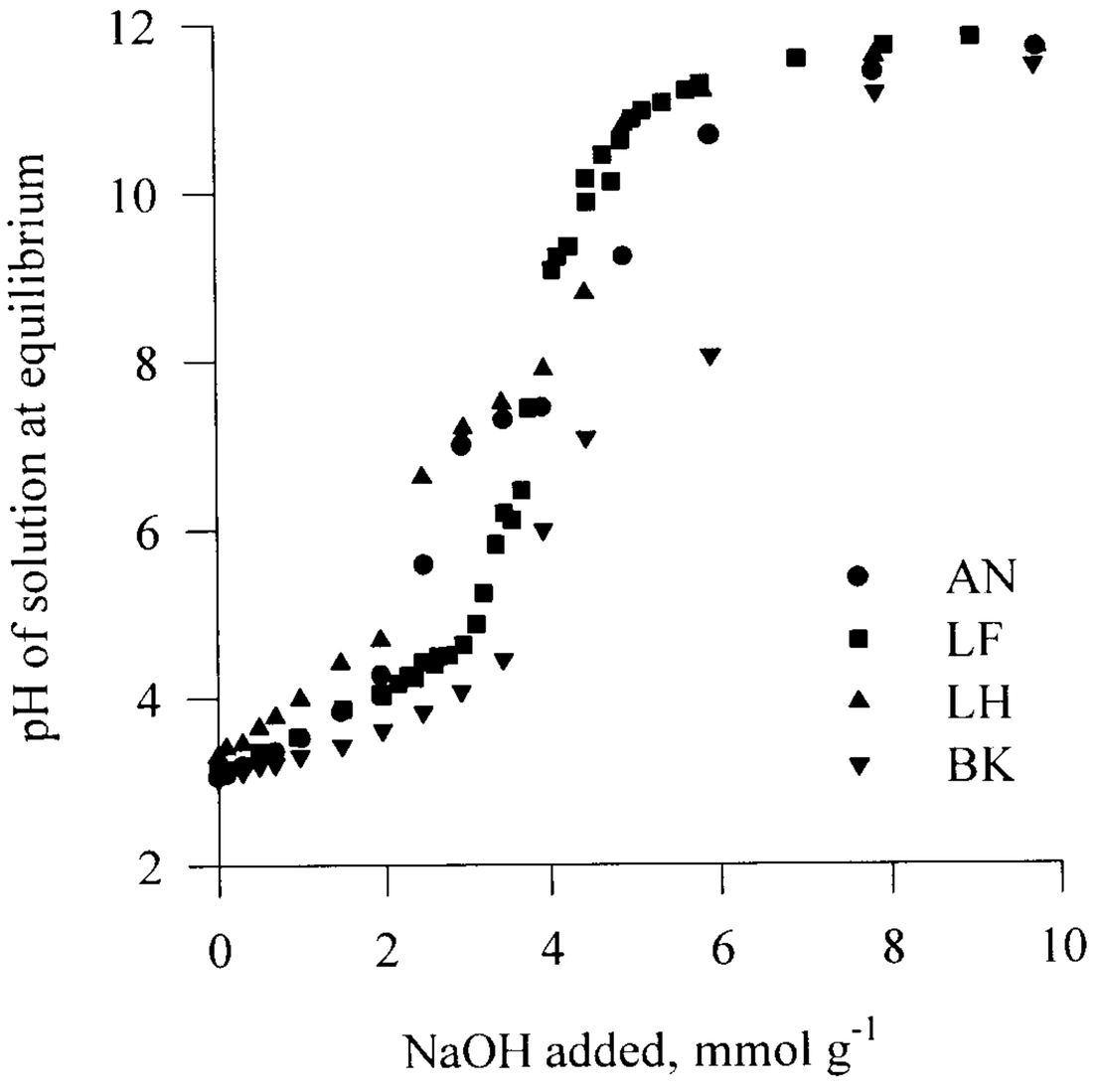

Figure 2.3. Potentiometric titrations of various native algal biosorbents.

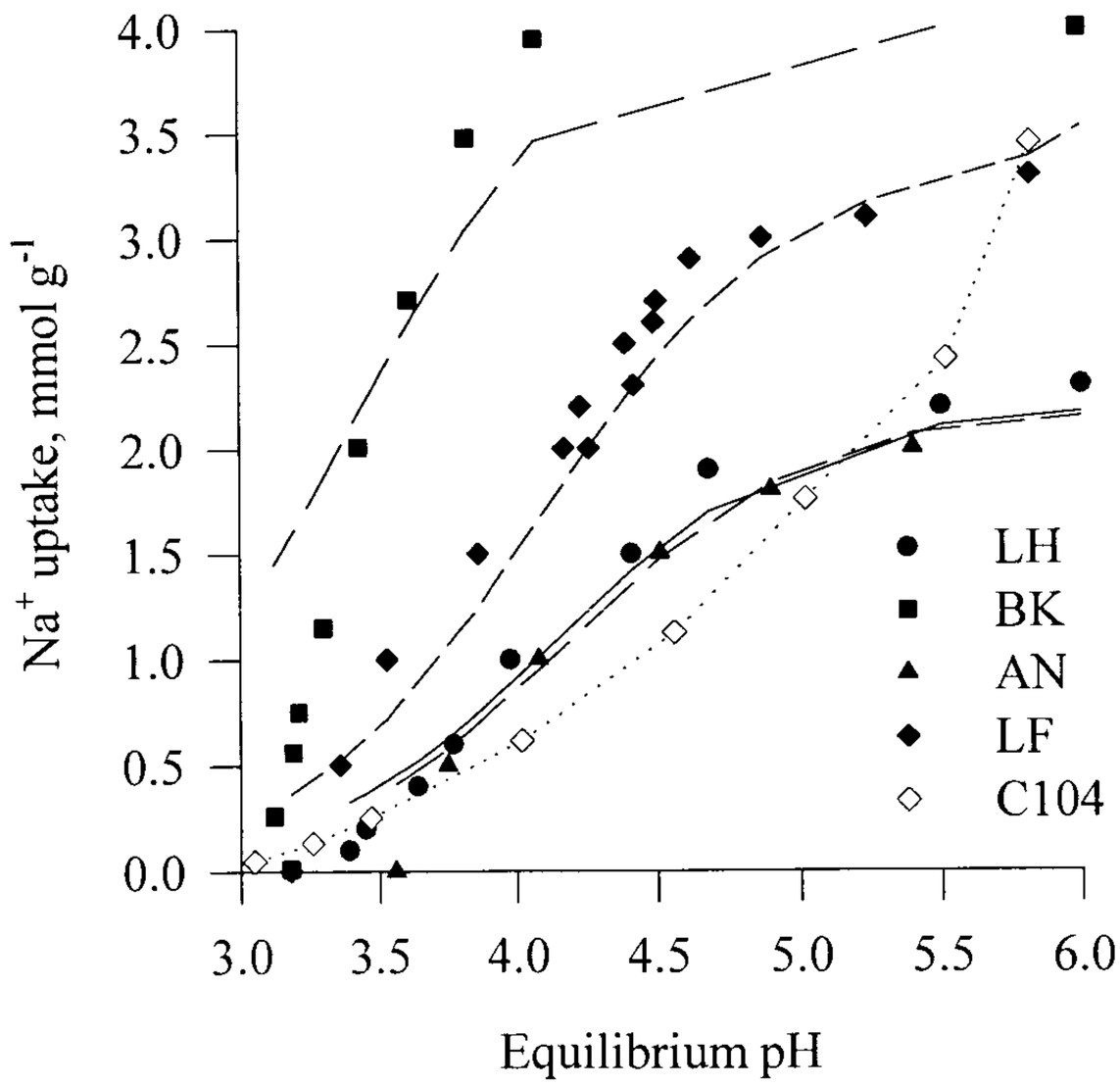

Figure 2.4. Comparison of sodium uptake as a function of pH by native algae.

The sodium sorption data obtained by potentiometric titration of alginic acid samples (see Fig. 2.5.) shows a plateau due to Na^+/H^+ exchange over the pH range 3-4. The dealginate seaweed samples show a marked reduction in acidity in comparison with native precursors (see Fig. 2.6.). The pH of the titres containing DAN/DLF rise steeply upon addition of small doses of alkali.

A second acid-dissociation constant exists for the native algal samples between pH 6-9. The contribution of these groups towards the overall Na^+ uptake capacity is significant for all the native seaweed varieties studied except LF. Only 13% of the total Na^+ uptake capacity of LF may be attributed to acidic groups dissociating between pH 6-8. In the case of AN and LH, about 50% of the overall Na^+ uptake capacity occurs above pH 6 while for BK, the contribution of these groups is around 30%. The inflection in the pH titration curves between pH 6-8 characterises functional groups other than carboxyl. Potentiometric titration curves for a brown algae, *Undaria pinnatifida*[6], also showed a similar inflection when titrated with a background electrolyte of 0.1M NaCl. It is possible that weakly dissociated phenolic type groups attached as side groups in the polysaccharide chains, may be responsible for reactivity toward Na^+ ions. Dealginate seaweed samples such as DAN show a slightly higher acid-dissociation constant value in comparison with the native precursor *Ascophyllum nodosum* (see Table 2.4.). The primary reason for this slightly higher pK_a may be due to the lower concentration of acid groups because most of the algin has been removed from the material. It is surprising, however, that processed seaweed samples still possess a relatively high number of active functional sites.

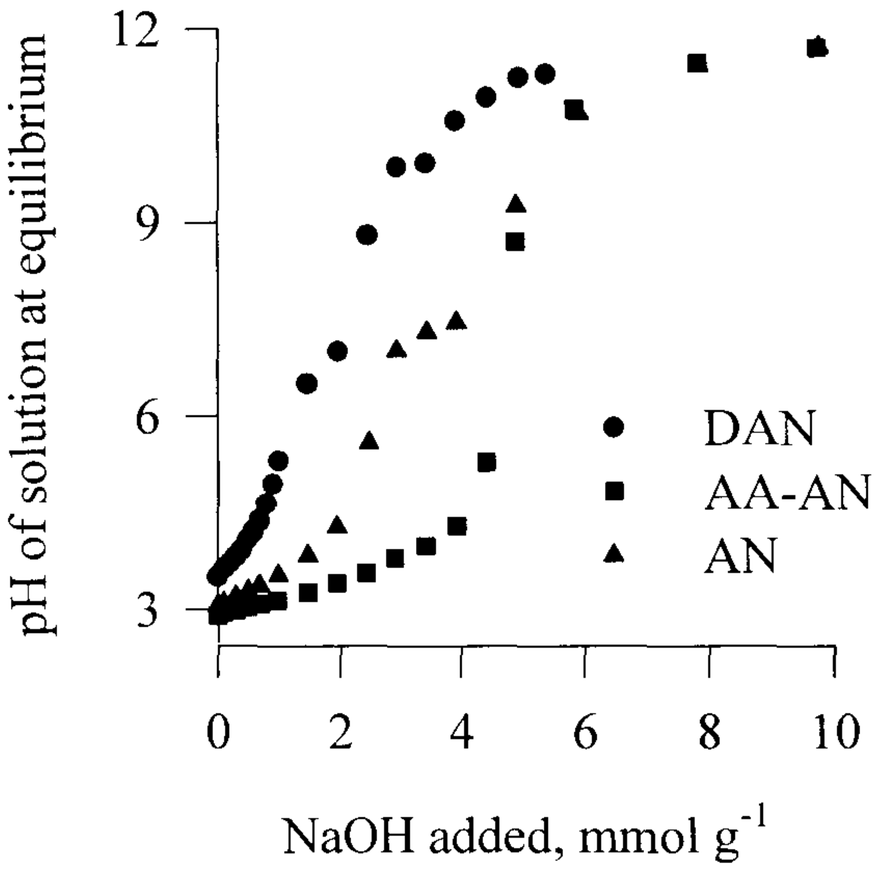

Figure 2.5. Potentiometric titration of AN, DAN and AA-AN.

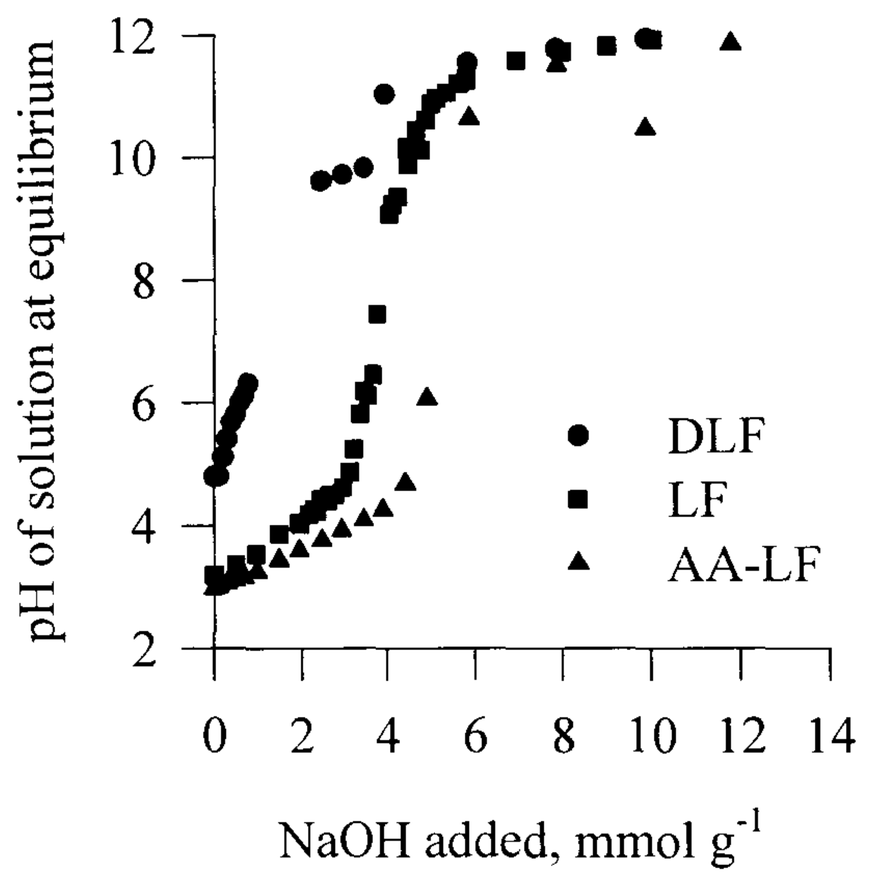

Figure 2.6. Potentiometric titration of LF, DLF and AA-LF.

Supernatant solutions in the individual batch equilibration samples were tested for solubilisation of alginate. The native algal samples showed a clear reduction in UV absorbance indicating complexation of the organic cation (PHMBHCl) with leached algin. In titres containing larger doses of alkali, an increase in the amount of algin was noticed (this was the case for all native algal samples). An increase in supernatant solution viscosity was also noted (indication that sodium alginate was present in solution). The higher alkali dosed batches resulted in solubilisation of the algal material with the supernatant solution turning a murky brown colour.

The results of testing commercial alginate samples in solution and the response of the PHMBHCl-assay method are depicted in Fig. 2.7. Difficulty was experienced in achieving complete solubilisation of sodium alginate in solution at high sodium alginate concentrations and this resulted in an increase in the spread of UV absorption values (see Fig. 2.7.). UV absorbance readings for algal alkalimetric titres showed a range of values (see Table 2.5.). Assuming the degree of polymerisation of algin in solution as 80^3 (Approx. molecular weight 18,000), average concentration values for algin in solution may be calculated (see Table 2.5.). The highest amount of algin detected was in titres of BK (0.2 mmol g^{-1}) whereas the dealginate samples showed the least amount of algin leaching. These calculated values are based on the rather weak assumptions regarding the molecular weight of algin in solution.

Quantitative determination of leached algin for the various seaweed samples was difficult, since the molecular weight of algin in solution is unknown. Hydrolysis of the glycosidic-linkage within the algin polymer results in a range of molecular weights present in alkali titres. In the literature[47], researchers suggest values ranging from 18,000 to around 150,000 (depending on the viscosity of the alginate solutions). Only qualitative comparisons may be made between the various samples analysed. BK leached more algin than the other native materials (in terms of the UV absorbance values) whereas LH leached the least amount of algin. Although algin presence was more pronounced in titre batches containing excess NaOH (i.e. in the later part of the

titration process), algin leaching was also found to occur in titre samples containing relatively small amounts of NaOH.

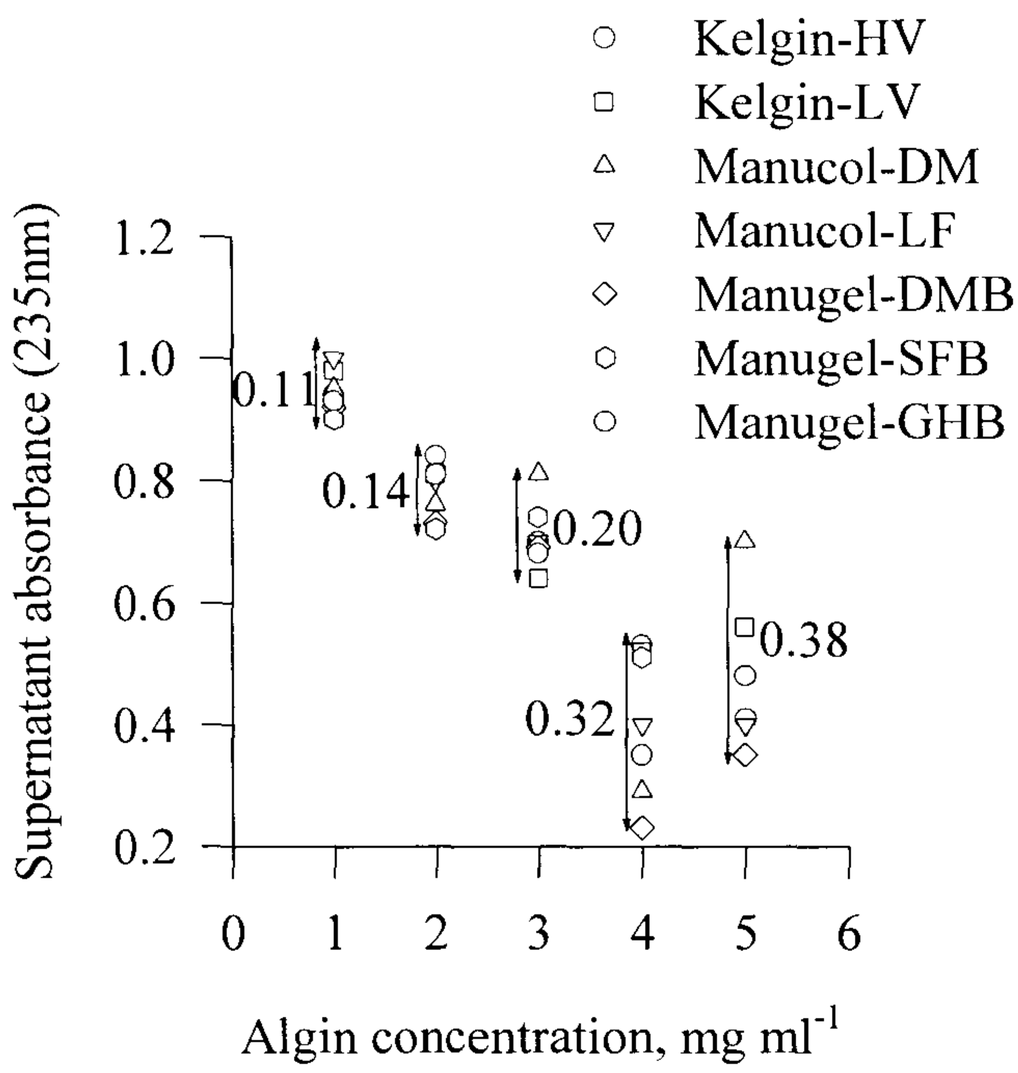

Figure 2.7. Response of various commercial sodium alginate samples to the PHMBHCl-assay.

The negative surface charge surrounding algal particles in solution, due to the dissociation of acidic functional groups, was also prevalent during zeta-potential measurements carried out on AN and BK. The zeta-potential curves of AN and BK resembled the curve measured for Purolite C104 weakly-acidic carboxylate ion exchanger. The isoelectric points lie somewhere between pH 0-2 for AN and pH 1.5 for BK compared with pH 1.9 for the Purolite C104 resin. The Purolite C104 resin has a similar sodium capacity (3.5 mmol g^{-1}) compared with AN and BK (see Table 2.4.) and therefore serves as a suitable material for comparison with the algal sorbent materials The results indicate the presence of a negative surface charge on algal

particles over most of the alkalimetric titration range (see Fig. 2.8.). The zeta potential of AN falls sharply below pH4 (from around -60 mV to -10 mV at about pH 2). This suggests that surface groups responsible for the high negative zeta-potential begin to interact with protons in solution, lowering the surface charge of the biosorbent particles. Kuyucak[48] reported a similar fall in measured zeta-potential for the brown algae *Sargassum natans*. The effect of high background electrolyte strength on the zeta-potential measurement of *A. nodosum* indicates a sharp decrease in zeta-potential at pH values less than 4 for a high background ionic strength (0.1M NaCl compared with 0.01M NaCl; see Fig. 2.8.). The overall zeta-potential however, is considerably more negative for titres equilibrated at higher ionic strength. Increasing electrolyte strength may cause the Stern layer to become more compact, i.e. the electric double layer is compressed. This should, in theory, result in the measurement of the true surface potential. The cross-over of the two zeta-potential curves occurs at pH 2-3, an exact value for the pznpc cannot be unambiguously determined. Schiewer[4] found that the apparent proton binding constant changed drastically with ionic strength for *Sargassum natans*; the values obtained ranged between pK 3-5. The observed shift in pK values is a common phenomenon in titrations of polyelectrolyte gels[49,50,51]. At low degrees of dissociation, electrostatic effects diminish and the pK value approaches the intrinsic pK. Schiewer[4] determined pK values for alginate and found it to be lower (pK 2.6-2.7) in comparison with *Sargassum natans* (pK~3).

Species	AN	LF	BK	LH	DAN	DLF	AA-AN	AA-LF
UV absorption (235nm)	1-0.6	1-0.6	1-0.5	1-0.8	1-0.9	1-0.9	1-0.4	1-0.4
algin, mg ml^{-1}	2-3	2-3	3-4	1-2	0-1	0-1	4-5	4-5
[1]algin mmol g^{-1}	0.14	0.14	0.19	0.08	0.03	0.03	0.25	0.25

[1]Note: Avg. molecular weight for algin used was 18,000.

Table 2.5. Algin quantification using PHMBHCl-assay method.

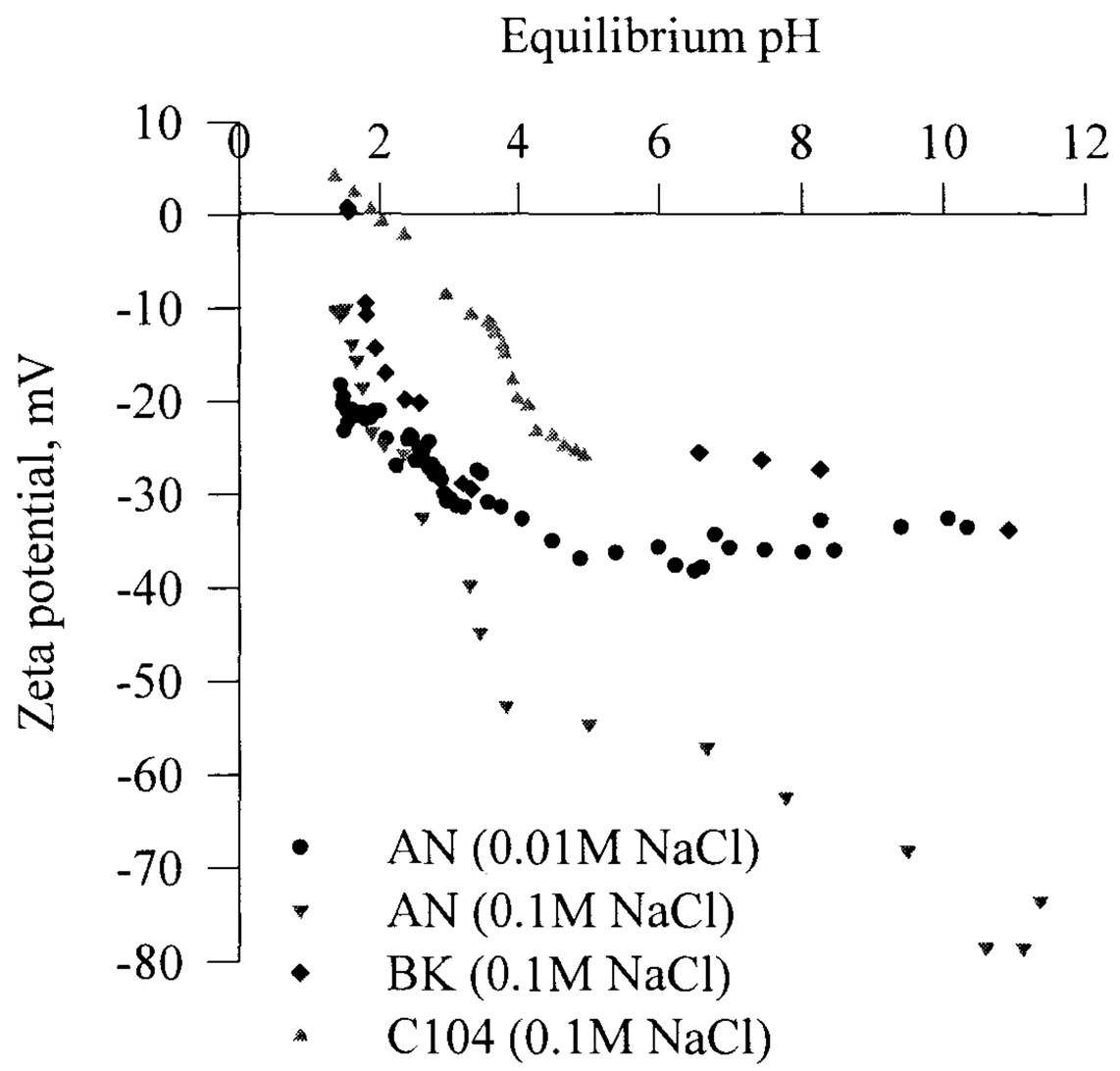

Figure 2.8. Zeta-potential curves for AN, BK and C104.

Chemical modification of metal binding sites

The influence of successive treatments of fresh methanolic hydrogen chloride or propylene oxide on algal biomass results in a reduction in subsequent copper sorption behaviour (see Table 2.6.). 48 hour methanolic/HCl treatment reduces the reactive surface functionality of native seaweed samples by over 70% (e.g. 0.3 mmol g^{-1} copper uptake by AN after 48h contact with methanol/HCl compared with 1 mmol g^{-1} by unesterified material). A subsequent cycle causes a further reduction of between 10-20% in residual binding sites for native materials (see Table 2.6.). Percival and McDowell[1] suggest that the acidity of alginic acid molecules makes complete methylation difficult. The processed seaweed samples of DAN and DLF show only 30% reduction in functionality during the first 48 hours of treatment although metal binding sites are reduced by over 70% after a further 48 hour treatment. In LF, as many as 90% of the copper binding sites are esterified. Treatment of native algae with methanol alone showed no noticeable effects on subsequent metal sorption behaviour. Base hydrolysis of these control samples showed absence of methanol release from algae. Extraction of polyphenolic type compounds from physodes vesicles in algae following acetone washing did not substantiate the claims of earlier researchers[34,35] that phloroglucinol polymers contribute toward the metal binding capacity of algal biomass. The slight increase in copper uptake by dealginate seaweed samples (see Table 2.6.) following acetone/water treatment may be explained in terms of partial purification of the metal sorption components by elimination of non-sorbing polyphenols thereby improving accessibility to the surface active sites.

Copper(II) sorption at pH4 by native algal samples was almost completely eliminated by esterification of the carboxylate groups present in seaweed. This result confirms the evidence of other researchers[52,53,54] who have reported the strong affinity of metal ions to algal biosorbents at pH 3 or above where carboxylate groups begin to dissociate.

Determination of methanol release following treatment of algal biomass with methanolic hydrogen chloride was an attempt to quantify the ratio of carboxylate groups esterified (on a mmol g^{-1} basis) with the reduction in copper binding. It was

found that about 2 mmol g^{-1} of methanol was released for 1 mmol g^{-1} reduction in copper(II) uptake for LF. However, the results did not support a bidentate binding mechanism for AN, DAN and DLF.

In this work, selective esterification was the strategy employed to investigate the contribution of carboxylate groups towards the overall metal-binding properties of algal biomass[44,55]. The method used here, employing HCl in absolute methanol to esterify carboxyl groups of galacturonic acid and polyuronides also results in parallel desulphonation reactions[56]. The transesterification of the sulphate group leads to a soluble methyl-ester. Fourest and Volesky[3] found that the two reactions proceed at the same slow rate, making it impossible to independently distinguish the contribution of each towards the overall metal sorption capacity of the algal material. Esterification using an aqueous solution of propylene oxide has been used since it is faster and more selective for carboxylic groups.

Propylene oxide treatment of algal samples causes solubilisation of alginic acid as propylene glycol alginate and the resultant reduction in copper (II) binding is attributed to this phenomenon. The lesser effect of propylene oxide treatment on the processed seaweed samples DAN and DLF may be explained by hydrolysis of the glycosidic linkage within the alginic acid molecule due to alkali treatment. This leads to break-down products which do not show similar reactivity towards propylene oxide.

The difficulty in achieving complete methylation of carboxyl groups in polyuronides of algae is demonstrated in an attempt to esterify alginic acid samples extracted from native algae AN and LF (see Table 2.6.). The presence of charged groups due to carboxyl functionality in the polyuronide structure hinders complete methylation of the polysaccharide[1]. Treatment of alginic acid samples with propylene oxide resulted in eventual solubilisation of the complete sample.

Chemical modification	Copper uptake, mmol g^{-1} (pH4)						wt loss, %	
	AN	LF	DAN	DLF	AA-AN	AA-LF	AN	DLF
no treatment	1	1.3	0.7	0.8	1.83	1.74	-	-
methanol control	1.1	1.3	0.85	0.85	2.0	1.72	14	6.1
methanol/HCl								
48h	0.3	0.2	0.5	0.6	0.9	1.0	14	4.5
96h	0.24	0.1	0.2	0.2	-	-	18	14.8
propylene oxide								
4h	0.7	0.8	0.7	0.7	-	-	9	3.9
48h	0.3	0.1	0.7	0.6	-	-	21	5.7
acetone/water	1	1.3	0.85	0.8	2.3	1.4	27	13.8
methanol release	3.1	2.6	0.6	0.7	-	-	-	-

Table 2.6. Influence of chemical modification on sorbent copper sorption capacity.

The various chemical modification treatments employed resulted in some loss of weight of the biomass samples. 18% loss in weight was recorded for AN following 96h of contact with methanolic-HCl whereas DLF showed a 15% reduction in weight. Cellular components extracted during this treatment may be similar for both native and processed material. This result suggests that the material extracted may be insoluble following alkali washing since the processed dealginate material had

undergone this treatment. The propylene oxide treatment of AN resulted in a 9% loss of weight after 4h and 21% reduction in weight after 48h of contact. This corresponds well with the fact that the copper sorption capacity fell by 30% after 4h of propylene oxide treatment, indicating a similar percentage of algin should have been washed out of the algae as propylene glycol alginate. Considering that AN contains around 25% algin by weight, the loss in copper capacity corresponds to 7.5% loss of weight in terms of algin washed out. This is quite close to the result obtained. Data for 48h treated sample matches the results described here.

The acetone/water treatment resulted in 27% loss in weight of AN and 14% loss in DLF. Tannin type polyphenols are probably solubilised during this treatment and result in significant reduction in weight of native as well as dealginate materials.

Surface area and pore size distribution

The nitrogen adsorption/desorption isotherms for native and dealginate sorbents showed Type II shape (according to IUPAC classification) which is characteristic of the multi-layer adsorption onto non-porous or macroporous solids (see Fig. 2.9.). It is evident from the data that the sorbents have very little sorption capacity for nitrogen. There is no significant sorption of nitrogen over the low pressure range, and therefore no discernible microporosity. Characterisation of the macropores from isotherm data near $\frac{P}{P_o} = 1$ is not practical since serious condensation on the sample tube walls begins near the saturated vapour pressure. Other techniques such as mercury intrusion porosimetry may be used for macroporosity determination, however, given the sponge-like compressible nature of algal biosorbents, this technique was not deemed practical and therefore was not considered.

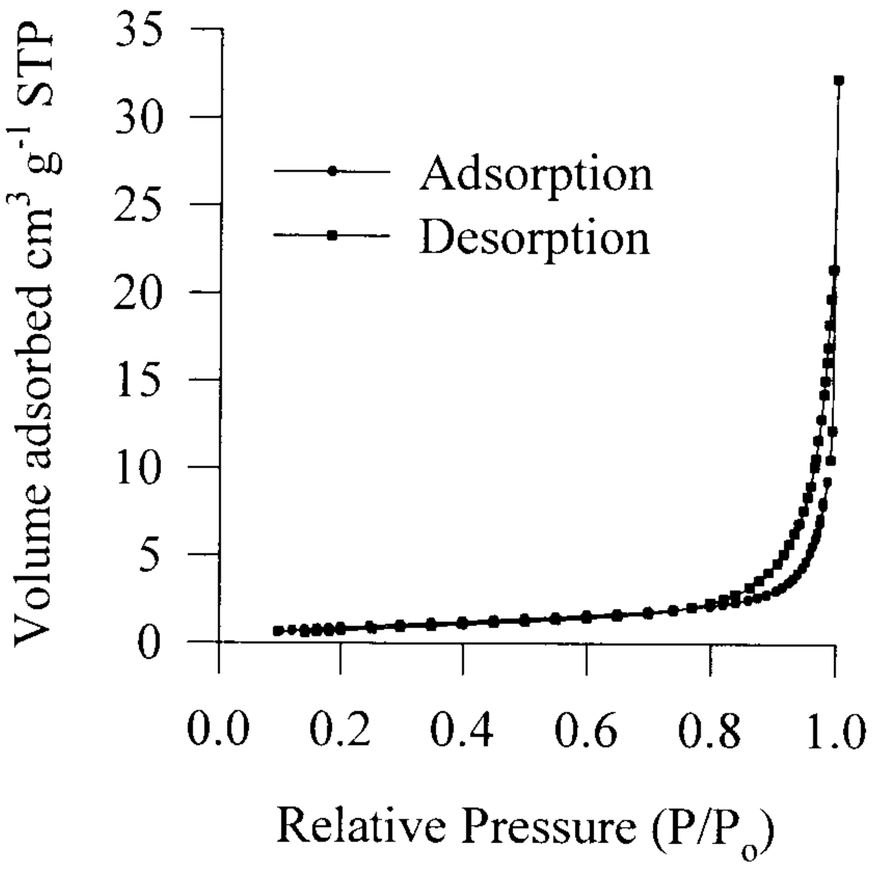

Figure 2.9. Nitrogen Adsorption/Desorption Isotherms for LF.

A large number of models can be applied to describe experimental adsorption isotherm data in order to obtain surface area and pore size distributions. Details of the equations for the Langmuir and B.E.T. theories are covered extensively in the literature and the reader is referred to the text by Gregg and Sing[57].

The Langmuir and BET isotherms are linear over the range 0.05-0.25 for the sorbents studied (see Fig. 2.10.). The low surface area values between 3-6.5 m^2 g^{-1} suggest that there is very little active sorption area. This may be due to incomplete moisture removal from the algal samples analysed. Considerable moisture was collected in the cold trap during degassing, indicating the presence of substantial moisture within the freeze dried algal samples. This moisture which is difficult to remove during freeze drying may be chemically bound to the algal structural polysaccharides. Removal may cause structural changes and therefore presents difficulty in accurately measuring the true surface area exhibited by algal biosorbents during metal sorption.

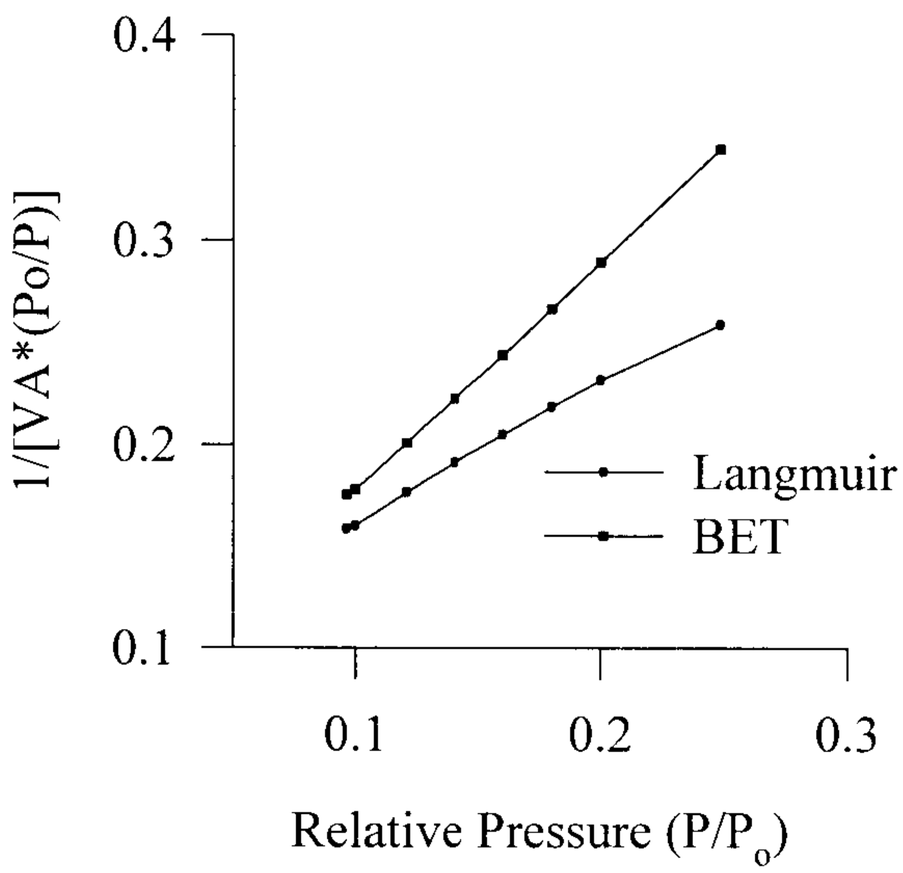

Figure 2.10. Langmuir and B.E.T. plots for LF.

The average pore diameter was calculated using the method of Barrett, Joyner and Halenda (B.J.H.)[58]. The inherent assumptions of the model concern the mechanisms describing the equilibrium between the gas phase during desorption: (1) physical adsorption on the pore walls, the thickness of which are calculated based on the theories of Schull[59] and (2) capillary condensation, modelled by the Kelvin equation. The B.J.H. method allows mesoporous materials to be characterised; however, pores below 15 Å cannot be characterised since the extension of the Kelvin equation to pores of very small radii does not hold. The B.J.H. adsorption average pore diameter for LF was calculated to be 203 Å compared with BJH desorption average pore diameter around 316 Å indicating the presence of predominantly large mesopores constituting the algal structure. This result is characteristic of the algal samples evaluated during this study.

Microscopy

SEMs of the water-washed processed dealginate particles clearly show the presence of salt crystals on the algal surface (see Fig. 2.11.). These crystals are probably $Ca(OH)_2$ precipitated during treatment of the dealginate algal particles (see section on algin extraction). Following acid-wash (protonation), the surface of the algal particles is clearly devoid of any crystalline deposits and gives a sponge-like appearance (see Fig. 2.12.). The topographical image of protonated native *L. flavicans* shows a mangled sheet-like surface devoid of any coherent structure and clearly no visible pore structure, thus supporting results obtained from nitrogen sorption studies (see Fig. 2.13.).

Methanolic-HCl treated samples clearly show washing away of the tissue-like material seen in the SEMs of protonated native algal particles. Obviously, a lot of the cellular material has been washed out leaving a bare-bone structure of the algal particles visible (see Fig. 2.14.). Propylene oxide treated native algal particles show even starker evidence of algal material having dissolved away with a definitive destruction of the pocket-like structure that was so evident in the methanolic-HCl treated samples (see Fig. 2.15.).

The SEMs provide visual confirmation of the results obtained from chemical modification and nitrogen sorption studies. The surface of the algal particles appear flat sheet-like and there is no real microporous structure. Treatment with propylene oxide seems to wash out key structural components (in all probability alginic acid) leaving a severely damaged structural appearance.

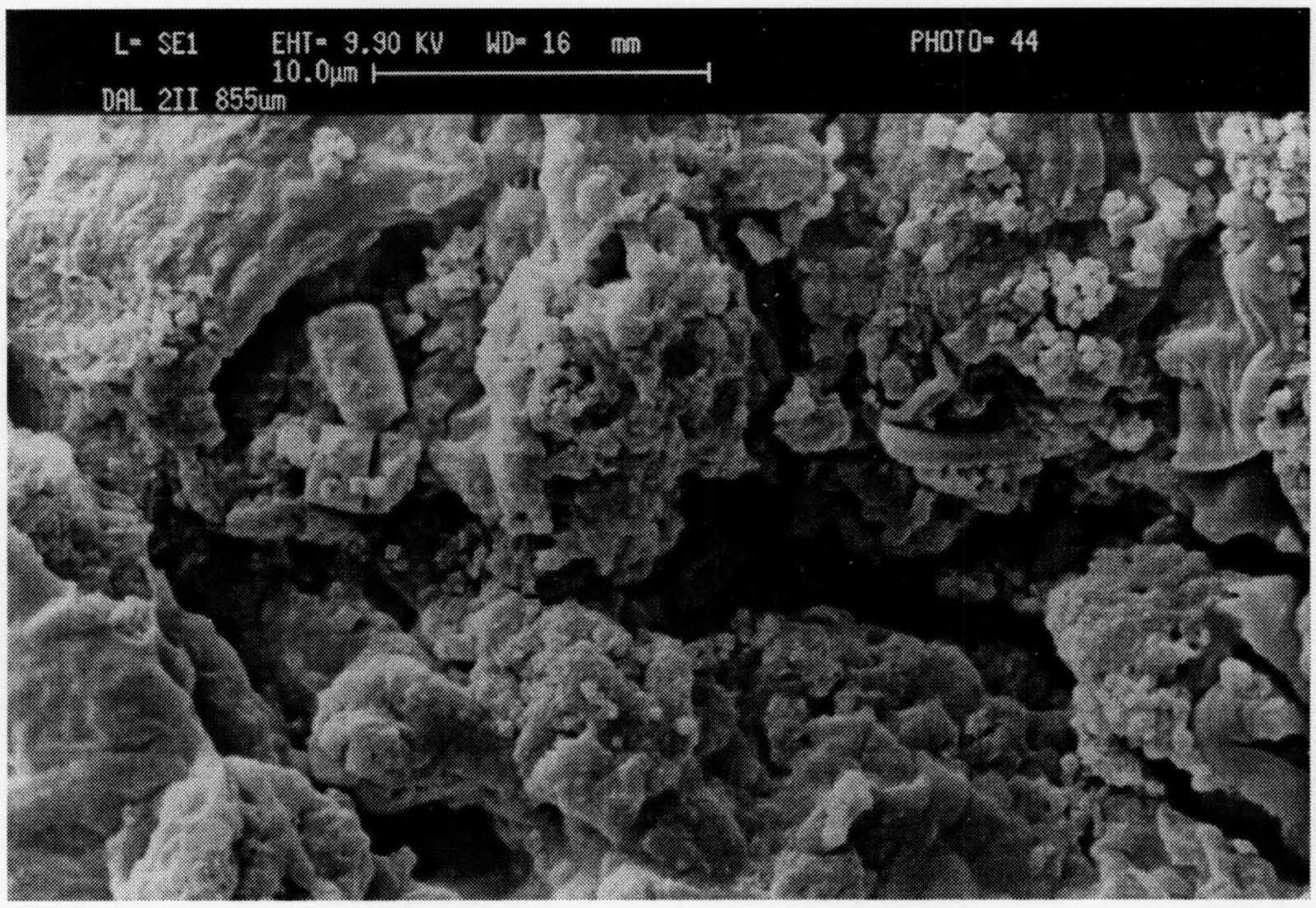

Figure 2.11. SEM topographical image of DLF (water-washed sample).

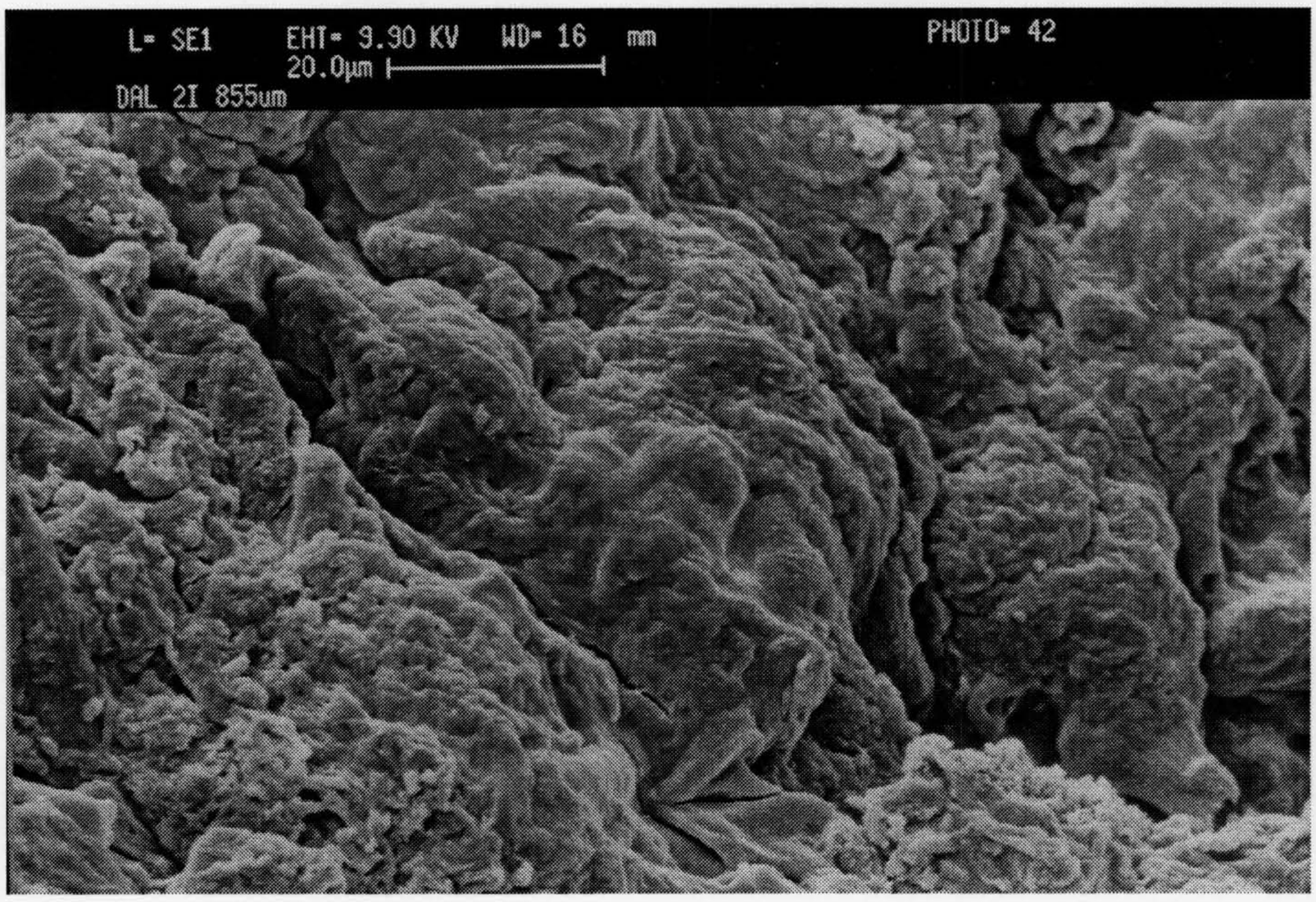

Figure 2.12. SEM topographical image of DLF (acid-washed sample).

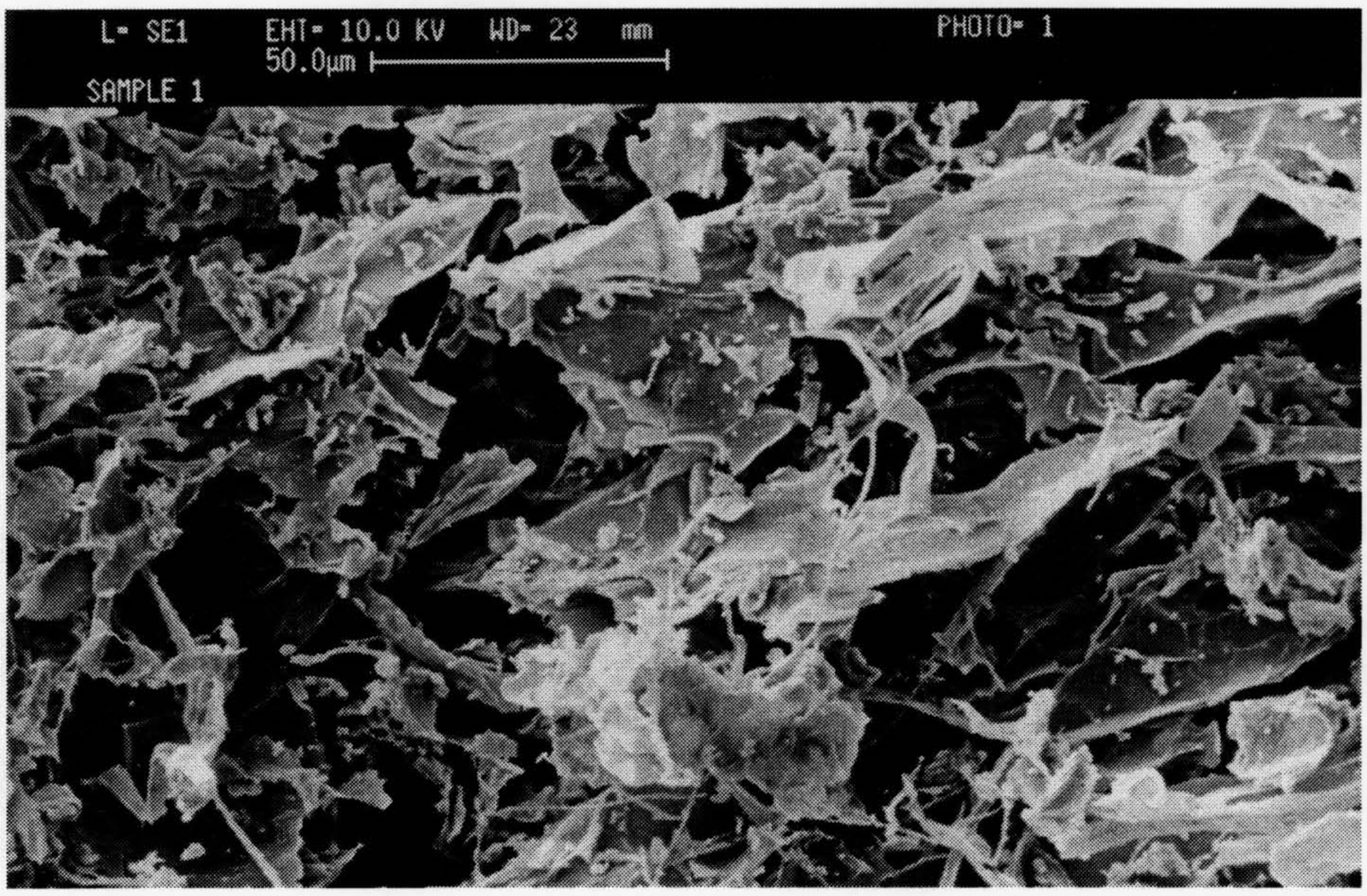

Figure 2.13. SEM topographical image of native *L. flavicans* (Protonated).

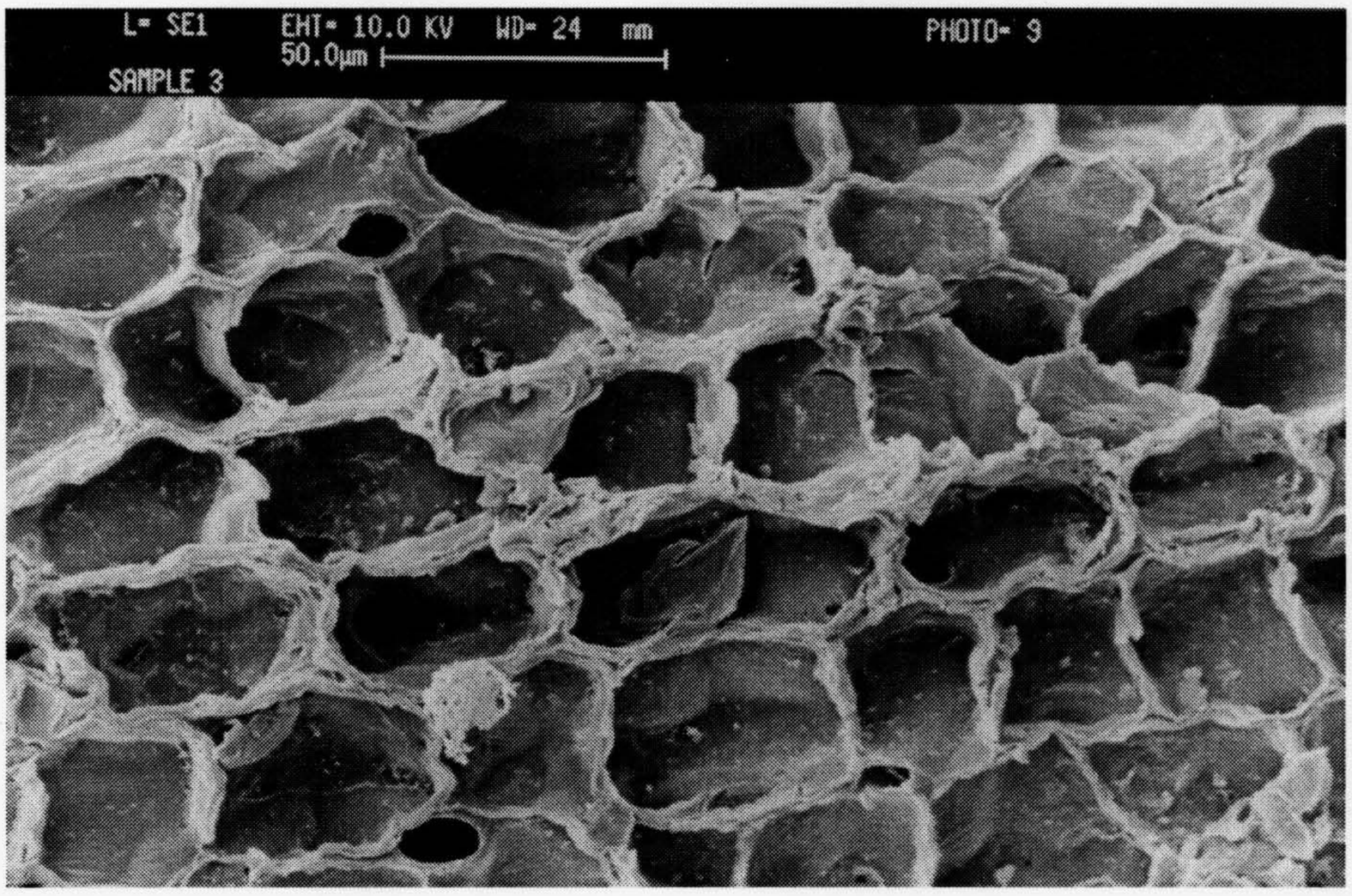

Figure 2.14. SEM topographical image of native *L. flavicans* (Methanol-HCl).

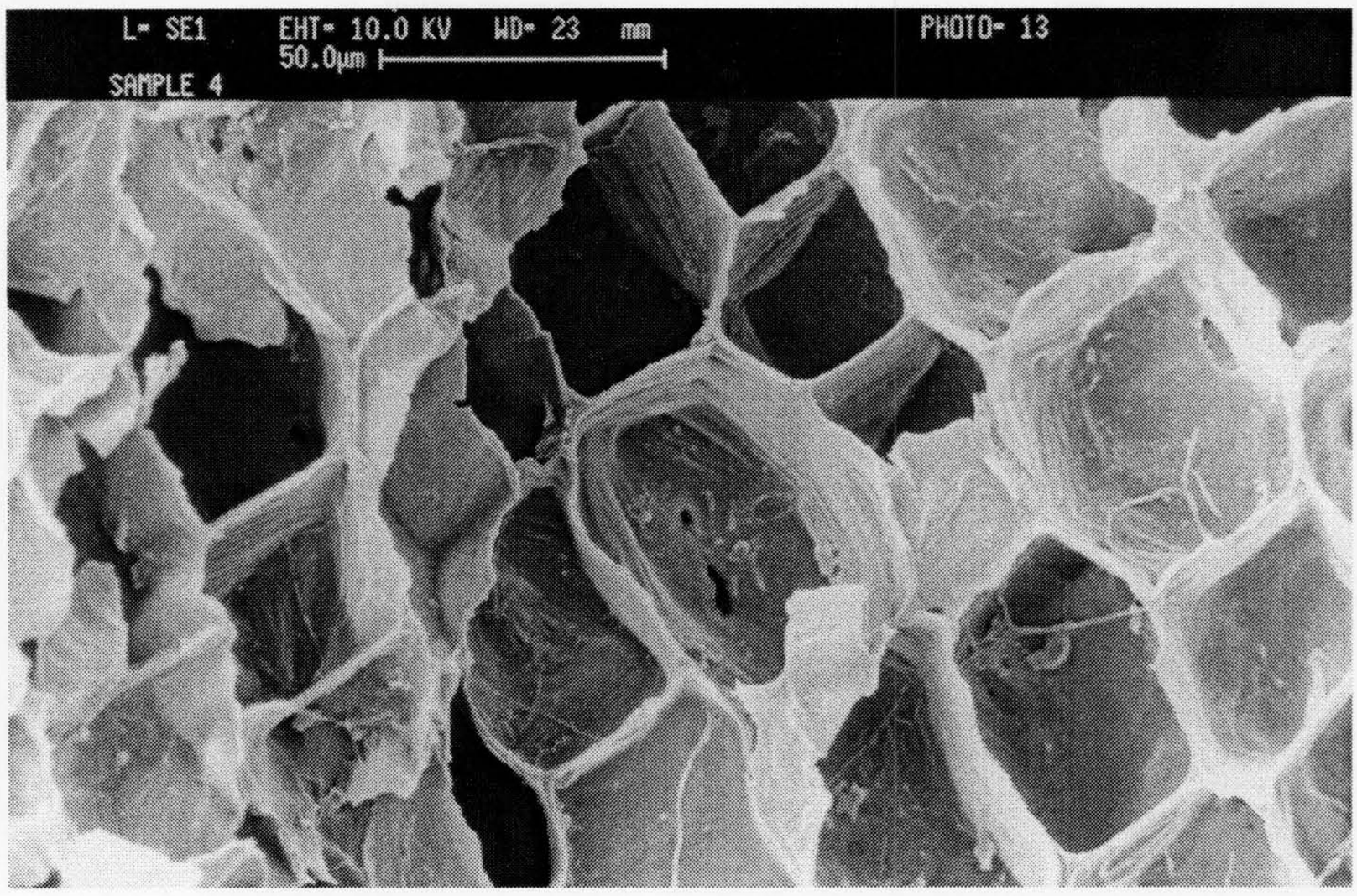

Figure 2.15. SEM topographical image of native *L. flavicans* (Propylene Oxide).

Infra-red Spectroscopy

FT-IR spectra of fucoidan, glucuronic acid, laminarin and mannitol (see Figures 2.16. - 2.19.) were obtained in order to identify characteristic stretching/rotational/bending vibrations associated with functional groups present in algae due to the presence of various polysaccharides constituting the algal cellular matrix (see Tables 2.7. and 2.8.; characteristic peaks found in the various polysaccharides are depicted). The sulphonate groups of fucoidan provide a distinct (C-O-S) vibration between 870-800 cm^{-1} and (S=O) stretching vibration around 1240 cm^{-1}. There was no indication of the presence of sulphonate type groups within the protonated algal matrix of LF, LH and BK (see Figures 2.21. and 2.22.). The spectra for AN showed a slight increase in absorbance around 820 cm^{-1} however at 1240 cm^{-1} there was no characteristic peak, thus indicating absence of the S=O vibration. This information coupled with the results from potentiometric titration data strongly suggest the absence of significant amounts of sulphonate type groups within the algal samples evaluated.

The native algal samples showed a distinct peak at 1736 cm^{-1}; characteristic of C=O stretching vibrations due to carboxylic groups. Native BK showed the highest absorbance peak in comparison with other native algae which suggests the possibility of higher concentrations of carboxylic groups within the sorbent matrix. The native materials also displayed a peak at around 1040 cm^{-1} similar to the peak exhibited by laminarin (see Fig. 2.18.) indicating (C-OH) stretching vibrations as well as (C-O-C) stretching vibrations.

A comparison of the FT-IR spectra of AN and AA-AN indicates a sharper peak at 1740 cm^{-1} by the alginic acid sample (see Fig. 2.20.). Also, intermolecular hydrogen bonding shifts the OH-stretching vibration to 3300 cm^{-1} in the spectra of AA-AN. The native biomass *A. nodosum* shows a vibration peak at 1520 cm^{-1} which is not displayed by the FT-IR spectra of alginic acid. This vibrational frequency is indicative of the presence of primary or secondary amides. The vibrations usually occur in the range 1650-1515 cm^{-1} as a consequence of NH_2 or NH bending; the amide II band. The native material also exhibits a broad absorption band between 1680-1580 cm^{-1} which may be attributed to C=O stretching vibrations of the amide I band. This shoulder to the peak at 1735 cm^{-1} is not displayed by the alginic acid sample nor the other pure polysaccharide samples evaluated (see Fig. 2.20.). LH also displayed a broad shallow peak around 1535 cm^{-1} as well as a peak at 1660 cm^{-1} which was of equal intensity compared with the C=O stretching vibration at 1730 cm^{-1} due to the presence of carboxylate groups. The FT-IR spectra of BK was less conclusive in this regard, with no distinct peaks between 1650-1500 cm^{-1}. Fourest[3] presented an FT-IR spectra of *Sargassum natans* which showed a peak at around 1520 cm^{-1} as well as a shoulder to the peak at 1740 cm^{-1}. However, no reference to groups responsible for these peaks was made in the text. Further evidence supporting the possible presence of amide groups within *A. nodosum* is found in a paper by Kuyucak[41] concerning cobalt sorption by native algae. An IR spectra in the range 4000-400 cm^{-1} for virgin *A. nodosum* showed characteristic bands at 1624, 1419, 1261 and 1036cm^{-1}. The combined effect of double bond stretching vibrations (mainly

C=O) and hydrogen bonding due to amide groups may be responsible for the band between (1650-1620) cm^{-1}.

Propylene oxide treated *A. nodosum* sample showed a reduced intensity peak at 1740 cm^{-1} indicating reduction in carboxyl groups within the algal matrix (see Fig. 2.23.) however, the methanolic-HCl treated sample did not show any discernible change at this frequency. Esterification of the hydroxyl groups would lead to a distinct (C-O-C) stretching vibration. However, the stretching vibration of this system is not greatly different from the C-C-C system[45] . Also since there anyway exists a (C-O-C) group in the six membered ring of alginic acid, discernible shifts or changes in the vibration frequency are unlikely.

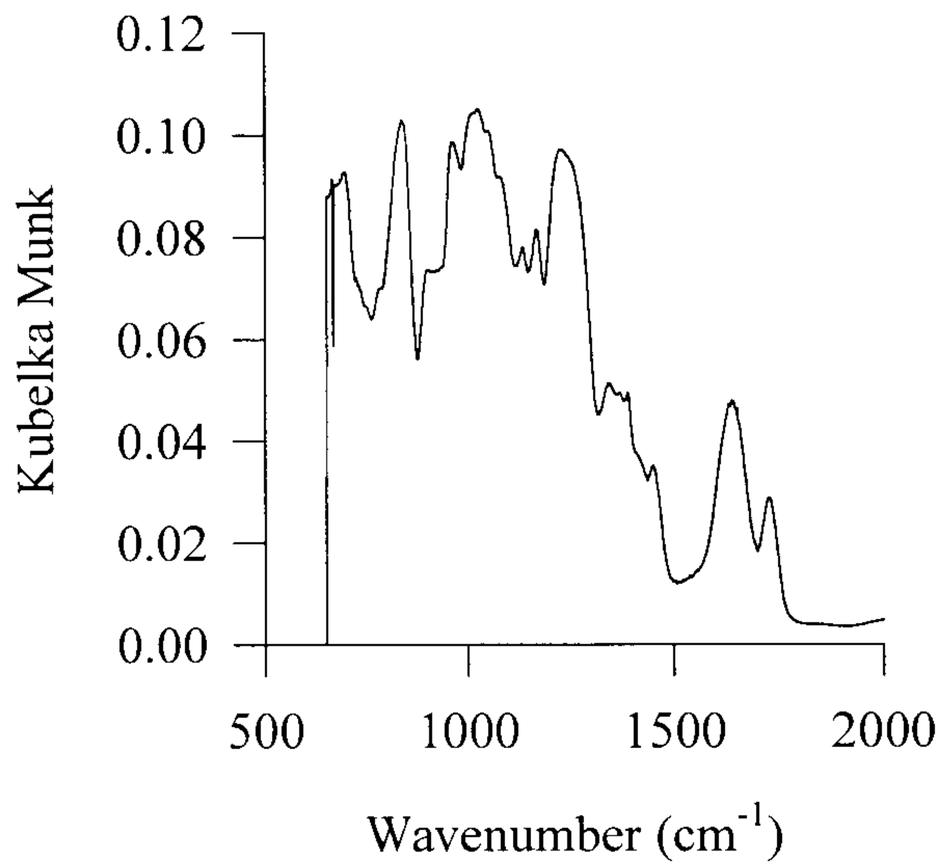

Figure 2.16. Diffuse reflectance FT-IR spectra of Fucoidan.

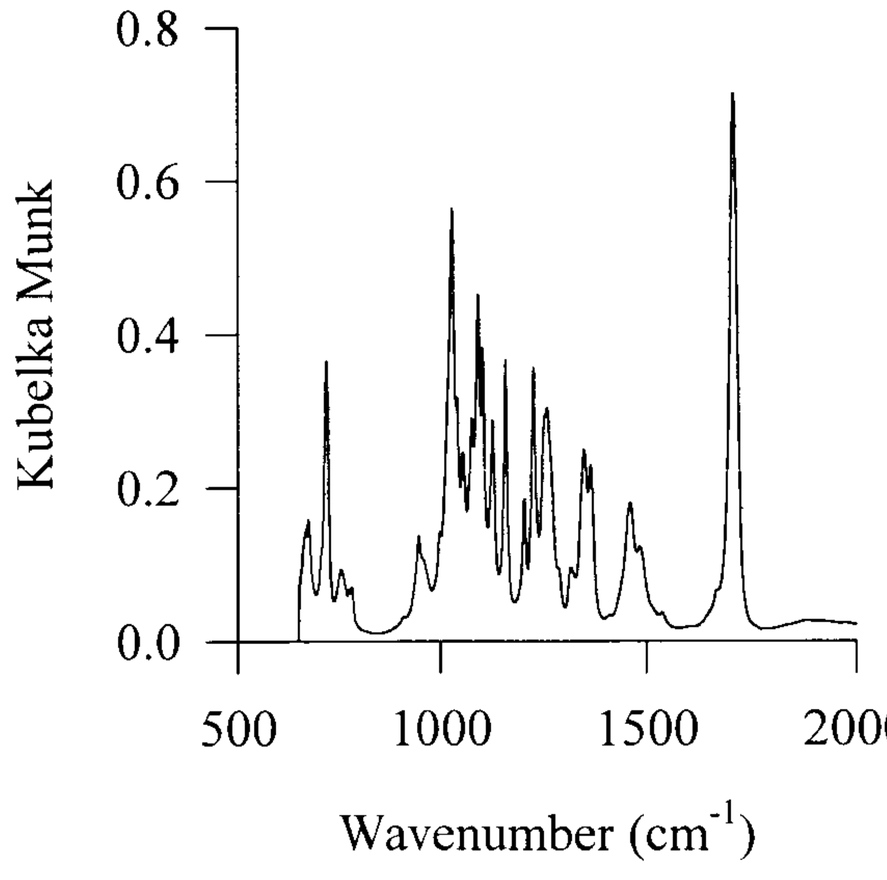

Figure 2.17. Diffuse reflectance FT-IR spectra of Glucuronic acid.

Polysaccharide	Groups	Band, cm^{-1}	Remarks
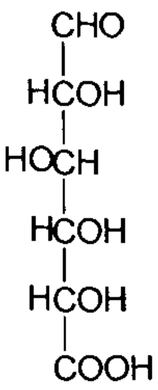 D-Glucuronic acid	O-H stretching	3400	Inter-molecular hydrogen bonding shifts free hydroxyl stretching vibrations from 3650-3584 cm^{-1} to 3550-3200 cm^{-1}.
	C=O stretching	1270-1240	Aldehyde. C-O stretching vibrations in alcohols produces strong band here.
	O-H in-plane bending vibration	1365 & 1347	
	C=O	1710	Carboxyl group C=O stretching vibration. Internal hydrogen bonding shifts the absorption to lower wave numbers (not present in mannitol: see below)
	C=O	1380-1330	C-O stretching in carboxylic acids
	C=O	1285-1210	O-H bending vibration in carboxylic acids
	C=O	1226	C-O stretching vibration band for dimers

Table 2.7. Summary of FT-IR absorption peaks found in D-Glucuronic acid samples.

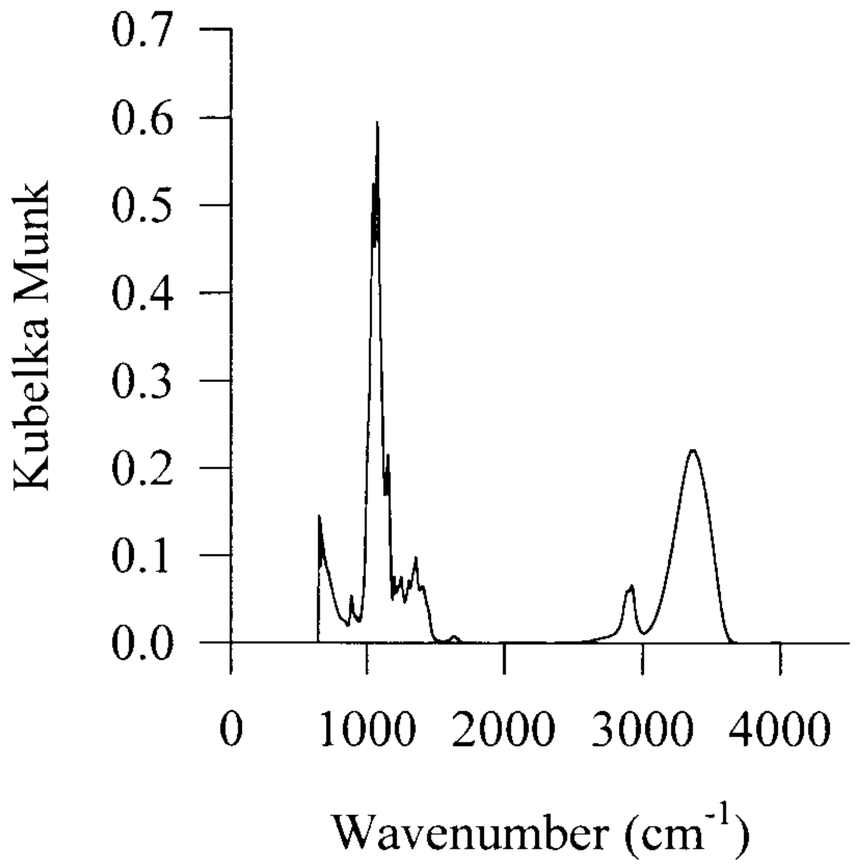

Figure 2.18. Diffuse reflectance FT-IR spectra of Laminarin.

Esterification of the carboxylic groups of alginic acid should lead to two characteristically strong absorption bands arising from C=O and C-O stretching. The intense C=O stretching vibration overlaps with those of acids, and the OH stretching and bending vibrations around 1735 cm^{-1} offers little help in distinguishing the acid from the ester (See Fig. 2.23.).

Polysaccharide	Groups	Band, cm^{-1}	Remarks
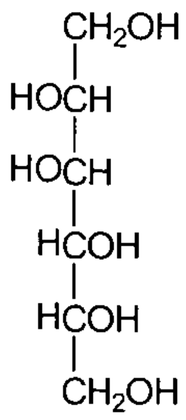	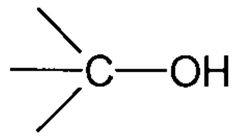	1125-1040	C-O stretching vibration Note: Absence of C=O vibration around 1730 cm^{-1}, characteristic of aldehyde and carboxylic groups
Mannitol	-O-H	1320-1260	O-H bending
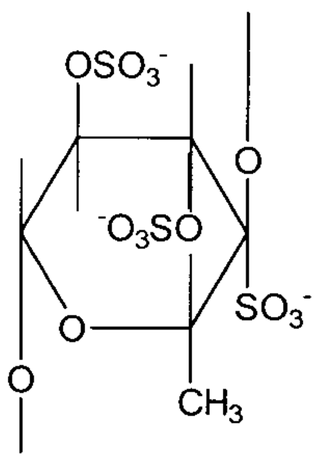	C-O-S	870-800	C-O-S vibration characteristic of ester-sulphate, 820 cm^{-1} (sulphated primary hydroxyl), 830 cm^{-1} (sulphated equatorial hydroxyl) and at 850 cm^{-1} (sulphated axial hydroxyl)
Fucoidan	S=O	1240	characteristic S=O stretching vibration
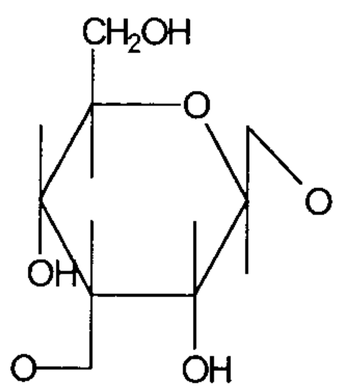	-OH	3600-3000	often broad, lower the frequency, higher the hydrogen bonding
Laminarin	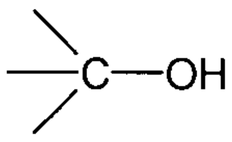	1060	C-O stretching vibration
	C-O-C	1060	C-O stretching vibration

Table 2.8. Summary of FT-IR absorption peaks found in Mannitol, Fucoidan and Laminarin samples.

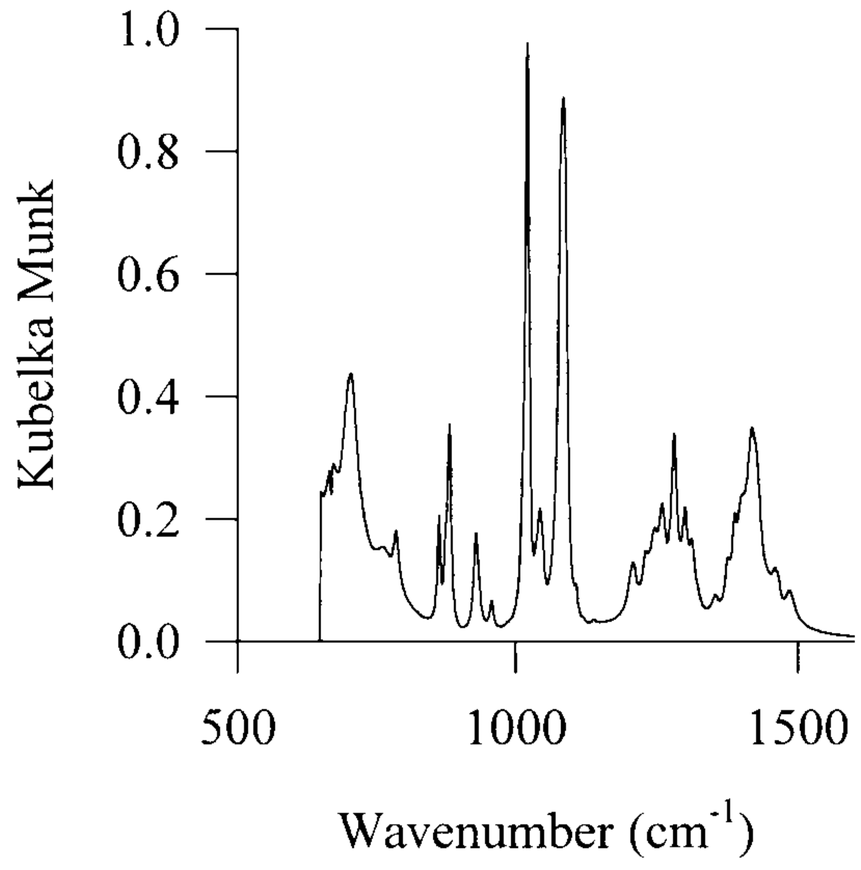

Figure 2.19. Diffuse reflectance FT-IR spectra of Mannitol.

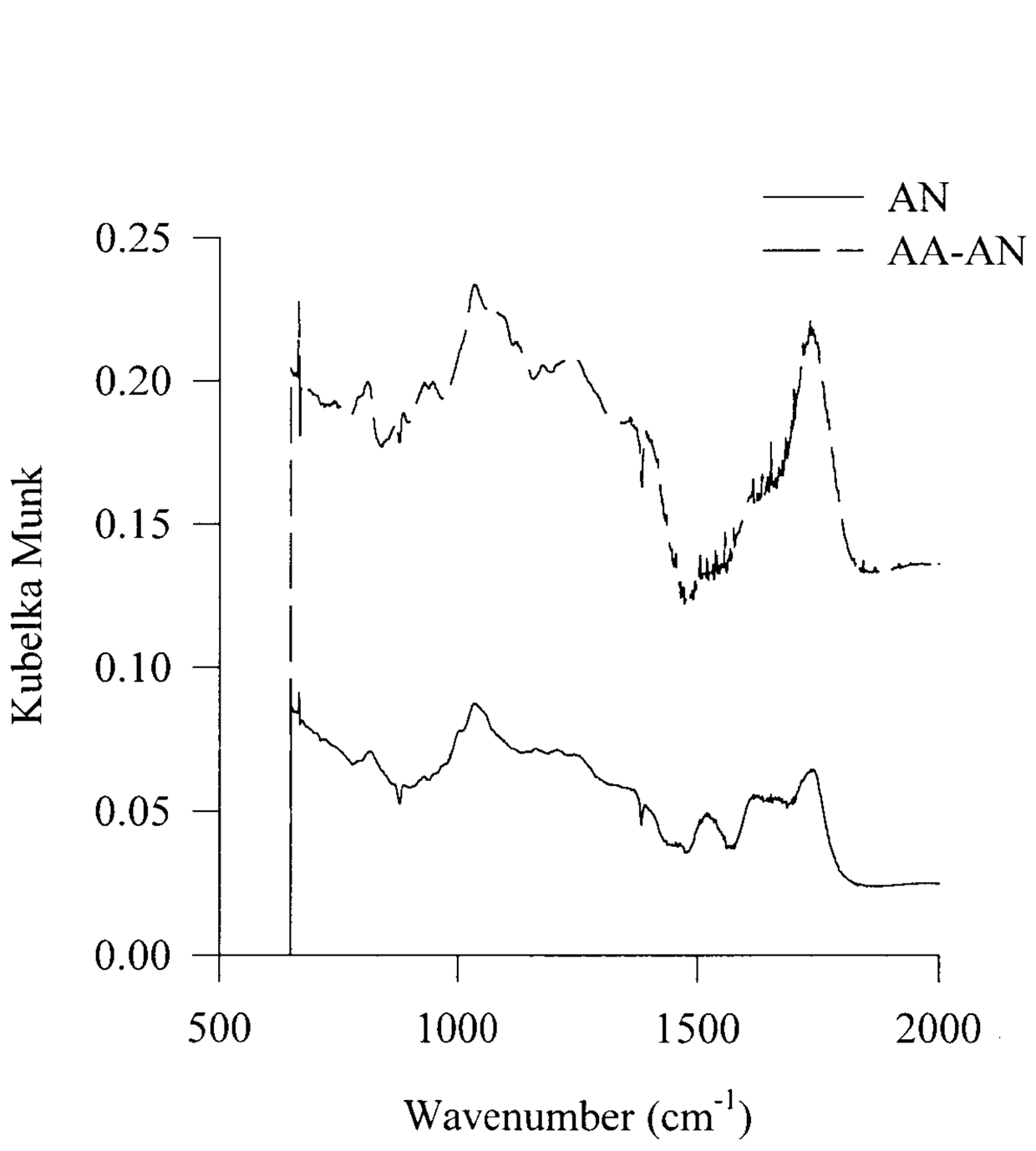

Figure 2.20. Diffuse reflectance FT-IR spectra of AN and AA-AN.

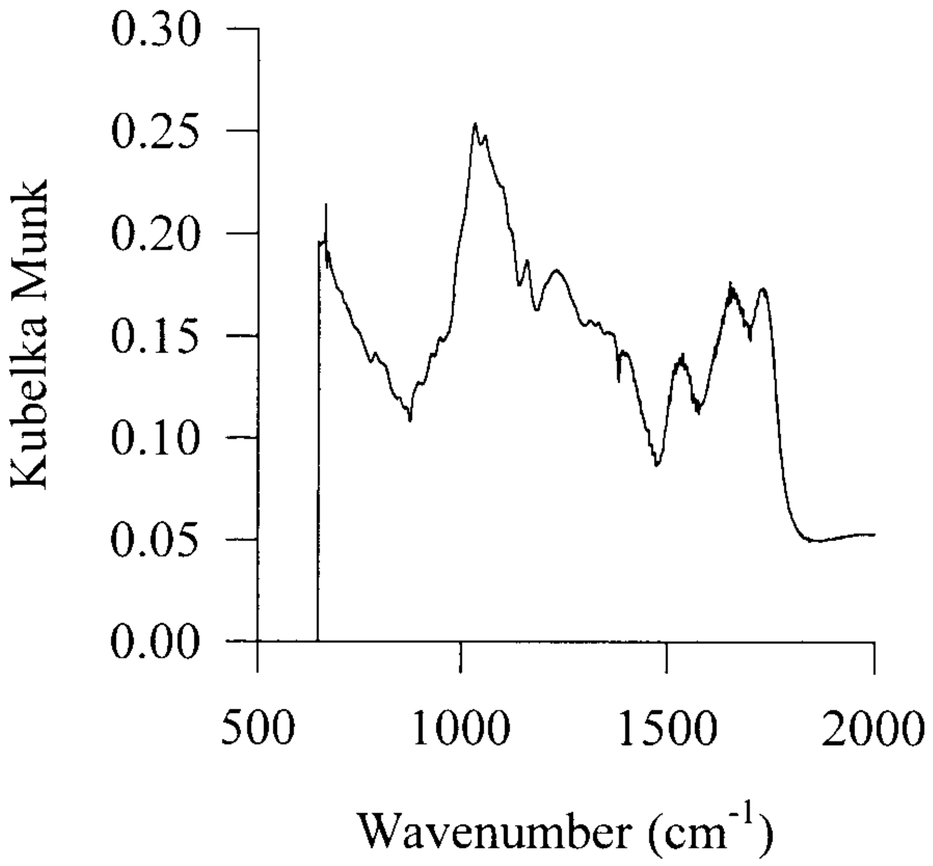

Figure 2.21. Diffuse reflectance FT-IR spectra of *L. Hyperborea*.

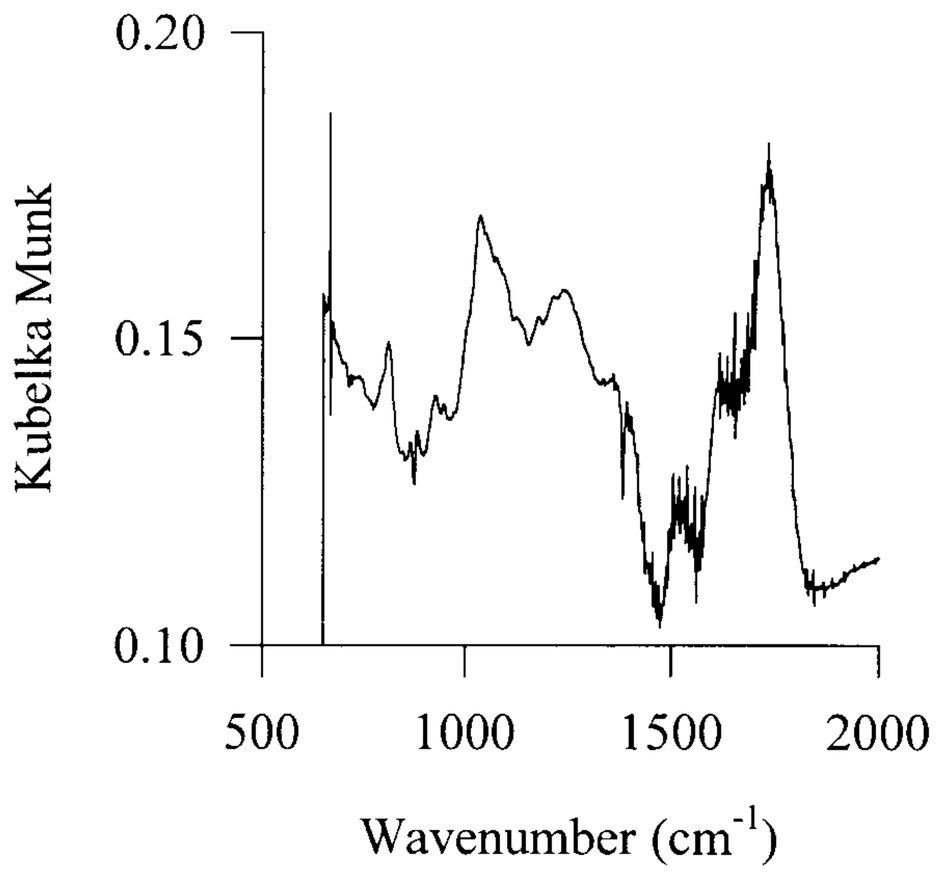

Figure 2.22. Diffuse reflectance FT-IR spectra of *D. Potatorum*.

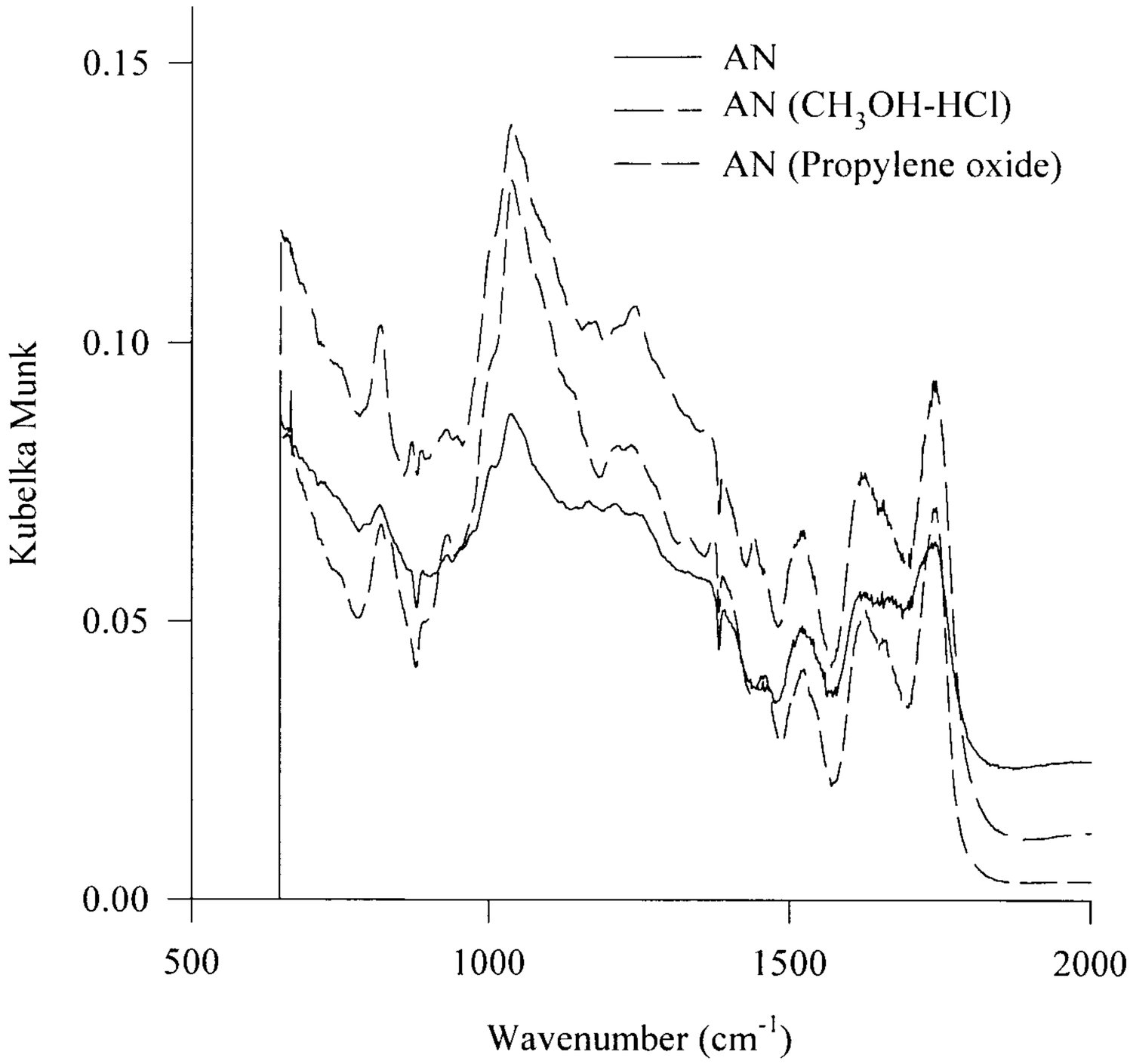

Figure 2.23. Diffuse reflectance FT-IR spectra of AN (Comparison of chemically modified samples).

Section 2.4. Conclusions

Native algal biosorbents showed significant swelling upon rewetting. This swelling phenomenon is related to the presence of alginic acid within the algal materials; in particular, guluronic acid segments may be responsible for water retention within brown algae. Potentiometric titration of algal samples suggests the presence of weakly acidic groups which dissociate around pH 3 and pH 6. Comparison of native algal samples and a carboxylate cation exchanger for sodium uptake as a function of

external solution pH suggests that carboxyl groups are the dominant metal binding sites within marine algae at solution pH 4. Zeta-potential measurement of the surface charge on algal particles indicates a strongly negative surface potential at pH values greater than pH 3.5. Coincidentally, acid-dissociation pK_a values of algal samples also occur at about the same pH value.

The use of selective esterification is successful in masking the reactivity of carboxyl functional groups. Processed seaweed residue samples also possess similar functionality as in the native precursor. Measurement of methanol release upon hydrolysis of esterified surface groups did not reveal a bidentate copper binding mechanism.

Investigations into the surface morphology of native algal samples reveals a structure devoid of microporosity and possessing very low surface area. In addition, water within the algal structure is rather difficult to remove and the possibility of chemically bound water to the structural polysaccharides of algae is proposed.

IR-spectroscopic studies reveal the absence of sulphonate-type functional groups related to the presence of fucoidan in algae. It is very likely that the washing and protonation procedure, followed during the pre-treatment of algal biomass, is responsible for washing out polysaccharides if present. Their role in the metal-binding properties of algae is therefore minimal.

In conclusion, carboxyl groups associated with the structural polysaccharide alginic acid are the dominant functional groups and are reactive during metal sorption in near-neutral aqueous solutions.

Section 2.5. Nomenclature

F	Faraday constant (C mol^{-1})
I	ionic strength (mol l^{-1})
K	acid-dissociation constant of acidic sites (mol dm^{-3})
N	number of acidic sites (mol g^{-1})
R	gas constant (J mol^{-1} K^{-1})
T	temperature (K)
V_D	dry volume (cm^3 g^{-1})
V_S	swollen volume (cm^3 g^{-1})
X_o	number of deprotonated acidic sites (mol g^{-1})

Greek Letters

Γ_i	surface charge of species "i" (mol m^{-2})
α	degree of dissociation of acidic sites (-)
ε	permittivity (F m^{-1})
ρ_D	dry bulk density (g cm^{-3})
ρ_S	wet bulk density (g cm^{-3})
σ_d	charge density in the diffuse layer (C m^{-2})
σ_H	surface charge density due to adsorbed protons (C m^{-2})
σ_{in}	intrinsic surface charge density (C m^{-2})
σ_o	charge density on biosorbent surface (C m^{-2})
σ_p	total particle charge density (C m^{-2})
σ_S	surface charge density in the Stern layer (C m^{-2})
ψ_d	electrical potential in the diffuse layer (V)
ψ_o	surface potential (V)

Section 2.6. References

1. Percival, E. and McDowell, R. H. 1967, Chemistry and enzymology of marine algal polysaccharides, Academic Press, London and New York.
2. Helfferich, F. 1995, Ion Exchange, Dover Publications Inc., New York.
3. Fourest, E. and Volesky, B. 1995, Environ. Sci. Technol., vol. 30, 277.
4. Schiewer, S. and Volesky, B. 1997, Environ. Sci. Technol., vol. 31, 1863.
5. Schiewer, S. and Volesky, B. 1995, Environ. Sci. Technol., vol. 29, 3049.
6. Seki, H. and Suzuki, A. 1998, J. Colloid Interface Sci., vol. 206, 297.
7. Percival,E. and Ross, A. G. 1948, J. Soc. Chem. Ind., vol. 67, 420.
8. Gregory, J. D. 1960, Archs. Biochem. Biophys., vol. 89, 157.
9. Brown, E. G. and Hayes, T. J. 1952, Analyst, Lond., vol. 77, 445.
10. Tollens, B. 1908, Ber., vol. 41, 1788.
11. Lefevre, K. W. and Tollens, B. 1907, Ber., vol. 40, 4513.
12. Bitter, T. and Muir, H. M. 1962, Anal. Biochem., vol. 4, 330.
13. Blumentrantz, N. and Asboe-Hansen, G. 1973, Anal. Biochem., vol. 54, 484.
14. Kennedy, J. F. and Bradshaw, I. J. 1984, Brit. Polym. J., vol. 16, 95.
15. Kennedy, J. F. and Bradshaw, I. J. 1987, Carbohydrate. Polymers vol. 7, 35.
16. Kennedy, J. F., Barker, S. F., Jones, P. and Bradshaw, J. F. 1981, Carbohydrate Polymers, vol. 1, 85.
17. Bernde, Y. G., Onoda, G. Y. and De Bruyn, P. L. 1967, Surf. Sci., vol. 8, 448.
18. Yates, D. E. and Thomas, W. H. 1980, J. Chem. Soc., Faraday Trans., vol. 1, no. 76, 9.
19. Cornell, R. M., Posner, A. M. and Quirk, J. P. 1975, J. Colloid Interface Sci., vol. 53, 6.
20. Bowden, J. W., Posner, A. M. and Quirk, J. P. 1977, Aust. J. Soil. Res., vol. 15, 121.
21. Marabini, A. M. and Barbaro, M. 1980, Int. J. Miner. Process., vol. 7, 159.
22. Siffert, B. and Hamieh, T. 1989, Colloids and Surfaces, vol. 35, 27.
23. Corapcioglu, M. O. and Huang, C. P. 1987, Carbon, vol. 25, no. 4, 569.
24. Lau, A. C., Furlong, D. N., Healy, T. W. and Gvieser, F. 1986, Colloids and Surfaces, vol. 18, 93.
25. Parker, G. A. 1978, In chemical oceanography, Riley, L. P. and Skirrow, G., (eds.), Academic Press.
26. Sposito, G. 1998, Environ. Sci. Technol., vol. 32, no. 19, 2815.
27. Everett, D. H. 1972, Pure Appl. Chem., vol. 31, 578.
28. Lopez-Rapon, M. V., Moraco-Cartilla, C., Rivera-Utrilla, J. and Hidalgo-Alvarez, R. 1993, Carbon, vol.31, no.5, 815.
29. Schut, P. H., Evans, R. D. and Scheider, W. A. 1986, Water air soil Pollut., vol.28, 225.
30. Walter, R. J., Sherman, R. M. and Lee, C. Y. 1983, J. Food Sci., vol.48, 1006.
31. McFeeters, R. F. and Armstrong, S. A. 1984, Anal. Biochem., vol. 139, 212.
32. Steiner, A. B. and McNeely, W. H. 1951, Ind. Eng. Chem., vol.43, 2073.
33. McDowell, R. H. 1986, Properties of alginates, Kelco International, commercial literature.
34. Haug, A. and Larsen, B. 1958, Acta. Chem. Scand., vol.12, 650.

35. Ragan, M. A. and Craigie, J. S. 1976, Can. J. Biochem, vol.54, 66.
36. Slabbert, N. 1992, In plant polyphenols; Hemmingway, R. H. and Lako, P. E. (eds.), Plenium Press, New York.
37. Fagerberg, W. R., Moon, R. and Truby, E. 1979, Protoplasma, vol. 99, 247.
38. Holan, R. and Volesky, B. 1994, Biotechnol. Bioeng., vol.43, 1001.
39. Chapman, A. R.O. 1978, Phaeophyta, In CRC handbook of microbiology, vol.2, 2nd edition, Laskin, A. I. and Lachevalier, H. A. (eds.), CRC Press, Boca Raton, Fl.
40. Kuyucak, N. and Volesky, B. 1989, Biotechnol. Bioeng., vol.33, 815.
41. Kuyucak, N. and Volesky, B. 1989, Biotechnol. Bioeng., vol.33, 823.
42. Grasdalen, H., Larsen, B. and Smidsrod, O. 1981, Carbohydr. Res., vol.89, 179.
43. Malvern Instruments Commercial literature. 1997, Getting started manual.
44. Gardea-Torresdey, J. L., Becker-Hapak, M. K., Hosea, J. M. and Darnall, D. W. 1990, Environ. Sci. Technol., vol. 24, no. 9, 1372.
45. Silverstein, R. M., Bassler, G. C. and Morrill, T. C. 1993, Spectrometric identification of organic compounds, 5th edition, John Wiley & Sons, Inc., New York.
46. Matheickel, J. T. and Yu, Q. 1996, Wat. Sci. Tech., vol. 34, no. 9, 1.
47. Fisher, F. G. and Dorfel, H. Z., 1955, Physiol. Chem., vol. 302, 186.
48. Kuyucak, N. 1987, Algal biosorbents for gold and cobalt, Ph.D. Thesis, McGill University, Canada.
49. Marinsky, J. A., Ephraim, J. 1986, Environ. Sci. Technol., vol. 20, 349.
50. Liu, F. G., Marinsky, J. A. 1993, React. Poly., vol. 19, 27.
51. Tipping, E., Backer, C. A. and Hurley, M. A. 1988, Water Res., vol. 22, 597.
52. Crist, R.H., Oberholser, K., McGarrity, J., Crist, D.R., Johnson, J.K. and Brittsan, J.M.,1992, Environ. Sci.Technol., 26: no.3, 496-502.
53. Lee, H.S., and Volesky, B., 1997, Water Res., vol. 31, no.12, 3082.
54. Kuyucak, N., and Volesky, B. 1989, Biotechnol. Bioeng., vol. 33, no.7, 809.
55. Fourest, E., Serre, A. and Roux, J. C. 1996, Toxicol. Environ. Chem., vol. 54, no. 1-4, 1.
56. Kantor, T. G. and Schubert, M. 1957, J. Am. Chem. Soc., vol.79, 152.
57. Gregg, S. J. and Sing, K. S. W. 1982, Adsorption, surface area and porosity, Academic Press, London.
58. Barrett, E. P., Joyner, L. G. and Halenda, P. P. 1951, J. Am. Chem. Soc., vol.13, 373.
59. Schull, C. G. 1948, J. Am. Chem. Soc., vol.70, 1405.

Heavy Metal Biosorption

"The important thing in science is not so much to obtain new facts as to discover new ways of thinking about them"

(Sir William Lawrence Bragg 1890-1971)

Chapter 3

Heavy Metal Biosorption

This chapter compares the performance of native and dealginate marine algae in sequestering heavy metal ions from aqueous solutions. Single metal biosorption isotherms for copper, cadmium, nickel and zinc ions have been obtained under carefully controlled experimental conditions. Study of proton-metal interactions with the algal surface has yielded information regarding the mechanisms of metal biosorption. The equilibrium sorption phenomenon has been modeled using a surface complex formation model.

Section 3.1. Theory and Literature Review

Sorption Performance of Biosorbents and Mathematical Description

Chapter 1 discussed metal biosorption from copper, cadmium, nickel and zinc bearing solutions by various marine algae. This section provides an overview of recent literature related to the mathematical description of equilibrium sorption isotherms. Conventional attempts at modeling ion exchange equilibria involve the use of chemical model equations such as the Langmuir and Freundlich relationships (see Table 3.1.).

It is important to note that these relationships do not reflect the physico-chemical mechanisms involved in biosorption. For all practical purposes, they are merely a convenient mathematical representation of the relationship between (q^*) vs. (C_{eq}) as experimentally observed. These relationships cannot offer an insight into the sorption mechanism. The usual concept of a porous sorbent with a large surface area does not closely resemble the appearance and behavior of biosorbent particles (see chapter 2; surface area and pore size distribution). Biosorbents with crosslinked, highly swollen gel-type structure may be easily penetrated by minute ions and protons. Ion exchange, which has been found to play a vital role in biosorption[1], involves exchange

of at least one ion from within the molecular structure of the sorbent with a counterion from the external solution. This exchange between surface ions and the aqueous medium needs to be accounted for during modeling of the biosorption phenomenon.

Model	Equation	Notes
Langmuir	$q^* = q_m^* \frac{bC_{eq}}{1+bC_{eq}}$	q_m^* is the maximum sorbate uptake under the given conditions, mmol g^{-1} b is a coefficient related to the affinity between the sorbent and sorbate.
Freundlich	$q^* = kC_{eq}^{\left(\frac{1}{n}\right)}$	k and n are Freundlich constants.
Brunauer-Emmett-Teller (BET)	$q^* = \frac{BQC_f}{(C_s - C)\left[1+(B-1)\left(\frac{C_{eq}}{C_s}\right)\right]}$	C_s is the saturation constant of the solute. B is a constant relating to the energy of interaction with the surface. Q is the number of moles of solute adsorbed per unit weight of adsorbents in forming a complete monolayer on the surface.
Dubinin-Radushkevich (DR)	$\ln q^* = \ln q_m^* - BE^2$ $E = RT\ln\left(1+\frac{1}{C_{eq}}\right)$	B is a constant related to the sorption energy. E is Polanyi potential.

Table 3.1. Classical model equations used to describe sorption equilibria.

Kratochvil et al.[1] modeled the biosorption of Cr^{3+} ions onto the seaweed *Sargassum*. The predominant species in solution between pH 3-4 was found to be the hydrolysis product $Cr(OH)^{2+}$ accounting for over 90% of all Cr^{3+} ions in solution. Protons undergo several reactions with the biomass surface so that pH changes occurring in solution do not provide information on the stoichiometry of the exchange. Ca^{2+}

loaded *Sargassum* yielded a Cr^{3+}:Ca^{2+} exchange ratio of 1:1 indicating $Cr(OH)^{2+}$ cations are sorbed by the algal particles. A mathematical expression for the sorption isotherm of a divalent cation sorbing onto *Sargassum* in the presence of protons is proposed. The model predicts the equilibrium of proton and metal ion binding as a function of metal ion concentration, pH and ionic strength. Electrophoretic mobility measurements of algal particles indicates a significant negative charge when the concentration of protons or covalently bound divalent metal ions is low (see chapter 2). Obviously, this charge must lead to electrostatic attraction of cations[2]. Modeling the influence of Na^+ in the biosorptive system may be accomplished by the introduction of a binding constant for Na^+ ions[3]. The advantage of this approach is that binding of such species can be calculated using a multicomponent isotherm. One disadvantage however, concerns the purely empirical nature of the binding constant which does not reflect the electrostatic nature of the Na^+ binding[4]. The effect of changes in background electrolyte can be described in terms of electrostatic models. Various attempts to describe the electrostatics have been adopted (see Table 3.2.). These range from numerical solutions of the Poisson-Boltzmann equation for spherical- and cylindrical-shaped particles[5,6] to Donnan-models in which the humic material is treated as a distinct electrically neutral phase[7]. The Donnan approach is computationally simple since it does not involve the solution of the Poisson-Boltzmann equation.

The Donnan-model[8] has been employed to predict the interaction of protons and metal ions with organic polyelectrolytes, including humic substances[9] and alginic acid[10]. A Donnan-type model for non-specific binding of electrolyte ions is combined with the non-ideal competition adsorption model for specific binding to represent ionic binding to humic substances[11]. Site heterogeneity, electrostatic interactions and multicomponent metal ion binding is accounted for in the model. The cation binding in humics is assumed to occur through specific interactions between the cation and negatively charged surface functional groups (described by non-ideal competitive adsorption) and by non-specific Coulombic binding at any residual negative charge (described by the Donnan-model). The specific binding is described by assuming a continuous distribution of affinity constants for the metal binding sites. Electrostatic

effects are incorporated into the model by using the concentration of ions near the binding sites rather than concentrations in the bulk solution. A bimodal distribution of proton affinities due to carboxylic and phenolic groups is obtained for humic and fulvic acids. In the Donnan-model, the humic material is considered to behave as an electrically neutral phase having a distinct volume. Throughout this volume there exists a uniform, averaged electrostatic potential designated as the Donnan potential, ψ_D. The Donnan-potential is dependent on a single unknown parameter; the Donnan volume, however, a critical aspect of the model relates to the way the Donnan-volume varies, or does not vary with changes in the solution chemistry. Benedetti et al.[7], found the Donnan volume to be highly sensitive to changes in ionic strength. The variation in Donnan-volume is assumed to follow an empirical relation in which a linear decrease of the logarithm of the particle volume with logarithm of the ionic strength is used. The binding of metal ions (Ca^{2+}, Cd^{2+}, Cu^{2+}, Pb^{2+}) to humic acid is described well by the model, however, the model requires a large number of fitting parameters. The model takes into account the very different behavior of different ions (H^+, Cu^{2+}, Cd^{2+}, Ca^{2+} etc.) and introduces the concept of ion-specific non-idealities.

Xue et al[12] used a Helmholtz model with constant capacitance to describe the charged interface of algal particles *Chlamydomonas rhienhardii*. With constant capacitance, it is not possible to predict ionic strength effects. Metal binding at different ionic strengths require a new value for the capacitance to be determined.

Tipping[13] took three possible competition mechanisms into account in order to interpret the binding of trace metals and alkaline earth cations (Mg^{2+}, Ca^{2+}) by fulvic-type humic substances. These are:

- Direct competition at discrete sites
- Competition for counterion accumulation
- Reduction in net electrical charge on the humic molecule due to alkaline earth cation binding to certain sites, thereby reducing electrostatic contributions to trace metal binding at other sites.

The advantage of this model is the economical way of using relatively few fitting parameters for the prediction of a wide range of experimental conditions. Only one or two parameters are needed in order to predict the distribution of ions within the sorbent-Donnan volume at different ionic strengths. Unfortunately, the relationship between Donnan-volume and ionic strength is empirical[13].

Schiewer and Volesky[2] propose a model to compare titrations of *Sargassum* and alginate at different ionic strengths with predictions by Donnan-models. Influence of ionic strength on the swelling of algal particles is accounted for by a simple linear relationship. Carboxyl groups are the sole specific ion binding sites used in the model. The total number of metal binding sites, the equilibrium constant for proton binding (obtained from potentiometric titrations) and one further parameter are necessary to account for the effect of ionic strength. The third parameter is the Donnan-swollen volume of algal particles. The model fits proton-binding data reasonably well. Another paper[14] extended the model to predict the equilibrium of proton and metal ion binding as a function of metal ion concentration, pH and ionic strength was carried out. This model is able to predict the competitive effects of Ca^{2+} ion during Cd^{2+}/H^{+} exchange.

A much simpler approach to predict multi-component metal biosorption equilibria using a Langmuir model proved unsuccessful[15]. Equilibrium constant values derived from binary exchange systems differed from values in ternary systems. The biosorption system is defined as non-ideal. The predictive power of the multi-component Langmuir model is relatively restricted.

Model/Reference	Type of Binding	Local isotherm	Affinity Distribution	Particle Size & Shape	Electrostatics/Model	Critical Parameters
NICA-Donnan Kinniburgh et al.[11]	Monodentate	Henderson-Hasselbach/Rudzinski	Continuous, bimodal quasi-Gaussian	Not considered	Donnan	Donnan volume
Fully Coupled Electrostatic Milne et al.[5,16]	Monodentate	Langmuir	Continuous, bimodal quasi-Gaussian	Cylindrical; single equivalent radius	Poisson-Boltzmann equation for cylinders	Equivalent radius of cylinder
Model V Tipping & Hurley[17] Tipping[18]	Monodentate + Bidentate	Langmuir	Bimodal, discretized	Not considered	Donnan	Empirical P factor relating proton charge to ionic strength
Oligo-electrolyte model Bartschat et al.[6]	Monodentate	Langmuir	Discrete: 3 sites for protons 2 sites for copper	Two classes of spheres	Poisson-Boltzmann equation for spheres	Radii of spheres and the relationship between charge and the electrostatic (Boltzmann factor)
Polyelectrolyte model Barak and Chen[19]	Monodentate	Langmuir	More than a single type of group	Cylinders; radius varies with charge	Poisson-Boltzmann equation for cylinders	Equivalent radius of cylinder
Polyelectrolyte model Ephraim & Marinsky[20]	Monodentate + Bidentate (bidentate recognized but not formulated)	Langmuir	Three major sites + one minor site for H^+ binding	Not considered	Donnan (but obscure)	1M curve

Table 3.2. Comparison of the approaches used in some models for metal ion binding by polyelectrolytes (e.g. humic substances).

Chen and Yiacoumi[21] successfully predicted the surface charge and equilibrium biosorption experimental data using a "Two-pK Basic Stern Model". The surface complexation model (SCM) accounts for the effects of pH, ionic strength, concentration of metal ions as well as other factors. Three processes occur simultaneously which are responsible for metal-biosorbent interactions:

- Surface ionization
- Complex formation
- Formation of an electrostatic double layer adjacent to the sorbent surface

The parameters required for model description include:

- Surface area of biosorbents
- Concentration of surface functional groups
- Equilibrium constants of surface protolysis and biosorption reactions
- Capacitance of the electrostatic double layer

The surface charge of biosorbent particles is obtained from potentiometric titrations. Two different sets of equilibrium constants of metal ion biosorption reactions are used for two different ionic strengths. The model is not capable of predicting the effect of ionic strength with a unique set of parameters. The model successfully predicts the effect of pH on metal ion biosorption by calcium alginate[21].

In the current study, the surface complex formation model (SCM) developed by Dr. W. Holl and his co-workers at Karlsruhe research center, Germany, has been employed to describe metal equilibrium biosorption in marine algae. The model has been used by the author in its entirety. The author does not claim any credit for its development. All programs and files were supplied by Dr. Holl and the model has been used with his consent. The model was originally developed for the study of ion exchange equilibria on weak acid resins (the following section is based on the paper by Holl et al.[22]).

The principal features of the surface complex formation model along with associated assumptions are outlined below.

1. An electric field is generated normal to the biosorbent surface due to electrical charges on dissociated functional groups.
2. Counter-ions are arranged in characteristic individual layers, called Stern layers.
3. The sequence of the layers (in case of multi-component equilibria) is in accordance with the selectivity series[23].
4. Protons interact with the surface such that they lie within the surface plane.
5. No interactions between counter-ions in the same layer or between adjacent layers occurs.
6. The biosorbent matrix is modeled as a plane sheet with a hypothetical surface area.
7. Surface functional groups are uniformly distributed across this surface (see Fig. 3.1.).
8. Swelling and/or shrinking of the biosorbent is ignored.

SCM regards the biosorbent as a monofunctional ion exchanger. Only reactions with weakly dissociated carboxyl groups are accounted for. The contribution of other surface groups including phenolic-type groups (identified during algal characterization; see chapter 2) have been ignored. The gross simplification of the biosorbent process is acknowledged, however, in order to initially assess the suitability of the model, this approach was considered appropriate. Otherwise, formulation of the model equations would have been a lot more complicated.

Apart from an ordered presence of counter-ions situated in the Stern layers, a diffuse layer of co-ions and counter-ions is located in a layer adjacent to the biosorbent surface (see Fig. 3.1.). The negative charge due to dissociated functional groups result in the presence of a negative surface potential ψ_S. This potential is lowered to $\psi_{St,n}$ due to counter-ions in the Stern layers, to ψ_d in the diffuse layer and finally to zero in the free solution[22].

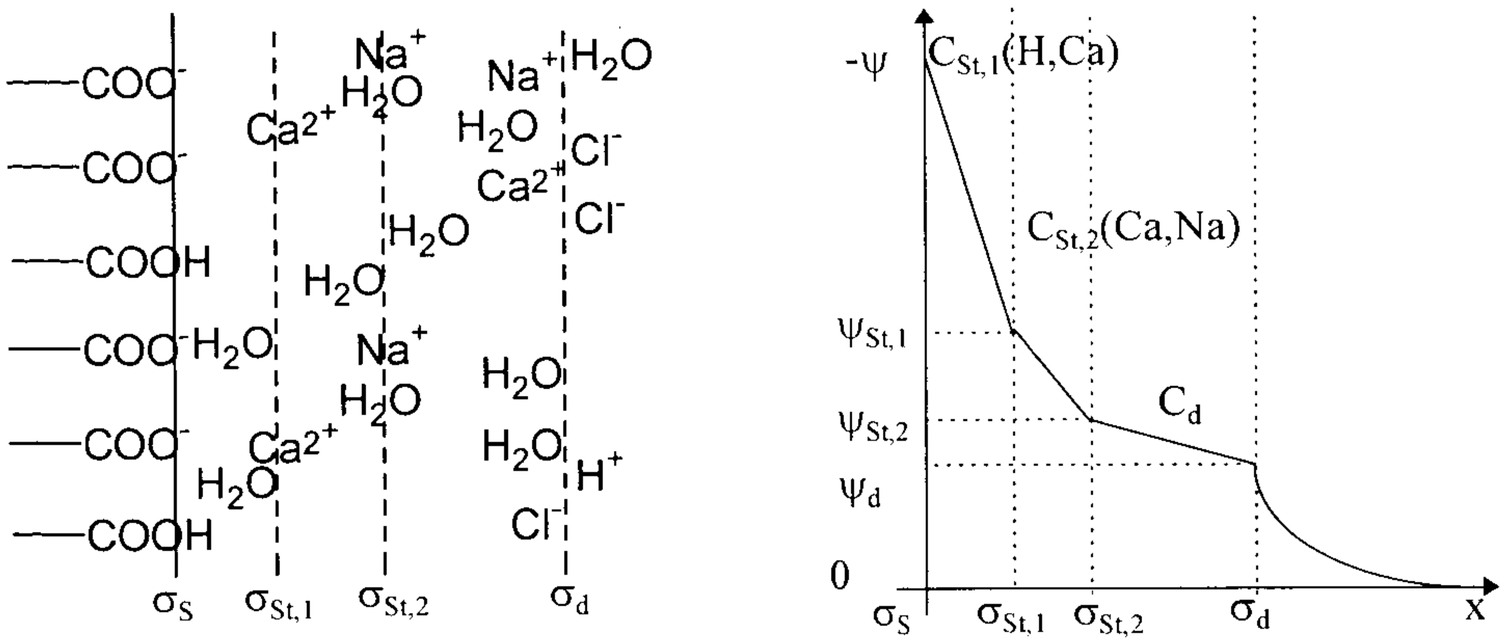

Figure 3.1. Schematic of biosorbent surface, counter-ions, sorption layers and surface potentials for the ternary exchange $H^+/Na^+/Ca^{2+}$.

Counter-ions located in individual Stern layers impart a surface charge density. As a consequence, any two layers form an electric capacitor and the biosorbent may be likened to a series of capacitors. Counter-ions interact with fixed sites on the biosorbent surface forming "surface complexes". These surface complexes are characterized by complex formation constants. Previous characterization studies of algal biosorbents suggests that the biosorbents may be represented as bivalent acids (refer to Chapter 2).

Considering binary exchange (Me^{2+}/H^+), there is only one Stern layer in which Me^{2+} ions are located. H^+ ions are sorbed directly onto the surface, forming undissociated carboxylic groups. The binding of protons and interaction of Me^{2+} ions with carboxylic-acid groups on the biosorbent surface may be considered as equilibrium reactions which are described by the mass action law:

$$R\left(COO^-\right)_2 + 2H^+ \leftrightarrow R(COOH)_2 \qquad (1)$$

$$K_H = \frac{\left[R(COOH)_2\right]}{\left[R\left(COO^-\right)_2\right]\left[\overline{H^+}\right]^2} \qquad (2)$$

K_H is the constant of the formation of surface complexes $(RCOOH)$. Complexes between $RCOO^-$ and H^+ ions result in undissociated carboxylic groups. $\left[\overline{H^+}\right]$ represents the equilibrium concentration of free protons at the surface, whereas $\left[H^+\right]$ represents free protons in the bulk solution. The Boltzmann-relationship is used to relate the concentration of species (i) as a function of the electric potential ψ_x at a distance x from the biosorbent surface[24]:

$$[i]_x = [i]\exp\left(-\frac{z(i)F\psi_x}{RT}\right) \qquad (3)$$

Combining eqs. (2) and (3), the concentration of undissociated carboxyl groups may be expressed as a function of the concentration of protons in the bulk solution:

$$\left[R(COOH)_2\right] = K_H\left[R(COO)_2^{2-}\right]\left[H^+\right]^2 \exp\left(-\frac{2F}{RT}\psi_s\right) \qquad (4)$$

In an analogous way, the sorption of metal counter-ions (Me^{2+}) may be represented as:

$$R\left(COO^-\right)_2 + \overline{Me^{2+}} \leftrightarrow R(COO)_2\,Me \qquad (5)$$

The constant for the formation of $R(COO)_2\,Me$ complexes is defined as:

$$K_{Me} = \frac{\left[R(COO)_2\,Me\right]}{\left[R(COO)_2^{2-}\left[\overline{Me^{2+}}\right]\right]} \qquad (6)$$

Me^{2+} counter-ions are assumed to be located in a Stern-layer where the electric potential is ψ_{St}. The Boltzmann-relationship provides the interdependence between the concentration of Me^{2+} ions in the Stern layer and those in the free solution:

$$\left[R(COO)_2\,Me\right] = K_{Me}\left[R(COO)_2^{2-}\right]\left[\overline{Me^{2+}}\right]\exp\left(-\frac{2F}{RT}\psi_{St}\right) \qquad (7)$$

Eqs. (4) and (7) provide a relation between the ions in the liquid phase and those bound within the biosorbent as surface complexes. The electric potential values ψ_S and ψ_{St} are as yet unknown; relationships about charge balance have to be considered.

The surface charge density σ_S at the biosorbent surface (see Fig. 3.1.) is related to the electric potentials ψ_S and ψ_{St} and the capacitance $C_{St}(H, Me)$ of the capacitor formed as a consequence of electric potentials at the surface and in the Stern layer:

$$\sigma_S = C_{St}(H, Me)(\psi_S - \psi_{St}) \qquad (8)$$

In a similar way, the charge density in the Stern layer results from:

$$\sigma_{St} = C_{St}(H, Me)(\psi_{St} - \psi_d) \qquad (9)$$

From the condition of electroneutrality:

$$\sigma_S + \sigma_{St} + \sigma_d = 0 \qquad (10)$$

The charge density σ_S at the surface results from dissociated carboxylic groups diminished by groups which form $R(COO)_2\,Me$ complexes:

$$\sigma_S = A\left(-2\left[R(COO)_2^{2-}\right] - 2\left[R(COO)_2\,Me\right]\right) \qquad (11)$$

The charge density σ_{St} in the Stern layer equals the charge equivalents of $R(COO)_2\,Me$:

$$\sigma_{St} = A\left(+2\left[R(COO)_2\,Me\right]\right) \qquad (12)$$

Where the factor A converts molar concentrations to charge densities:

$$A = \frac{FV}{SM} \qquad (13)$$

F = Faraday constant, S = Surface area parameter, V = Volume of liquid, M = Mass of biosorbent.

Integrating the Poisson-Boltzmann distribution provides the relationship of interdependence between ψ_d and σ_d across the entire diffuse double layer:

$$\sigma_d = \int_d^{\alpha} \varepsilon \frac{d^2\psi}{dx^2} dx = -\varepsilon \left(\frac{d\psi}{dx} \right)_{x=d} \qquad (14)$$

If the electric potential term in the Stern layer is known (ψ_{St}), eq.(7) provides the concentration of counter-ions present in this layer. In addition to counter-ions present in the Stern layer, those present in the diffuse layer may be accounted for by integrating across the diffuse layer.

$$[i]_d = \frac{A_o S}{z(i) L} \int_{\psi_d}^{0} \left\{ [i] \left(\exp\left(- Az(i)\psi \right) - 1 \right) \right\} \left\{ \frac{2RT}{\varepsilon \sum_j [j]} \left(\exp\left(- Az(j) - 1 \right) \right) \right\}^{-\frac{1}{2}} d\psi \qquad (15)$$

A charge balance across the diffuse double layer enables quantification of counter-ions which are required for neutralization of negative surface charges:

$$2\left[R(COO^-)_2 \right] = z(H^+)[H^+] + z(Me^{2+})[Me^{2+}]_d \qquad (16)$$

Following mathematical manipulation, the following expression is obtained:

$$[i]_d = \frac{[i]}{z(i)F} \frac{\sigma_d A_o S}{\sum_j [j] F(j,i) L} \qquad (17)$$

The relationships (4, 7, 8-14, 15 and 17) form a set of eleven equations with eleven unknown quantities of the system. This system of non-linear equations was solved numerically using the Newton-Raphson method. Concentrations were corrected for by using the Larsen-Busswell approximation. The numerical solution is outlined in the paper by Horst et al[22].

A logarithmic equilibrium parameter may be defined by taking the ratio of eqs.(3) and (7):

$$K_{Me}^{H} = \frac{K_H}{K_{Me}} = Q_{Me}^{H} \exp\left(2A_o\psi_S - 2A_o\psi_{St}\right) \qquad (18)$$

where:

$$Q_{Me}^{H} = \frac{[R(COOH)_2][Me^{2+}]}{[R(COO)_2][H^+]^2} \qquad (19)$$

Q_{Me}^{H} the equilibrium parameter may be obtained from experimental metal sorption data.

For biosorbents (weak-acid exchangers), the concentration of counter-ions in the diffuse layer may be assumed to be negligible, hence:

$$[R(COOH)_2] = \frac{1}{2} q_H \frac{S}{L} \qquad (20)$$

$$[R(COO)_2\, Me] = \frac{1}{2} q_{Me} \frac{S}{L} \qquad (21)$$

Dividing (20) by (21) gives the ratio:

$$\frac{\left[R(COOH)_2\right]}{\left[R(COO)_2\,Me\right]} = \frac{q_H}{q_{Me}} \qquad (22)$$

Replacing this relationship in eq.(19) and taking logarithms:

$$\log Q_{Me}^{H} = 2\,pH + \log\frac{q_H}{q_{Me}} + \log[\,Me] \qquad (23)$$

Eq.(23) defines a logarithmic equilibrium parameter for the binary exchange of protons against divalent metal ions. From eq.(18), a relationship between Q_{Me}^{H} and the surface complex formation constants may be obtained:

$$\log Q_{Me}^{H} = \log K_{Me}^{H} - 0.8686\,A_o\left(\psi_S - \psi_{St}\right) \qquad (24)$$

Eqs.(8) and (11) provide a relationship for the difference of the unknown potentials:

$$\left(\psi_S - \psi_{St}\right) = \frac{A}{C_{St}\left(H, Me\right)}\left(-2\left[R(COO)_2^{2-}\right] - 2\left[R(COO)_2\,Me\right]\right) \qquad (25)$$

As a consequence of the condition of electroneutrality, the charges of dissociated carboxyl groups have to be balanced by an equivalent number of charges of counter-ions present in the diffuse layer:

$$2\left[R(COO)_2^{2-}\right]=\left[H^+\right]_d=2\left[Me^{2+}\right]_d \qquad (26)$$

If the concentration of protons in the diffuse layer is neglected:

$$-2\left[R(COO)_2^{2-}\right]-2\left[R(COO)_2\,Me\right]\approx q_m y\left(Me^{2+}\right)\frac{S}{L} \qquad (27)$$

where q_{max} is the total capacity of the biosorbent and $y(Me^{2+})$ is the equivalent fraction of the functional sites which are neutralized by "Me^{2+}" ions. Eq. (24) may therefore be written in its final form:

$$\log Q_{Me}^{H}=\log K_{Me}^{H}+0.8686\frac{F^2 q_{\max}}{A_o C_{St}(H,Me)RT}y(Me^{2+}) \qquad (28)$$

Eq.28 is the equation of a straight line relating the logarithmic selectivity coefficient Q_{Me}^{H} as a function of the loadings with ions "Me". A plot of $\log Q_{Me}^{H}$ vs. $y(Me^{2+})$ should result in a straight line, the gradient of which provides the product of the parameters $C_{St}(H,Me)$ and A_o and ordinate the difference of the logarithms of the complex formation constants $\log K_H$-$\log K_{Me}$.

The interdependence of binary and multicomponent parameters is highlighted in the following section. As an example, the case of a ternary system with divalent counter-ions A^{2+}, monovalent counter-ions B^{+} and protons is considered. The selectivity sequence is as follows:

$$H^{+}>A^{2+}>B^{+}$$

therefore, A^{2+} are assumed to be located in the first Stern layer and B^{+} ions in a second Stern layer further from the surface. The difference in potential between the surface and the first Stern layer may now be represented as:

$$\left(\psi_S - \psi_{St,1}\right) = \frac{A}{C_{St}\left(H, Me\right)}\left[-2\left[R(COO)_2^{2-}\right] - 2\left[R(COO)_2 A\right] - 2\left[R(COO)_2 B_2\right]\right] \quad (29)$$

The logarithmic equilibrium parameter may therefore be written as the sum of loadings with A^{2+} and B^{+}:

$$\log Q_A^H = \log K_A^H + 0.8686\frac{F^2 q_{\max}}{A_o C_{St}\left(H, A\right)RT}\left(y(A^{2+}) + y\left(B^{+}\right)\right) \quad (30)$$

Similarly:

$$\log Q_B^A = \log K_B^A + 0.8686\frac{F^2 q_{\max}}{A_o C_{St}\left(A, B\right)RT} y(B^{+}) \quad (31)$$

with:

$$\log Q_B^A = -\log\left[A^{2+}\right] + \log\frac{q_A}{q_B} + 2\log\left[B^{+}\right] \qquad (32)$$

Eq.(31) contains two unknown quantities; $\log K_B^A$ may be written as:

$$\log K_B^A = \log_A^H - \log_B^H \qquad (33)$$

while C_{St}(A,B) is simply written using the relationship of capacitors in series:

$$\frac{1}{C_{St}(H,B)} = \frac{1}{C_{St}(H,A)} + \frac{1}{C_{St}(A,B)} \qquad (34)$$

A comparison of relationships (30) and (31) indicates that the selectivity parameter Q_A^H is a function of the sum y(A^{2+}) + y(B^{+}), whereas Q_B^A is a function of y(B^{+}) only. Therefore, for any Stern layer, the values of Q_j^H may be expressed as a function of metal loadings of the outer sorption layers. Provided, the sequence of layers with counter-ions reflects the correct selectivity sequence of biosorbent for counter-ions, linear relationships are obtained with positive slopes. As a consequence, multicomponent equilibria may be predicted using parameters from binary exchange measurements.

Holl et al.[22] demonstrated that for weakly-acidic carboxyl ion exchange resins, $\log Q_i^H$ did not depend on the ionic strength of the liquid phase. Therefore, the same set of parameters (K_j^i and $C_{St}(H,i)$) holds for any initial condition, a fact which is rather important. If for a ternary exchange system, the values of Q_A^H are plotted vs. $y(A^{2+}) + y(B^{+})$, the slope of the straight line should be the same as in the binary exchange of protons vs. A^{2+}. This agreement is a rather sensitive check of the validity of the model.

Influence of pH and ionic strength on metal biosorption

Crist et al.[25] reported on the interaction between protons in solution and metal-laden algae. Metal ion displacement by protons upon acidification (pH change from 7 to 1) resulted in two distinct inflections; one at ca. pH 5 which was attributed to carboxylate anions and the other at ca. pH 1.5 to sulfate groups. The process of metal-proton exchange was considered to be one of ion exchange. Kuyucak and Volesky[26] suggested that pH affects the solution chemistry of the metal ions as well as the activity of the functional groups in the biomass. This affects the competitive behavior of metal ions for the binding sites within algae. Matheickal et al.[27] found that sorption of lead increased with solution pH and reached a plateau at pH 5. At lower pH values, acidic functional groups of algal polysaccharides were rendered labile by protons competing with metal ions for the binding sites. Aldor et al[28] carefully studied the interaction of protons in solution with cadmium-laden algae. The H^{+}/Cd^{2+} exchange was found to be reversible and a stoichiometric coefficient of 1.24 was obtained. It was suggested that metal uptake by algae was a consequence of coordination and electrostatic interactions. Unfortunately, these measurements were not carried out at high solid/liquid ratios and therefore it is not correct to draw conclusions regarding the mechanisms of proton-metal exchange from the stoichiometric coefficient values obtained. At low solid/liquid ratios, protons in solution may interact with sites within the biosorbent other than those occupied by

divalent metal ions. Thus proton uptake is not necessarily associated with an equivalent release of metal ions even though this might actually be the mechanism of metal sorption. Several researchers have reported release of H^+ or Ca^{2+} into the solution phase due to heavy meal uptake[29]. Kratochvil et al.[29] concluded, that biosorption of Cu^{2+} by *Sargassum fluitans* in both H^+ and Ca^{2+} form may be viewed as an ion exchange process. Difficulty in accurate measurement of H^+ concentrations at low pH values was attributed to the non-bidentate binding relationship obtained from the sorption data. It is quite likely that copper binding by protonated algae is rather more complex than a straight forward H^+/Cu^{2+} ion exchange process. Lee and Volesky[30] studied the affinity series of light metals towards protonated *Sargassum fluitans* and found the proton displacement of Na^+ and Ca^{2+} may be considered as an ion exchange process. The measured stoichiometry of H^+/Na^+ exchange was close to 1 whereas for the H^+/Ca^{2+} system, 1.85 moles of protons were required for 1 mole of Ca^{2+} released.

Selective uptake of metal ions from multi-metal bearing solutions

The literature on metal biosorption from multi-metal bearing solutions is rather scant. Relatively little work has been carried out to investigate the selective behavior of marine algae towards a certain metal ion or groups of metal ions. Holan and Volesky[31] found that the presence of copper and zinc ions in solution had a significant negative effect on cadmium sorption by reinforced *A. nodosum*. Selectivity coefficient values were obtained for the affinity of an alginate for a metal in comparison with sodium[32,33]. High selectivity for copper ions was displayed by alginate derived from *L. digitata* (K=230) and *L. hyperborea* (K=340). The ratio of mannuronic/guluronic acid fragments constituting the algin played an important role in the selectivity of alginate towards certain metal ions. It was shown that the high selectivity coefficients for some metals depends on the guluronic acid blocks in the alginate molecules[34]. A thorough treatment of selective metal sorption by ion exchange materials is discussed by Helfferich[35] (the reader is referred to this text for further reading).

Section 3.2. Experimental Parameters

Biosorption of copper, cadmium, nickel and zinc

Typically, equilibrium sorption experiments were carried out by weighing 100 mg samples of biosorbent into polypropylene bottles of 500 ml nominal capacity with leak proof screw tops. 500 ml of solution containing a known quantity of metal ions was added to each bottle. Blank samples of the same solution with no biosorbent added were prepared under identical conditions for comparison with equilibrated samples. Metal biosorption isotherms were obtained at controlled solution pH 4 by addition of known amounts of sodium hydroxide or hydrochloric acid to the batch samples using a micro-pipette. The batch samples were equilibrated at a temperature of 25°C (±2°C) in an orbital shaker (C25 Incubator shaker, New Brunswick Scientific). Every 24 hours, the pH of each sample was measured and adjusted to pH 4 by addition of alkali (NaOH: 1 mol l^{-1}/0.1 mol l^{-1}). The samples achieved equilibrium when no significant change in solution pH (±0.1 pH units) was observed over a 48 hour period. The equilibrium metal concentration in each sample as well as the blank were measured after filtering the sample through a 0.2 μm Whatman (PTFE) disposable filter using AAS at the appropriate wavelength (see above). The equilibrium metal uptake (q) was calculated using the following equation:

$$q = \frac{\left(C_{in} - C_{eq}\right)V}{m_{sw}} \qquad (35)$$

The initial metal concentrations used were between (25 μmol l^{-1}-1 mmole l^{-1}). Automatic dilution of samples was done using an on-line sample dilution (SIPS) unit as the linear range for metal detection varies for the different metals analysed; Cu^{2+}(0-0.16) mmol l^{-1}, Cd^{2+}(0-0.027) mmol l^{-1} and Ni^{2+}(0-0.17) mmol l^{-1}. The lower limits of detection for metal ions in solution were measured by comparing results from AAS and the graphite furnace AAS technique. Results were in close agreement for the metal concentration ranges studied and therefore, flame AAS was used in all

experiments. The wavelengths used for metal detection were: copper (324.7nm), cadmium (228.8nm), nickel (232.0nm) and zinc (213.9nm).

Influence of pH and ionic strength on metal biosorption

The experimental procedure for determining the influence of pH and ionic strength on metal biosorption was identical to determination of surface complex formation parameters (see below).

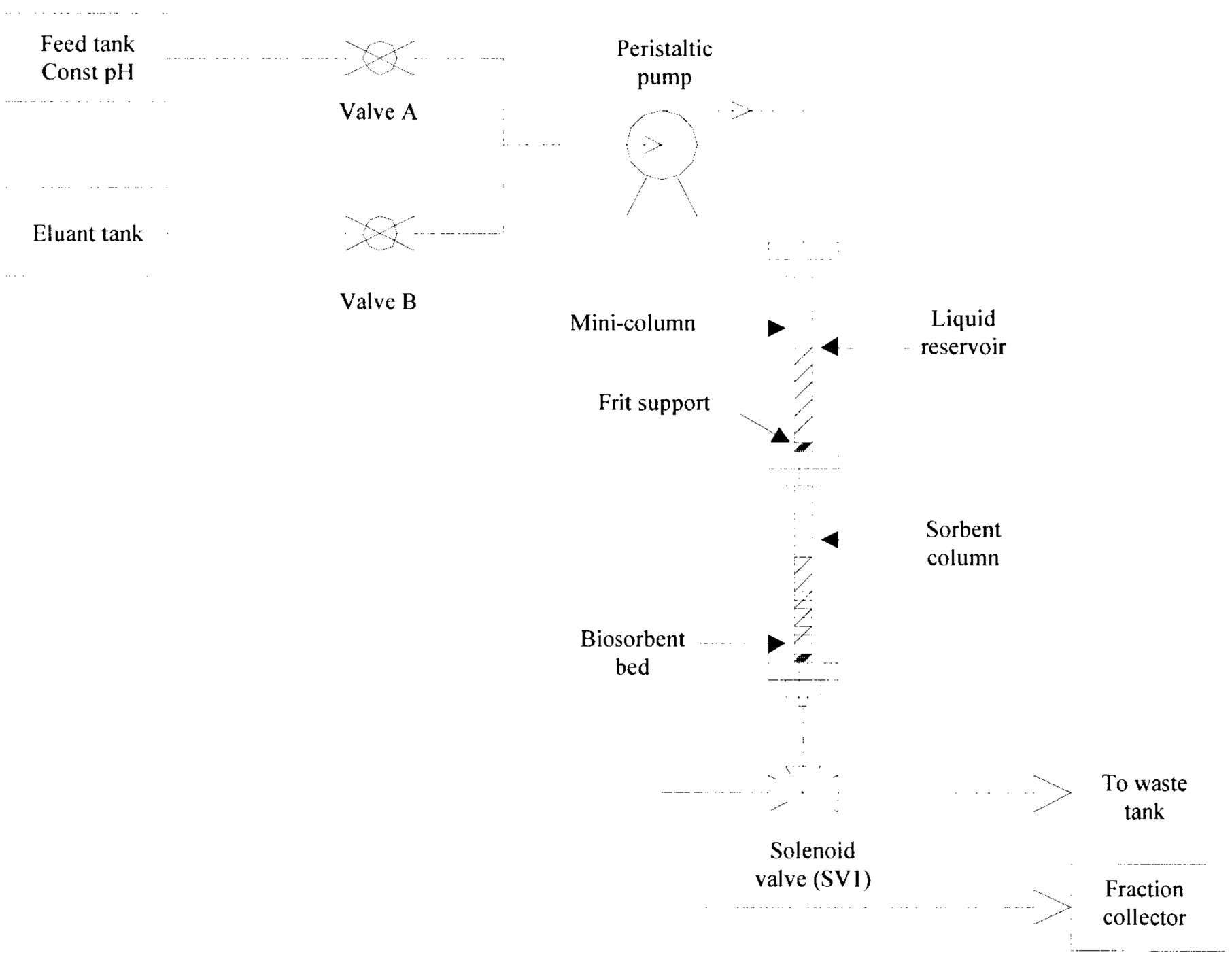

Figure 3.2. Schematic set-up used for selective-sorption studies.

Selective uptake of metal ions from multi-metal bearing solutions

Selective sorption of metal ions from multi-metal bearing solutions was studied using the set-up depicted in Figure 3.2. 50 mg of algal particles were placed in a mini-column (isolute SPE columns of nominal capacity 3 ml, supplied by Jones Chromatography Limited, Mid-Glamorgan, UK) with 20μm polyethylene frits as bed supports. Feed containing multi-metal salt solution (pH adjusted beforehand)

supplied the biosorbent bed with solution using a Masterflex multi-cartridge peristaltic pump. The effluent solution was allowed to flow into a clean waste tank. Effluent samples were periodically collected using a solenoid valve (SV1) which diverted solution to a fraction collector. Metal concentration was analysed using AAS in flame mode (see above for details). Following saturation of the sorbent bed, 10 ml of DDW was used to flush out residual metal ions present in the interstitial pores of the biosorbent bed. The associated tubing was flushed with 0.1M HCl to remove any metal ions present. Finally, 0.1M HCl solution was pumped at low flow rates (≈ 15 ml h^{-1}) through the metal-laden biosorbent bed to achieve elution of metal ions. 100 ml of the eluant was collected in sample vials and analysed for metal concentration using AAS. In addition to experiments at equal molar metal concentrations and pH 4, the influence of lower solution pH and excess of a particular metal ion in solution was also studied.

Sorption performance of biosorbents and mathematical description

In order to predict multicomponent exchange equilibria, numerical values of the following parameters need to be determined experimentally:

1. Equilibrium constants K_H, K_{Me1}, K_{Me2} of the formation of surface complexes.

2. The surface parameter A_o, m^2 g^{-1} sorbent.

3. The electric capacitance $C_{st,n}$ and C_d of Stern and diffuse layers, μF cm^{-2}.

Conversion of protonated algal biosorbents in a reference state (i.e. copper form, nickel form etc.) was achieved by contacting 5g of algal particles with 1 mM of metal salt solution in DDW. Following equilibration (24h), the solution pH was measured and the algal solution mixture was filtered using a Buchner-vaccum filtration system. New metal-salt solution was prepared and the algal particles were re-equilibrated with this fresh solution. This procedure was followed until the pH of the equilibrated solution exceeded pH 4. Several equilibrations were necessary since the initial

solution pH was found to be significantly low due to H^+/Me^{2+} exchange. Since metal biosorption is highly pH dependent, it was necessary to follow successive equilibration steps. Each equilibration occurred at a slightly higher solution pH until the equilibration pH value approached near-neutral conditions. Once the biosorbent was saturated with metal, the algal particles were washed with DDW to remove interstitial metal ions and then freeze dried ready for subsequent sorption experiments. In addition, 100 mg of freeze-dried metal saturated algal particles were contacted with 0.1M HCl by passing 100 ml of the acid solution through a mini-column of the biosorbent material. Eluted metal ions were quantified using AAS and this enabled determination of the saturated metal uptake capacity of the algal particles.

Binary exchange equilibria were measured by contacting a series of samples of metal-loaded biosorbent material, 10 mg-500 mg with 100 ml of DDW at initial pH 2.55 in 100 ml nominal capacity Erlenmeyer flasks. The algal particles were left equilibrating in an orbital shaker (25°C) for seven days, thereafter, the equilibrium pH was recorded using a calibrated Mettler Toledo 340 pH meter. Quantification of metal ions in solution was performed using a Varian SpectrAA-200 atomic absorption spectrophotometer (AAS) in flame mode employing an air-acetylene flame. A mass balance relating metal ions in solution and residual metal ions within the biomass enabled representation of Me^{2+}/H^+ exchange equilibria according to eq.(28). $\log K_{Me}^{H}$ and m(H,Me) values were obtained by carrying out linear regressions on the experimental data obtained.

Ternary exchange equilibria were measured in a similar manner to binary exchange equilibria except, in addition to protons in solution, each batch sample contained a fixed initial concentration of competing metal ionic species (e.g. 0.1 mM Cd^{2+} at pH 2.55, equilibrated with copper laden *A. nodosum*, in order to obtain a $Cu^{2+}/Cd^{2+}/H^+$ ternary system). Binary equilibrium parameters were used to fit ternary equilibria data to show whether the surface complexation model had predictive capabilities.

Section 3.3. Results and Discussion

Biosorption of copper, cadmium, nickel and zinc

Experimental q^* values and Langmuir parameters (according to the expression $q = \frac{\overline{q^*}bC_{eq}}{1+bC_{eq}}$) for the biosorbents (see Table 3.3. a-d) show high copper affinity for BK, LH and LF (see also Fig. 3.3.). Thus, for relatively dilute copper bearing solutions BK, LH and LF offer promise as potential biosorbents. Taking into account the high wet bulk volume of LF, the sodium capacity of AN and BK is higher than that of LF on a volume basis (see Table 3.4.). The processed seaweed residues of DAN and DLF show significant copper sorption capacities; the copper uptake values are about 50% lower than their native precursors. Given that the materials are waste products of the algin extraction industry and are therefore a potentially cheap biosorbent source, the high residual sorption capacity for metals is very encouraging.

	Copper			
Species	q*	$\overline{q^*}$	b	r^2
	mmol g^{-1}	mmol g^{-1}		
AN	1.0	1.4	13	0.94
LF	1.3	1.3	74	0.9
BK	1.5	1.7	22	0.98
LH	1.1	1.1	59	0.99
DAN	0.6	0.7	17	0.99
DLF	0.7	0.8	35	0.98
AA-AN	1.9	1.9	43	0.95
AA-LF	1.6	1.6	51	0.91

Table 3.3.a. Comparison of Langmuir parameters and experimental copper uptake data for biosorbents.

Copper sorption by DLF is surprisingly favourable in comparison with the native precursor on a swollen volume basis; i.e. 0.12 mol l^{-1} for LF compared with 0.2 mol l^{-1} for DLF, an increase of over 60%. A similar comparison for the other metals studied (see Figures 3.4. and 3.5.) reinforces the conclusion that waste dealginate materials are attractive potential sorbents for the treatment of dilute metal-bearing solutions.

Species	Cadmium			
	q*	$\overline{q*}$	b	r^2
	mmol g^{-1}	mmol g^{-1}		
AN	1.0	0.9	42	0.99
LF	0.9	0.8	73	0.92
BK	1.4	1.0	49	0.99
LH	1.1	0.9	86	0.85
DAN	0.5	0.3	49	0.77
DLF	0.4	0.4	20	0.89
AA-AN	1.3	1.2	50	0.9
AA-LF	0.9	0.9	70	0.88

Table 3.3.b. Comparison of Langmuir parameters and experimental cadmium uptake data for biosorbents.

Species	Nickel			
	q*	$\overline{q*}$	b	r^2
	mmol g^{-1}	mmol g^{-1}		
AN	0.5	0.5	17	0.95
LF	0.8	0.6	55	0.91
BK	0.4	0.6	39	0.94
LH	0.8	0.9	19	0.99
DAN	0.5	0.4	16	0.97
DLF	0.4	0.3	34	0.97
AA-AN	0.8	0.7	2.4	0.98
AA-LF	0.9	1.0	9	0.85

Table 3.3.c. Comparison of Langmuir parameters and experimental nickel uptake data for biosorbents.

Species	Zinc			
	q*	$\overline{q*}$	b	r^2
	mmol g^{-1}	mmol g^{-1}		
AN	0.3	0.22	255	0.87
LF	0.7	0.23	227	0.9
BK	0.7	0.3	174	0.7
LH	0.5	0.29	140	0.72
DAN	0.2	0.2	47	0.63
DLF	0.3	0.52	9.6	0.81
AA-AN	0.5	0.48	40	0.95
AA-LF	0.5	0.5	35	0.95

Table 3.3.d. Comparison of Langmuir parameters and experimental zinc uptake data for biosorbents.

The Langmuir equation provides a reasonable fit [values of r^2>0.95 in most cases] to metal equilibrium sorption data for the sorbents studied (see Table 3.3. a-d and Figures 3.3. - 3.6.). It is important to recognise that the mechanism of metal sorption cannot be concluded directly from the fit. One of the principal assumptions of the Langmuir model is mono-molecular deposition of sorbate caused by surface adsorption.

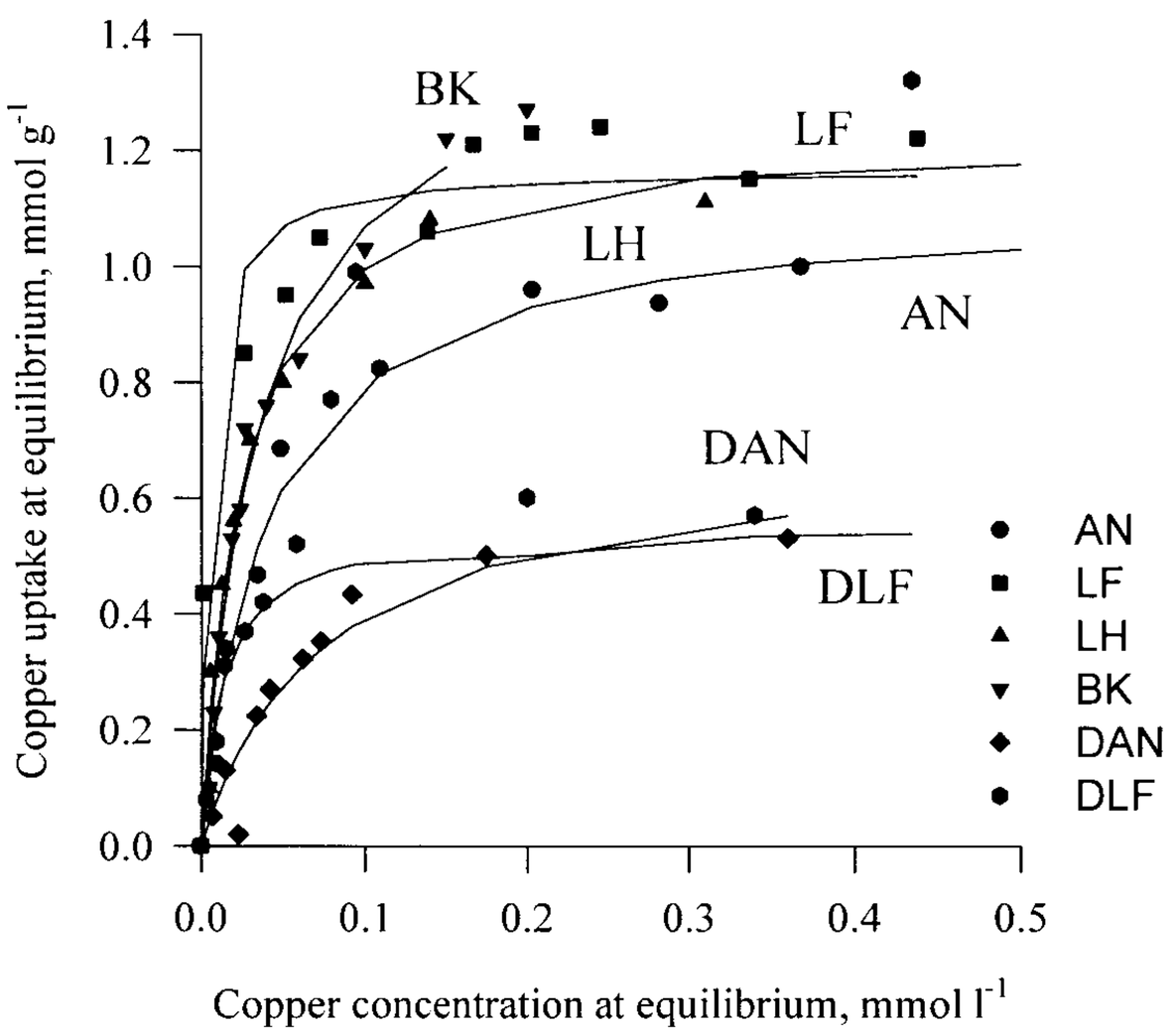

Figure 3.3. Copper sorption isotherm at equilibrium pH 4.

	AN	LF	BK	LH	DAN	DLF
[1]Dry bulk volume, V_{dry} ml g^{-1}	1.6	5.6	1.4	1.6	1.5	1.5
Wet bulk volume, V_{wet} ml g^{-1}	4	11.1	3.6	4.5	3	3.6
[2]Na^+ capacity, mmol g^{-1}	2.0	3.0	4.0	<2.0	1.0	<0.5
Na^+ capacity, mmol ml^{-1}	0.5	0.3	1.1	<0.4	0.33	<0.14
pK_a	4.2	4.1	3.4	4.2	-	-

Table 3.4. Comparison of some properties of native algal biosorbents.

[1](Particle size range 300-355 μm)

[2]The sodium uptake capacity is quoted for pH <6. This is the effective capacity for metal sorption studies where precipitation of metal species is to be avoided.

The data for metal uptake by DAN and DLF show noticeable scatter at C_{eq}>0.1mmol l^{-1}. Na^{+} added during pH adjustment of batch samples may compete with heavy metal ions for surface functional groups. In batch samples where more alkali was added, residual alginate may leach out of the algal particles, thus reducing metal binding capacity and enhancing the scatter of metal sorption data. Another possible reason for

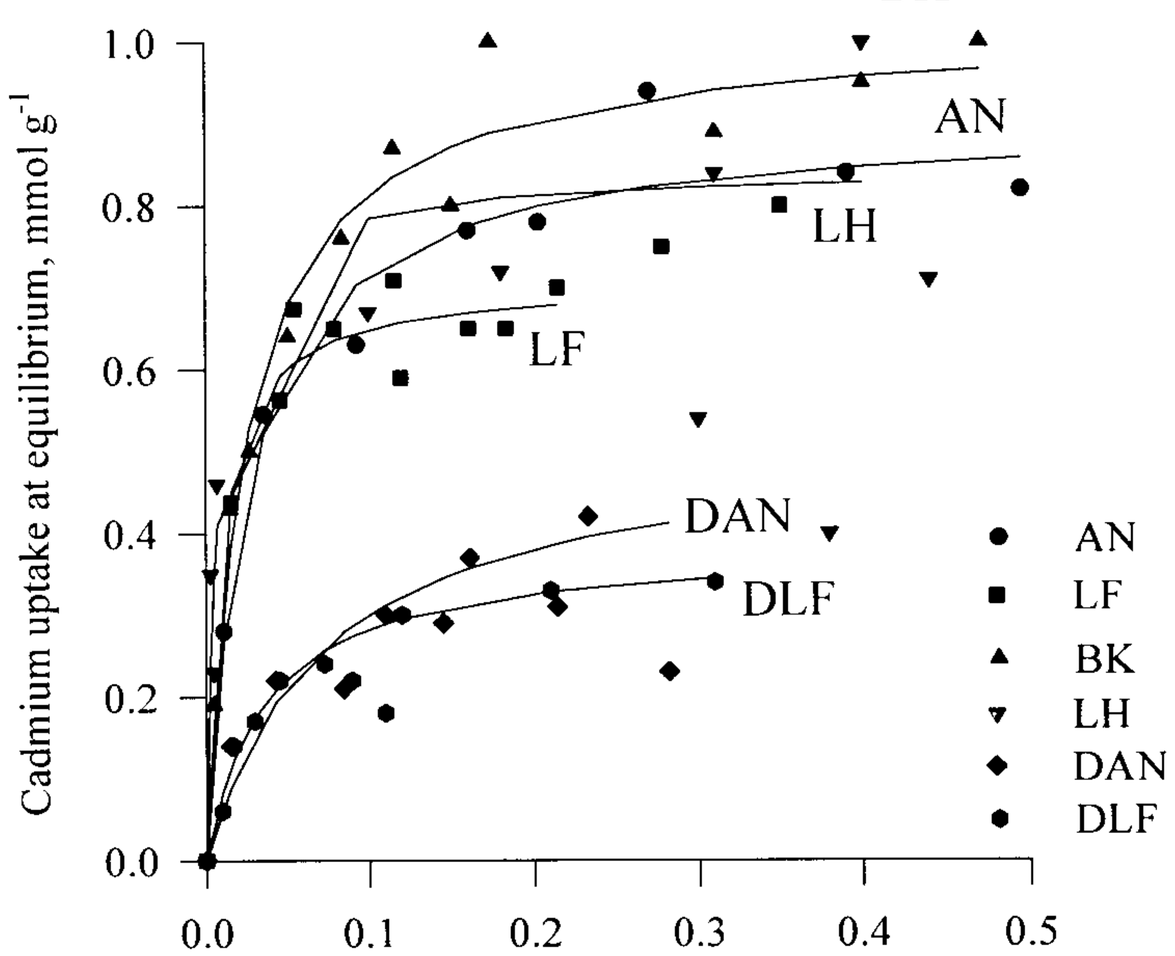

Figure 3.4. Cadmium sorption isotherm at equilibrium pH 4.

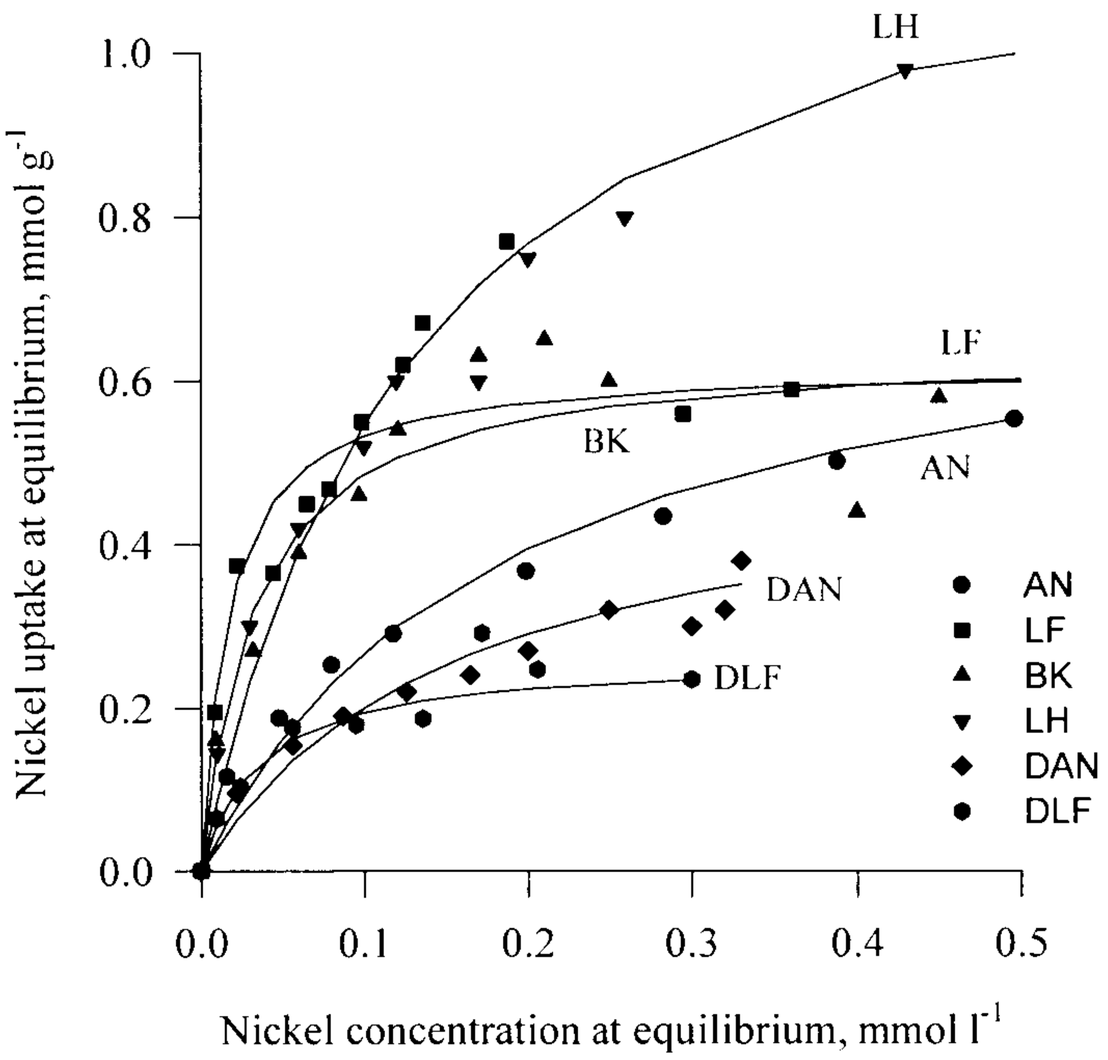

Figure 3.5. Nickel sorption isotherm at equilibrium pH 4.

the scatter may be due to variability of the material. The algin industry uses both leafy stipes as well as fronds for the extraction of algin. Various parts of the plant are known to exhibit varying biosorptive properties due to differing polysaccharide composition making up the cellular structure[36]. Particles of crushed algal material may therefore provide different biosorption capacities within the same algae type, depending on the proportion of specific polysaccharides present.

In addition to the seasonal fluctuations in the algin content of various algae, variations in the different proportions of mannuronic (M) and guluronic acid (G) residues making up the alginic acid polymer are common[37]. LH has the highest proportion of guluronic acid segments found in commercial seaweeds[38]; about 65% of algin has guluronic conformation. Although LH has a lower overall algin content in comparison with BK (LH~20% by weight compared with BK~50%), it shows relatively high metal sorption values for all metal ions studied (see Table 3.3. a-d). It has been found that a high proportion of guluronic acid segments in alginates are responsible for the higher selectivity coefficient values for equilibria between sodium

ions, divalent metal ions and alginate[39]. The high G content in LH undoubtedly plays a role in the high affinity of divalent metal ions towards LH.

Even though the processed dealginate biomass was subjected to alkali treatment during the algin extraction process [mixture of sodium carbonate (1% wt/wt) and sodium hydroxide (0.1% wt/wt)] there was still significant residual metal sorption capacity. The high pH of the extraction process may result in a β-elimination reaction with the formation of αβ-unsaturated uronic acid derivatives[12]. The leaching out of hydrolysis products may be a diffusion controlled process, given the gelatinous nature of alkali treated algae. During successive treatments of native biomass with alkali, disintegration and solubilisation of the material was observed with severe loss of weight. Further breakdown of α,β-unsaturated uronic acid derivatives may occur. The residual capacity displayed by processed dealginate seaweed waste may arise as a consequence of breakdown hydrolysis products that have not leached out of the cellular matrix during the algin extraction process. Evidence that these products may possess weak acid carboxylate functionality has been confirmed by the reduction in copper biosorption following methylation of the algae by treatment with methanolic hydrogen chloride. The insignificant effect of the propylene oxide treatment further reinforces the fact that metal removal does not occur as a consequence of residual algin in the algal matrix since this algin would have leached out as propylene glycol ester (see chapter 2).

Alkali-washing of algae strips out essential polysaccharides constituting the cellular matrix of the native material. The dealginate residue may be considered as the remnant back-bone of the virgin biomass consisting of hemicellulosic type carbohydrates. These may include different sugar residues including D-xylose, L-arabinose, D-glucuronic acid, 4-O-methyl-D-glucuronic acid, D-galactose, D-mannose, L-rhamnose and L-fucose[40]. It is clear therefore, that the amorphous mass left after alkali treatment of seaweed comprises a medley of different polysaccharides which provide significant metal binding sites in the dealginate residue.

The high algin content of native seaweed (see Table 2.5.) may suggest significantly high metal sorption values for the virgin material in comparison with dealginate materials. This is clearly not the case and the processed biomass shows only 50% reduction in metal sorption capacity compared with the native precursor (see Table 3.4.). Low molecular weight compounds; break-down products due to alkali hydrolysis, possessing weakly-acidic groups are responsible for enhancing the capacity of the processed material even though most of the algin has been extracted.

Zinc sorption studies by native and dealginate materials showed significant scatter in zinc-sorption data at Ceq>0.1mM (not shown in Fig. 3.6.). Zinc interacts with alginic acid producing zinc alginate which according to some sources may be partially water soluble[41]. It is possible, that at Ceq>0.1mM some algal-bound zinc leaches out of the sorbent materials resulting in a reduction in overall zinc sorption capacity. No published data on the solubility of zinc alginate in water has been found. In the present study, maximum zinc uptake values are quoted on the basis of the highest experimental values obtained during sorption experiments. The results do not suggest a flattening of the sorption isotherm at this value. The native materials showed high affinity towards zinc at trace metal equilibrium concentrations in solution (see Fig. 3.6.) for uptake values below C_{eq} 0.05 mM.

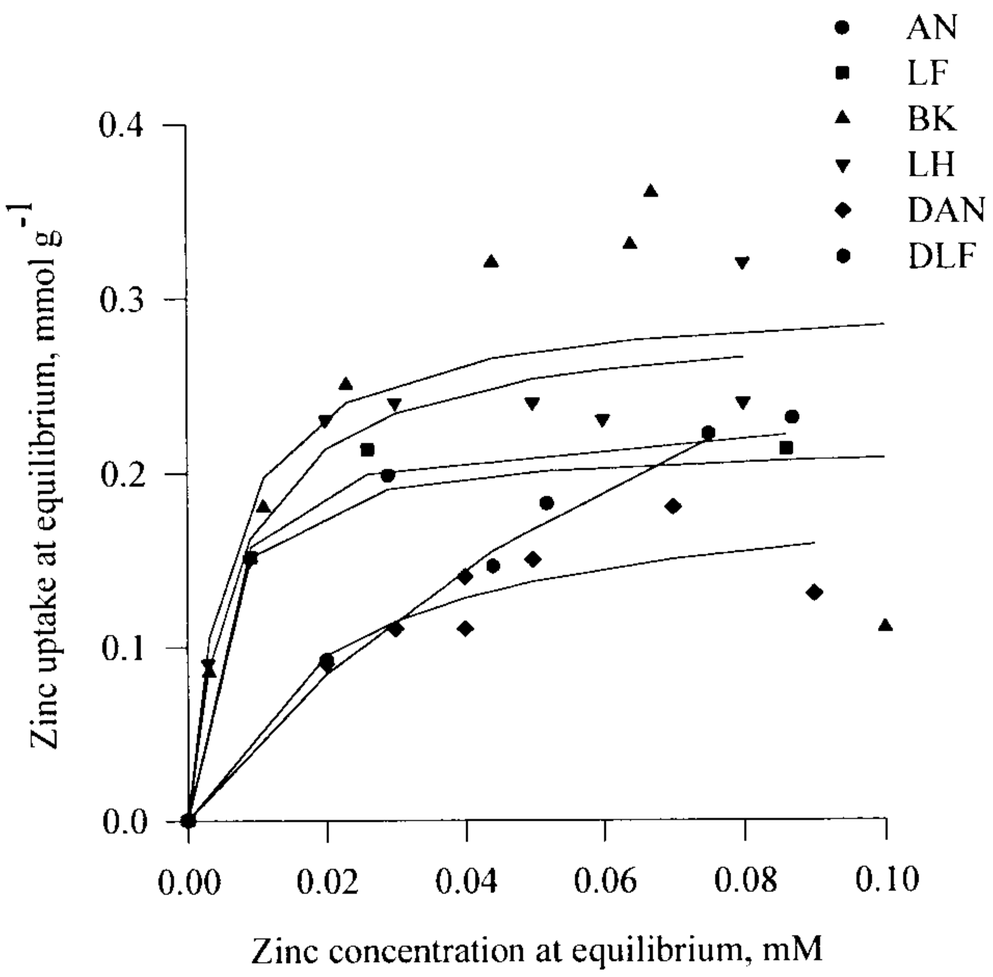

Figure 3.6. Zinc sorption isotherm at equilibrium pH 4.

The zinc sorption isotherm of alginic acid (AA-AN) did not show scatter in equilibrium uptake data over the concentration range 0-0.5 mM. The data fits the Langmuir-type isotherm quite well. This result suggests that solubilisation of zinc-alginate is not a very likely explanation for the scatter observed in zinc-sorption data for all biosorbents studied. Alginic acid samples showed low nickel and zinc sorption capacity compared with affinity for copper and cadmium (see Figures 3.7. and 3.8.). This result is comparable with nickel and zinc sorption values obtained for algal biomass and this suggests that copper and cadmium ions may interact with sites on the biomass which do not show the same affinity to metal ions including nickel and zinc. A comparison of the hydrated ionic radii of the metal ions in solution indicates very similar sizes (see Table 3.5.). Electrostatic attraction of metal ions to fixed ionic groups may result in their localisation in the neighbourhood of the fixed ionic groups. The strength of the electrostatic attraction depends on the ionic charge and also on the distance of closest approach between the solvated counter-ion and the fixed ionic groups in the biosorbent. The Debye-Huckel parameter $\overset{o}{a}$ represents the distance of closest approach between the counter-ions and the fixed ionogenic groups[42].

Electrostatic attraction is inversely proportional to the square of the distance between charges, so that ions with smaller $\overset{o}{a}$ are held more strongly. The more polarised the counterion, the smaller the distance of closest approach and therefore greater the tendency to be retained within the biosorbent particle[43,44] (see Table 3.5.). The relatively similar polarisability values provide little to distinguish between the heavy metal ions under investigation.

Ion	D_i	CN, R_i	R_s	R_H	Polarisability
	10^{-5} cm^2 s^{-1}	$\overset{o}{A}$	$\overset{o}{A}$	$\overset{o}{A}$	10^{-24} cm^3
Cu^{2+}	0.714	6,0.73	3.25	4.19	6.1
Cd^{2+}	0.719	6,0.95	3.41	4.26	7.2
Ni^{2+}	0.661	6,0.69	2.92	4.04	6.8
Zn^{2+}	0.703	6,0.74	3.49	4.30	7.1

Table 3.5. Properties of selected metal ions in aqueous solutions.

Benedetti et al[45] proposed that phenolic groups contribute significantly to copper binding in humic-type substances over a wide pH range including mild acidic solutions. Carboxylic groups were found to be more important from near neutral pH solutions at high equilibrium copper concentrations. The high copper sorption capacity displayed by all biosorbents in the current study may be explained in terms of interaction with (-OH) groups present in polysaccharides. Interaction of copper ions with phenolic-type groups even in relatively acidic solutions have been reported in literature[45]. Potentiometric titration data (see Table 2.4.) indicate that on average 5 mmol g^{-1} of negatively charged (monovalent) binding sites are available in alginic acid (AA-AN) at about pH 5 (sorption isotherms evaluated at pH 4). This would suggest uptake of divalent copper ions of around 2.5 mmol g^{-1}. Sorption isotherm data indicates copper removal of about 2 mmol g^{-1}. Sorption capacity for the other metals is significantly lower suggesting somewhat different interactions between these ions and the algal surface.

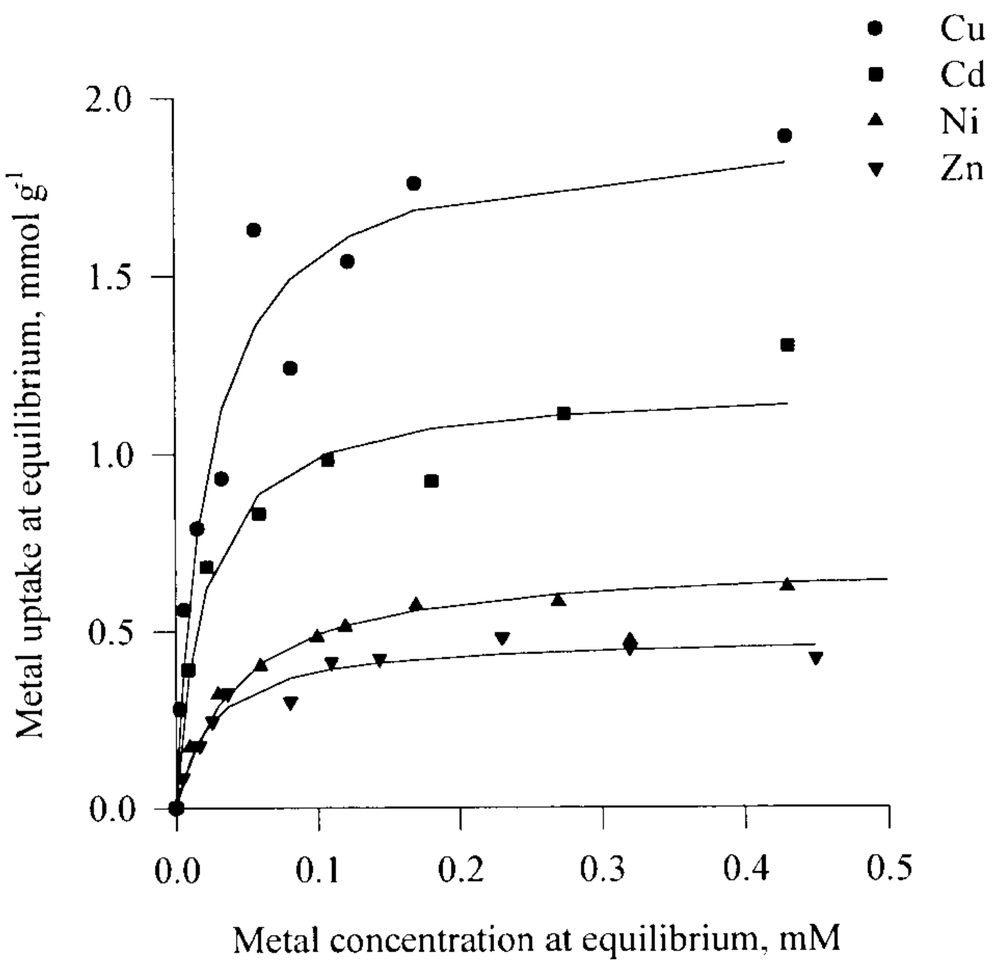

Figure 3.7. Metal sorption isotherm for AA-AN at equilibrium pH 4.

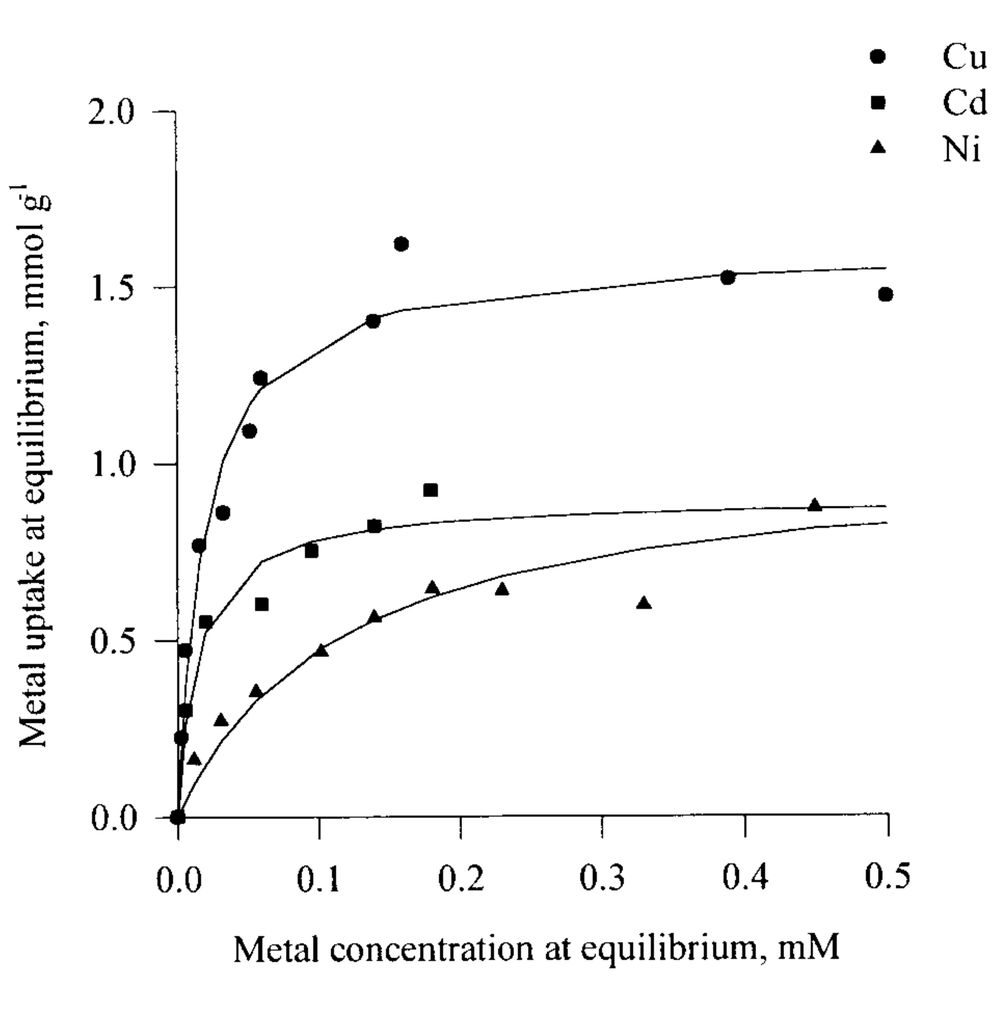

Figure 3.8. Metal sorption isotherm for AA-LF at equilibrium pH 4.

Influence of pH and ionic strength on metal biosorption

The metal sorption capacity of all the algal biosorbents studied showed significant dependence upon the external solution pH. Protons in solution strongly interact with the surface of the algae. In particular, at low solid/liquid concentrations, proton sorption by algae far exceeded the stoichiometric uptake of protons expected as a consequence of release of metal ions from previously metal saturated algal biomass. This buffering effect exhibited by algae, whereby protons in solution are mopped-up from solution indicates the strong affinity of the biosorbent surface for protons. Below solution pH 3.5 the metal binding sites began releasing previously sequestered copper and cadmium ions thereby showing preference for protons; this phenomenon is strongly indicative of the interaction of metal ions with weakly-acidic functional groups present within the algal biomass. Nickel and zinc ions were released at higher pH values in comparison with copper and cadmium ions indicating that they are considerably less strongly bound to the algal surface. In addition, the maximum biosorption capacity for nickel and zinc ions is noticeably lower in comparison with biosorption of copper and cadmium ions. In the case of BK for example, previously held nickel and zinc ions were displaced at relatively higher solution pH values compared with copper and cadmium (see Fig. 3.9.). During metal biosorption all algal sorbents showed reduced affinity towards metal ions in the presence of competing H^+ ions, i.e. at pH values around or below pH 2.5 (see Fig. 3.10.): in this instance, the metal sorption curves are similar to titration curves and are a mirror reflection of curves obtained during desorption of metal laden algae. Plots of proton uptake obtained from pH measurements vs. metal ions released from algae suggest a bidentate binding mechanism for copper sorption by *A. nodosum* (see Fig. 3.11.). The stoichiometric coefficient for H^+/Cu^{2+} exchange is 2, indicating 2 mmoles of H^+ taken up for every mmole of metal ions released. This indicates that a chelating type binding mechanism similar to that displayed by chelating ion exchange resins e.g. iminodiacetic resins may be partially responsible for metal biosorption. Protons are capable of breaking chelating bonds between metal ions and surface functional groups under acidic pH conditions. Similar measurements for cadmium and zinc exchange

indicate lower coefficient values (see Table 3.6.). The stoichiometric coefficient values for nickel release by *A. nodosum* indicates 4 mmoles of protons are required for the release of 1 mmole of algal bound nickel. This result is anomalous as it suggests that tetravalent nickel is desorbed by the algae with uptake of equivalent number of protons from solution. In comparison, nickel release by BK showed a stoichiometric coefficient closer to 2 (see Fig. 3.12.). The proton sorption data has been calculated from external solution pH measurements. These values are only as accurate as the pH probe used to measure the solution pH. Also, the error involved in measuring pH values varies with the proton concentration in solution. An alternative measurement of proton concentration, e.g. direct titration of residual protons in solution, may increase confidence in the data obtained in the present case. Proton concentration adjacent to the biosorbent surface may be rather different from the measured bulk solution pH. Nevertheless, the strong dependence of metal biosorption on external solution pH is clearly a very important parameter which will have an important bearing on the overall efficiency and effectiveness of any water treatment process utilising algal biosorbents.

Competition between protons and metal ions for metal binding sites on the algal surface indicates that an ion exchange mechanism is responsible for the biosorption phenomenon. Reduction in solution pH upon metal sorption by algae was clearly evident during the development of biosorption isotherms. Dosing of batches with alkali resulted in further uptake of metal ions from solution and subsequent release of protons from within the algae which resulted in lowering of the solution pH. Recently, other researchers[30] have reported a stoichiometry of 1 for H^+/Na^+ exchange during proton exchange rate studies with Na^+ and Ca^{2+} laden *Sargassum fluitans*, thus providing further evidence of the important role of surface bound protons in metal biosorption.

It is worth noting that a stoichiometric exchange of protons with divalent metal ions was encountered at high solid/liquid ratios. As the preloaded biosorbent concentration in solution was reduced (i.e. low solid/liquid ratios), protons in solution were mopped up far in excess of the corresponding stoichiometric release of divalent

metal ions. This result suggests that protons are initially attracted to the highly charged surface sites (dissociated functional groups). Once these sites are occupied, the remaining protons are attracted to any residual negative charge on the algal surface (see chapter 2; zeta potential section). During proton sorption by preloaded metal bearing algae, in the presence of excess of metal binding sites (i.e. high solid/liquid ratio), protons were only able to interact with functional groups to which metal ions were adhering. The competition between protons and metal ions swung in favour of protons with stoichiometric release of metal ions.

The metal sorption/desorption curves plotted as a function of external solution pH clearly represent titration of metal binding sites with protons. The sudden rise in metal biosorption between pH 2.5-3.5 (see Fig. 3.10.) corresponds to the dissociation pK of the surface functional groups.

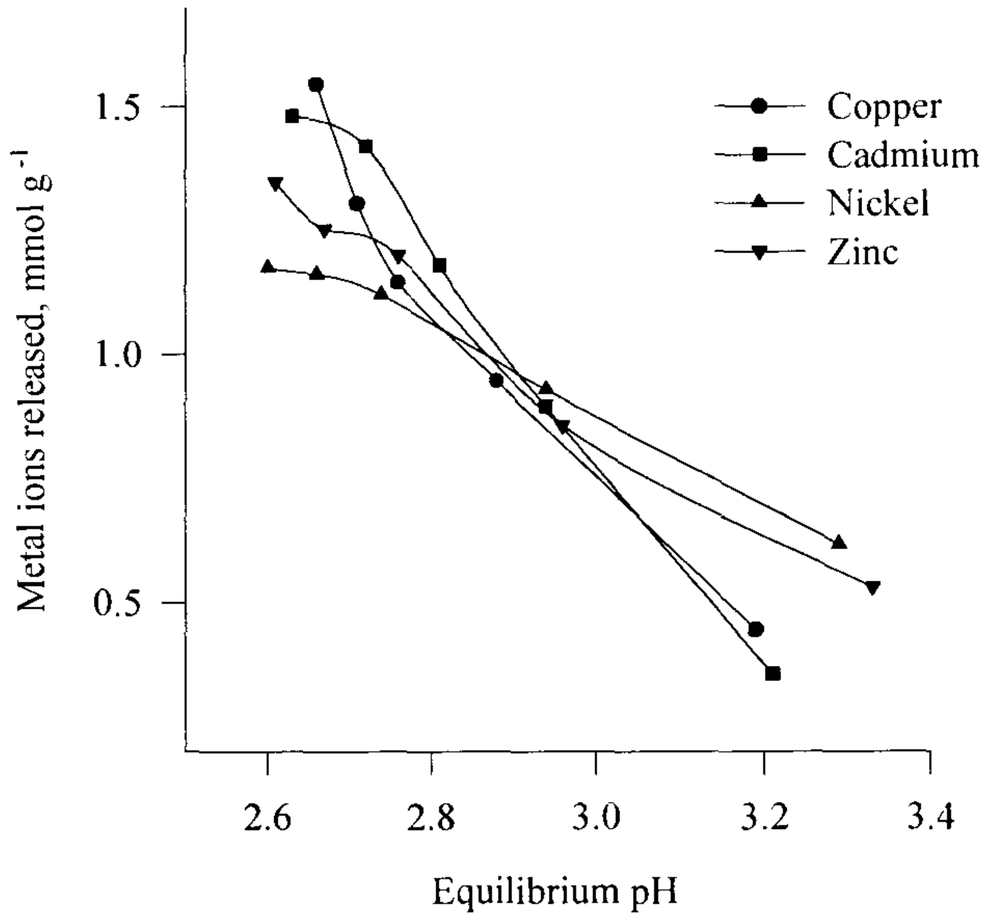

Figure 3.9. Release of metal ions as a function of external pH by BK.

Species	Stoichiometric coefficient H^+/Me^{2+}			
	Cu^{2+}	Cd^{2+}	Ni^{2+}	Zn^{2+}
AN	2.0	1.46	4.0	1.82
BK	2.89	2.5	2.4	2.3

Table 3.6. Some representative stoichiometric coefficient values for H^+/Me^{2+} exchange.

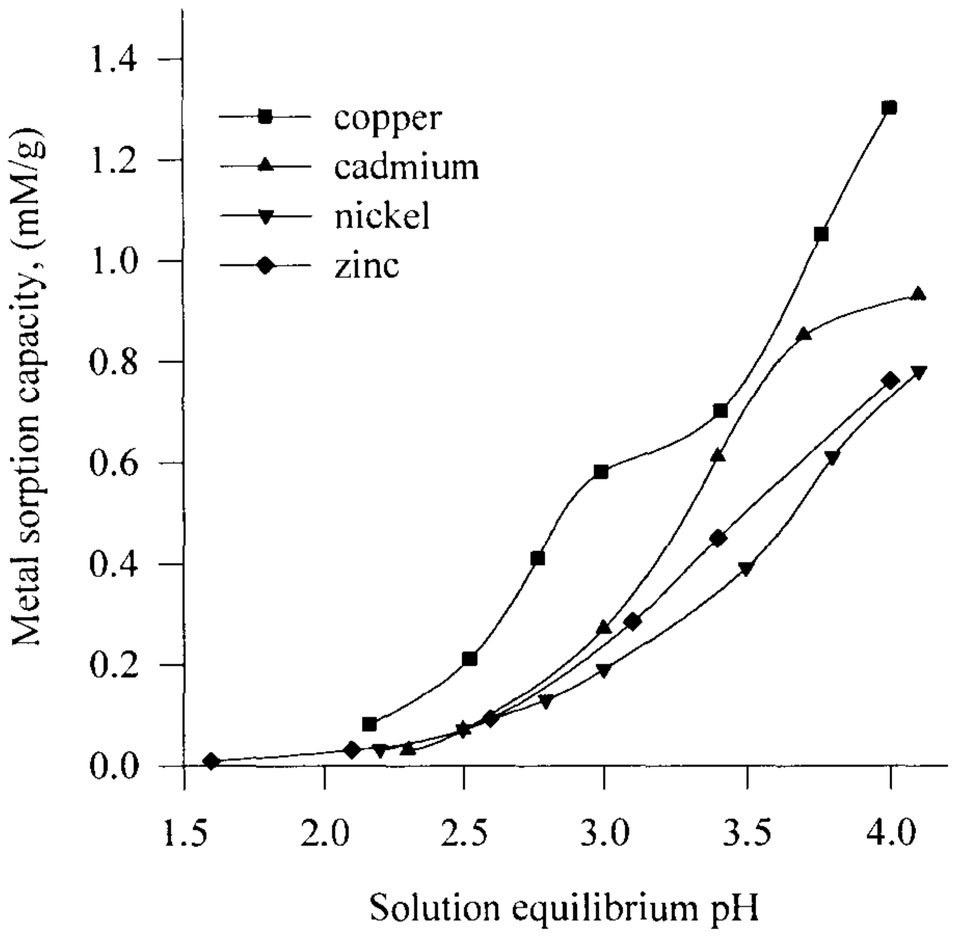

Figure 3.10. Sorption of metal ions as a function of external pH by LF.

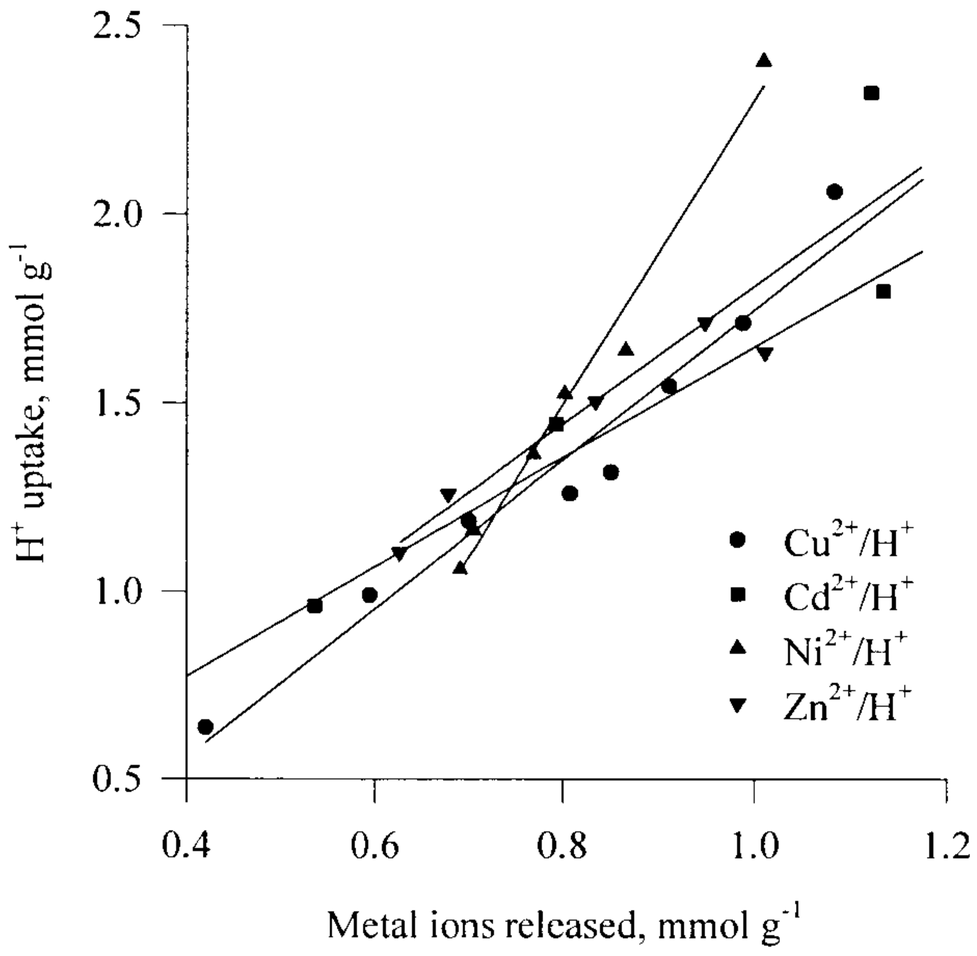

Figure 3.11. Stoichiometry of H^+/Me^{2+} exchange by AN.

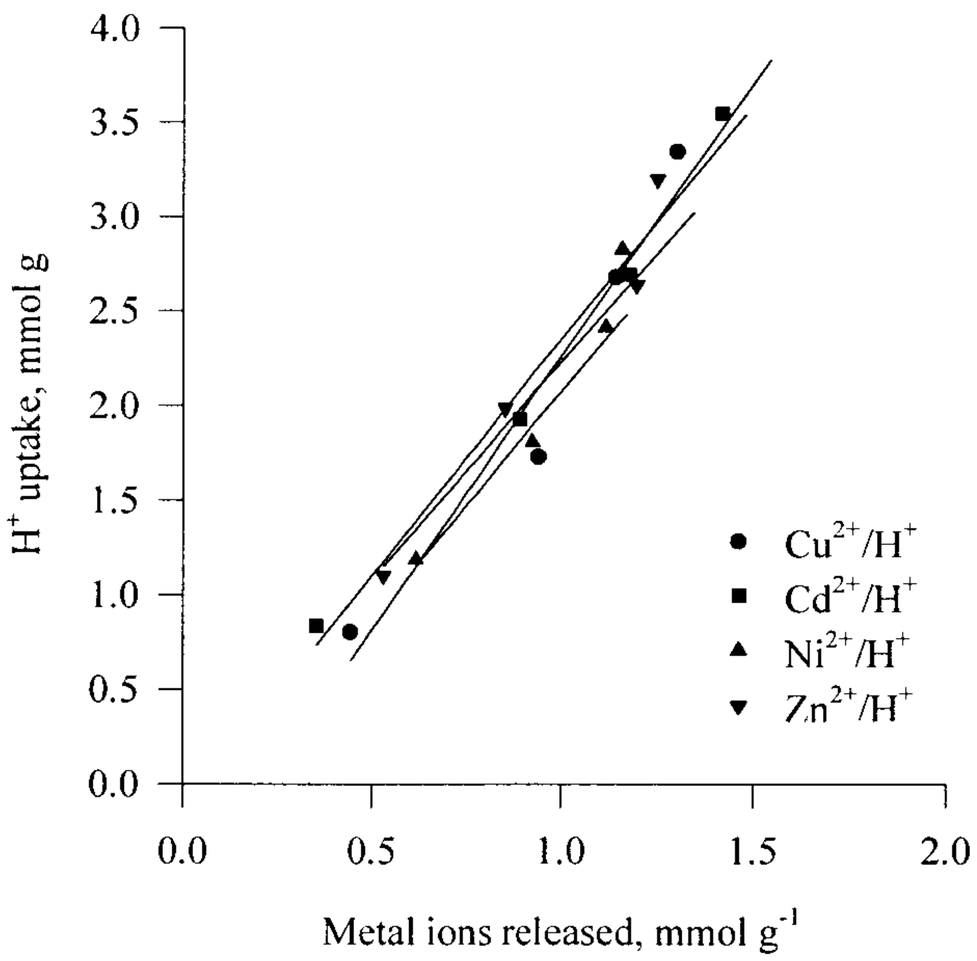

Figure 3.12. Stoichiometry of H^+/Me^{2+} exchange by BK.

High background ionic strength due to the presence of Na^+ ions did result in reduction in the overall heavy metal biosorption capacity of algal biosorbents. Copper sorption

by *L. flavicans* reduced from 1.3 mmol g^{-1} in the absence of background NaCl to 0.65 mmol g^{-1} (I=100 mM) and 0.35 mmol g^{-1} (I=500 mM) respectively. This reduction in heavy metal biosorption capacity is typical for all biosorbents studied and is a direct consequence of electrostatic interaction of Na^+ to the negatively charged biomass surface. This results in reducing the negative surface potential of algal particles with consequent weak interactions with other heavy metal ions present in solution. Schiewer and Volesky[14] found that electrostatic effects were negligible only at a very high ionic strength, i.e. at a high concentration of Na^+ or other ions for cadmium binding to *Sargassum* particles. As a consequence, ionic strength effects should always be considered in the modelling of biosorption by algae. The presence of alkali and alkali-earth metal ions in solution do result in competitive interactions with algae. At trace concentrations, the strong interactions of divalent metal ions with the algal surface far outweigh electrostatic interactions between monovalent ions and the algal surface. However, at higher concentrations, these interactions cannot be ignored.

Mathematical description of biosorption isotherms

Biosorbent loadings were calculated by carrying out material balances for exchange between H^+ ions in solution and metal ions previously sequestered onto algal particles (preloaded biomass). pH values were measured directly (providing a balance of protons taken up by the algal particles). Equilibrium concentrations (expressed in mol l^{-1}) and $\log Q_i^H$ values were calculated according to eq.(28) and plotted as a function of y(Me) (see Figures 3.13.-3.15.). Corresponding $\log K_{Me}^H$ and m(H,Me) values were obtained from these plots (see Table 3.7.). Typical results for Cu^{2+}/H^+, Cd^{2+}/H^+, Ni^{2+}/H^+ and Zn^{2+}/H^+ exchange equilibria and model predictions for AN, BK and LH are depicted in Figures 3.16. - 3.18.

Using the characteristic SCM parameters [$\log K_{Me}^H$ and m(H,Me)] for binary exchange equilibria, theoretical predictions of H^+/Cu^{2+} exchange, H^+/Cd^{2+} exchange etc. have been calculated. The isotherms are similar to titration curves showing the characteristic rise in metal binding with increase in solution pH. Since initially, the biomass was preloaded with metal ions, therefore, the curves were calculated for metal ions realeased from the biosorbents as a consequence of interactions of protons

in solution with algal sites in metal form. The exchange occurs around the pK values of the surface functional groups as metal ions are released from the algae since protons are preferred at lower solution pH values.

Theoretical predictions of heavy metal binding affinity clearly shows that nickel and zinc ions are removed from solution at a higher pH value in comparison with copper and cadmium ions (see Fig. 3.16.). This is in agreement with experimental observations. Also, the equilibrium metal sorption values for AN are significantly lower in the case of nickel and zinc ions compared with copper and cadmium ions for the same equilibrium pH values. Qualitatively good agreement between the theoretical predictions and experimental values of heavy metal sorption onto *A. nodosum* have been obtained. In the case of copper biosorption by AN, the model under predicts the uptake of copper ions at lower pH values (pH<3) (see Fig. 3.16.). Since the surface functional groups on algae have been modelled as simple carboxyl groups, any chelating and coordination reactions as well as reactions with other surface functional groups including phenolic type groups were not taken into account. The under prediction of copper biosorption by the SCM model is due to the simplifying assumption of mono-functionality of the algal biomass which does not fully represent the multitude of surface reactions of metal ions with the metal binding surface sites found in algae. Complete release of previously bound copper ions by AN is difficult to achieve even at low solution pH values around pH 2.8 ($y(Cu^{2+}) \approx 0.6$). This is due to the strong interactions between copper ions and metal binding sites in algae. $R(COO)_2Cu$ type complexes similar to those occurring with chelating ion exchange resins (e.g. iminodiacetic resin) are thought to be responsible for the strong binding of copper ions to the algal surface.

The theoretical predictions of metal biosorption by BK are not in excellent agreement with the experimental data (see Fig. 3.17.). Both theoretical curves for copper and cadmium biosorption by BK are considerably below the experimentally observed values. Surface reactions which are not accounted for during model development probably play an important contribution towards metal biosorption by BK. These surface reactions need to be incorporated into SCM to better represent the biosorption

phenomenon occurring within BK. Nickel sorption equilibria for BK could not be represented by the surface complex formation model due to the ill-defined curvature (towards the x-axis) of the $\log Q_i^H$ vs. y(i) plot (see Fig. 3.14.). Nickel sorption by BK may be dominated by electrostatic attraction to the negatively charged surface of BK (see Fig. 2.8.). The surface complex formation model does not therefore portray a very accurate picture of the nickel biosorption phenomenon. A different modelling approach better suited to describing electrostatic interactions between metal ions in solution and the negatively charged sorbent surface would be fundamentally more accurate in describing nickel biosorption.

Theoretical prediction of copper biosorption by LH is in excellent agreement with the experimentally observed sorption values (see Fig. 3.18.). LH is slightly different from AN and BK due to its higher guluronic acid content (see Table 1.2.). Clearly, copper biosorption by LH may be represented by simple ion exchange between guluronic acid segments and copper ions in solution. The $\log Q_i^H$ vs. y(i) plot for LH (see Fig. 3.15.) shows a change in gradient only around y(i) ~ 0.2 compared with the other biosorbents where the transition occurs around y(i)~0.4. This suggests, that, formation of complexes such as $R(COO)_2Cu$ occur to a lesser extent in LH compared with the other marine algal biosorbents. If this is indeed true, then, exchange of copper ions within marine algae may be directly related to the presence of guluronic acid segments within marine algae. Differences in the relative amounts and the conformation of different algal polysaccharides (e.g. mannuronic and guluronic acid segments) may be responsible for determining the extent to which metal ions are removed by the marine algae due to ion exchange and/or chelation.

Ternary exchange equilibria for copper loaded *A. nodosum* were calculated using the binary exchange parameters except that, with multiple counter-ions, each metal species was assumed to be sorbed according to a selectivity series ($Cu^{2+}>Cd^{2+}>Zn^{2+}>Ni^{2+}$). The greater the selectivity of the material for a particular ion, the closer that ion is located to the biosorbent surface. Competition between cadmium ions and protons in solution for surface sites preloaded with copper ions are depicted in Figure 3.19. The high affinity of copper ions for AN metal binding sites is

clearly apparent from the ternary equilibrium data (see Fig. 3.19.). Cadmium ions were unable to displace previously loaded copper ions from the algae. Displacement of previously bound copper ions by protons in solution is the dominating exchange reaction. The theoretical predictions of copper displacement from AN due to the presence of cadmium ions and protons in solution agree reasonably well with the experimental data. However, cadmium sorption by AN is considerably over predicted by the model, especially at the lower pH values. A sensitivity check of the validity of SCM i.e. plot of $\log Q_i^H$ vs. [y(Cu^{2+})+y(Cd^{2+})] did not yield an identical value for the slope compared with the value obtained from binary exchange experiments. This obviously suggests that the parameters for binary exchange may not be extended for predicting ternary exchange equilibria as they do not remain constant for the two processes. Copper release by competitive nickel sorption is predicted reasonably well over the entire pH range except at pH values around 2.5 (see Fig. 3.20.). Zinc sorption by copper loaded AN is extremely low and therefore, the sorption curves essentially depict Cu^{2+}/H^+ exchange. The sensitivity check (as mentioned earlier) did not yield identical gradient values compared with binary equilibrium parameters used for predicting the ternary equilibria. There is insufficient data to really comment on the model's ability to predict ternary data from binary exchange parameters.

Considering that the surface reactions chosen to represent the interactions between metal ions in solution and the algal biomass surface were extremely simplified for model development, the initial predictions of binary exchange equilibria have provided valuable insight into the biosorption phenomenon. The importance of metal chelation by algal polysaccharides and the possible role of guluronic acid segments in ion exchange highlights the wide variation of surface reactions that need to be taken into account if reliable predictions of algal-metal interactions are to be successful. The present attempt at predicting algal heavy-metal biosorption by the surface complex formation model marks a first step in understanding the biosorption process so that any future attempts take the important mechanisms responsible for algal-metal interactions into account.

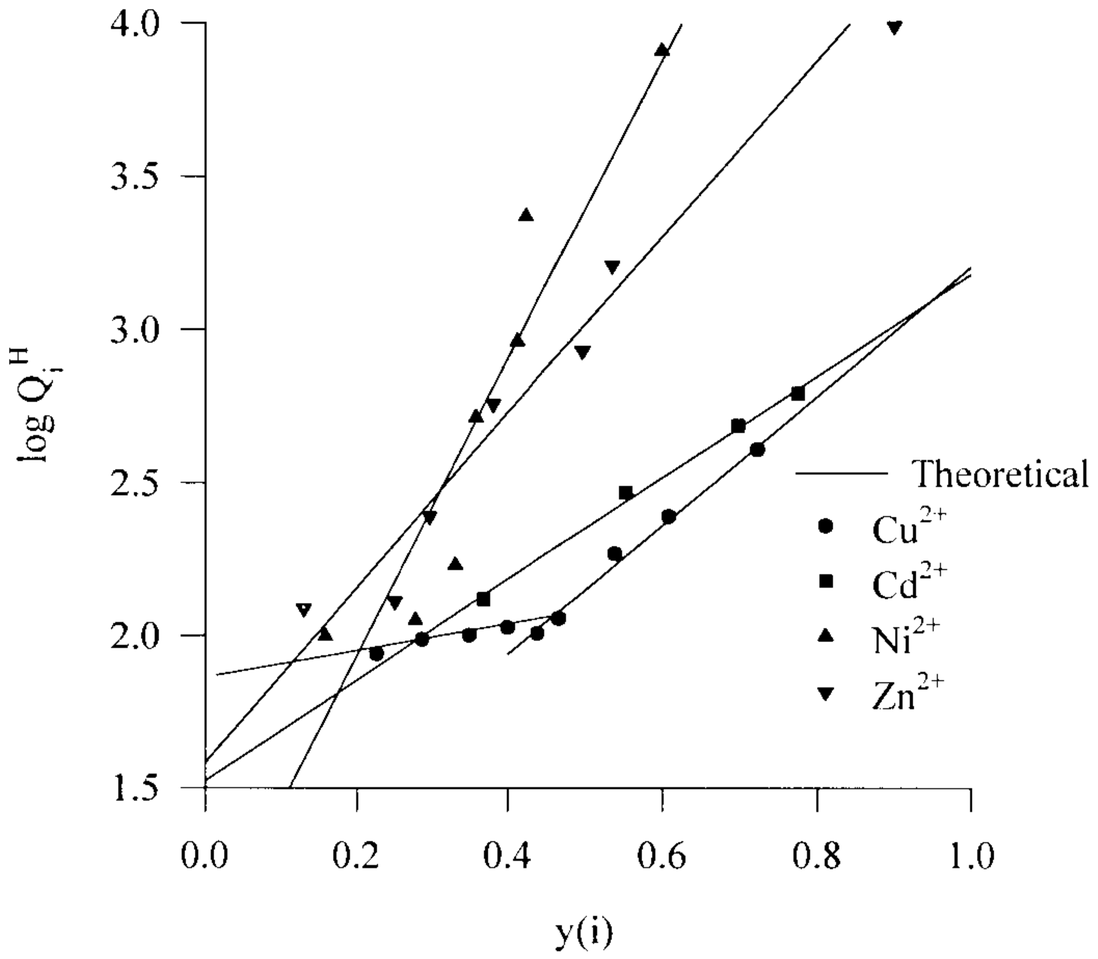

Figure 3.13. AN plot of log Q vs y(i) for different counterions.

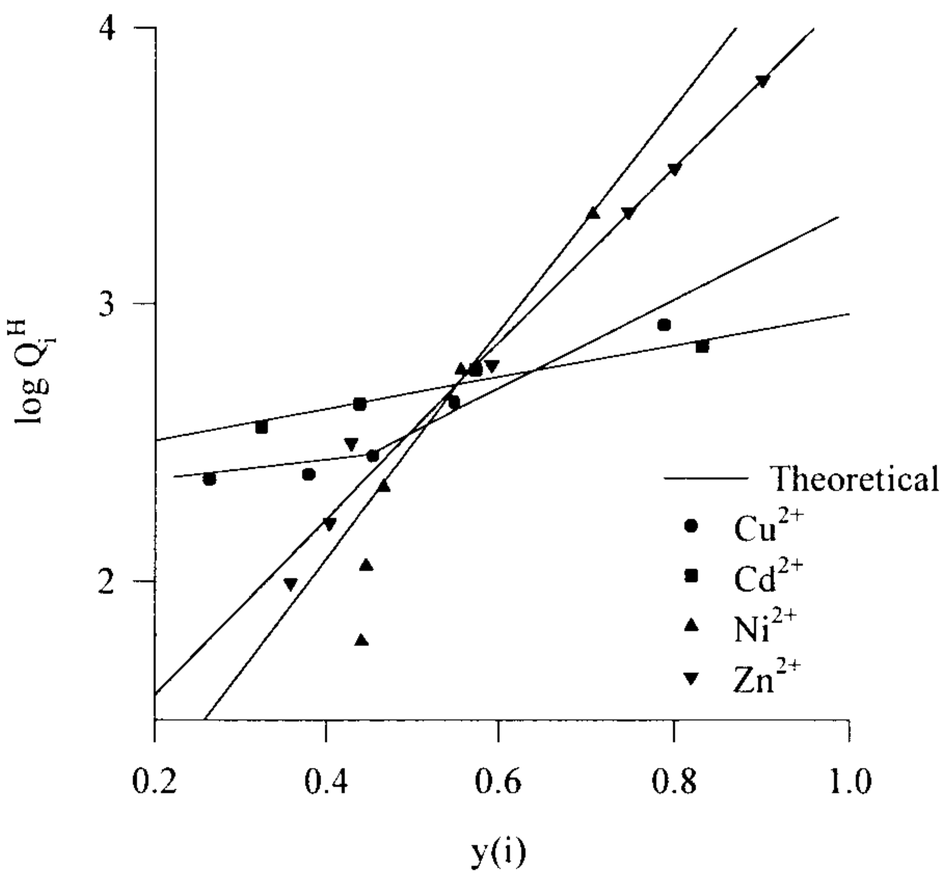

Figure 3.14. BK plot of log Q vs y(i) for different counterions.

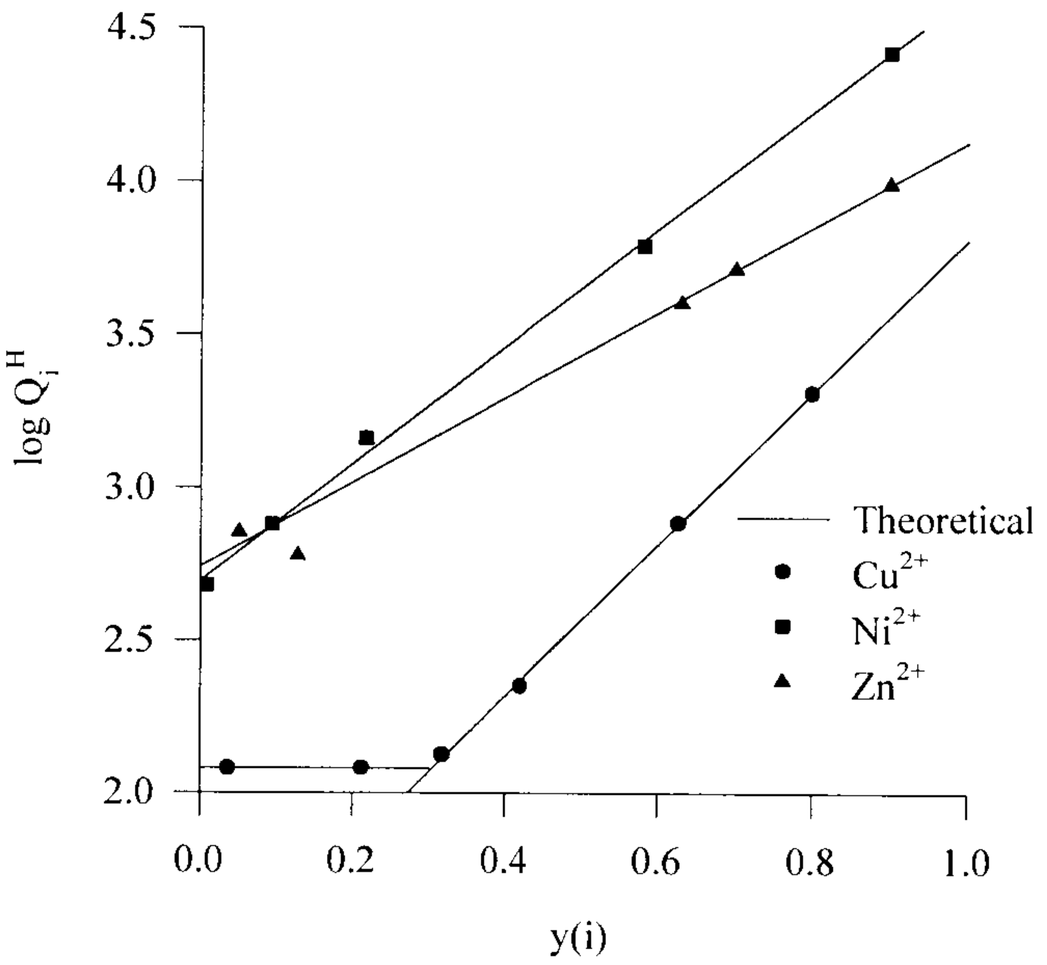

Figure 3.15. LH plot of log Q vs y(i) for different counterions.

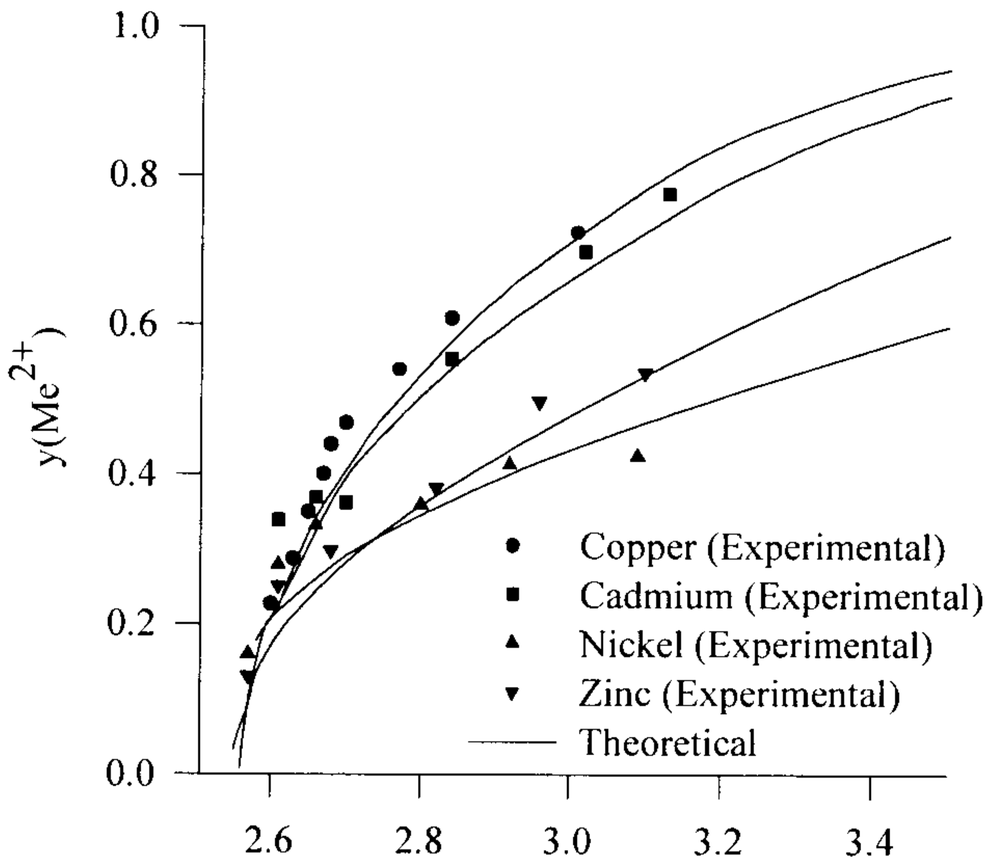

Figure 3.16. Comparison of experimental and theoretical equilibria for AN.

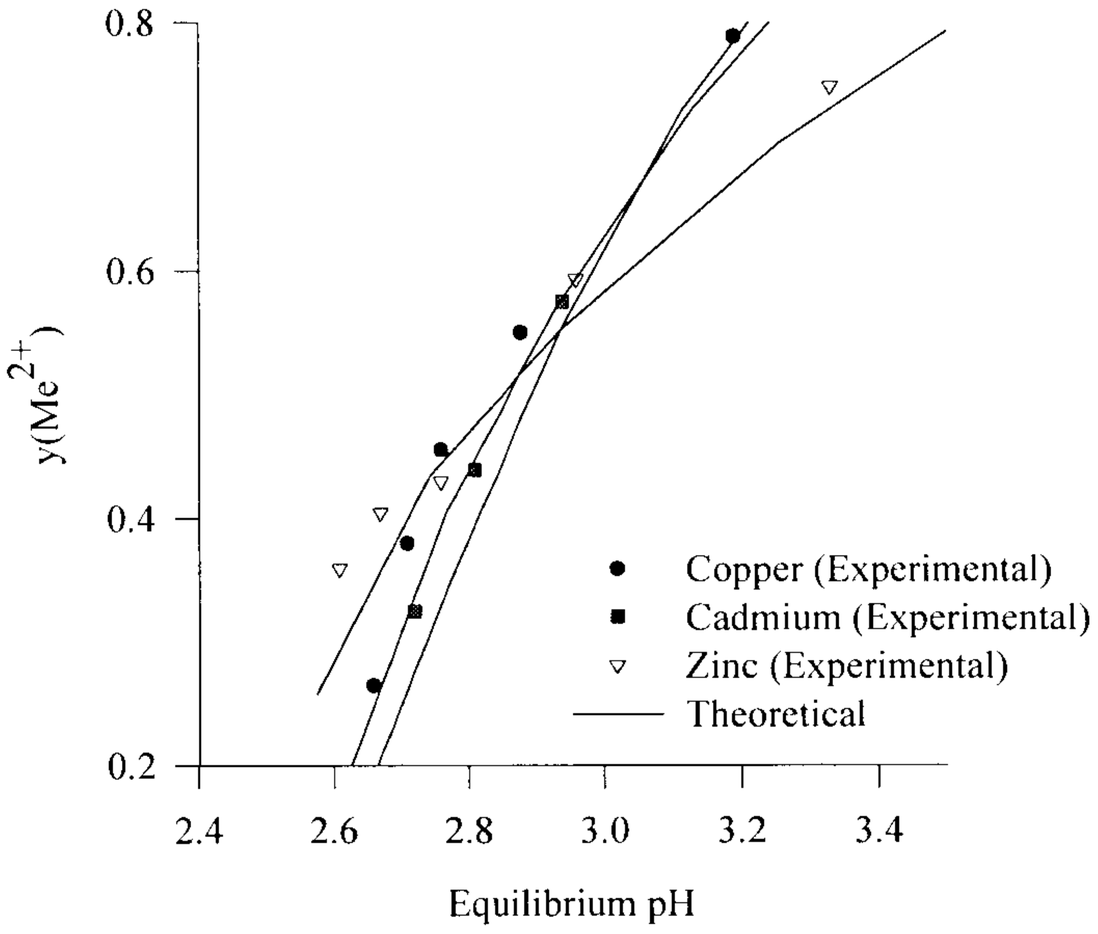

Figure 3.17. Comparison of experimental and theoretical equilibria for BK.

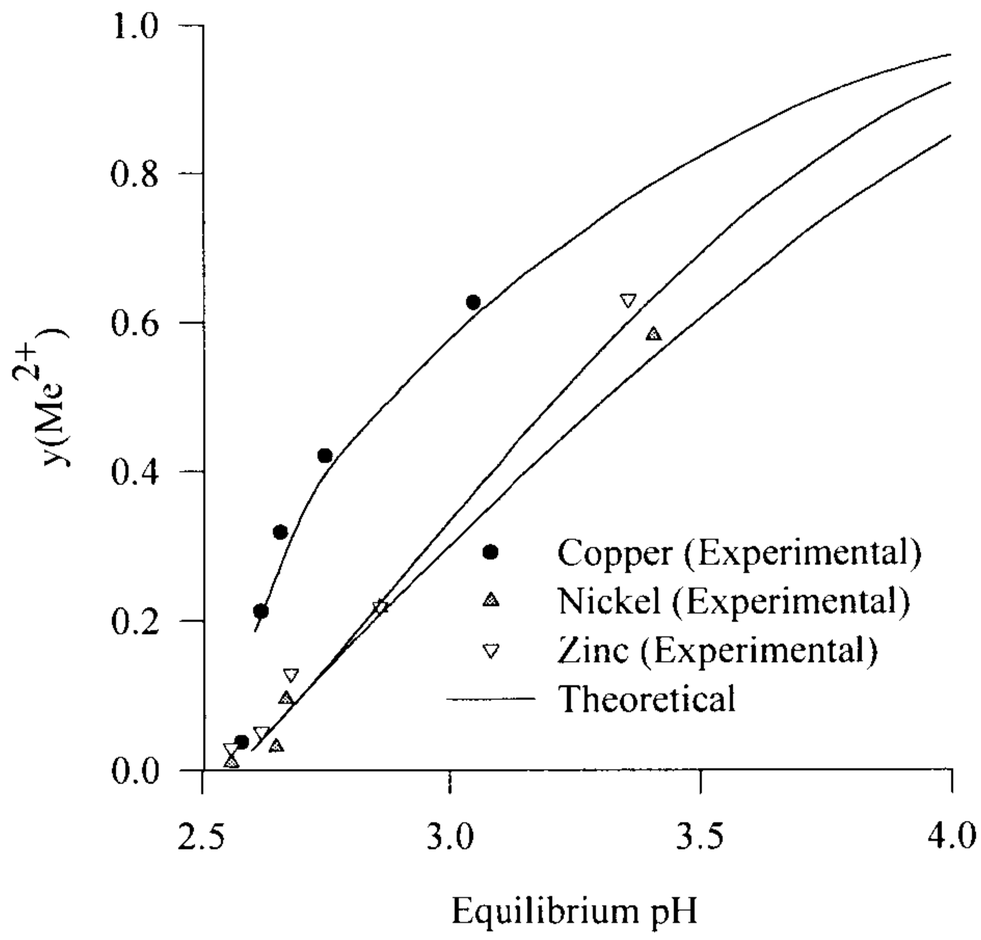

Figure 3.18. Comparison of experimental and theoretical equilibria for LH.

Ionic species	log K	$m(H^+,Me^{2+})$	range y(Me)
H^+/Cu^{2+}	1.1	2.1	0.5-1.0
H^+/Cd^{2+}	1.5	1.7	all
H^+/Ni^{2+}	0.96	4.9	all
H^+/Zn^{2+}	1.6	2.9	all

Table 3.7.a. Formation constants of surface complexes and gradients of regression analysis for AN.

Ionic species	log K	$m(H^+,Me^{2+})$	range y(Me)
H^+/Cu^{2+}	2.0	1.2	0.4-1.0
H^+/Cd^{2+}	2.4	0.6	all
H^+/Ni^{2+}	0.45	4.1	all
H^+/Zn^{2+}	0.95	3.2	all

Table 3.7.b. Formation constants of surface complexes and gradients of regression analysis for BK.

Ionic species	log K	$m(H^+,Me^{2+})$	range y(Me)
H^+/Cu^{2+}	1.3	2.5	0.3-1
H^+/Ni^{2+}	2.7	1.9	all
H^+/Zn^{2+}	2.7	1.4	all

Table 3.7.c. Formation constants of surface complexes and gradients of regression analysis for LH.

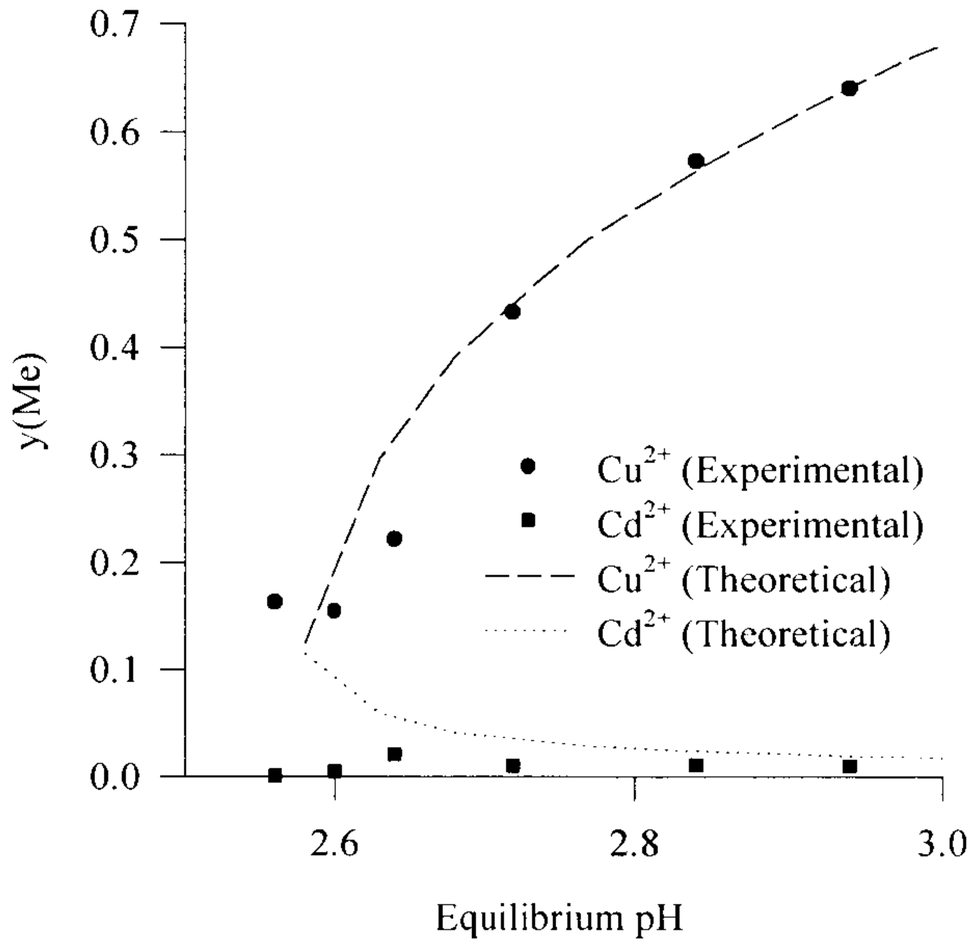

Figure 3.19. AN plot of ternary equilibrium data and calculated isotherms (Cu/Cd/H).

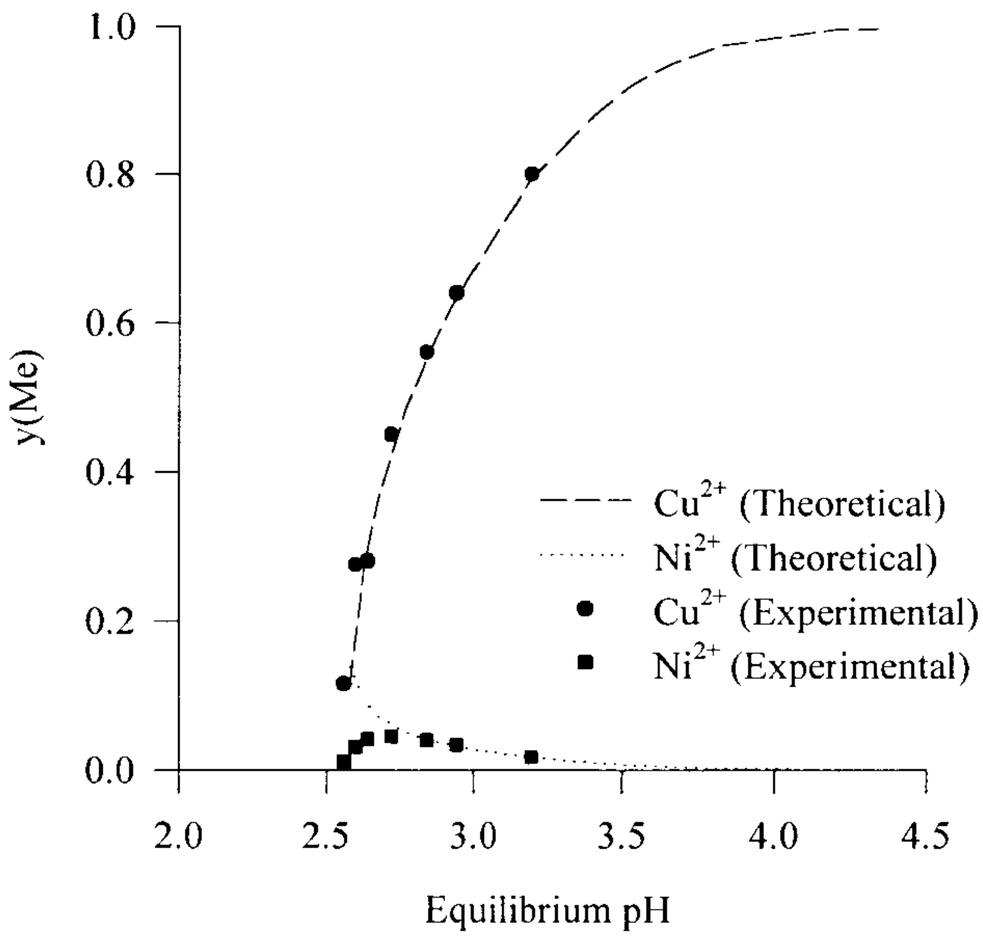

Figure 3.20. AN plot of ternary equilibrium data and calculated isotherms (Cu/Ni/H).

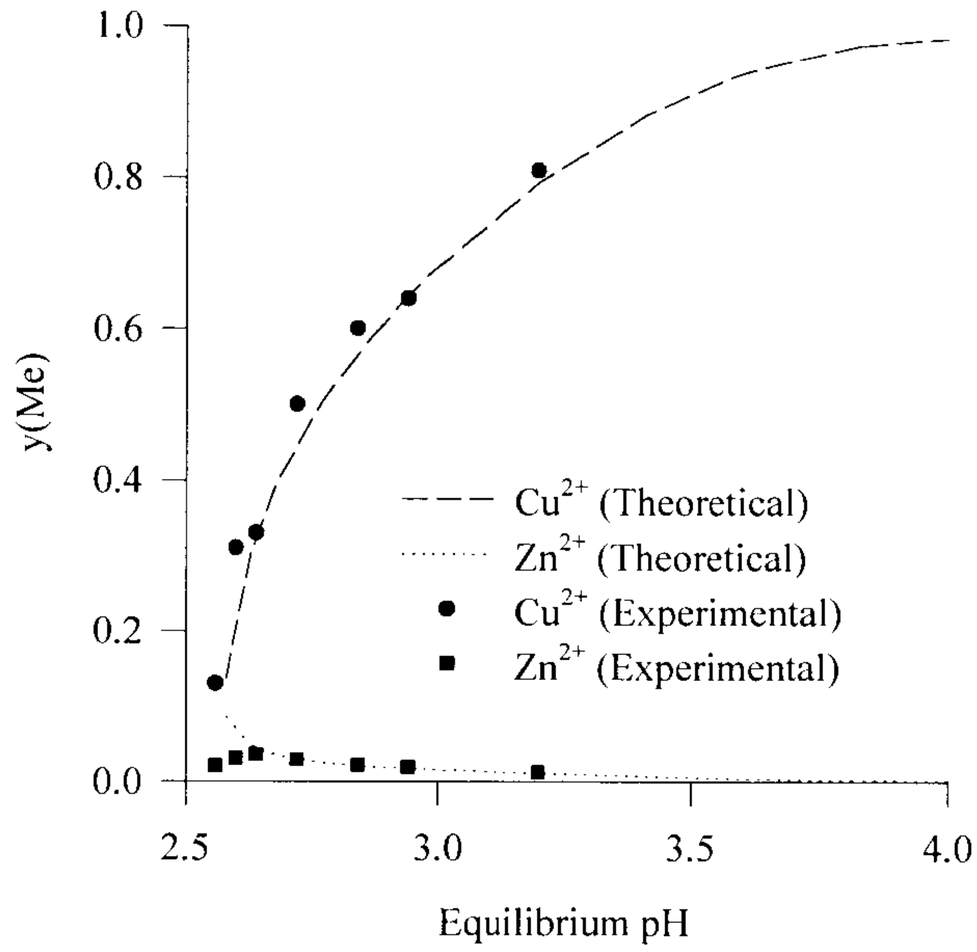

Figure 3.21. AN plot of ternary equilibrium data and calculated isotherms (Cu/Zn/H).

Selective uptake of metal ions from multi-metal bearing solutions

All algal biosorbents showed selective uptake of copper from mixed-metal bearing solutions (see Table 3.8.). LH showed the highest selectivity coefficient values for copper. The selectivity coefficient values did not remain constant when the concentrations were varied over a wide range, however, by keeping to standardised conditions, these values may be used for comparison of the affinities of different metals for algae. BK showed a slightly higher affinity towards cadmium in comparison with other virgin biomass. Copper was nevertheless the most preferred metal ion from mixed-metal solutions. Cadmium was preferred over nickel and zinc. Cadmium ions are more polarised than nickel or zinc. Carboxyl groups within algae are excellent proton acceptors, as a consequence, carboxyl groups prefer the more polarised, more strongly hydrated and larger cadmium ions compared with the other two cations[35]. Zinc is slightly preferred over nickel, thus the following affinity sequence may be drawn up:

$$Cu^{2+} \rangle\rangle Cd^{2+} \rangle Zn^{2+} \geq Ni^{2+}$$

This affinity sequence is similar to the selectivity of metal ions interacting with alginates (see Table 3.8.). Also, the selectivity sequence is in good agreement with results obtained from the surface complex formation model.

The total amount of metal ions taken up by the various biosorbents remained constant as long as copper or cadmium ions were present in solution. Binary mixtures of nickel and zinc resulted in lower uptake for each metal compared with sorption results from single metal bearing solutions. However, the sum total of metal ions taken up by the algae remained the same.

Species	$K_{Cd}^{'Cu}$	$K_{Ni}^{'Cu}$	$K_{Zn}^{'Cu}$	$K_{Ni}^{'Cd}$	$K_{Zn}^{'Cd}$	$K_{Zn}^{'Ni}$
AN	11.2	64	39	26	8	0.4
LF	13.4	85	81	31	12	0.6
BK	7.6	169	86	30	13	0.4
LH	22.7	88	110	17	5	0.4
AA-AN	5.8	176	104	44	14	0.6
AA-LF	13.1	204	103	46	16	0.3

Note: Results are for the following experimental conditions: pH4, 0.5 mM (each metal).

Table 3.8. Selectivity coefficients for equilibria between divalent metal ions.

Reducing the concentration of copper in solution increased the selectivity for the metal by algae resulting in higher selectivity coefficient values compared with those calculated for equal molar solutions. This result is consistent with established theories of ion exchange[35]. Selectivity of a divalent metal ion increases with solution dilution due to increased Donnan potential effects. LH shows the highest affinity for copper from a mixture of copper and cadmium ions in solution. This selectivity is even greater in comparison with copper selectivity exhibited by purified alginic acid samples (see Table 3.8.). The high guluronic acid residues constituting algin in LH may be attributed for the high selectivity towards copper ions in solution. The

diaxially linked 1C conformation of guluronic acid residues may result in interaction between the hydroxyl group on C2 and the oxygen atom of the carboxyl group in adjacent units (see also chapter 1). In contrast, LH shows lower selectivity than the other native algae towards cadmium ions from mixtures containing nickel and zinc ions as well. The other native algae e.g. BK, contain algin rich in mannuronic acid residues. All native algae except LH showed similar selectivity towards cadmium, nickel and zinc as alginic acid samples containing higher ratio of mannuronic acid residues. The stronger interaction of these cations with mannuronic acid segments rather than guluronic acid segments is a distinct possibility which might explain the subtle selectivity differences exhibited by the various algal biosorbents.

Section 3.4. Conclusions

Native marine algae have shown high sorption capacity for concentrating heavy metal ions from trace metal bearing aqueous solutions. In addition, dealginate seaweed waste has shown substantial metal sorption capacity for removing cadmium, nickel and zinc ions from near-neutral solutions. Proton-algal interactions are extremely important in the metal biosorption process which is a reversible phenomenon. The high algin content of BK results in this marine algae exhibiting the highest metal sorption capacity of all virgin biomass studied.

All algal biosorbents evaluated during the present study displayed selectivity towards the more polarised copper and cadmium ions. Nickel and zinc sorption affinities to the algal surface was noticeably lower by comparison. Modeling of the equilibrium sorption phenomenon has indicated that the reactions between copper ions in solution and the algal surface cannot alone be described by simple ion exchange. Covalent bond formation between copper ions and acidic surface functional groups in algae by chelation reactions may be the reason for the strong binding of these metal ions to marine algal biomass. Stoichiometric exchange coefficients of around 2 strongly suggests that when divalent heavy metal ions are sequestered by the biomass surface, a corresponding release of two monovalent ions (usually protons) occurs.

Preliminary attempts at applying a surface complex formation model to predict multicomponent exchange equilibria have met with limited success. Copper desorption due to competitive effects of cadmium, nickel and zinc ions in solution were predicted with marginal success. The effect of pH on sorption isotherms was well represented by the model.

Section 3.5. Nomenclature

A abbreviation for F/RT (V^{-1})

A_o surface parameter ($m^2\ g^{-1}$)

b affinity parameter of solute (-)

C_{eq} equilibrium metal concentration (mmol l^{-1})

C_{in} initial metal concentration (mmol l^{-1})

$C_{St,n}$ electric capacitance of Stern layer "n" (F m^{-2})

D_i diffusivity of species "i" ($cm^2\ s^{-1}$)

F Faraday constant (C eq^{-1})

F(j,i) distribution factor, $\frac{\left[\exp\left(-0.5z(j)A\psi_d\right)-1\right]}{\left[\exp\left(-0.5z(i)A\psi_d\right)-1\right]}$ (-)

K_i constant of the formation of a surface complex with counterions "i" (l mol^{-1})

K^i_j molar selectivity coefficient for exchange of i from a mixture of i and j (-)

L volume of liquid (l)

m_{sw} dry weight of sorbent (g)

Q_i^H selectivity coefficient (-)

q equilibrium metal uptake (mmol g^{-1})

q* maximum sorption capacity (mmol g^{-1})

$\overline{q^*}$ theoretical maximum sorption capacity (mmol g^{-1})

q(i) loading of sorbent phase with counterions "I" (meq g^{-1})

q_m exchange capacity (meq g^{-1})

R gas constant (J $mol^{-1}\ K^{-1}$)

R_H hydrated ionic radius ($\mathring{A}$)

R_i crystal ionic radius ($\mathring{A}$)

R_S Stokes ionic radius ($\mathring{A}$)

S sorbent quantity (kg)

T temperature (K)

V solution volume (l)

x(i) equivalent fraction of species "i" in liquid phase (-)

y(i) equivalent fraction of species "i" in solid phase (-)

z(i) valence number of species "i" (-)

Greek Letters

ε permittivity (F m^{-1})

σ_d charge density in the diffuse double layer (C m^{-2})

σ_S surface charge density (C m^{-2})

$\sigma_{St,n}$ charge density in the nth Stern layer (C m^{-2})

ψ_d electric potential of the diffuse double layer (V)

ψ_S electric potential at sorbent surface (V)

$\psi_{St,i}$ electric potential of ith Stern layer (V)

ψ_x electric potential at distance x from surface (V)

Section 3.6. References

1. Kratochvil, D., Pimentel, P. F. and Volesky, B. 1998, Envrion. Sci. Technol., vol. 32, no. 18, 2693.
2. Schiewer, S. and Volesky, B. 1997, Environ. Sci. Technol., vol. 31, no. 7, 1863.
3. Westall, J. C., Jones, J. D., Turner, G. D. and Zachara, J. M. 1995, Environ. Sci. Technol., vol. 29, no. 4, 951.
4. Schiewer, S. and Volesky, B. 1997, Environ. Sci. Technol, vol. 31, no.7, 1863.
5. Milne, C. J., Kinniburgh, D. G., deWit, J. C. M., Van Riemsdijk, W. H. and Koopal, L. K. 1995, Geochim. Cosmochim. Acta., vol. 59, 1101.
6. Bartschat, B. M., Cabaniss, S. E., Morel, F. M. M. 1992, Environ. Sci. Technol., vol. 26, 284.
7. Benedetti, M. F., Van Riemsdijk, W. H., Koopal, L. K. 1996, Environ. Sci. Technol., vol. 30, no. 6, 1805.
8. Donnan, F. G. 1911, Z. Electroch., vol. 17, 572.
9. Marinsky, J. A. and Ephraim, J. 1986, Environ. Sci. Technol., vol. 20, no. 4, 349.
10. Lin, F. G. and Marinsky, J. A. 1993, Reactive Polymers, vol. 19, no. 1-2, 27.
11. Kinniburgh, D. G., Milne, C. J., Benedetti, M. C., Pinheiro, J. P., Filius, J., Joopal, L. K. and Van Riemsdijk, W. H. 1996, Environ. Sci. Technol., vol. 30, no. 5, 1687.
12. Xue, H. and Sigg, L. 1993, Limnol. Oceanogr., vol. 38, 1200.
13. Tipping, E. 1993, Environ. Sci. Technol., vol. 27, no. 3, 520.
14. Schiewer, S. and Volesky, B. 1997, Environ. Sci. Technol., vol. 31, no. 7, 2478.
15. Chong, K. H. and Volesky, B. 1996, Biotechnol. Bioeng., vol. 49, no. 6, 629.
16. Milne, C. J., Kinniburgh, D. G., deWit, J. C. M., Van Riemsdijk, W. H. and Koopal, L. K. 1995, Geochim. Cosmochim. Acta., vol. 59, no. 6, 1101.
17. Tipping, E. and Hurley, M. A. 1992, Geochim. Cosmochim. Acta., vol. 56, 3627.
18. Tipping, E. 1993, Colloids Surf. A: Physiochem. Eng. Aspects, vol. 73, 117.
19. Barak, P. and Chen, Y. 1992, Soil Science, vol. 154, no. 3, 184.
20. Ephraim, J. and Marinsky, J. A. 1986, Environ. Sci. Technol., vol. 20, no. 4, 367.
21. Chen, J. and Yiacoumi, S. 1997, Sep. Sci. Technol., vol. 32, no. 1-4, 51.
22. Horst, J., Holl, W. H. and Eberle, S. H. 1990, Reactive Polymers, vol.13, no. 3, 209.
23. Eisenmann, G. 1983, In "Mass transfer and kinetics in ion exchange", Liberty, L., and Helfferich, F. G., (Eds.), Martinus Nijhoff, The Hague.
24. Yiacoumi, S. and Tien, C. 1995, Kinetics of metal ion adsorption from aqueous solutions, Kluwer Academic Publishers, Boston, USA.
25. Crist, R. H., Oberholser, K. and McGarrity, J. 1992, Environ. Sci. Technol., vol. 26, no. 3, 496.
26. Kuyucak, N. and Volesky, B. 1988, Biotechnol. Letters, vol. 10, no. 2, 137.
27. Matheickal, J. T. and Qiming, Y. 1996, Wat. Sci. Tech., vol. 34, no. 9, 1.
28. Aldor, I., Fourest, E. and Volesky, B. 1995, Can. J. Chem. Eng., vol. 73, no. 4, 516.
29. Kratochvil, D., Volesky, B. and Demopoulos, G. 1997, Water Res., vol. 31, no.9, 2327.
30. Lee, H. S. and Volesky, B. 1997, Water Res., vol. 31, no. 12, 3082.
31. Holan, Z. R. and Volesky, B. 1995, Biotechnology Prog., vol. 11, 235.

32. Haug, A. 1959, Acta. Chem. Scand., vol. 13, 1250
33. Mongar, J. L. and Wassermann, A. 1949, Discussions Faraday Soc., vol. 7, 118.
34. Haug, A., Myklestad, A., Larsen, B. and Smidsrod, O. 1967, Acta. Chem. Scand., vol. 21, 768.
35. Helfferich, F. 1995, Ion exchange, Dover Publications Inc., New York, USA.
36. Williams, C.J. and Edyvean, R.G.J., 1997, Biotechnol. Prog., vol. 13: no.4, 424-428.
37. Fisher, F. G. and Dorfel, H. Z., 1955, Physiol. Chem. vol. 302, 186.
38. McDowell, R.H, 1986, Properties of alginates, 4-5 (Published by Kelco International Ltd.).
39. Haug, A., and Smidsrod, O., 1965, Acta. Chem. Scand., vol. 19, no.2, 329-341.
40. Percival, E. G. V. and Percival, E. 1962, Structural carbohydrate chemistry, J. G. Miller, Ltd., UK.
41. Greig, J. A. 1998, Personal Communication, Monsanto plc.
42. Harned, H. S. and Owen, B. B. 1958, "The physical chemistry of electrolytic solutions", 3rd edition, Reinhold Publishing Corporation, New York.
43. Boyd, G. E., Schubert, J. and Adamson, A. W. 1947, J. Am. Chem. Soc., vol. 69, 2818.
44. Kressman, T. R. E. and Kitchner, J. A. 1949, J. Chem. Soc., 1190.
45. Benedetti, M. F., Milne, C., Kinniburgh, D. G., Van Riemsdijk, W. H. and Koopal, L. K. 1995, Environ. Sci. Technol., vol. 29, no. 2, 447.

Regeneration and Kinetics of Metal Biosorption

"The history of scientific and technical discovery teaches us that the human race is poor in independent thinking and creative imagination. Even when the external and scientific requirements for the birth of an idea have long been there, it generally needs an external stimulus to make it actually happen; man has, so to speak, to stumble right up against the thing before the right idea comes."

(Albert Einstein 1879-1955)

Chapter 4

Regeneration and Kinetics of Metal Biosorption

This chapter compares the rate of heavy metal biosorption by native and dealginate marine algae from aqueous solutions. The important rate determining parameters have been identified and values of ionic diffusivities estimated. Regeneration of metal-saturated algae using a spectrum of eluants has helped in identifying possible potent eluants.

Section 4.1. Theory and Literature Review

Regeneration of metal-laden biosorbents

Regeneration of metal-laden algal biomass has not attracted much attention. Little systematic effort has been devoted to an important topic worthy of greater attention. What is to become of the metal-laden algal biomass? An obvious solution is to concentrate the metal in as small a volume as possible. Ideally, the eluted solution should contain high concentrations of metal, hundreds or thousand-fold increase in concentrations compared with the original metal bearing solution to be treated. Aldor et al[1] studied the elution of cadmium laden *Sargassum fluitans* using hydrochloric acid. Concentration ratios of 70 were successfully obtained. No loss of cadmium sorption capacity was observed in three consecutive metal uptake/desorption cycles. In another study[2], elution of gold-laden *Sargassum natans* using thiourea as eluant resulted in deterioration of the uptake capacity in subsequent sorption cycles.

Kinetics of metal biosorption

Study of the sorption kinetics of algae-metal interactions in aqueous solutions is essential for improved understanding of transport mechanisms which control the sorption rate. Evaluation of rate constants, intraparticle diffusivity or diffusion coefficient values from single metal kinetic studies represents the first step in the determination of the interdependence between equilibrium and mass transport

phenomenon[3]. These parameters provide an essential basis for the establishment of a suitable model necessary for process design and performance prediction.

Ion exchange between ionic species in solution and algal polysaccharides; particularly between algin in the cellular walls and metal ions in solution is thought to be the dominant mechanism for metal biosorption[4]. Ion exchange is considered a diffusional phenomenon in porous sorbents with five possible rate-limiting steps[5]:

1. Diffusion of counter-ions from the bulk solution to the surface of the ion exchange biosorbent particle.
2. Diffusion of counter-ions within the solid particle.
3. Exchange of counter-ions with those on the biosorbent matrix.
4. Diffusion of exchange ions out of the sorbent matrix towards the outer surface of the sorbent particle.
5. Diffusion of the displaced ions from the exchanger surface into the bulk solution.

In the bulk solution, concentration gradients are constantly leveled out by agitation of the sorbent solution mixture. The agitation however, has little effect on the interior of the sorbent particles nor on a liquid layer which adheres to the sorbent surface. Thus, within the sorbent particle and through this adhering film, transport may occur by diffusion only. Consequently, the two potential rate determining steps are:

1. Inter-diffusion of counter-ions within the exchanger itself (particle-diffusion)
2. Inter-diffusion of counter-ions in the adherent films (film-diffusion)

Either may be rate controlling while in intermediate cases, the rate may be affected by both steps. Helfferich[6] provides kinetic rate theories and mathematical expressions correlating effective diffusion coefficient values (the reader is referred to this text for a thorough treatment of this subject). Another useful text by Slater[7] reviews recent developments in the area of kinetics for predicting ion exchange sorption rates. Pore diffusion, ion exchange with chemical reaction in the sorbent and shrinking-core models are discussed. Representative resin bead self-diffusion coefficients for common metal ions are tabulated with references citing pertinent literature.

The kinetics of single metal biosorption in a batch system has received some attention in the literature. Intraparticle diffusivity for Cu^{2+} sorption by calcium alginate beads was calculated by Jang et al.[8] using a shrinking-core model. Apel and Torma[9] confirmed that Cd^{2+}, Zn^{2+}, and Ba^{2+} sorption in calcium alginate beads was intraparticle diffusion control limited. Cd^{2+} diffusivity values were one or two orders of magnitude lower than the corresponding molecular value. Yang and Volesky[3] presented a model incorporating linear and Langmuir equilibrium isotherms into a rate equation for the intraparticle diffusion of Cd^{2+} during desorption from formaldehyde crosslinked *Sargassum fluitans* algal particles. The desorption rate of Cd^{2+} increased with decreasing particle size indicating that the overall desorption process was governed by intraparticle diffusion. During desorption experiments, the particle-to-fluid mass transfer resistance was eliminated by sufficient stirring. The typical mass conservation equation was solved numerically using appropriate boundary conditions. Incorporation of the nonlinear Langmuir isotherm equation made an analytical solution impossible. Desorption rate studies at pH 1 could be modeled using a linear equilibrium sorption isotherm. An analytical solution for this case was possible. Calculated Cd^{2+} diffusivity values ranged from (2.73×10^{-6}-3.5×10^{-6}) $cm^2\ s^{-1}$ at pH 1 for different particle sizes and 1.65×10^{-6} $cm^2\ s^{-1}$ at pH 2. Molecular diffusivity of cadmium ions in aqueous solution is 7.19×10^{-6} $cm^2\ s^{-1}$ (see Table 3.5.).

In a slightly different approach, Yiacoumi and Tien[10] modeled adsorption rates in terms of three separate yet interacting phenomenon: surface ionization, complex formation and the presence of an electrostatic double layer adjacent to the adsorbent surface. Matching of experimental results with model calculations was accomplished following a combined macropore and micropore diffusion model. The calculated dependence of sorption profiles on solution pH agreed well with experimental data. However, the effect of total metal ion concentration on adsorption history was not described well. Inaccurate description of adsorption density at equilibrium was thought to be the cause of the discrepancies.

The strong affinity of metal ions to algal biomass and results of metal sorption rate studies on calcium alginate beads provides some evidence that the ion exchange process within algae may be represented as a fast chemical reaction. The interacting ions progress in shells into the biosorbent matrix. Covalently bound metal ions in the biomass may result in undissociated surface groups. The presence of moving boundaries within ion exchange resin particles has been demonstrated by microphotography[11,12,13]. The shrinking core model was originally developed to describe burn-off of carbonaceous deposits from catalyst particles[14]. Application to ion exchange systems was the work of Helfferich[15]. The assumption of Fickian diffusion with a constant intraparticle diffusivity lead to an analytical solution[16]. No specific interactions within the ion exchanger were accounted for, hence ions were assumed to simply diffuse through the outer reacted layer without hindrance. Yoshida et al.,[17,18] presented a series of papers with analytical solutions applicable for weak-acid ion exchangers based on the shrinking core model but using the Nernst-Planck equation to account for electric field effects to describe the transport process.

Initially, rate laws based on simple diffusion processes were used to fit experimental rate data and determine effective diffusion coefficient values. Conventional plots of $\ln(1-F^2)$ vs (t) and $\ln(1-F)$ vs (t) (where F is the fractional conversion of biosorbent into metal form and t is time) were unsuccessful in representing biosorption rate data.

Since this approach is best suited to describe diffusional transport of non ionic species (isotopic exchange), the inability to describe metal biosorption rate data was not surprising. In biosorption, the fluxes of at least two ions (protons on algae and metal ions in solution) are coupled with one another. The electric coupling of ionic fluxes distinguishes metal biosorption from simple diffusional processes. An approximate numerical solution for the continuity equation where the Nernst-Planck equation was used to account for electric field effects in ion exchange resins is provided by Helfferich[6]. This solution was applied to fit metal biosorption data, however, due to the assumption of co-ion exclusion from the sorbent matrix, this solution did not provide a good theoretical fit to experimental data (co-ion exclusion may be true in strong-acid resins due to Donnan exclusion, however, in weakly dissociated ion exchange materials, the assumption is not entirely valid).

In the previous chapter, the possibility of covalent bond formation between copper ions and the metal binding sites in algae has been highlighted. If copper sorption by algal particles may be considered as an irreversible process due to covalent bond formation between metal ions and the surface functional groups (under the sorption conditions), then the applicability of the shrinking core model is reasonably justified. In the current study, an analytical solution for diffusion limited transport with all ionic species obeying the Nernst-Planck equation in algal biosorbent particles has been applied in order to extract ionic diffusivity values from sorption rate data. The model is based on the solution by Yoshida et al[18] however, all equations have been derived by the author (not provided in the original paper; see Appendix 1). The principal assumptions and an outline of the equations used are provided below:

The exchange reaction between the biomass surface and metal ions in solution may be represented by the reaction:

(1)

where B denotes a certain metallic cation and R is the biosorbent matrix. The ion exchange reaction may be represented by the reversible reaction:

$$z_B R^- - H^+ + B^{z_B+} \leftrightarrow (R^- -)_{Z_B} B^{Z_B^+} + z_B H^+ \qquad (2)$$

The reaction between the surface functional groups and the metallic ions may be considered an instantaneous reaction. Also, the strong affinity of the metal ions to the surface functional groups lead to undissociated surface-metal groups. Hence (2) may be written as an irreversible reaction:

$$z_B R^- - H^+ + B^{z_B+} \rightarrow (R^- -)_{Z_B} B^{Z_B^+} + z_B H^+ \qquad (3)$$

The biosorbent particle is divided into a unreacted core of $R^- - H^+$ and an outer reacted shell converted to the corresponding metal form $\overline{R-B}$ (see Fig. 4.1.). Thus the following statements may be written:

$$q_H = Q \qquad 0 \le r \le \delta \qquad (4)$$

$$z_B q_{\overline{RB}} = Q \qquad \delta \le r \le r_o \qquad (5)$$

The metal ions B^{2+} diffuse through the reacted outer shell towards the carboxyl groups in the unreacted core of the biosorbent particles. Considering that the diffusion process is limited by conditions of electroneutrality and no net electric current in the shell, the following statements may be written:

$$q_H + z_B q_B = z_E q_E \qquad \delta \le r \le r_o \qquad (6)$$

$$J_H + z_B J_B = z_E J_E \qquad \delta \le r \le r_o \qquad (7)$$

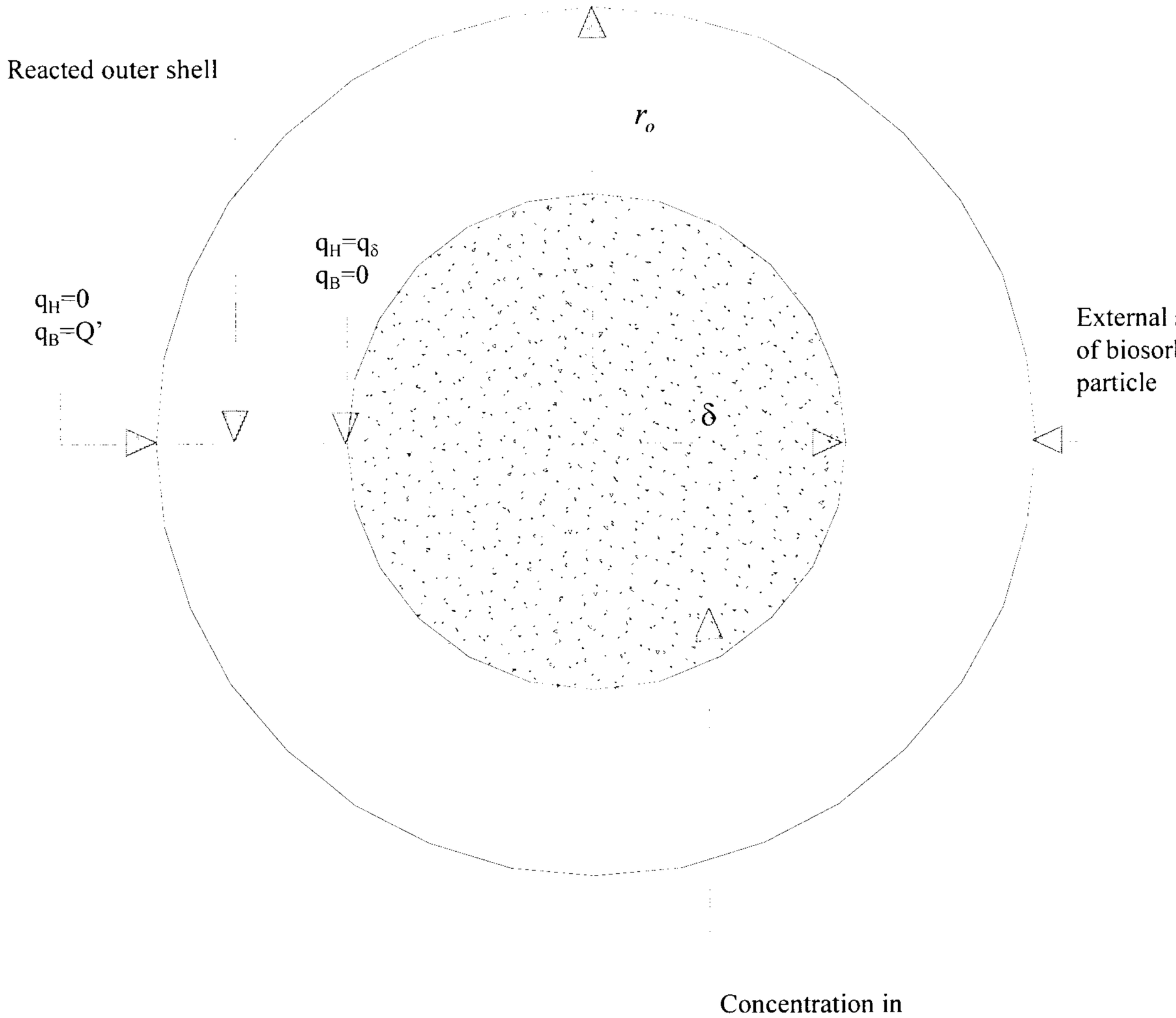

Figure 4.1. Schematic representation of shrinking core model of a biosorbent particle.

The coion is not consumed or produced by the reaction (3) hence, the flux J_E may be neglected:

$$J_E = 0 \qquad (8)$$

Expressions for the fluxes of H and B are obtained from (6), (7) and (8) coupled with the Nernst-Planck equation (See full derivation Appendix 1, Section 1). The fluxes are related to the concentration gradient within the biosorbent particles.

$$J_H = -D_H\left[\frac{\left(z_E + z_B\right)U_B + \left(1 + z_E\right)U_H}{\left(z_E + z_B\right)U_B + \left(\alpha + z_E\right)U_H}\right]\frac{\partial q_H}{\partial r} \qquad (9)$$

$$J_B = -D_B\alpha\left[\frac{\left(z_E + z_B\right)U_B + \left(1 + z_E\right)U_H}{\left(\alpha z_E + z_B\right)U_B + \left(1 + z_E\right)\alpha U_H}\right]\frac{\partial q_B}{\partial r} \qquad (10)$$

Initial and boundary conditions are given as follows:

Initial conditions:

$$q_H = Q \text{ and } q_B = Q_{\overline{RB}} = 0\,;\ \text{t=0} \qquad (11)$$

$$\delta = r_o\,;\ \text{t=0} \qquad (12)$$

Boundary conditions:

$$q_H = 0\,;\ \text{r=r}_\text{o} \qquad (13)$$

$$q_B = Q'\,;\ \text{r=r}_\text{o} \qquad (14)$$

$$q_H = z_E q_E = q_\delta\,;\ \text{r=}\delta \qquad (15)$$

$$q_B = 0\,;\ \text{r=}\delta \qquad (16)$$

$$J_H = -z_B J_B = -Q\frac{d\delta}{dt}\,;\ \text{r=}\delta \qquad (17)$$

Equation (18) is the relation between U_{Na} and U_B in the shell and is obtained from eqs. (6)-(10), (13) and (14):

$$\left(U_{Na} + U_B\right)\left(GU_{Na} + U_B\right)^S = U_{Bo}^{1+S}\,;\ \rho_\delta \le \rho \le 1 \qquad (18)$$

The derivation of eq(18) is given in Appendix 1, Section 2. Using equation (18) and the assumption of a pseudo-steady state, eq(19) is derived in Appendix 1, Section 3.

$$\frac{\partial}{\partial \rho}\left[\rho^2\left\{\left(z_B-1\right)\left(\frac{U_{Bo}}{U_E}\right)^{\frac{1+S}{S}}-G\left(z_B+z_E\right)+\left(1+z_E\right)\right\}\frac{\partial U_E}{\partial \rho}\right]=0,\ \rho_\delta \le \rho \le 1 \quad (19)$$

Equation (20) the boundary condition at ρ_δ is obtained from eqs. (15), (16) and (18):

$$U_E^\delta = U_{Bo}G^{-\frac{S}{1+S}}, \rho = \rho_\delta \quad (20)$$

Equation (20) is derived in Appendix 1, Section 4. Integrating the partial differential equation (19) twice (See Appendix 1, Section 4) eq(21) is obtained:

$$2\rho_\delta^3-3\rho_\delta^2+1=\left\{\frac{S\left(z_B-1\right)\left(1-G^{\frac{1}{1+S}}\right)+\left\{G\left(z_B+z_E\right)-\left(1+z_B\right)\right\}\left[1-G^{\frac{S}{1+S}}\right]}{z_E\left(1-\alpha\right)\left(1-G\right)}\right\}\frac{6\alpha U_{Bo}D_B}{r_0^2}t \quad (21)$$

The fractional approach to equilibrium (F) is given by:

$$F=1-\rho_\delta^3 \quad (22)$$

Eq(21) may be written in the final form:

$$3-2F-3\left(1-F\right)^{\frac{2}{3}}=\left\{\frac{S\left(z_B-1\right)\left(1-G^{\frac{1}{1+S}}\right)+\left\{G\left(z_B+z_E\right)-\left(1+z_B\right)\right\}\left[1-G^{\frac{S}{1+S}}\right]}{z_E\left(1-\alpha\right)\left(1-G\right)}\right\}6U_{Bo}\tau \quad (23)$$

Experimental rate data was fitted to eq(23). Ionic diffusivity values were extracted from the gradient values of the regressed data.

Section 4.2. Experimental Parameters

Regeneration of metal-laden biosorbents

Preliminary regeneration experiments using hydrochloric acid as eluant for copper and cadmium laden *A. nodosum* had indicated near complete regeneration at solution pH values below pH 2[19]. In the current study, several eluants were tested for desorbing metal ions from saturated algal biosorbent beds in an attempt to elucidate the interactions of various cations and anions with potential metal binding sites within the biosorbents. Inorganic acids (HCl, HNO_3, and H_2SO_4) were studied to see the effect of different anions on metal elution. $CaCl_2$, NH_4Cl and NaCl were studied to see whether these cations could compete for metal binding sites previously occupied by various heavy metal ions. Na_2CO_3 and $NaHCO_3$ were used since they have a tendency to solubilise algin and thus liberate metals. Complexing agents such as Na_2EDTA were used to interact with metal ions on the biosorbent and break complexes between algal functional groups and metal ions.

Metal saturated *A. nodosum* algal particles were used in the elution study. Total metal content of algal particles was calculated by digesting the metal-laden biosorbent particles in concentrated perchloric acid. Following dilution, metal uptake by the algal particles was calculated by analyzing the solution using AAS. This metal uptake capacity was used to compare the desorption efficiency of the various eluants tested. 50mg of the metal-laden biomass was placed in an ion exchange column. 50ml of eluant was pumped through the algal bed (10 ml hr^{-1}) with effluent collected in a sample container. Final metal concentration in the effluent was measured using AAS. A comparison with the metal content of the algal particles determined from the digestion experiment provided a simple method of determining the efficiency of the elution process. The initial pH of the solution passed through the bed was also noted.

The influence of S/L ratios (defined later) on achieving high concentration factors in the eluant was studied in order to optimise the regeneration process. The ratio of the loaded biomass weight (mg) to the eluant volume (ml) was defined as the solid-to-

liquid ratio (S/L) which was varied in the range from 0 to 2 for the preliminary evaluation of its effect on the concentration factor. Concentration factor is defined as the ratio of metal concentration in the eluant at equilibrium compared with feed solution used to saturate the sorbent material initially (0.5mM in this case). *A. nodosum* previously exposed to a cadmium chloride containing solution sequestered the metal at an appropriate cadmium loading of around 1.5 mmol g^{-1}. The column set-up depicted in Figure 3.2. was employed except, that, the eluant solution after passing through the column was recycled back to the feed tank. The sorbent was therefore equilibrated with the eluant solution which was continuously recycled through the algal bed until no change in solution pH or metal concentration was recorded. 48h was experimentally confirmed to be sufficient time for the attainment of desorption equilibrium. Metal solution in the eluant was analysed using AAS in flame mode.

Kinetics of metal biosorption

A schematic of the rig used to study metal sorption rates by the algal biosorbents is depicted in Figure 4.2. A variable speed stirrer (Heidolph RZR 2020) was used to ensure good mixing within the reaction vessel. The stirrer speed was measured by using a digital tachometer (TM-3011 non contact, optical sensor type). The stirrer was made of glass and connected to the motor with a stainless steel rod covered in PVC tubing to avoid vibrations at high speeds. The motor was allowed to warm up for 30 minutes before each experiment to ensure constant speed. Freeze dried seaweed samples were ground in a laboratory coffee grinder and then dry sieved to obtain fractions (45-90 μm) and (300-355 μm). All test solutions were made from analytical grade metal salts in DDW of resistivity greater than 15 MΩ cm^{-1}.

200mg of algal particles were swollen in 75ml of DDW for 20 minutes. Previous experiments had shown that using dry particles for metal uptake rate measurements was not suitable as the rate of uptake was much slower than if the particles had been pre-wetted. Swelling of the algal particles is important in order to allow accessibility of metal sorption sites within the biosorbent matrix. 1925ml of metal ion solution was prepared by weighing the appropriate amount of metal chloride salt and dissolved in DDW (the pH of the solution was adjusted to pH 3.85 by addition of HCl). This

solution was poured into a 2l round bottomed glass reactor. The concentration of metal solution was measured by withdrawing a 5ml sample and analyzing for metal concentration using AAS. The algal slurry was poured into the reactor containing the metal solution. It was assumed that the small quantity of water added to the reactor volume mixed almost instantaneously with the bulk solution.

A one minute time delay was usually needed to allow the system to settle once the metal containing solution was added to the reactor. Samples were withdrawn frequently during the first hour as preliminary tests had suggested relatively fast kinetics. Sample volume withdrawal was kept as small as possible to prevent greater than 5% volume reduction. Sample volumes of 5ml/sample were withdrawn. After the first hour, samples were withdrawn every hour for the next five hours. A final sample was withdrawn after a minimum of 12 hours of sorbent/solution contact time.

The experiments reported here were conducted at room temperature (20-25°C). A low starting solution pH was employed to avoid using a buffer. Algal particles were used in hydrogen form, thus the pH of the solution fell as hydrogen ions were released into the solution and metal ions were taken up. The metal sorption capacity of the seaweed was found to be highly pH dependent (see chapter 3). Preliminary experiments showed that hydrogen ions released during metal exchange reduced the pH of the solution from 4 to below 3.5. There is a significant change in the metal uptake capacity over this pH range. If however, the initial solution pH was around 3.8, following metal sorption this final solution pH was marginally lower (~ pH 3.5). Therefore, the lower pH range was chosen for the sorption rate investigations since the effect of pH changes on sorption capacity is limited over this pH range.

1. Thermostat
2. Sampling syringe
3. 20 micron PTFE Filter
4. Solution/Sorbent mixture
5. Water bath
6. Thermometer
7. Glass impeller
8. Variable speed motor

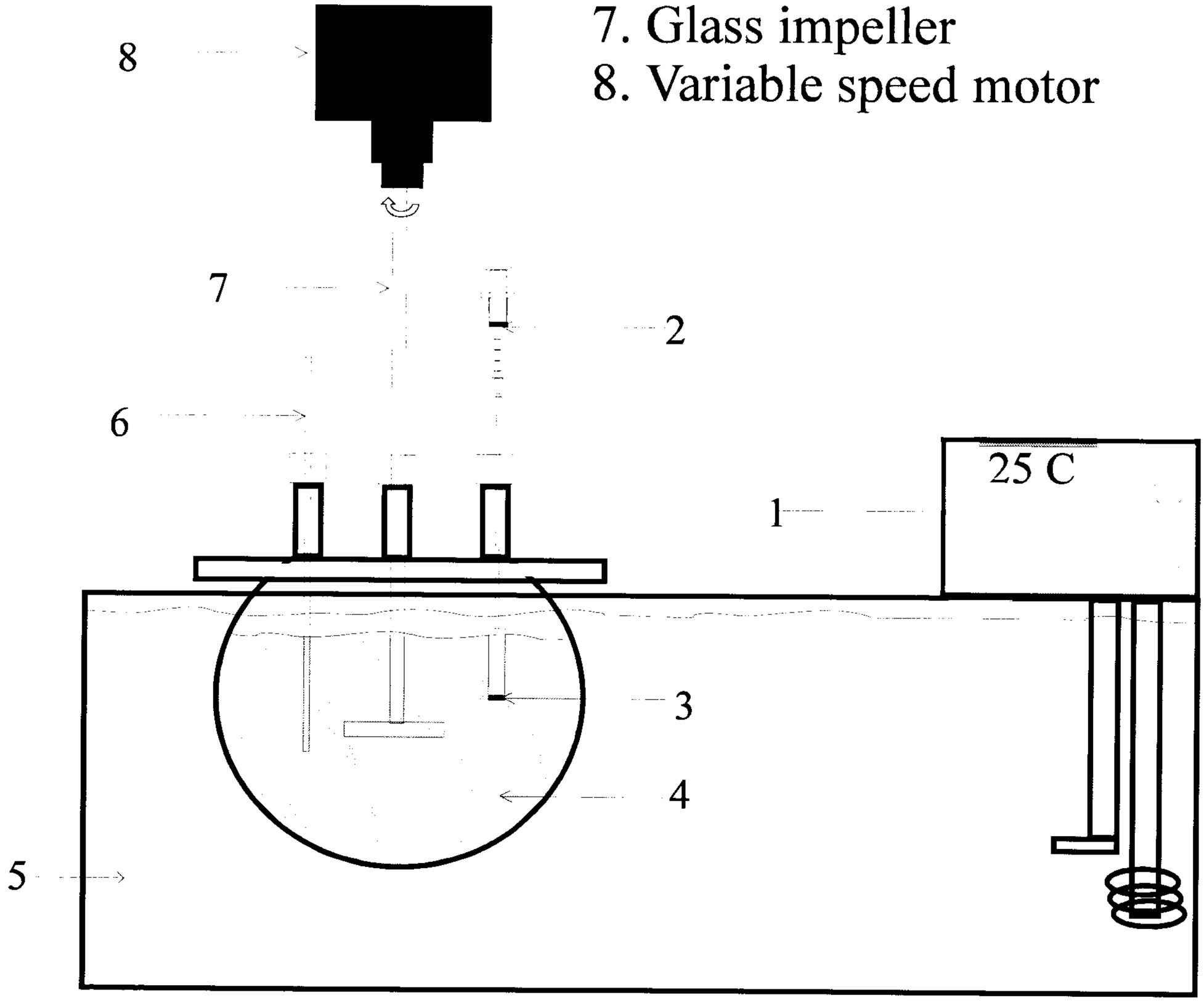

Figure 4.2. Schematic of kinetic reactor set-up used to study metal sorption rates.

The influence of metal ion concentration on the uptake rate was studied over the concentration range (0.1-1) mM. Higher concentrations were not possible because the kinetics was too fast to obtain sufficient reliable readings. All experiments were conducted at room temperature (20-25°C) with starting solution pH 3.8. The stirrer speed was set at 400 min^{-1}. The particle size range of the algal biomass AN studied was (300-355)μm.

The effect of stirrer speed was studied at two concentrations, 0.1mM and 0.5mM, and stirrer settings of 400 min^{-1}, 800 min^{-1} and 1000 min^{-1}. The experiments were conducted at room temperature (25°C) with algal particles of AN in the particle size range (300-355) μm.

The effect of particle size on copper sorption rates by AN was studied for two particle size ranges (45-90)μm and (300-355) μm. At high metal concentrations greater than 0.5 mM, the uptake kinetics for the size range (45-90)μm was extremely fast and no accurate measurements could be taken. Therefore, results at 0.1 mM concentration were obtained.

Section 4.3. Results and Discussion

Regeneration of metal-laden biosorbents

Nine different types of eluting solutions were selected and tested in the course of the present work. Almost all acidic solutions showed good metal elution behavior which clearly indicates the role of proton-metal interactions in the metal sorption/desorption process (see Figures 4.3. to 4.6.). The ability of alkaline solutions to elute previously sequestered metal ions provides valuable information on the affinity or strength of interactions of metal species with the surface functional groups. Previous metal selectivity experiments have suggested that copper and cadmium ions interact with the algal matrix much more strongly in comparison with nickel and zinc ions. Metal elution by $NaHCO_3$ and Na_2CO_3 shows that a very small portion of sorbed copper is eluted, whereas hardly any cadmium is mobilized by these eluants. In contrast, between (20-40)% of nickel and zinc ions were eluted from the algal matrix. This may be attributed to the leaching of algin from the algal matrix; the effluent leaving the biosorbent bed was discolored and the granular structure of the biomass was replaced by a paste-like texture.

Sodium chloride was found to be a good eluant for nickel and zinc, i.e. competing for metal-laden sites and desorbing metal ions from sites already previously occupied by

the metal ions. Copper and cadmium ions were less easily eluted once they were bound to the algal sites. This suggests that copper and cadmium ions interact more strongly to sites within the algal matrix in comparison with nickel or zinc. 0.1M nitric acid was found to be the best overall eluant since it showed high elution for all four metals studied. Cadmium desorption however, was slightly poorer than for the other metals. HCl and $CaCl_2$ were the best eluants for cadmium. Calcium ions interact strongly with alginates forming an 'egg box' like structure which is very stable and is used commercially to form stable hydrogels (see Fig. 1.6.). The interaction energy between calcium ions in solution and surface functional groups within the algal walls is sufficient to desorb previously bound cadmium ions. This suggests that a bidentate type binding mechanism is responsible for cadmium biosorption. The concentration of cadmium ions in solution using calcium chloride as eluant is of potential interest since the elution pH was between 9-10 pH units This fairly mild pH range may avoid possible damage to the structure of algal polysaccharides due to absence of hydrolysis of the glycosidic bonds linking monomers in the polymer network of alginic acid. Multiple reuse of the biosorbent should therefore be possible using mild eluants such as calcium chloride. Microscopic observation of calcium chloride eluted algal particles revealed no visible damage to the algal particles (not shown here) which retained their granular appearance.

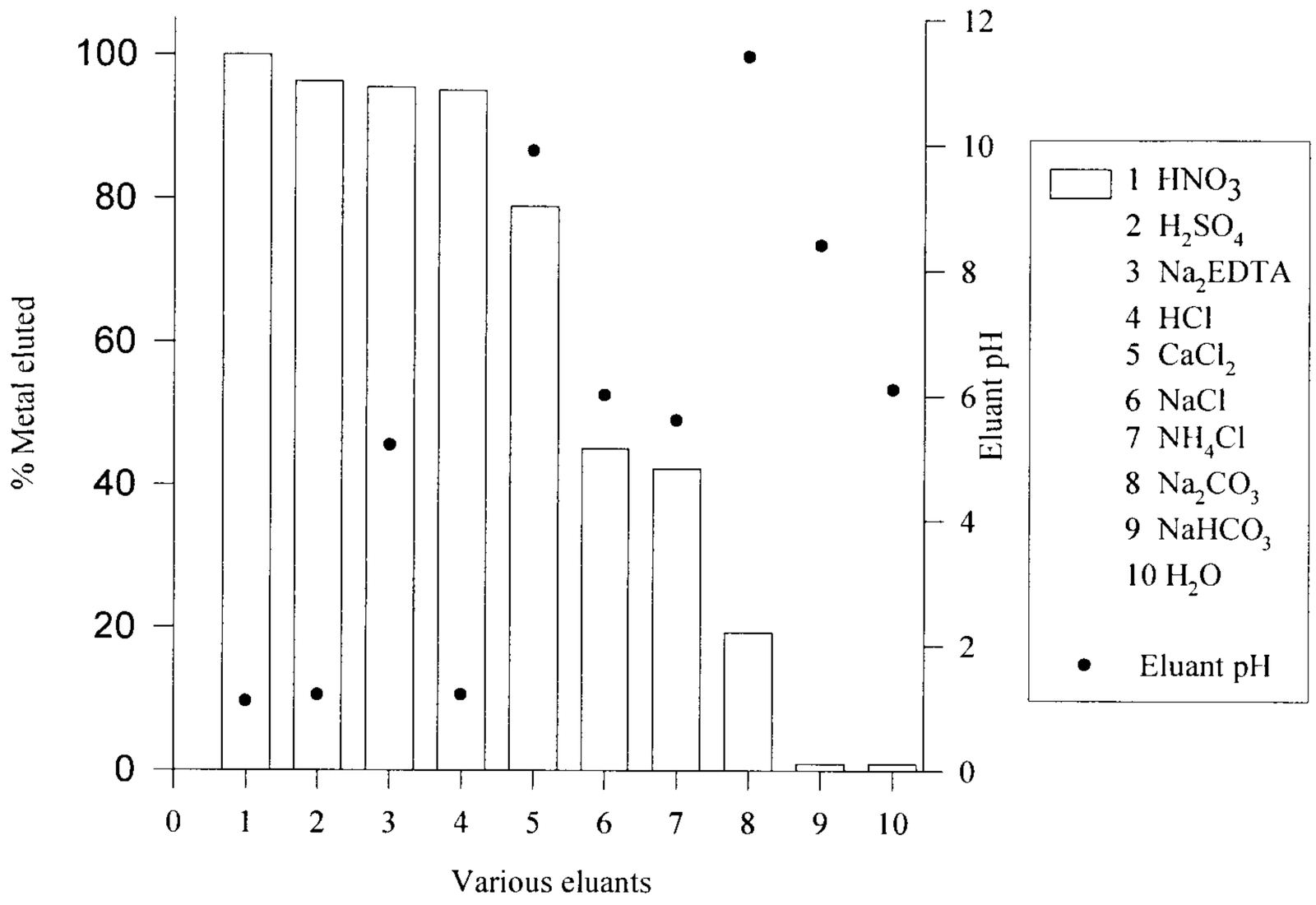

Figure 4.3. Copper elution performance of various eluants on *A. nodosum*.

Ammonium chloride was a particularly good eluant for algal-bound zinc ions (see Fig. 4.6.). This indicates strong electrostatic interactions between zinc ions and the algal biomass. Na_2EDTA was capable of complexing algal bound copper and zinc ions quite well. Cadmium and nickel ions were eluted to a lesser extent. The subtle differences in the elution abilities of various eluants indicates slightly different interactions between functional groups and metal ions within the algal cell walls.

The effectiveness of 0.1M sodium chloride solution as eluant was tested at different pH values. At pH 6 around 80% cadmium was desorbed while at pH 3 this had increased to 98%. The optimum pH for the most efficient cadmium elution lies between pH 2-3. Cadmium loaded *A. nodosum* biomass samples were eluted with 0.1M HCl and 1.0M HCl. Different S/L ratios were employed to see the effect on desorption efficiency and concentration factors. It is clear that increasing the S/L ratio results in greater concentration of metal ions in the eluant. Unfortunately, this occurs

at the expense of a lower desorption efficiency which results in reduced sorption capacity for the following sorption cycle (see Fig. 4.7.). This effect on reduction in desorption efficiency was most pronounced in the case of NaCl. 1.0M HCl showed little effect on desorption efficiency at higher S/L ratios. However, the low eluant pH resulted in changes to the texture of the algal biomass with significant reduction in resorption capacity. It was desirable to use the least possible eluting volume in order to elute previously bound metal from the biosorbent and thus obtain the highest concentration of the metal ions in the eluant. Preliminary results show that a compromise between concentration factors and good elution efficiency is clearly needed in order to optimise the metal elution process.

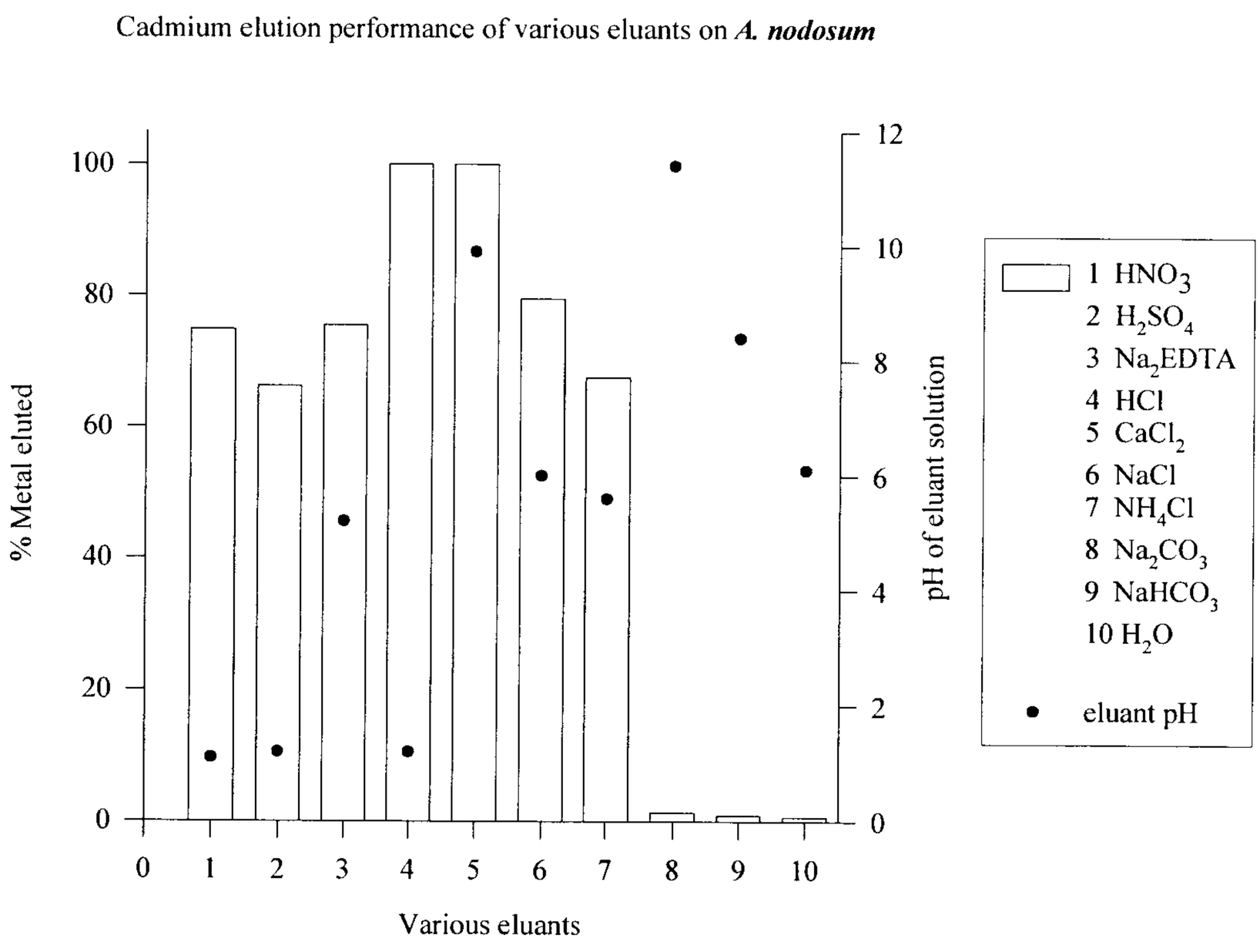

Figure 4.4. Cadmium elution performance of various eluants on *A. nodosum*.

The experimental results show that while some of the eluants tested are efficient in releasing the sorbed metal ions from the algal biomass, however, their application has a negative effect on the subsequent metal sorption cycle. The role of protons in eluting sequestered metal ions is obvious. An ion exchange mechanism is highly

probable. Successful metal elution using NaCl and NH_4Cl suggests that electrostatic interactions play an important role in metal biosorption, particularly in the sorption of nickel and zinc ions by algal biomass. Cadmium ions may be eluted by formation of cadmium-ammonium complexes which are known to occur in solution (refer to chapter 5). This complex formation may be strong enough to break previously formed covalent bonds between cadmium ions and carboxyl groups attached to structural polysaccharides in algae.

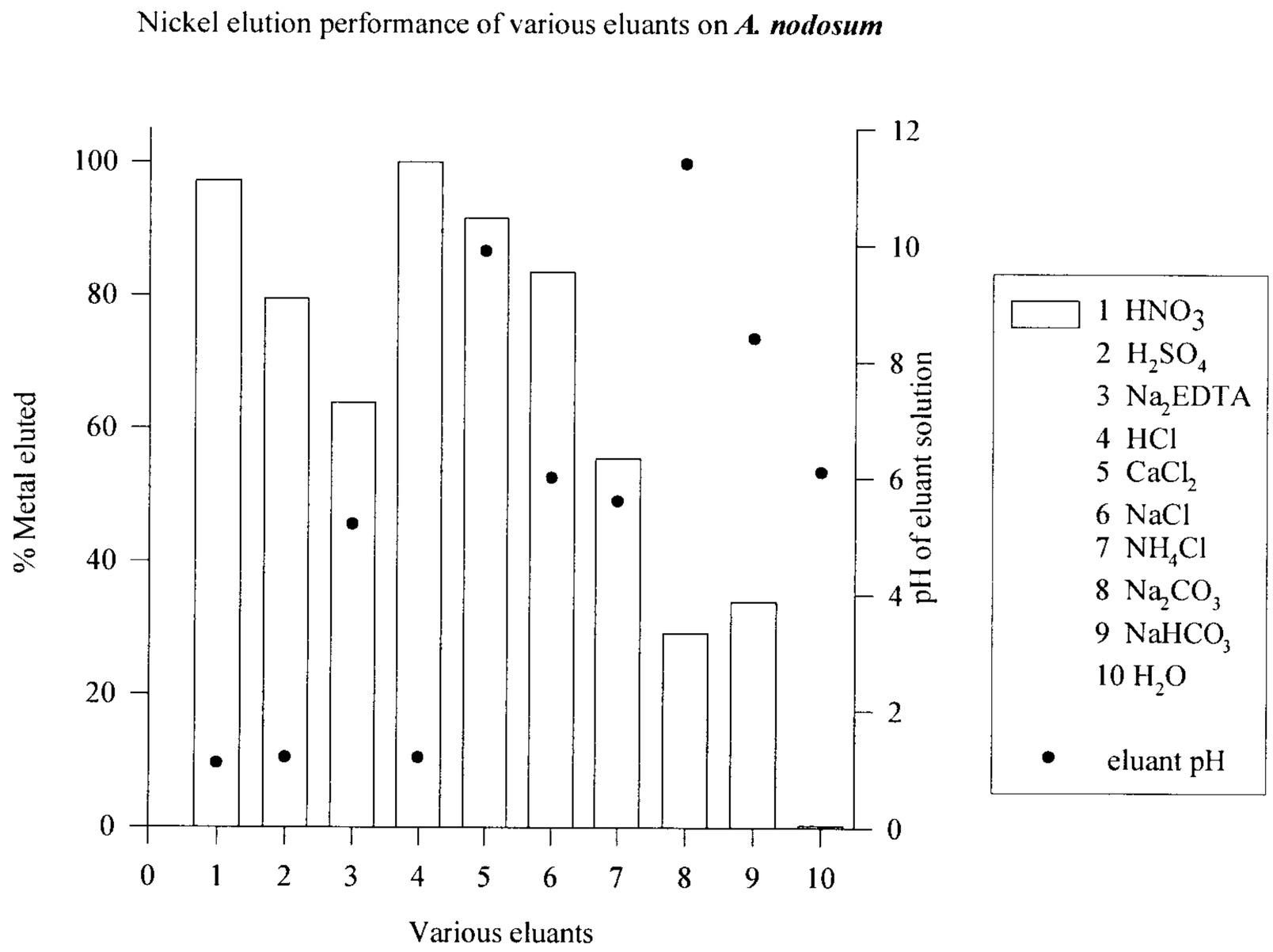

Figure 4.5. Nickel elution performance of various eluants on *A. nodosum*.

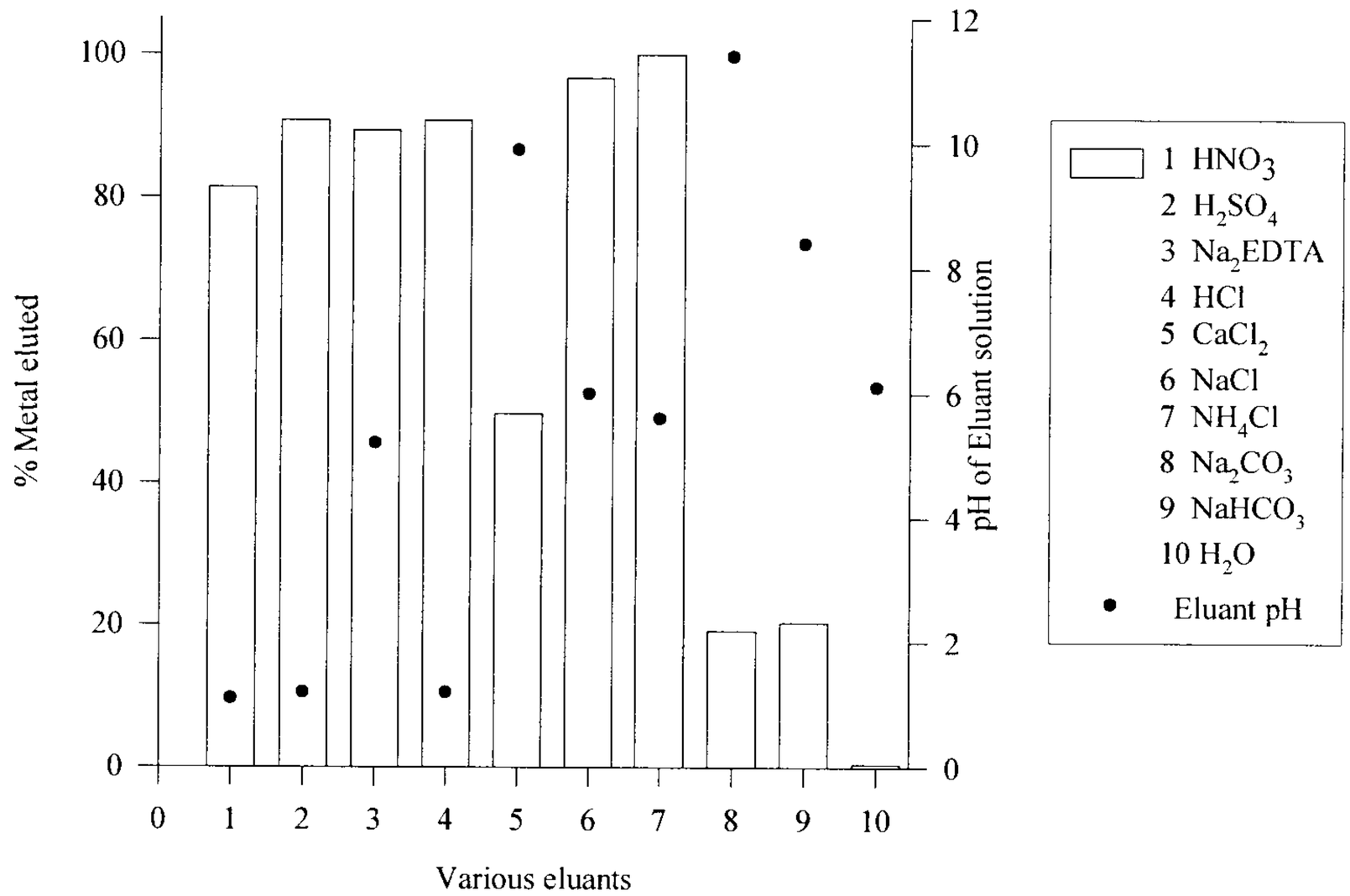

Figure 4.6. Zinc elution performance of various eluants on *A. nodosum*.

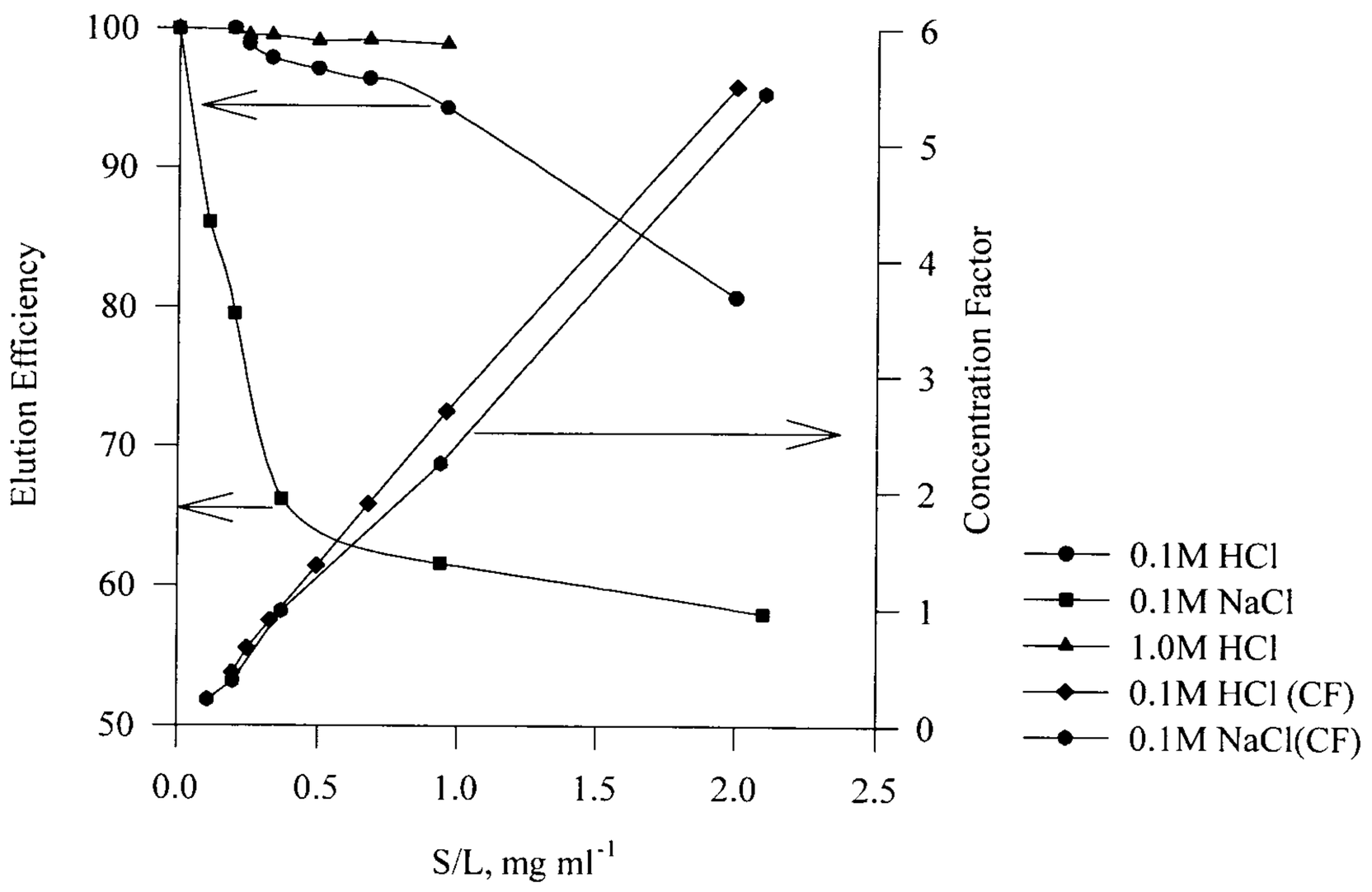

Figure 4.7. Influence of S/L on elution efficiency and concentration factors.

Kinetics of metal biosorption

The rate of biosorption is important for the optimum design of sorption systems. Investigation of the time dependence of metal biosorption leads to an improved understanding of the mechanisms and mass transport occurring within algal particles. Comparison of the rates of copper sorption by native algal varieties shows that *L. flavicans* has a significantly faster metal sorption rate in comparison to the other seaweed varieties (see Fig. 4.8.). One possible explanation for this phenomenon may relate to the swelling behavior of the various algal biosorbents. LF shows considerably greater swelling in comparison with the rest of the native materials studied (see Table 2.3.). *L. Hyperborea*, however, lies between *A. nodosum* and *L. flavicans* with regard to degree of swelling, but shows the slowest copper sorption rate in comparison with other native seaweed varieties. Swelling behavior alone may not explain this difference in copper sorption rate. *L. hyperborea* contains the highest proportion of guluronic acid segments of all the seaweed varieties studied. Interaction of copper ions with G-segments may be different from M-segments which may manifest itself in the slower copper sorption kinetics displayed by LH. Chelation reactions for example, tend to be slower than simple ion exchange reactions[6]. G-segments however, have been shown to display greater selectivity for most divalent ions, particularly copper ions, in alginates containing a higher G/M content and therefore reduced rate of metal biosorption on their account may be ruled out[20]. A more likely explanation may be the relatively low algin content of LH in comparison with the other native materials (see Table 1.2. and Table 2.5.). The higher copper sorption rate displayed by AN compared with BK (higher algin content) suggests that other factors, in particular differences in the morphology of the algal biomass may play a critical role in determining the rate of metal biosorption exhibited by the various algal species.

Comparison of copper sorption rates of native, processed seaweed based biosorbents and purified alginic acid samples (see Figures 4.9. and 4.10.) show that the native material possesses faster metal sorption kinetics in comparison with the processed residue (the uptake rate is comparable to the rate of metal sorption by free alginates

derived from the precursor material). The lower metal sorption rates of dealginate biosorbents may be attributed to a lower concentration of metal binding sites within the processed biosorbent materials in comparison with the native algae (see Table 2.4.). The driving force for metal ion removal by the algal matrix may be reduced due to the lower concentration of metal binding functional groups in the processed dealginate materials. The lower surface potential of dealginate residue may result in reduced electrostatic interactions between metal ions and the biosorbent surface. Electrostatic interactions between metal ions may play an important role in increasing the rate of biosorption as displayed by native algae due to non-specific interactions with metal ions in solution.

The influence of stirring rate on copper sorption kinetics by *A. nodosum* indicated only a marginal increase in copper uptake rate for stirring rates of 800 min^{-1} and 1000 min^{-1} compared with copper sorption rate at 400 min^{-1} (see Fig. 4.11.). A similar affect was seen for other metal ions as well, e.g. nickel sorption by AN (see Fig. 4.12.). This indicates that film diffusional resistance is relatively insignificant and may be ignored as the dominant mass transport resistance during metal biosorption.

The shrinking core model (discussed earlier; see section 4.1.) for sorption of metallic ions by algal biosorbents has been used to evaluate metal ionic diffusivities within the algal matrix where film diffusion effects had been overcome by vigorous agitation of algal-metal solution. The principal resistance to mass transfer was assumed to be intraparticle diffusion controlled. The Nernst-Planck equation[18] was applied for the flux of ions in the biosorbent particles. An analytical solution for diffusion control based on the shrinking core model gave the fractional removal of metal ions as a function of the diffusivities and valencies of the counter-ions (see Table 4.1. for calculated copper diffusivity values within various biosorbents).

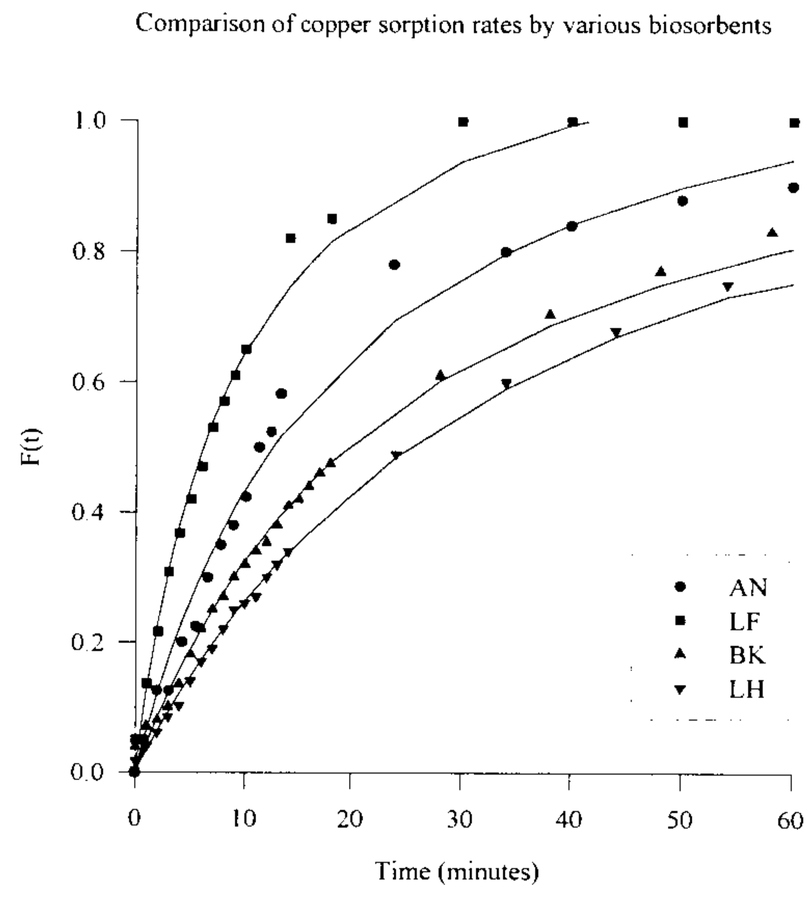

Figure 4.8. Comparison of copper sorption rates by various biosorbents.

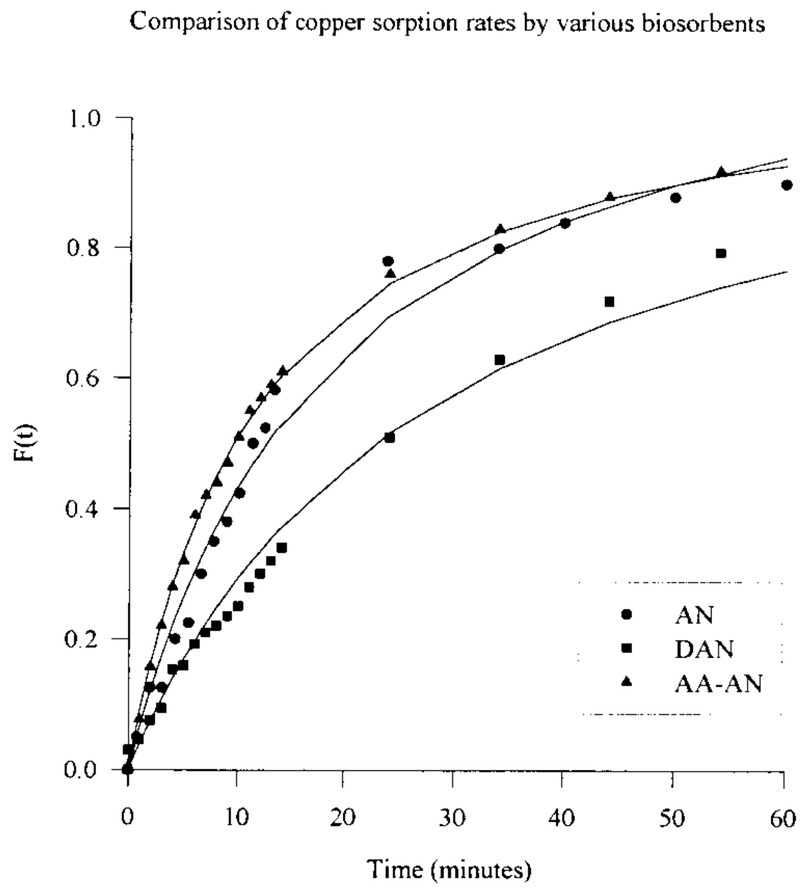

Figure 4.9. Comparison of copper sorption rates by various biosorbents.

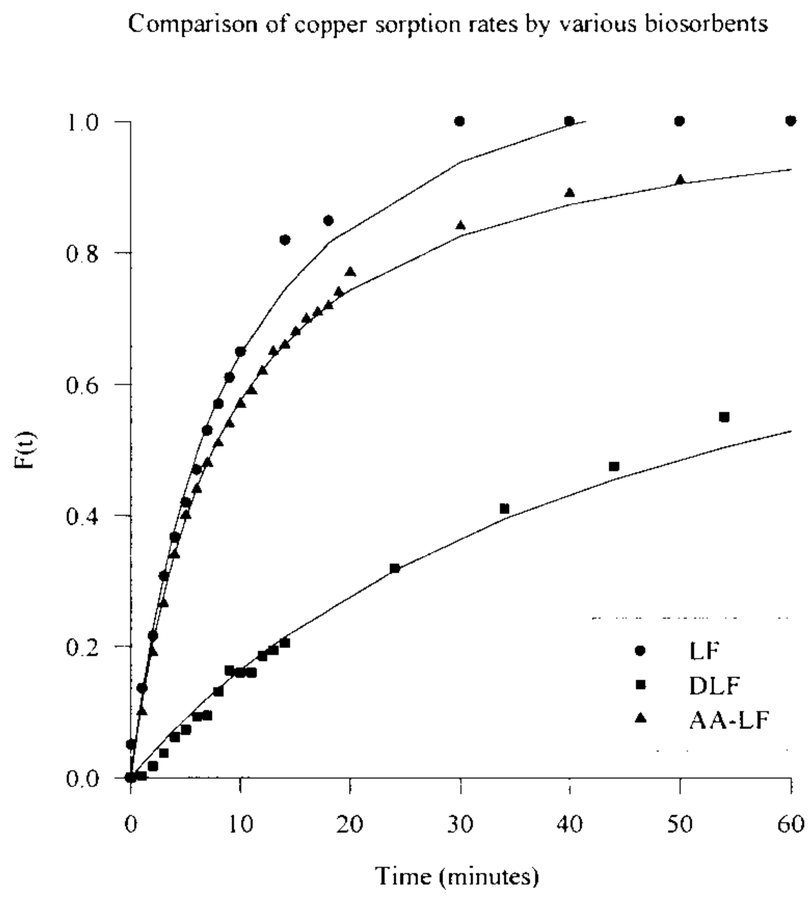

Figure 4.10. Comparison of copper sorption rates by various biosorbents.

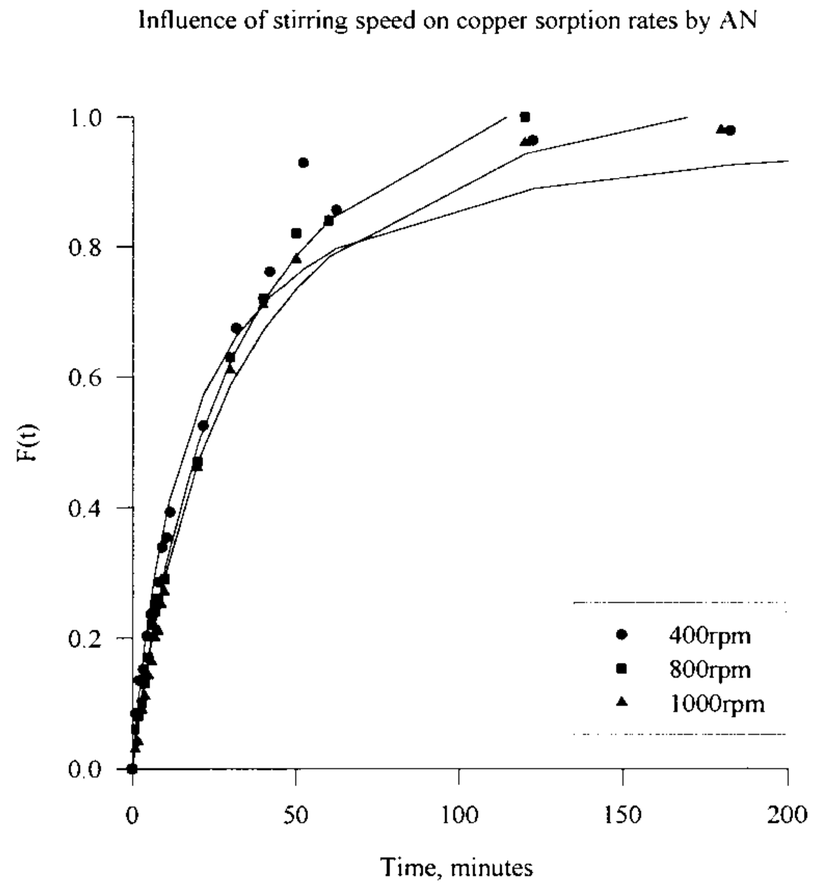

Figure 4.11. Influence of stirring speed on copper sorption rates by *A. nodosum*.

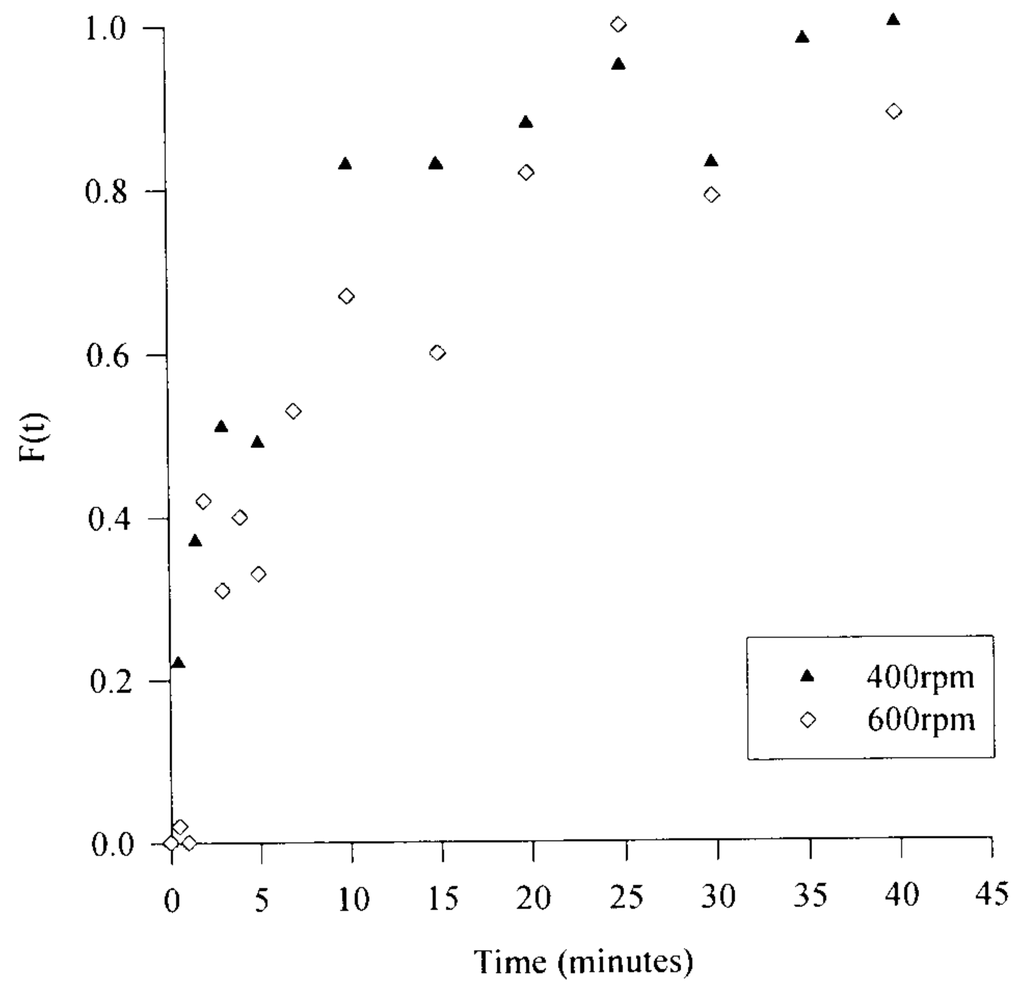

Figure 4.12. Influence of stirring rate on nickel sorption by *A. nodosum*.

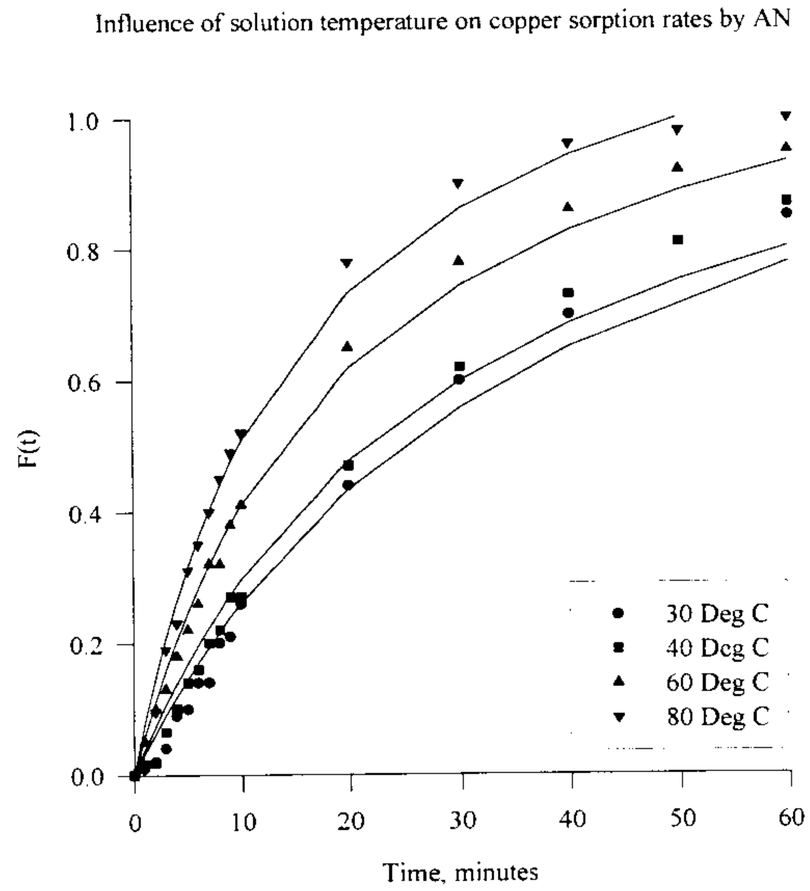

Figure 4.13. Influence of solution temperature on copper sorption rates by AN.

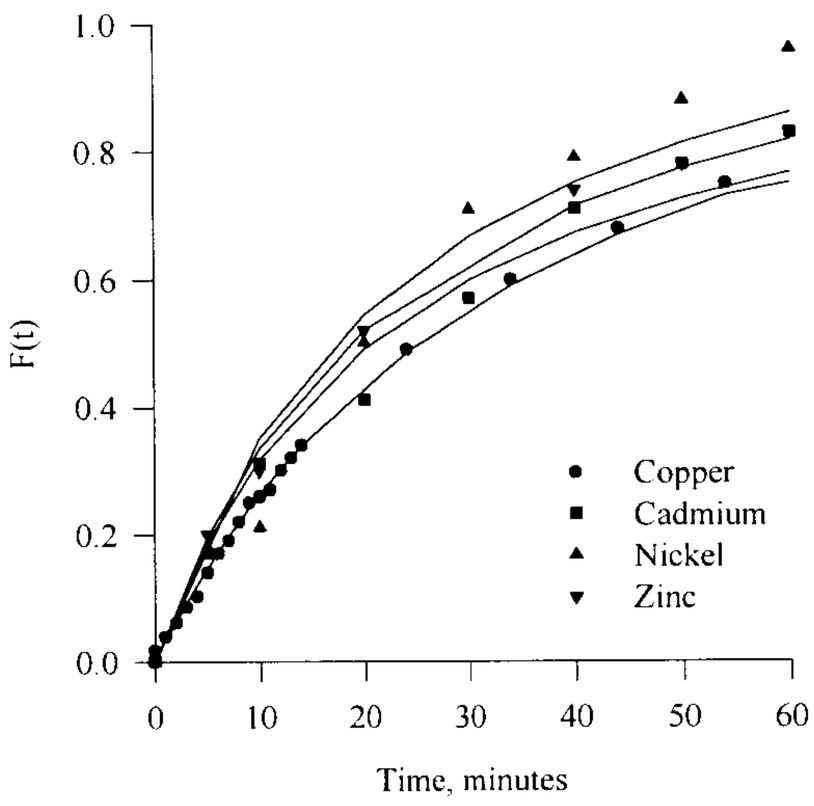

Figure 4.14. Comparison of the uptake rates of various metal ions by LH.

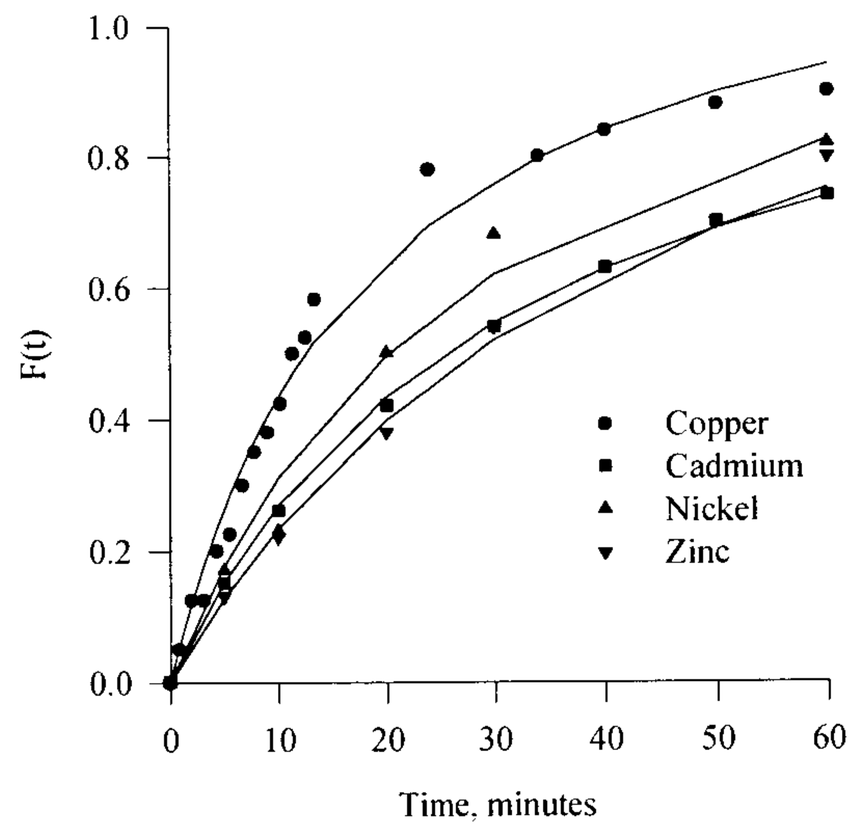

Figure 4.15. Comparison of the uptake rates of various metal ions by AN.

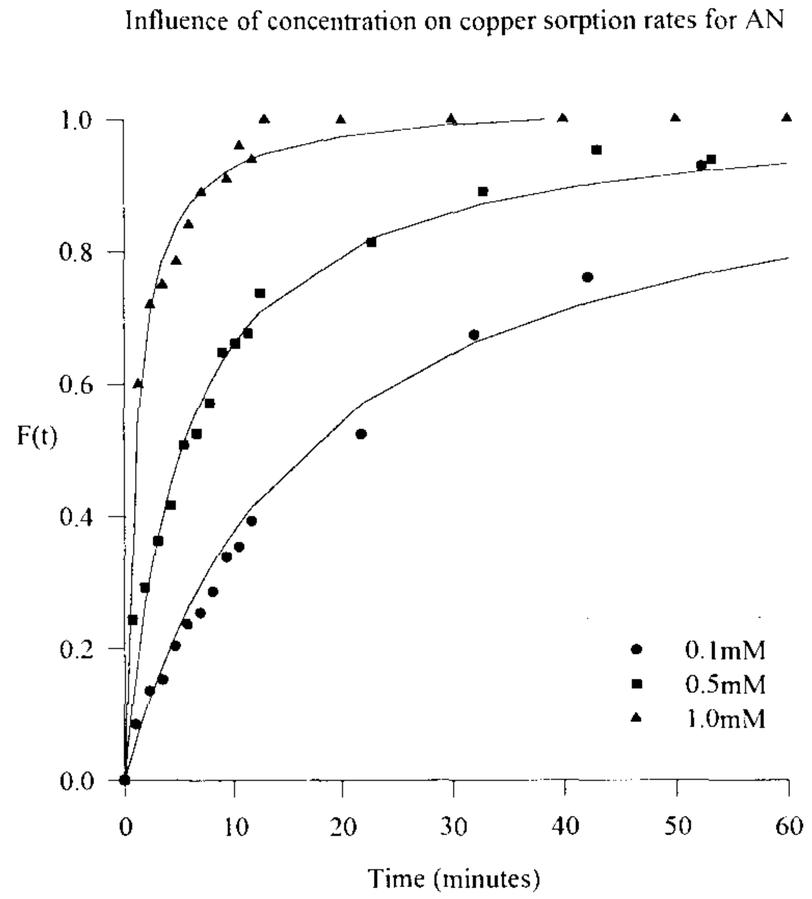

Figure 4.16. Influence of concentration on copper sorption rates for AN.

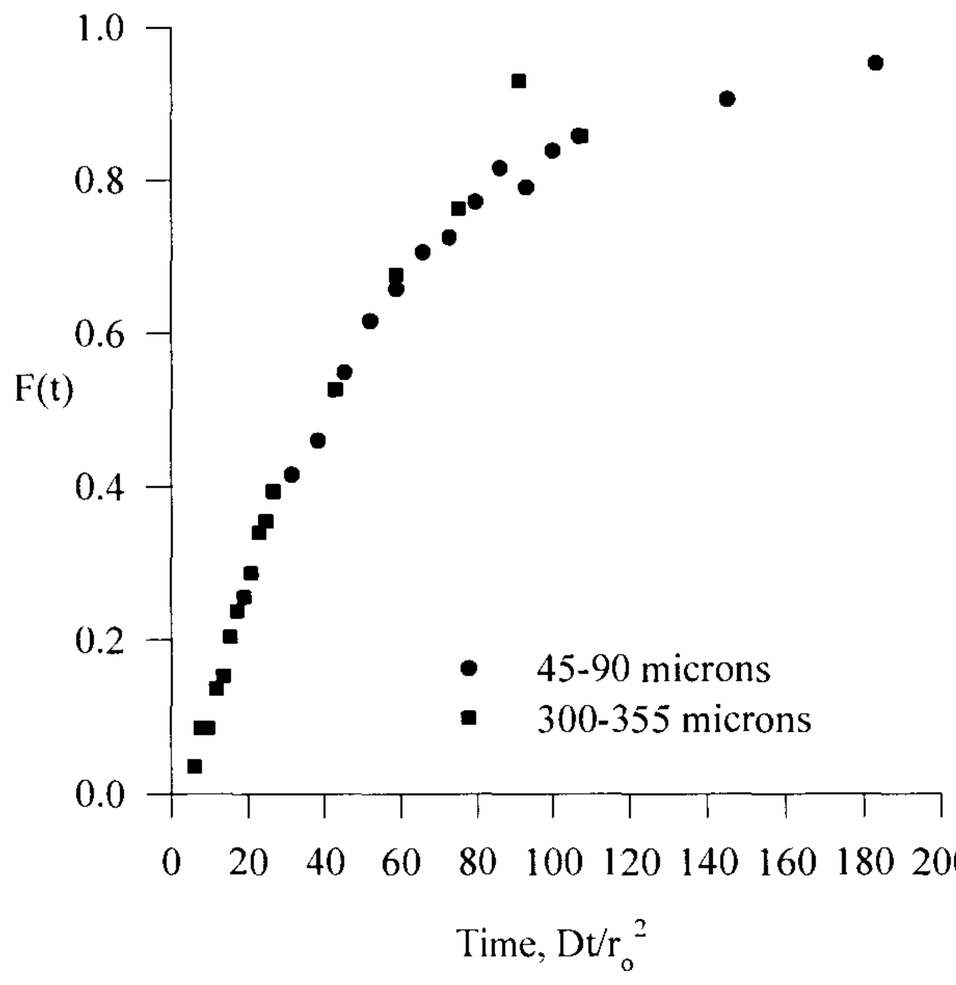

Figure 4.17. Influence of particle size on copper sorption rates for AN.

The rate of copper sorption by *A. nodosum* at various solution temperatures shows a marginal increase in copper sorption rates for temperatures between (25-40)°C (see Fig. 4.13.). There is however, a significant increase in copper sorption rate at temperatures of 60°C and 80°C in comparison with the uptake rate at 25°C. Diffusion coefficients for copper ions in the biosorbent were found to increase with increasing temperature (values for copper diffusivity were calculated using the shrinking core model: $2.3x10^{-12}$ m^2 s^{-1} at 30°C, $3.1x10^{-12}$ m^2 s^{-1} at 60°C, and $6.8x10^{-12}$ m^2 s^{-1} at 80°C). The diffusivity values are not proportional to the absolute temperature raised to the power 1.5 which is usually the case for pore diffusion transport limitations. This suggests that the principal resistance to the ionic mobility within the biosorbent lies in the solid matrix i.e. the cell walls of algae. This effect is similar to diffusional resistance in solids e.g. ion exchange membranes[6]. The increase in diffusivity values at higher temperatures may be explained in terms of decreased retarding effects due to specific or electrostatic interactions and reduced size of ions (solvation shells surrounding metal ions decrease at high temperatures). An Arrhenius plot was used to calculate activation energy values for copper sorption by *A. nodosum* for a particle diffusion controlled case. Activation energy for copper sorption was calculated to be 23 kJ $mole^{-1}$ which is of the same order of magnitude as those found for standard ion exchange resins[6] (25.1-41.8 kJ $mole^{-1}$).

Species	Ionic Diffusivity m^2 s^{-1}
	Copper
AN	$2.2x10^{-12}$
LF	$8.2x10^{-12}$
BK	$2.5x10^{-12}$
LH	$1.4x10^{-12}$
DAN	$9.6x10^{-13}$
DLF	$9.6x10^{-13}$

Table 4.1. Comparison of copper diffusivity in various biosorbents.

A comparison of the sorption rates of different metal species by *A. nodosum* and *L. hyperborea* show that the uptake of nickel ions is relatively faster than cadmium and zinc (see Figures 4.14. and 4.15.). This may be explained in terms of higher affinity

of metal species with surface functional groups of the cellular polysaccharides. It must be pointed out however, that selectivity coefficient values at equilibrium are much higher for cadmium ions relative to those for nickel or zinc. A simple explanation for the higher uptake rate for nickel is therefore not available. There was a marked increase in copper sorption rate with increase in solution concentration and reduction in algal particle size (see Figures 4.16. and 4.17.). The dependence of copper biosorption rate on solution concentration may be explained in terms of the low concentration of dissociated carboxyl groups. Electroneutrality will permit only as many mobile cations as there are dissociated anionic functional groups. The scarcity of such groups in the algal particle (due to weak dissociation of acidic sites on the biomass surface and/or undissociated groups following covalent bond formation between metal ions and functional groups) results in almost complete elimination of Donnan exclusion of mobile co-ions[15]. Hence Cu^{2+} and Cl^{-} ions from the solution can invade the neutralized outer shell and thereby greatly boost the inter-diffusion rate. Hence, the exchange rate, although controlled by particle diffusion of counterions does depend on the solution concentration (see Fig. 4.16.). The influence of particle size on copper biosorption rates clearly indicates that intraparticle limitations are dominant due to the accessibility of metal-binding sites within the algal particles (see Figure 4.17.). The rate of copper biosorption is proportional to $\frac{1}{r^2}$ which is characteristic of particle diffusion limited systems[6].

Ionic diffusivity values were extracted from experimental sorption rate data employing eq(57). Figure 4.18. depicts some theoretical predictions of copper sorption rates by various algal biosorbents using the shrinking core model. Ionic diffusivity values used for theoretical calculations are tabulated (see Table 4.1.). The theoretical curves over predict the rate of copper sorption exhibited by native algae in all cases during the initial sorption period ($t<10$ min.). Film diffusional effects as well as improper mixing of algae/metal solution mixture may be responsible for the relatively lower sorption rate observed for all algal samples. Nevertheless, some idea of the ionic diffusivities within algae may be gauged from the results obtained thus far. The extremely low copper diffusivity values within the algal particles is possibly

related with diffusion through a relatively non-porous sorbent. Surface area and pore size distribution analysis using nitrogen sorption studies have previously indicated the low porosity and surface area displayed by algal particles (see chapter 2). It is extremely likely, that, the principal resistance to metal ions migrating to the metal binding sites lies in the cellular membrane surrounding the algal cells.

Copper diffusivities in the algal matrix are smaller than ionic mobilities in free solution (see Table 3.5.) by an order of magnitude of at least 100. In dealginate biomass samples, calculated ionic mobilities are even smaller reflecting even greater hindrance to transport of ions from the bulk solution to the metal binding sites within algae. The diffusivity values obtained for algal biomass are of the same order of magnitude as those reported for weak-acid weakly cross-linked ion exchange resins[7].

The applicability of the shrinking core model as representative of the mechanisms involved in algal biosorption is clearly doubtful. However, since the model does not consider external mass transfer effects and also does not make assumptions regarding the structure of the sorbent whilst at the same time accounting for electric field effects within the biomass therefore, for the present study, it is reasonable to employ it in order to obtain some idea of the order of magnitude of ionic diffusivities within algal biomass. From preliminary studies of algal biosorption rates, it is clear that the principal resistance to algal biosorption arises as a consequence of mass transport limitations within algal particles. These may arise as a consequence of specific interactions and/or steric hindrances in the algal cell wall towards the metal ions. Any biosorption system needs to allow for appropriate contact time between algal particles and the metal bearing solution. This contact time must be similar to that employed for ion exchange resins since the ionic diffusivities are of similar order of magnitude.

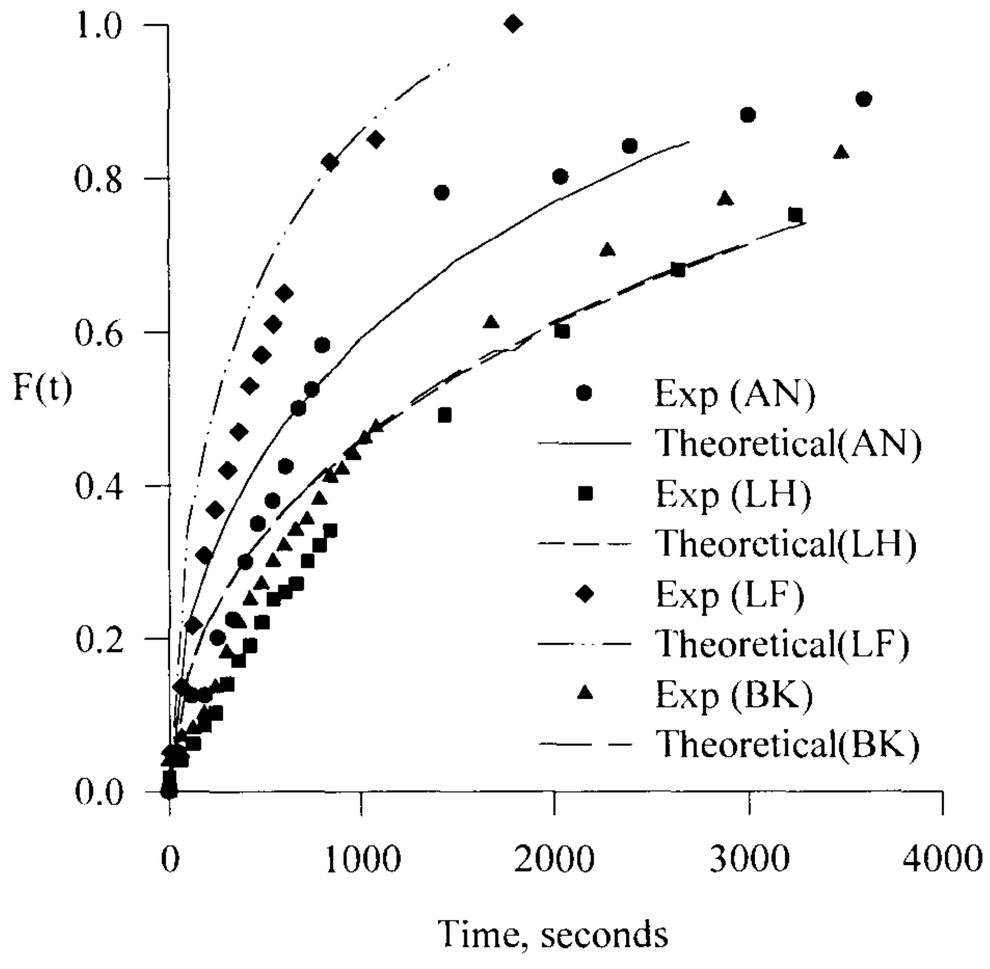

Figure 4.18. Comparison of experimental and theoretical predictions for copper sorption rates.

Section 4.4. Conclusions

Metal ions sequestered by algal biomass can be reversibly eluted using inorganic acids as well as acidified salt solutions such as $CaCl_2$ and NaCl. Metal desorption from algae by calcium ions indicates a bidentate binding mechanism whereas Na^+ at high concentrations compete with previously sorbed nickel and zinc ions quite effectively. This suggests electrostatic interactions between metal ions in solution and algal biomass surface may be partly responsible for the metal biosorption process.

Kinetics of metal biosorption in algal particles is found to be transport limited with particle diffusion control the dominant factor in rate determination. Application of a shrinking-core model provides approximate values for ionic diffusivity values which may be used to compare resistance to ion transport within algal particles for different metal ions as well as various algal species. The metal biosorption rate is affected by increase in temperature as well as metal concentration in the external solution.

Section 4.5. Nomenclature

B metallic ion

E co-ion

D intraparticle diffusivity ($m^2\ s^{-1}$)

F fractional attainment of equilibrium (-)

G $\dfrac{(1+z_E)\alpha}{(z_B+z_E)}$ (-)

J flux of ion (mol $m^{-2}\ s^{-1}$)

Q concentration of fixed groups in sorbent (mol m^{-3} sorbent)

Q' equilibrium concentration of electrolyte in sorbent phase with the concentration in the bulk solution (mol m^{-3} sorbent)

q sorbent-phase concentration (mol m^{-3} sorbent)

r radial dimension (m)

r_o radius of sorbent particle (m)

S $\dfrac{z_E(\alpha-1)}{(\alpha-z_B)}$

t time (s)

U $\dfrac{zq}{Q}$ (-)

U_{Bo} $\dfrac{z_B Q'}{Q}$ (-)

Greek Letters

α $\dfrac{D_H}{D_B}$ (-)

δ distance from centre of sorbent particle to reaction plane (m)

ρ $\dfrac{r}{r_o}$ (-)

ρ_δ $\dfrac{\delta}{r_o}$ (-)

τ $\dfrac{D_B t}{r_o^2}$ (-)

Application of Algal Biosorbents in Fixed-Bed Columns

"The pursuit of science can be organised....in no other manner than by granting complete independence to all mature scientists. They will then distribute themselves over the whole field of possible discoveries, each applying his own special ability to the task that appears most profitable to him. The function of public authorities is not to plan research, but only to provide opportunities for its pursuit. All they have to do is to provide facilities for every good scientist to follow his own interest in science."

(Michael Polanyi 1891-1976)

Section 4.6. References

1. Aldor, I., Fourest, E. and Volesky, B. 1995, Can. J. Chem. Eng., vol. 73, no. 4, 516.
2. Kuyucak, N. 1987, Algal Biosorbents for Gold and Cobalt, PhD thesis, McGill University.
3. Yang, J. and Volesky, B. 1996, J. Chem. Tech. Biotechnol., vol. 66, no. 4, 355.
4. Matheickal, J. T., Yu, Q. and Feltham, J. 1997, Environ. Technol., vol. 18, no. 1, 25.
5. Boyd, G. E. and Hayes, T. J. 1952, Analyst, Lond., vol. 77, 445.
6. Helfferich, F. 1995, Ion Exchange, Dover Publications Inc., New York, USA.
7. Slater, M. J. 1991, Principles of ion exchange technology, Butterworth-Heinemann Ltd., Oxford, UK.
8. Jang, L. K., Brand, W., Resong, M., Mainieri, W. and Geesey, G. G. 1990, Environ. Prog., vol. 9, no. 4, 269.
9. Apel, M. L. and Torma, A. E. 1993, Can. J. Chem. Eng., vol. 71, no. 4, 652.
10. Yiacoumi, S. and Tien, C. 1995, J. Colloid Interface Sci., vol. 175, no. 2, 347.
11. Dana, P. R. and Weelock, T. D. 1974, Ind. Eng. Chem. Fund., vol. 13, no. 1, 20.
12. Hoell, W. and Sontheimer, H. 1975, Chem. Ing. Technik., vol. 47, no. 14, 615.
13. Hoell, W. 1984, Reactive Polymers, vol. 2, no. (1-2), 93.
14. Weisz, P. B. and Goodwin, R. D. 1963, J. Catalysis, vol. 2, no. 5, 397.
15. Helfferich, F. 1965, J. Phys. Chem., vol. 69, no. 4, 1178.
16. Nativ, M., Goldstein, S. and Schmuckler, G. 1975, J. Inorg. Nucl. Chem., vol. 37, no. 9, 1951.
17. Kataoka, T. and Yoshida, H. 1981, Can. J. Chem. Eng., vol. 59, no. 4, 475.
18. Yoshida, H., Kataoka, T. and Fujikawa, S. 1986, Chem. Eng. Sci., vol. 41, no. 10, 2517.
19. M. Streat, Tai, M.H., Saha, B. and Malik, D.J. 1998, Development of advanced ion exchange materials and methods for the removal of toxic metals from metallurgical waste effluents, Progress report (Nov. '97 - April '98), EC Contract no. BRPR-CT96-0158.
20. McDowell, R.H. 1986, Properties of alginates, Kelco International, (Company product information).

Chapter 5

Application of Algal Biosorbents in Fixed-Bed Columns

This chapter looks at the performance of fixed-bed algal columns in treating simulant metal plating effluent streams. Industrial aircraft plating rinse waters have been treated and a comparison of column breakthrough profiles between the biosorbents and conventional organic ion exchange resins has been made. The important parameters affecting the development of constant pattern breakthrough profiles have been determined.

Section 5.1. Theory and Literature Review

Performance of fixed-bed algal biosorbent columns

The majority of ion exchange processes related to water treatment e.g. water softening applications, employ sorbent materials in fixed-bed columns. The principal advantage of employing columns is the extremely good decontamination factors that may be achieved. The feed solution continuously contacts with layers of fresh sorbent in the ion exchange columns resulting in efficient removal of ions by the sorbent material. The equivalent batch process would require a very large number of contact vessels containing fresh sorbent material in order to obtain similar solute removal. Helfferich[1] provides a good overview of the various theoretical approaches to predict column performance. The theories may be divided into two substantially distinct groups; equilibrium theories and rate theories. In the equilibrium theories, local equilibrium between layers in the bed and finite solution volume is assumed. The sorbent bed is divided into layers of finite height (determined experimentally). It is assumed that solution attains equilibrium with sorbent before moving to the next layer (or plate). The obvious advantage of equilibrium theories lies in their relative simplicity.

Rate theories are more realistic since there are no assumptions of local equilibrium. Instead, calculations are made for continuous flow through the columns with finite

rates of sorption. There is no need for empirical quantities and hence column performance can be predicted from fundamental data; at the expense of considerable mathematical effort. The effect of optimum operating conditions including flow rate, feed concentration, particle size, etc., on breakthrough profiles may be predicted.

Slater[2] provides an up-to-date review of literature pertaining to calculation of the performance of fixed beds. Typical initial and boundary conditions are listed and associated assumptions are discussed. The important role of the equilibrium relationship in determining constant pattern and proportionate pattern behavior is outlined. Constant pattern behavior applies only for very favorable equilibria (marine algae display favorable equilibria for heavy metal ions; see chapter 3). The assumption of constant pattern behavior greatly simplifies the design equations, however, column length may be excessive. In addition, various equilibrium relationships employed in the literature to predict breakthrough profiles for liquid film rate controlled and resin bead rate controlled cases are provided in this text[2]. Although limited to binary exchange, these relationships serve to categorize the principal types of behavior before more sophisticated analysis is attempted. Calculation of mass transfer zone heights using the method of Michaels[3] is recommended and has been employed in the current study. Several of the more advanced models account for coupled film/particle, film/pore or other similar combinations and axial diffusion utilize linear sorption isotherms for model development[4,5]. Linear sorption isotherms are obviously not well suited for favorable equilibria and selective sorption systems. Peel and Benedek[6] use a liquid film coefficient together with Vermeulen's quadratic driving force equation[7] for fixed-bed adsorption. Flow idealities such as plug-flow conditions and a Freundlich isotherm are used to successfully show the influence of both liquid film and particle diffusion on breakthrough profiles.

There are relatively few modeling studies of metal biosorption in fixed-bed column operation. The adsorption approach used on activated carbon has been closely followed[7,8] by researchers, who have attempted to model metal biosorption breakthrough profiles. In part, the lack of literature on the application of algal

biomass stems from the fact that metal uptake by different biomaterials is still not fully understood[8]. In addition, improvement in the textural rigidity of algal particles by using immobilization and/or granulation techniques are required to overcome the lack of physical strength of most algal biomass.

Kratochvil and Volesky[9] modeled copper biosorption on a fixed-bed of *Sargassum* biomass. They consider copper biosorption to be predominantly an ion exchange phenomenon and therefore applied the simplified model of Tan and Spinner[10] which was developed to describe the dynamics of multicomponent ion exchange in a fixed bed. Employing relatively shallow beds (20 cm high) necessitated axial dispersion effects of the fluid in the packed bed to be taken into account. The kinetics of metal biosorption is represented by a linear driving force and a combined film and intraparticle mass transfer resistance. A non-linear equilibrium sorption isotherm based on equilibrium binding constants of protons and metals is used to represent the distribution of metal ions between the biosorbent and the aqueous phase. The overall mass transfer coefficient and the axial dispersion coefficient values were obtained by fitting the fixed-bed model to an experimental breakthrough curve. Fair agreement between the theoretical and experimental breakthrough curves was obtained for copper sorption onto protonated biomass in fixed-bed columns. The inability of the model to fully represent the sharpening of the breakthrough profile for the longer column (40 cm) was responsible for worse predictions of copper biosorption in this case.

Kratochvil et al.,[11] investigated copper biosorption by *Sargassum* using both native untreated and protonated biomass. The unwashed algal bed leached out light metal ions upon sorption of copper ions from solution in accordance with the affinity sequence for algae i.e. $Na^{+} \leq K^{+} \leq Mg^{2+} \leq Ca^{2+}$. The protonated algal bed did not leach out any residual alkali and alkali-earth metal ions. The pressure drop across the column was found to vary linearly with the superficial velocity of the liquid pumped through the algal bed. In addition, the pressure drop across the native biosorbent bed varied with the ionic composition of the effluent from the bed whereas the protonated algal column showed no such behavior.

Matheickal and Yu[12] developed effluent profiles for *E. Radiata* at different feed concentrations of lead ions in solution. The effluent history followed the typical S-shaped curve with about 2.5l of 0.4 mM solution treated before metal breakthrough occurred. Sorbent bed usage values were high with about 90% of equilibrium sorption capacity utilized. This was characterized by sharp breakthrough curves due to favorable sorption conditions prevailing within the biosorbent column. Copper effluent profiles for *E. Radiata* indicated that an ion exchange mechanism was dominant in metal biosorption[13]. The cumulative light-metal ions desorbed during copper biosorption matched reasonably well with the amount of copper ions sequestered by *E. Radiata*.

Formaldehyde crosslinked biomass particles of *A. nodosum* were evaluated for cadmium biosorption in a fixed-bed column[8]. The rate of metal uptake varied linearly with the difference between concentration in solution at any time and the equilibrium concentration. This indicates first-order sorption kinetics. A linear relationship between breakthrough time and bed depth for a given equilibrium concentration was obtained by solving the kinetic and equilibrium relations. Varying column operating conditions yielded information leading to optimum sorbent usage rates.

The application of marine algae in flow-through sorption columns is the theme of the current chapter. The objectives of this investigation concern obtaining key biosorption process design parameters which may be employed to predict the concentration-history profiles of the treated effluent streams. Synthetic single-metal bearing solutions were initially employed to study the effect of effluent throughput rates and bed height on the metal breakthrough profiles. These experiments identified potential biosorbent materials which had scope for evaluation against real industrial waste streams. In particular, preliminary column studies helped in selecting the most promising native and dealginate algal biosorbents which were then tested against aircraft metal plating rinse waters arising from a commercial airline plating shop.

Metal-plating and effluent rinse waters

The contribution towards water pollution of metal-bearing effluents arising from the metal-finishing and related industries is a source of increasing environmental concern. Large volumes of water are employed for cleaning and rinsing processes to produce various types of decorative or resistant finishes by the use of a variety of chemicals. This in turn results in the production of effluents possessing a wide range of characteristics and composition.

In 1973, an estimate of the water consumption by the metal finishing industry in the UK, yielded a value of 4% of the total water used by industry overall. Brower et al.,[14] commented in the same report, that, around two-thirds of the companies produced less than 50,000 m^3 y^{-1} with only 4% discharging effluents exceeding 500,000 m^3 y^{-1}. This suggests that a lot of these discharging sources are so small that on-site large scale water treatment processes are out of the question. The feasibility of end-of-pipe treatment using an ion exchange cartridge seems a likely possibility. In particular, cheap materials like novel algal biosorbents might have an inherent advantage over expensive organic ion exchange resins for once through treatment systems without the need for regeneration. Low cost would be the primary concern for small enterprises such as plating shops which generally tend to have relatively low effluent flow rates.

The principal sources of metal-laden effluents within the metal finishing industry are the used plating solutions of which there are a number of different types as well as brightening dips used to improve the corrosion resistance and appearance of the product.

The composition of some rinse waters from plating baths used in aircraft plating operations are depicted in Table 5.2. The most widely used treatment method for reducing the metal content of the waste waters involves chemical precipitation. Precipitation is a relatively simple process for single metal contamination, however, in more complex systems, problems may arise due to:

- choice of the optimum effluent pH where a number of metals are present
- formation of soluble metal chelates due to complexation with organic matter
- resolubilisation of some metal ions as a consequence of their amphoteric nature

Disposal of precipitated sludge by land fill is of obvious environmental concern. The cost of such a disposal is escalating due to limitations of space and stringent environmental regulations. Biosorption of heavy metals from trace metal-bearing solutions arising from aircraft plating rinse waters has been investigated as part of the current study.

Column trials were carried out at Finnair's plating shop in Helsinki. Finnair is the national airline for Finland and a major international carrier. At Helsinki airport, Finnair carry out routine maintenance of all their own aircraft and offer contract services to other airlines for overhauling aircraft engines and landing gear. Every ten years or so, aircraft engines and landing gear need to be stripped down, checked for corrosion and wear. Any parts showing signs of wear need to be re-plated according to the specifications of the manufacturer. This plating is carried out at Finnair's plating shop. The most common metal platings include those of cadmium, nickel and chromium.

The aircraft parts are initially coated with a hot wax (see Fig. 5.1.). The parts needing replating are first stripped of the previous coating using acid stripping baths containing complexing agents. In order to expose the part requiring plating, the wax is removed from the relevant area (see Fig. 5.2.). The part is then placed in a stripping bath to remove the previous coating. Following acid-stripping, the part is raised above the bath and moved sideways above a rinsing bath where spray jets are used to remove any adhering metal by washing with water. In some cases, the coating stripped part is dipped into a second rinsing bath before it is ready to be replated. The cleaned and coating stripped part is then lowered into the metal plating bath (see Fig. 5.3.) and the electrolysis process monitored to ensure an even coating of the surface (see Fig. 5.4.). Following replating, the part is washed above a rinsing bath as before; there may be a cascade of rinsing baths to optimize the use of rinse waters (see Fig.

5.5.). The concentration of metal ions accumulating in the rinse tank are monitored. When the concentration reaches an unacceptable level, the rinse water is discharged to the treatment system (usually precipitation). If cyanide ions are present, oxidation using ozone treatment may be needed before pH adjustment can be carried out.

Preliminary batch sorption tests were carried out to test the feasibility of employing algal biosorbents in treating the different rinse waters arising from the metal plating process. The results of these batch tests helped in the selection of biosorbents and solutions which were studied in fixed-bed columns. The optimum operating conditions (flow rates, pH, bed height etc.) obtained from studies with single metal simulant solutions were used during trials with real industrial effluents at the plating shop.

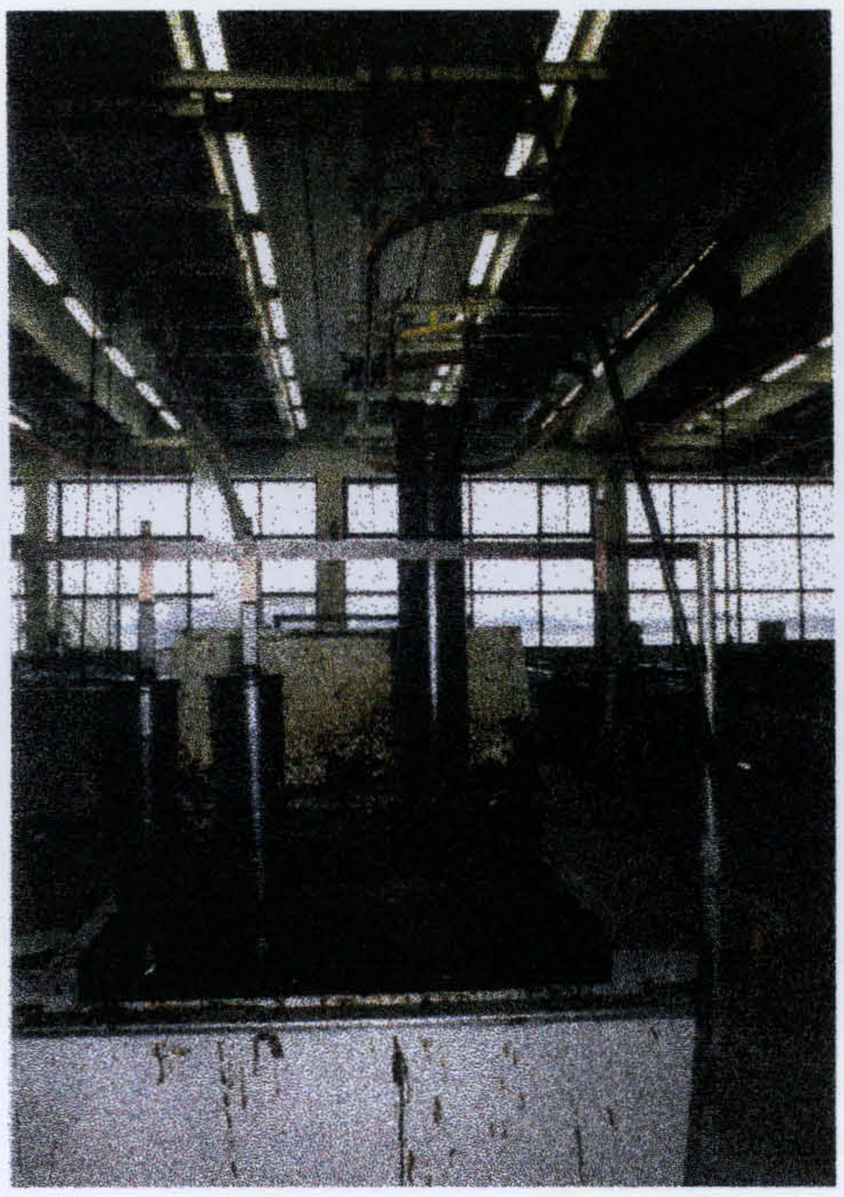

Figure 5.1. Wax coating bath.

Figure 5.2. Wax removed from specific areas to allow stripping of old coating.

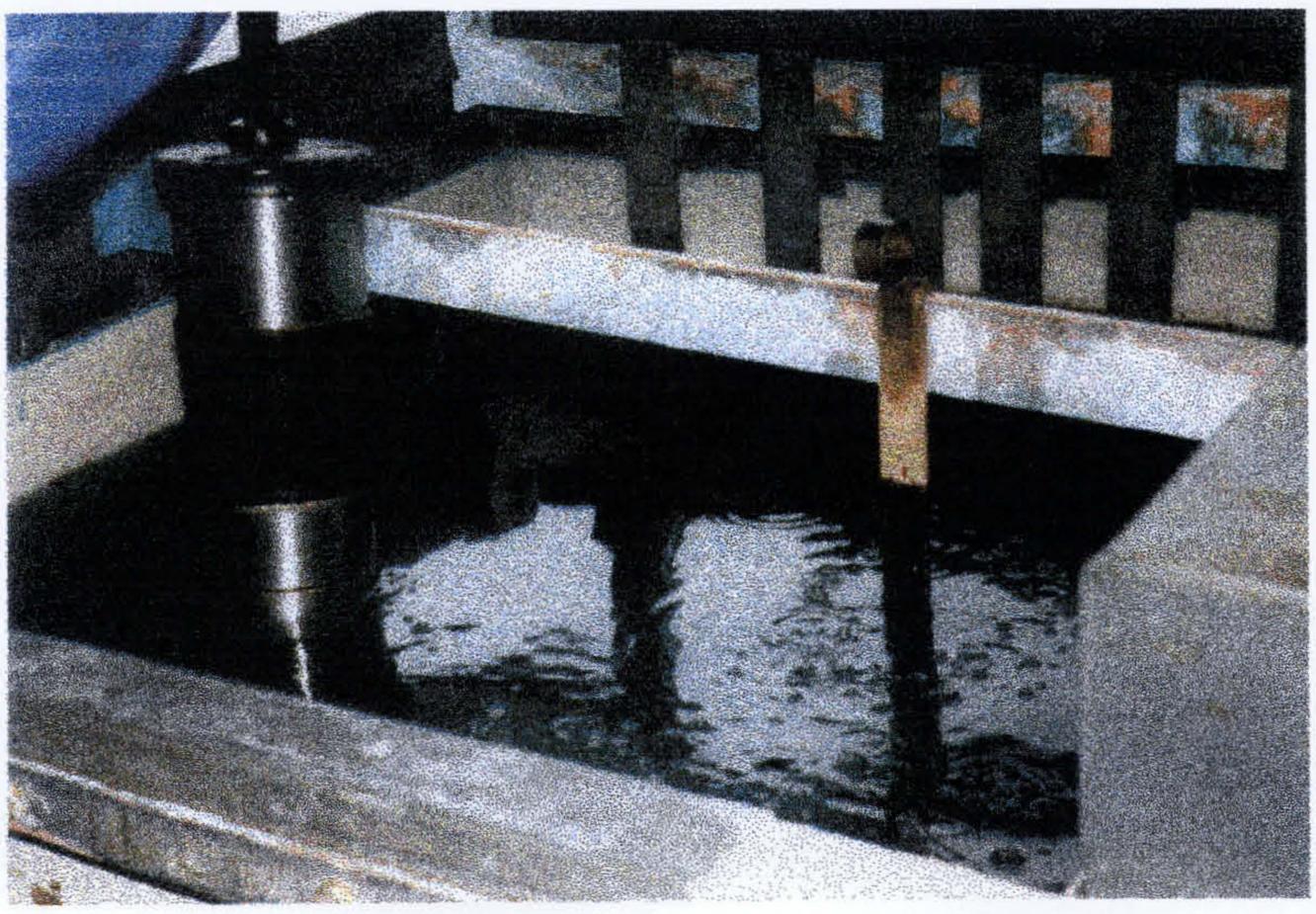

Figure 5.3. Aircraft part being lowered into metal plating bath.

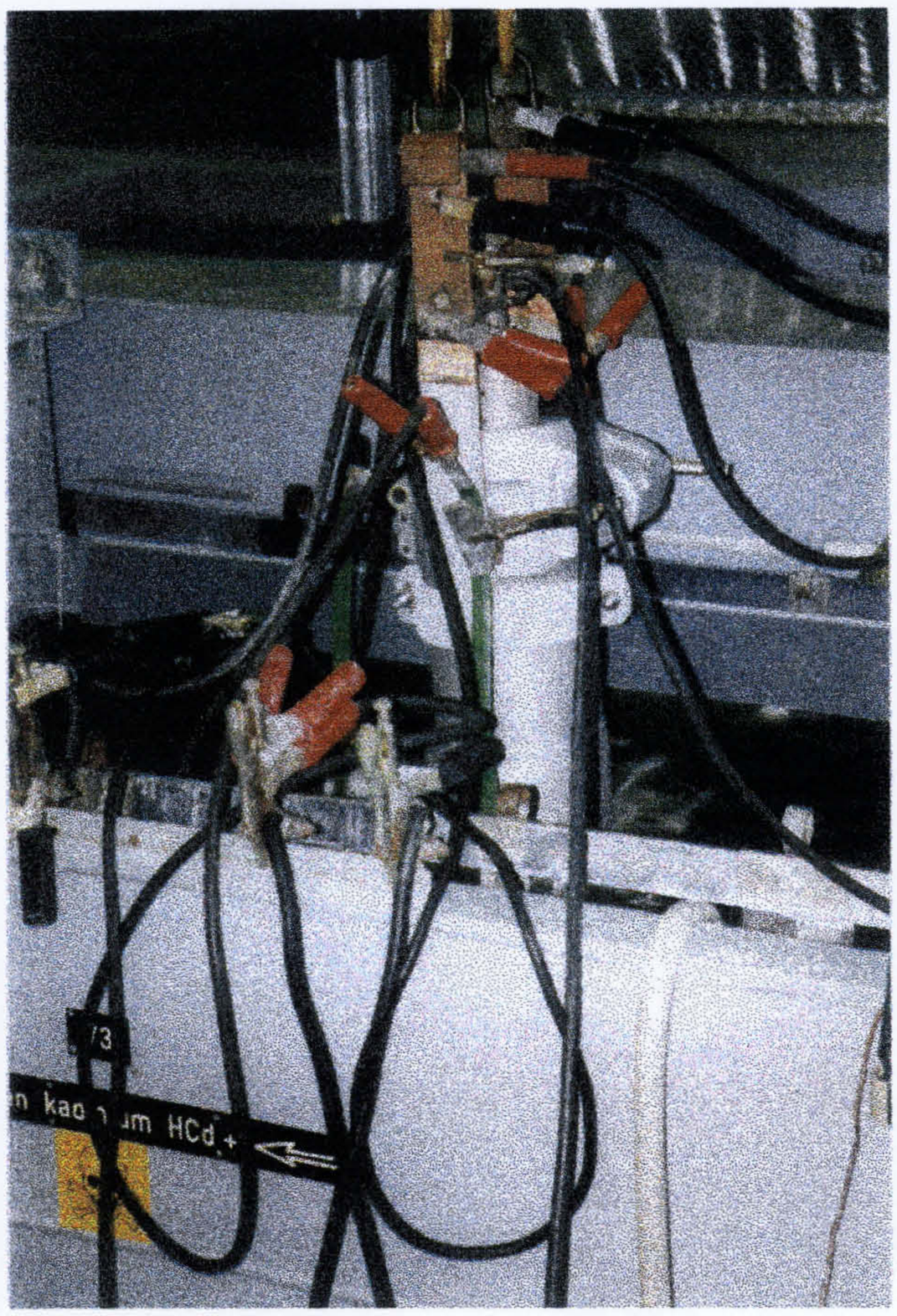

Figure 5.4. Cadmium plating of aircraft landing gear in progress.

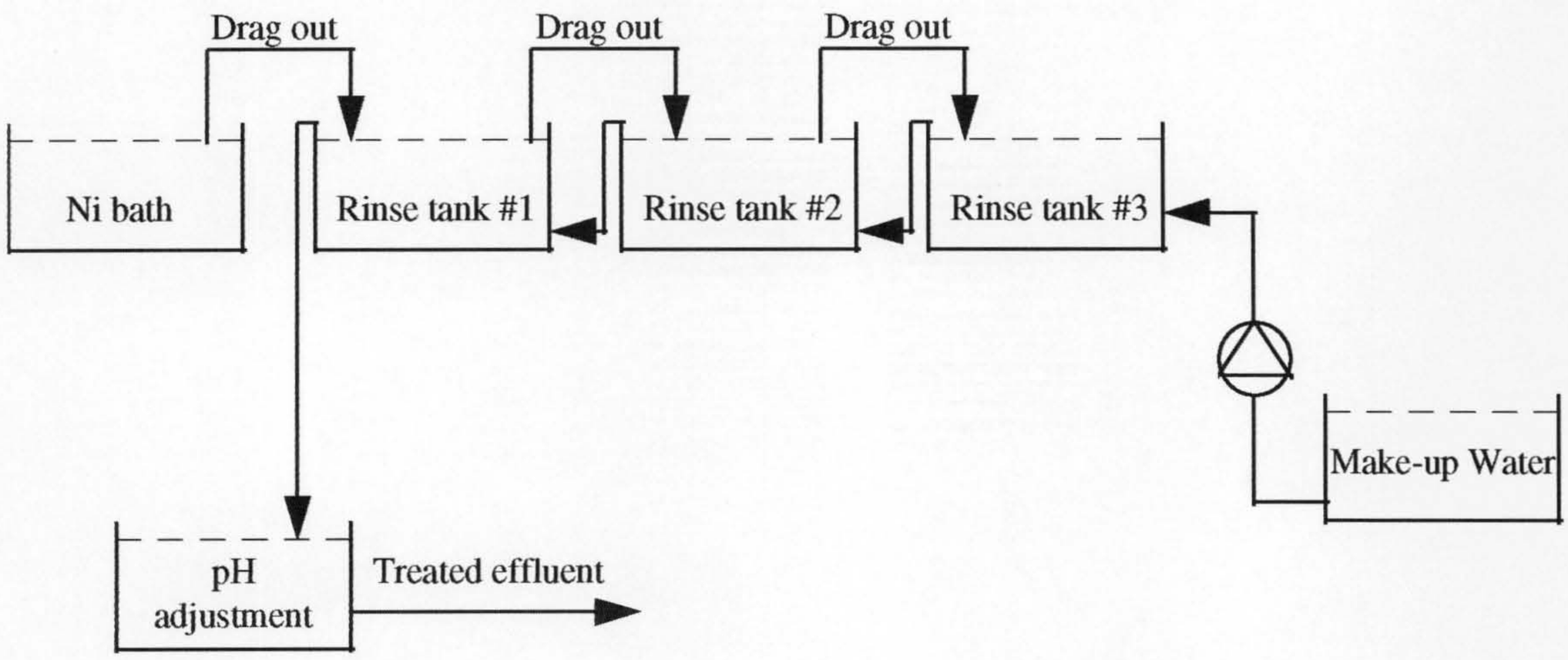

Figure 5.5. Cascade of rinsing baths used during metal plating.

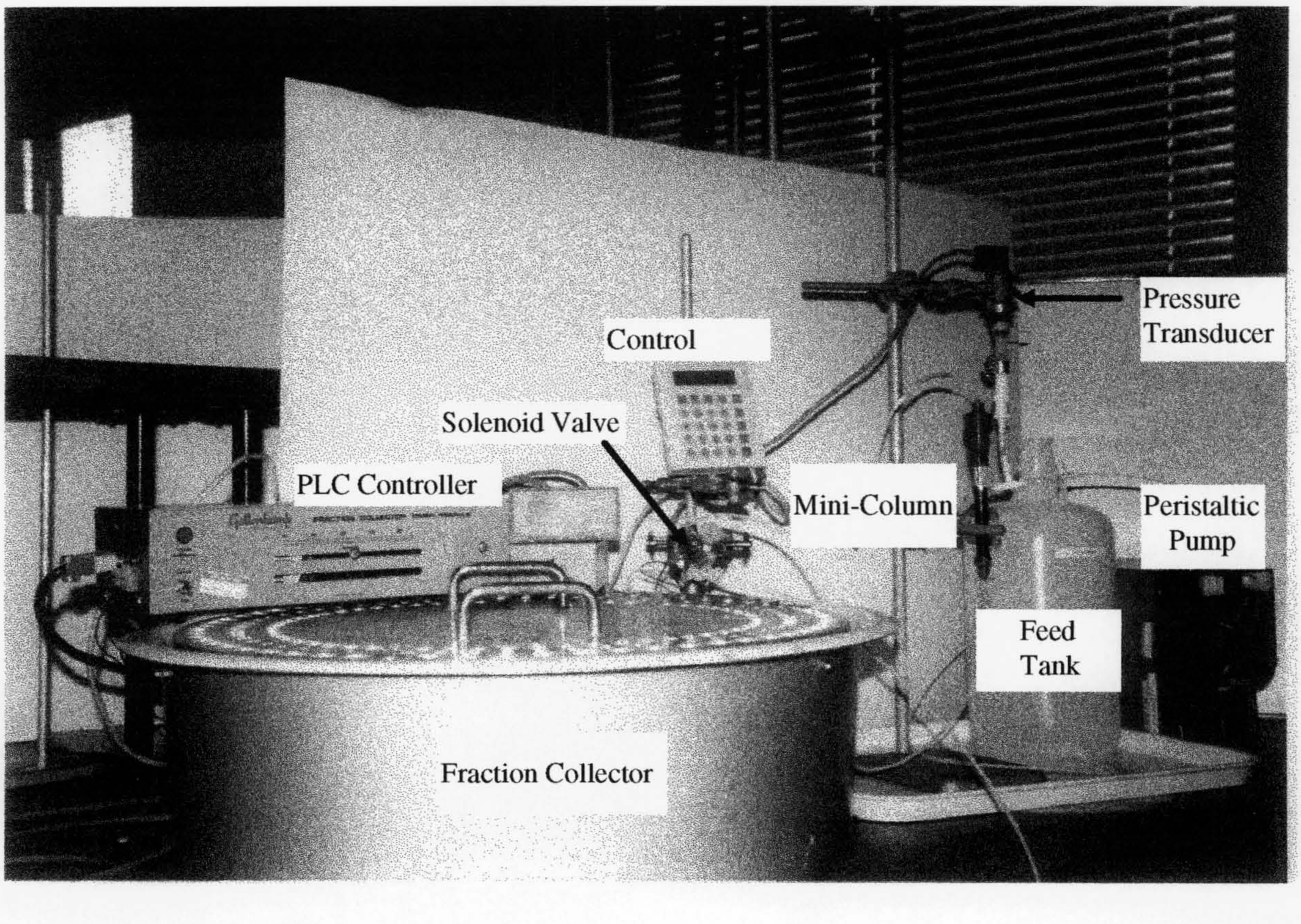

Figure 5.6. Mini-Column set-up for metal breakthrough profile development.

Biosorbent materials BK, AN, DAN and DLF were selected for study with real metal plating solutions from the Finnair plating shop. The selection was made on the basis of promising results obtained from studies on single metal breakthrough profiles as well as equilibrium sorption studies. BK contains the highest amount of algin amongst the four algae evaluated in the current study. Of all the brown marine algal varieties, AN has been most widely studied for metal biosorption (see chapter 1). A large amount of equilibrium metal sorption data are available. AN was selected as a bench mark against which other biosorbents may be compared. These two native materials were, therefore, selected for tests against plating effluent solutions. Dealginate seaweed samples DLF and DAN were selected as representative waste residues arising from an industrial algin extraction process.

Trials were carried out against two target metal bearing rinse water solutions; a cadmium stripping bath solution and a combined nickel chloride/nickel sulphamate plating bath solution. Nickel and cadmium bearing rinse waters were selected as the target effluent streams since biosorption studies indicated good sorption affinity of these heavy metal ions for algal metal binding sites.

Comparison of algae based biosorbents with conventional ion exchange and chelating resins as well as an oxidized active carbon was studied. An aminophosphonate resin (Purolite S950) and iminodiacetic resin (Purolite S930) were tested in nickel and cadmium bearing rinse waters of plating/pre-plating baths. The organic ion exchangers (Purolite S930 and S950) are chelating resins with a macroporous polystyrene back-bone matrix crosslinked with divinylbenzene. The resins were received from Purolite International Ltd., Pontyclun, UK. The 207C (OII) is a coconut-based active carbon oxidized by exposure to hot nitric acid for a period of 24h. The surface functional groups in the carbon closely resemble weakly acidic carboxyl and phenolic type groups.

Cross-flow microfiltration

In addition to using fixed-bed sorption columns, a cross-flow microfiltration process was employed to investigate the use of this alternative technology. The principal advantage of this process is that it employs algal particles with a wide range of particle size distributions. This avoids the need to granulate and separate algal particles. A smaller particle size distribution would result in improved sorption kinetics (see chapter 4). Problems associated with lack of structural integrity of algal particles would be of less concern in the microfiltration process.

Section 5.2. Experimental Parameters

Performance of fixed-bed algal biosorbent columns

Protonated and washed algal particles (native and dealginate) dry sieved size range (300-355 μm) were used in all fixed-bed column experiments. Smaller particle sizes resulted in excessive pressure drops and blockage of the 20μm frit support. Individual experimental conditions for each breakthrough profile are tabulated beneath the appropriate figure in the text. Algal particles were pre-wetted before the slurry was poured into the ion exchange columns to prevent entrapment of air bubbles. The algal slurry was washed several times with DDW until the supernatant solution appeared acceptably clear to the naked eye to prevent blocking of the frits. DDW (pH adjusted to 4) was pumped through the algal bed using a Watson-Marlow 501U peristaltic pump after loading the column with algal particles. Bed voidage was measured by draining a settled bed of biomass slurry using suction. An RS(256-720) pressure transducer (calibrated between 0-1 barG) was connected in-line with the pump and column inlet (see Fig. 5.6.). The effluent leaving the column was diverted to a Gallenkamp fraction collector using a two-way solenoid valve actuated using a Mitsubishi (FX_o 10P-E) Programmable Logic Controller unit with a digital control panel to alter the parameters associated with sample and delay times. pH of the effluent samples was measured individually using a Mettler-Toledo 340 pH meter. The metal ion concentration was measured using AAS in flame mode as described earlier (see chapter 3).

The influence of flow rates on the sorbent usage rate (volume of effluent solution treated g^{-1} of sorbent at 10% breakthrough) was calculated for an algal bed of fixed bed height and varying flow rates. The mass transfer zone height was calculated according to the method of Michaels[3] and the average uptake capacity calculated in the usual way by integrating the area above the breakthrough curve. These experiments were restricted to *A. nodosum* and copper bearing solutions. It is anticipated that most of the algal biosorbents will show similar trends in breakthrough profile development as those displayed by AN.

Cross-flow microfiltration

An integrated technology comprising biosorption and cross-flow microfiltration (MF) has been studied (see Fig. 5.7.). This process, referred to as the MF-BIOSORB process, may allow improved utilization of the high sorption capacities of particulate seaweed based biosorbents as mentioned earlier.

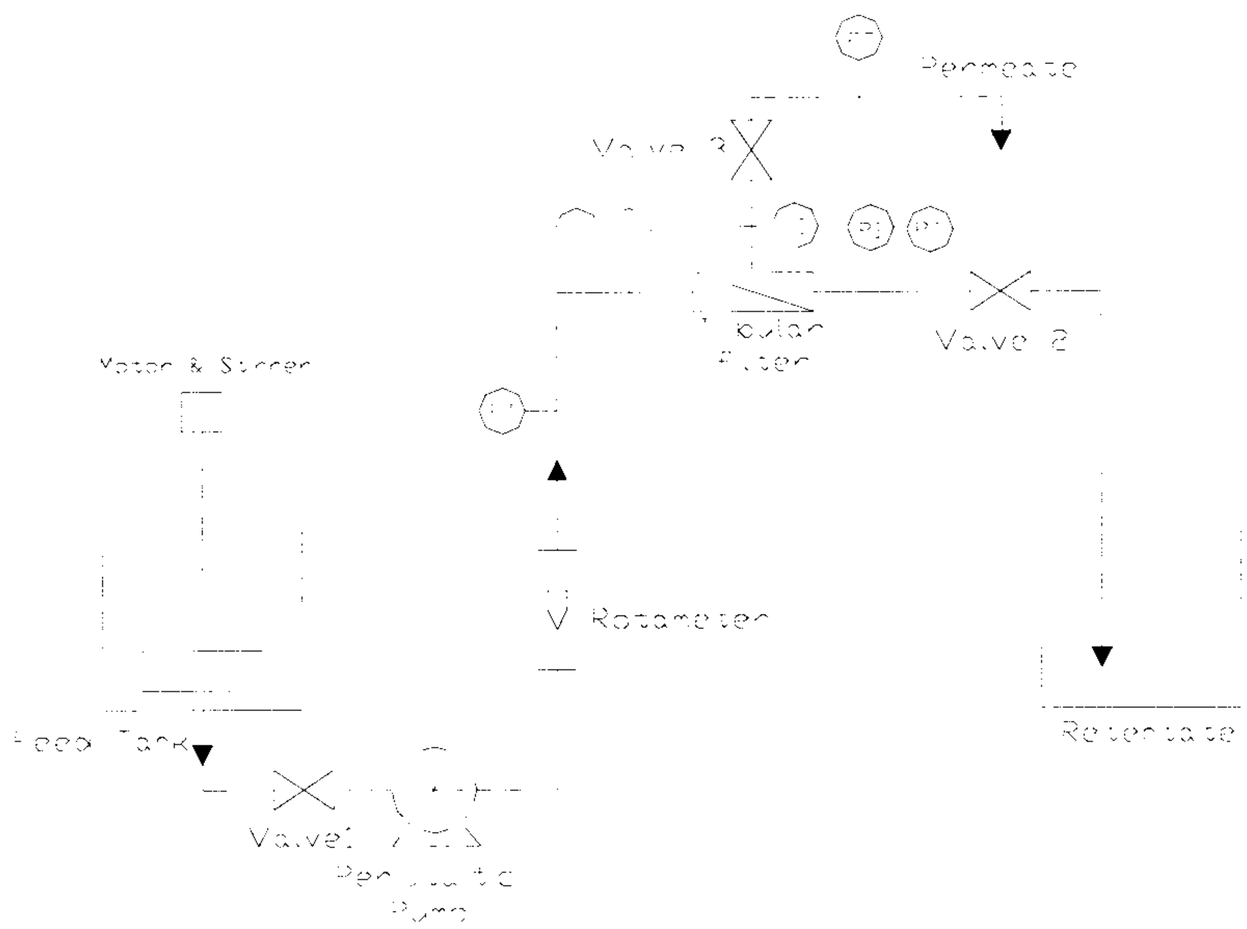

Figure 5.7. Schematic of MF-BIOSORB process.

The process employs a tubular cross-flow membrane filter module (nickel membrane with 18μm holes and an open area of 1% approx.) in which the feed stream (a slurry of algal sorbent particles and metal bearing effluent) flows tangentially along the membrane. The feasibility of obtaining a reasonable permeate flux for a slurry of DLF

particles (sieve fraction size 45-710μm) was initially investigated. A sorbent concentration of 200 ppm was pumped around the filtration loop (see Fig. 5.7.). A 20l slurry of DLF was stirred in a batch reactor. A peristaltic pump was used to circulate the slurry through the tubular filter before returning it to the reactor vessel. The valve downstream of the tubular cross-flow filter was partially closed to raise the filtration pressure (i.e. the transmembrane pressure P_{tr}). This valve was left untouched during the remainder of the filtration experiment. The inlet pressure P_{in}, outlet pressure P_{out}, and filtrate pressure P_{ft}, were continuously monitored during the filtration run using pressure transducers (the pressure transducers were connected to a data logger that continuously recorded the data which was available for analysis at the end of the filtration run).

The permeate flux was measured by opening the permeate valve and collecting known volumes of the permeate while measuring the time required for permeate collection. It was found, however, that the permeate flux declined considerably over the filtration run and it was impossible to keep the permeate volume fixed over the entire experimental run. The collected volume was therefore reduced in order to reflect the reduction in permeate flux.

The experiment was stopped after around 5 hours by fully opening the valve downstream from the membrane and closing the permeate valve. The outlet valve was partially closed for a short time to judge the effect of transmembrane pressure on the permeate flux. This resulted in a sudden surge of permeate through the membrane indicating a potential increase in flux at higher transmembrane pressures. In order to reduce membrane fouling, back flushing using compressed air was carried out in a subsequent experiment.

Ashing of algal biosorbent particles

The ash content of native and dealginate seaweed particles was determined as a possible route for final disposal of spent biomass once the sorbent material has degraded. Two sets of experiments were conducted; one set was carried out with

unwashed material as supplied by Monsanto plc., whereas the second set was carried out with protonated washed material.

A clean empty ceramic crucible was placed in a Carbolite oven (equipped with Eurotherm 91E temperature controller) at 600°C for one hour in order to remove any contaminants present. The crucible was allowed to cool in a dessicator over silica gel and was then weighed. The dry weight value of the empty crucible was recorded. 5g of algal particles (previously freeze dried) were weighed into the crucible and the weight was recorded. The crucible was placed in a preheated oven (set at 600°C) for six hours. Complete ashing of algal particles occurs within the first hour. However, to ensure that no error is introduced, all materials were studied under identical conditions and for an extended ashing period. Following ashing, the crucible was allowed to cool in a dessicator over silica gel before the ash content of the algal sample was recorded. Native AN, LH and BK along with dealginate seaweed samples DAN and DLF were tested for ash content. The unwashed seaweed samples were not freeze dried before ashing (only sun dried) and therefore, any residual moisture present in the materials would result in reduction in the ash content value.

Section 5.3. Results And Discussion

Performance of fixed-bed algal biosorbent columns

The influence of key experimental parameters, particularly effluent flow rates and bed height affecting the performance of sorbents in column systems have been evaluated for algal biosorbents. Copper bearing solution (0.5 mM, pH 4) was passed through two columns (in parallel) having different bed heights in order to assess the development of constant or proportionate pattern breakthrough profiles (as recommended by Slater[2]). The breakthrough curves for copper are self-sharpening indicating favorable equilibrium between copper ions in solution and the metal binding sites in algae (see Fig. 5.8.). This is not surprising, since the high affinity of copper ions for native algae was demonstrated during equilibrium sorption studies (see chapter 3). Copper ions in solution are readily removed by the biosorbent bed as the progressive front passes through the column and copper ions are prevented from

moving much in advance of the sorption front. Thus, a sharp boundary exists between high and low copper concentrations in solution and the concentration gradient in the direction of flow is steep[2]. The self-sharpening process is affected by flow abnormalities due to non-uniform packing of the algal bed resulting in channeling etc. This may be the underlying reason behind the slight differences in the breakthrough profiles for the two bed depths depicted in Figure 5.8. Only two bed heights have been evaluated in the current study (5 cm and 10 cm). It is important to realize that in a relatively shallow bed entry effects will distort the shape of breakthrough profiles. Experiments with algal bed heights of around 50 cm are recommended in order to overcome entry effects and achieve constant pattern behavior[2].

Solution flow rate plays an important role in determining the efficiency and consequently the volume of effluent treated per unit mass of biosorbent. As expected, the optimal sorbent usage (the least amount of sorbent for a given volume of treated effluent) occurs in the low flow rate region. Under these conditions, the algal bed is properly contacted with solution as it flows through the column and the dynamic bed mass transfer front is relatively small (see Table 5.1. and Fig. 5.9.). At high flow rates, increase in the mass transfer zone height due to departures from local equilibrium conditions causes flattening of the breakthrough profiles thereby reducing the sorbent sorption efficiency (see Fig. 5.10.). The mass transfer zone height increases linearly (almost) with the solution flow rate. Slater[2] suggested dependence on flow rate to the power between 0.33-0.5 as indicative of liquid film rate control. This is apparently not true for algal biosorbents and intraparticle limitations play an important role in determining the rate of biosorption within the algal bed.

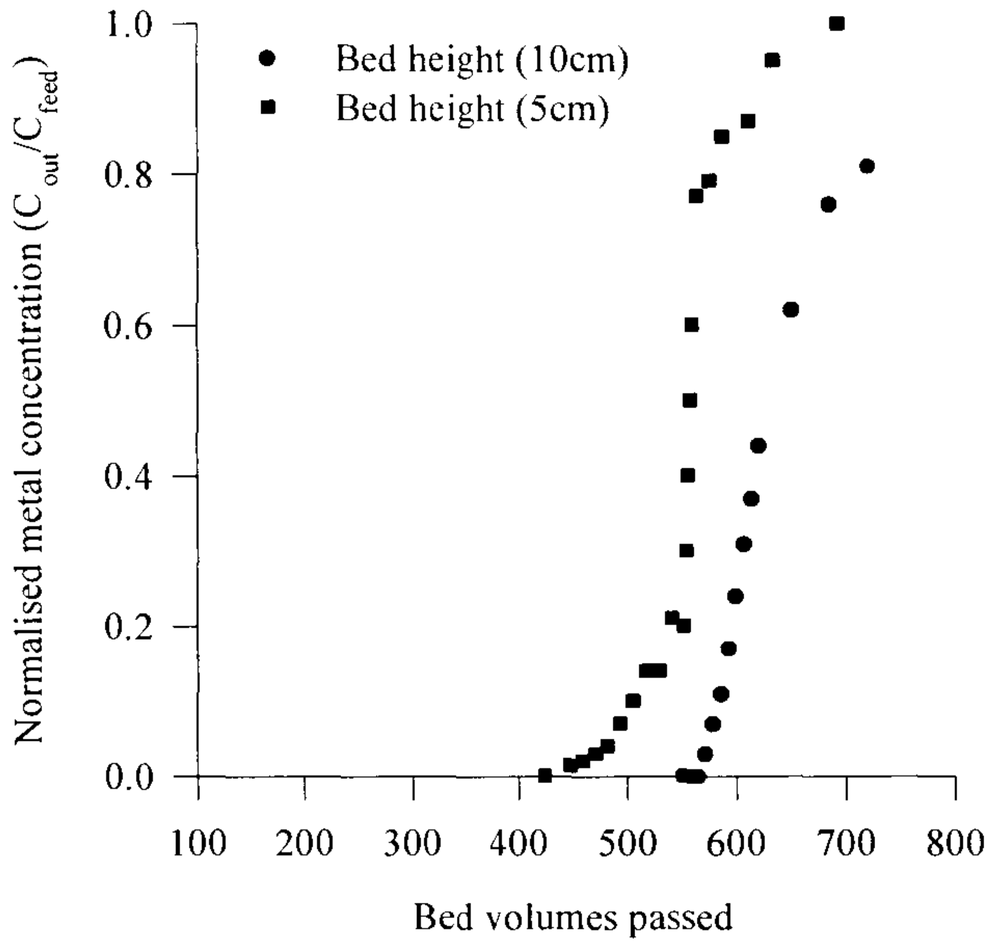

Experimental parameters

C_f mM	Bed height cm	Bed volume ml	Flow rate l hr^{-1} m^{-2}	Specific usage g $(1000l)^{-1}$	Service capacity mmol g^{-1}	EBCT min
0.5	9.75	7.7	46	444	0.9	12.8
0.5	4.6	3.6	36	549	0.9	7.6

Figure 5.8. Self-sharpening constant pattern curves for A. nodosum.

Flow rate $l\ hr^{-1}\ cm^{-2}$	Bed height cm	[1] $t_{0.1}$ hr	[2] $t_{1.0}$ hr	[3] specific usage g/1000l	[4] service capacity mmol g^{-1}	[5] EBCT min
46	8.8	124	169	444	0.9	12.8
138	8.8	27	41	667	0.6	4.3
214	8.8	14	28	833	0.58	2.4
688	8.8	3.9	11	943	0.53	0.6
16	4.6	123	161	647	0.7	17.2
36	4.6	65	88	549	0.9	7.6
290	4.6	6.1	16.4	725	0.69	1.0

Table 5.1. Influence of bed depth and flow rates on mini-column breakthrough profiles.

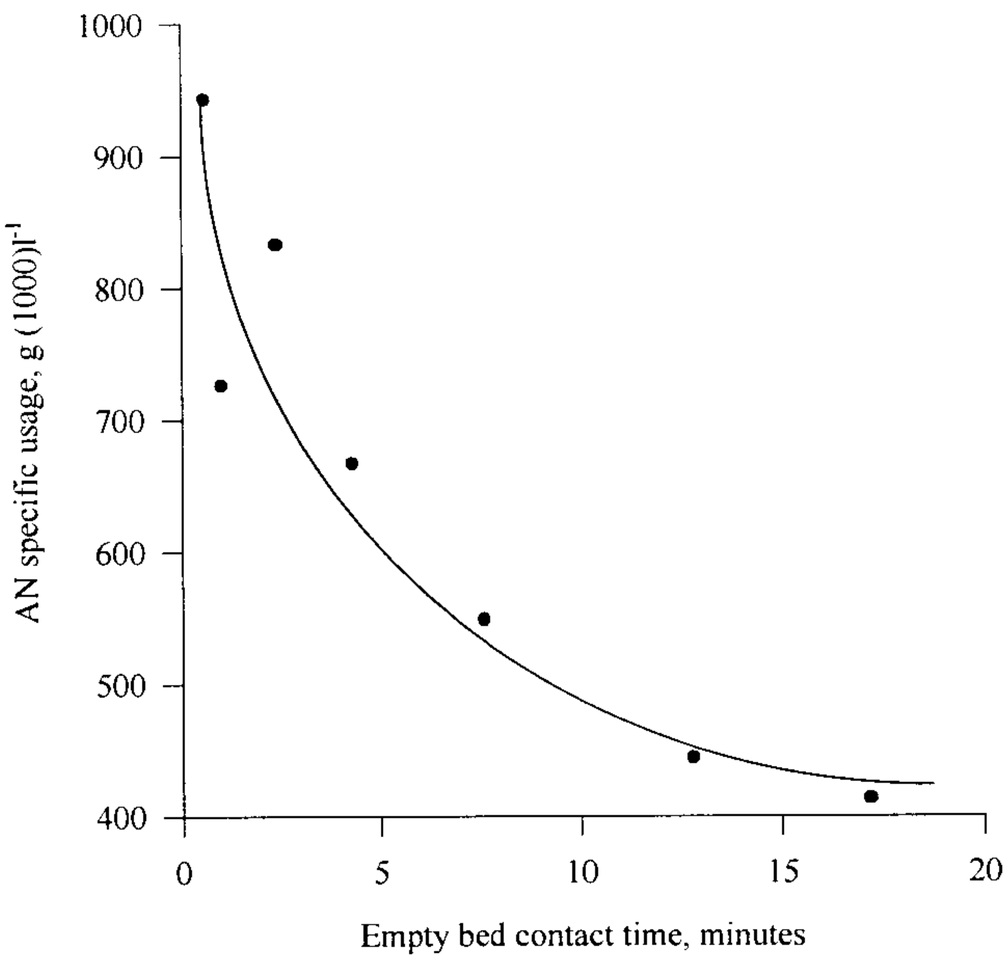

Experimental parameters

Target metal	C_f, mM	Bed height, cm	Bed volume, ml	Flow rate $l\ hr^{-1}\ m^{-2}$	Solution pH
Cu^{2+}	0.5	10	7.85	variable	4

Figure 5.9. Effect of effluent residence time on specific usage of *A. nodosum.*

[1] 10% breakthrough i.e. when effluent metal concentration reached 10% of the influent concentration.
[2] 100% breakthrough i.e. when effluent metal concentration reached 100% of the influent concentration.
[3] Amount of sorbent required to treat 1000 litres of metal bearing solution.
[4] Average metal uptake at 10% breakthrough.
[5] Empty bed contact time indicates the liquid residence time in the column.

After four sorption/desorption cycles, the service capacity of the AN algal bed fell from 0.9 mmol g^{-1} to around 0.5 mmol g^{-1} (see Fig. 5.11.). There was a marked reduction in service capacity following the first sorption/elution cycle. In subsequent copper sorption cycles, the shape of the breakthrough profiles became shallower, indicating possible changes in the sorption characteristics of the algal bed. The algal particles within the column showed signs of textural changes; there was a definite lack of granularity after four successive sorption cycles. In addition, degradation and washing out of algal constituents from the sorbent bed resulted in reduction in bed height from around 10 cm in the first cycle to less than 7.5 cm after the fourth cycle. The flattening of the breakthrough curves also resulted in increasing the difference between the breakthrough time ($t_{0.1}$) and the full saturation time ($t_{1.0}$).

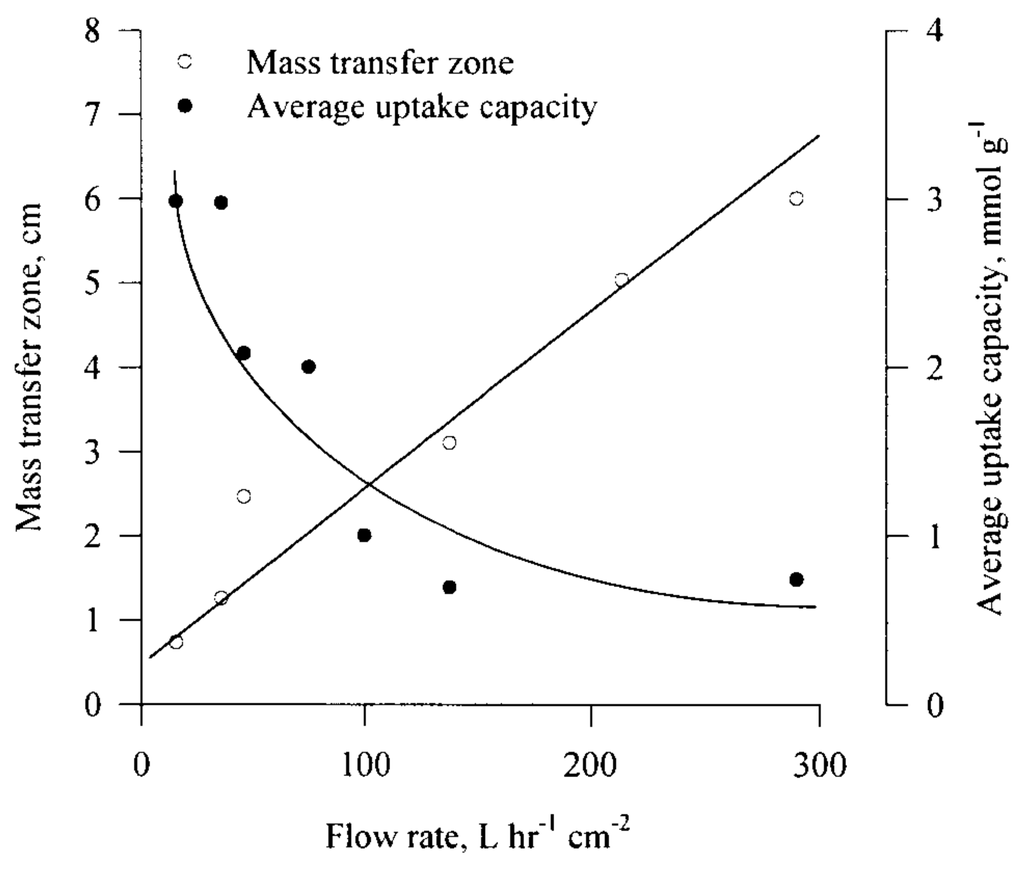

Figure 5.10. Influence of flow rate on mini-column copper breakthrough profiles for *A. nodosum*.

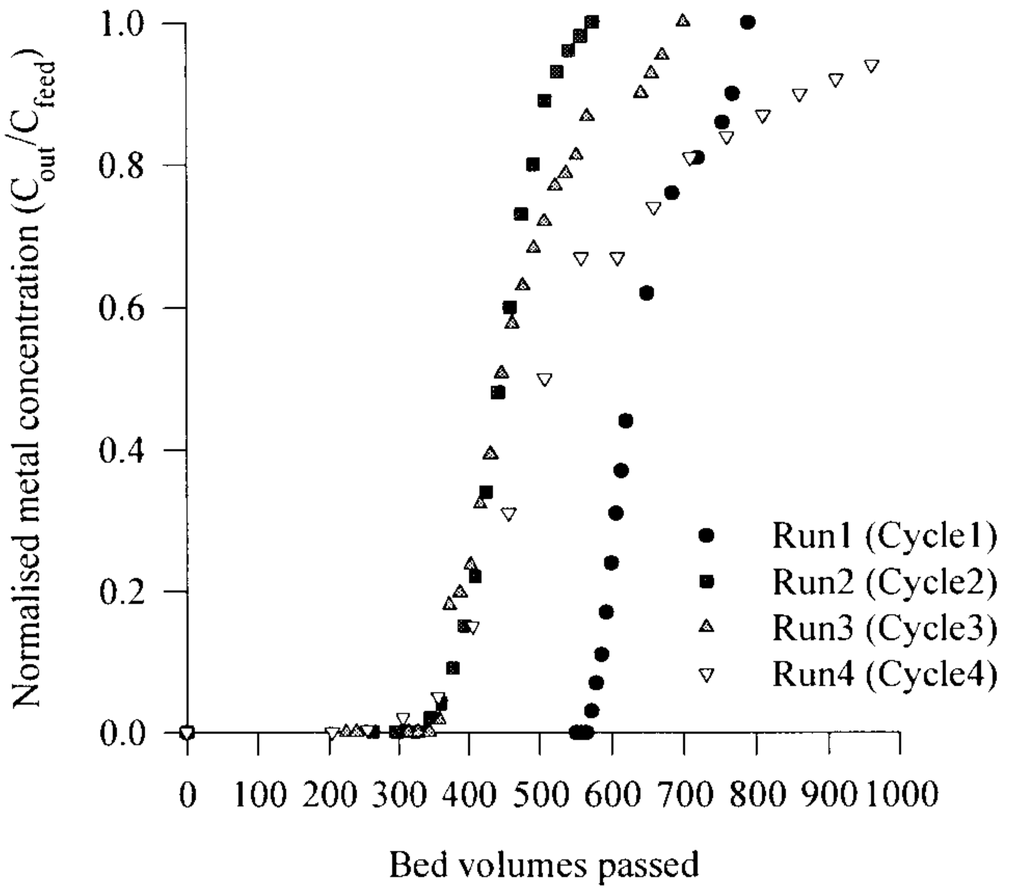

Figure 5.11. Breakthrough profiles for several copper sorption cycles by *A. nodosum.*

The reduction in treated effluent volume following the first sorption/elution cycle may be attributed to a combination of factors. Acid elution probably results in hydrolysis of glycosidic linkages in structural polysaccharides constituting the cellular make-up of algal cell walls. The reason for the lower volume of effluent treated after the first sorption cycle may be related to the washing out of key components responsible for providing metal-binding sites within the biosorbents. However, the significant change in sorbent sorption capacity after the first cycle cannot alone be explained by degradation of metal binding sites following acid elution. Otherwise, further reduction after the second and third sorption cycles would have been as dramatic. It is obvious that a large proportion of metal-binding sites available during the first sorption cycle were masked during successive sorption cycles. Copper ions may bind to surface functional groups by chelation and covalent bond formation in addition to simple ion exchange. These ions may not be easily eluted during the regeneration step, thereby reducing the sorbent sorption capacity in subsequent sorption cycles. The consistent breakthrough of copper ions in sorption cycles 2 to 4 after treating around 350 bed volumes of effluent is clear indication that copper-binding sites in

algae may be divided into those that can be regenerated and those that cannot (see Fig. 5.11.). The copper-binding sites that are regenerated by treatment with hydrochloric acid may represent sites undergoing simple ion exchange reactions between protons in solution and copper ions on the algal surface. These sites are responsible for about 70% of the effluent treated during the first sorption cycle and almost entirely responsible for copper sorption during successive sorption cycles when the chelating sites are already occupied by previously sorbed copper ions (the binding mechanism for these sites probably involves covalent bond formation).

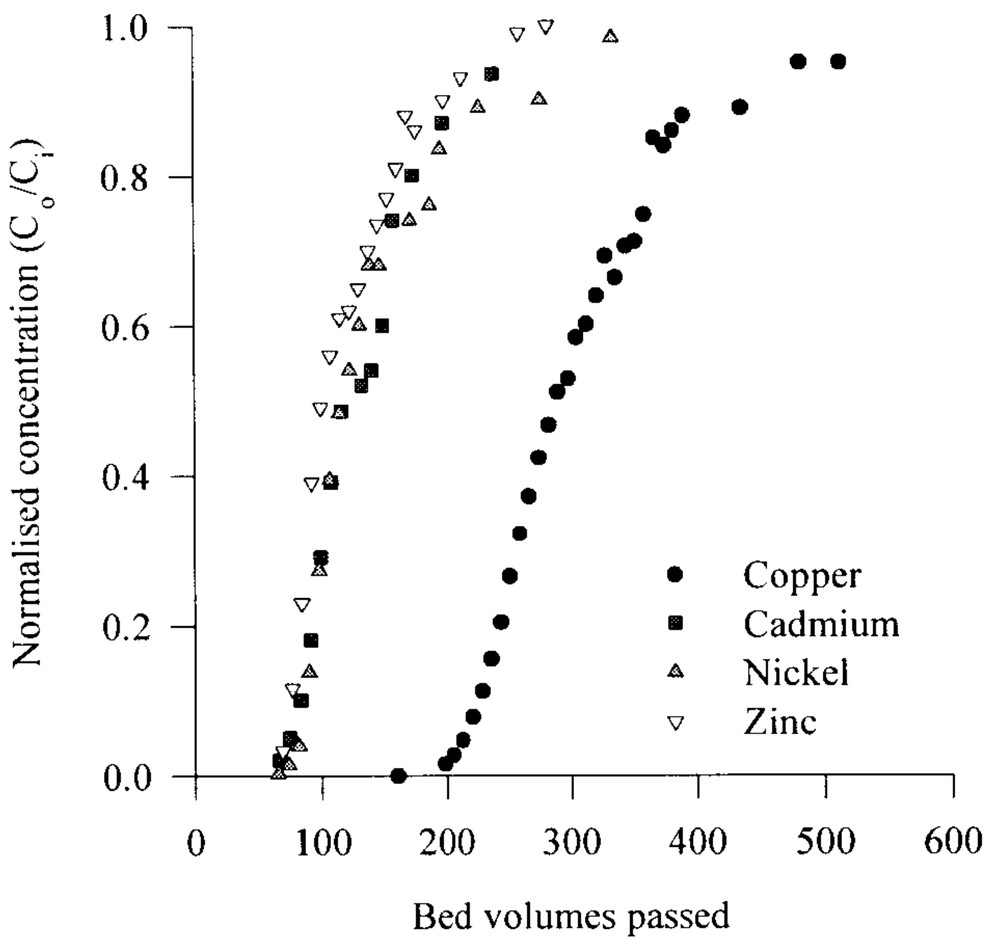

Experimental parameters

Target metal	C_f mM	Bed height cm	Bed volume ml	Flow rate $l\ hr^{-1}\ m^{-2}$	specific usage g/1000l	service capacity mmol g^{-1}	EBCT min
Cu^{2+}	0.86	5.4	6.5	41	1710	0.50	7.9
Cd^{2+}	0.70	5.4	6.5	44	5818	0.12	7.4
Ni^{2+}	0.89	5.4	6.5	44	4488	0.2	8.9
Zn^{2+}	0.66	5.4	6.5	44	6840	0.1	7.4

Figure 5.12. Single-metal breakthrough profiles for *A. nodosum.*

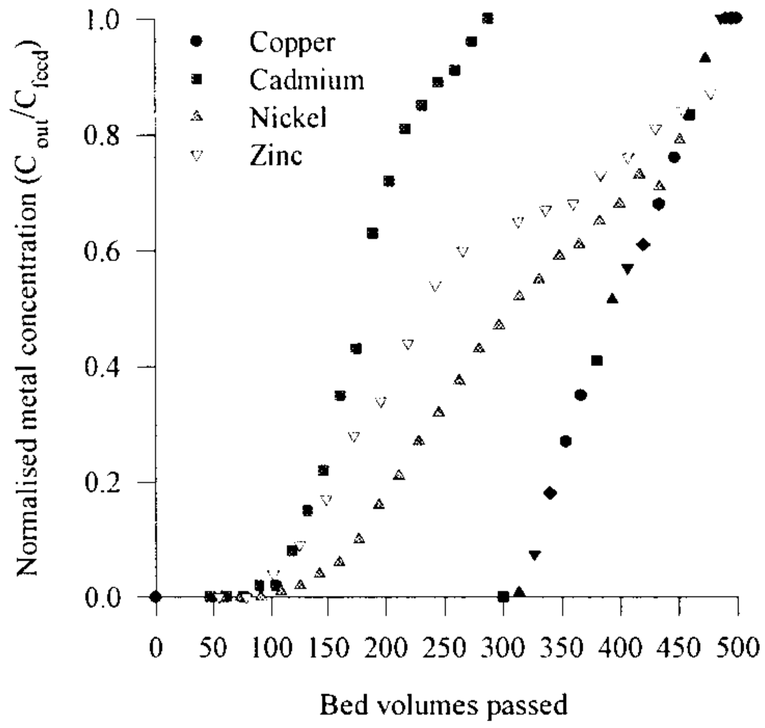

Experimental Parameters

Target metal	C_f mM	Bed height cm	Bed volume ml	Flow rate l hr^{-1} m^{-2}	specific usage g/1000l	service capacity mmol g^{-1}	EBCT min
Cu^{2+}	0.8	3.4	4.5	9.5	1802	0.44	21.5
Cd^{2+}	0.55	2.0	1.2	18.4	6211	0.09	6.1
Ni^{2+}	1.0	2.2	1.4	25.2	2094	0.48	5.2
Zn^{2+}	0.94	1.8	1.2	28.3	3609	0.26	4.0

Figure 5.13. Mini-column breakthrough curves for *D. Potatorum* (single metal).

Single-metal bearing solutions of copper, cadmium, nickel and zinc ions were passed through algal beds of native and dealginate seaweeds. Metal breakthrough profiles were recorded (see Figures 5.12. to 5.15.). Copper ions were the preferred species and the volume of copper solution treated by the algal beds was significantly greater in comparison with the other metal ions. AN treated over 200 bed volumes of copper solution whereas only 75 bed volumes of solution containing the other heavy metal ions was passed before breakthrough of metal ions was detected (see Fig. 5.12.). The breakthrough profiles were relatively sharp for all metal ions under identical flow conditions. The BK breakthrough curves displayed significantly flat effluent concentration profiles (see Fig. 5.13.). Nickel and zinc concentrations in the effluent failed to approach the feed concentration even after 450 bed volumes of solution was passed through the algal bed. The shallow beds (bed height ~ 2 cm) used for the development of these breakthrough profiles were not sufficient to achieve constant

pattern flow conditions within the algal bed. Increasing the bed height to ~ 3.5 cm did slightly increase the gradient of the copper breakthrough profile which clearly indicates the need for deeper algal beds (at least 5 cm) in order to study metal biosorption using mini-columns. Increasing the contact time between the effluent solution and the sorbent material also helped in approaching constant pattern conditions within the algal column. This behavior was displayed by shallow LH columns (bed height < 3 cm) where the empty bed contact time had been increased to around 10 minutes (see Fig. 5.14.). Reducing the contact time (i.e. increasing the flow rate) results in shallower breakthrough curves. The breakthrough profiles for nickel and zinc were obtained for higher feed metal concentration (~ 1 mM) which has the effect of increasing the height of the mass transfer zone.

The breakthrough profiles for dealginate seaweed showed remarkably similar performance in comparison with the native virgin biomass (see Fig. 5.15.). DLF was capable of treating around 200 bed volumes of copper solution and ~75 bed volumes of cadmium, nickel or zinc solutions without breakthrough of heavy metal ions (compare results with native LH; see Fig. 5.14.). This result is clearly important in light of the fact that dealginate seaweed residue is a waste by-product of the algin extraction industry and as a consequence would command a significantly lower cost in comparison with the more valuable algin-rich native seaweed. The sorption profiles for DLF were obtained at higher flow rates (EBCT between 3-5 minutes) and for high feed metal concentrations (~ 1 mM) compared with profiles obtained for LH. The lower swollen volume of dealginate seaweed residues in comparison with the native seaweeds (see Table 2.3.) is partially responsible for the better performance of these materials in column operation. The slower sorption kinetics previously displayed by the dealginate residues (see chapter 4) do not seem to significantly affect the performance of the material in column operation. The S-shaped breakthrough profiles are reasonably steep; at least during the initial part of the breakthrough curve. The multi-metal breakthrough profiles for a mixture of cadmium, nickel and zinc ions shows identical breakthrough of metal ions after around 20 bed volumes of solution had passed through the DLF column (see Fig. 5.16.). The high concentration of metal ions (~1 mM each) in the feed solution resulted in an early breakthrough with no

metal ions showing particular selective sorption within the dealginate seaweed column.

It is clear from preliminary studies of algal fixed-bed columns, that, the important parameters governing sorbent usage efficiency and development of sharp breakthrough profiles relate to flow rate and height of the algal bed. A minimum bed height of 5 cm and EBCT ~ 6 minutes is recommended in order to obtain constant pattern breakthrough profiles. The corresponding height of the mass transfer zone determined using Michaels method[3] is around 3 cm (see Appendix 2 for method of calculation). The algal beds may be re-used over several sorption/elution cycles except in the case of copper ions where some sorption capacity is lost following the first sorption cycle due to chelate-type surface reactions.

Preliminary mini-column studies have identified the optimum operating conditions required for testing selected biosorbents against real plating effluent streams (this is discussed in the following section).

Measurement of the effluent pH profile exiting the biosorbent column provides insight into the processes occurring within the algal bed. Several interesting observations are worth noting. The pH of the effluent solution rapidly fell below the influent pH (influent pH 4) which was constant during the entire sorption experiment (see Fig. 5.17.). An increase in the effluent pH coincided with the breakthrough of the metal ions from the biosorbent bed. The low effluent pH during copper sorption clearly indicates interaction of metal ions with protons of the functional groups.

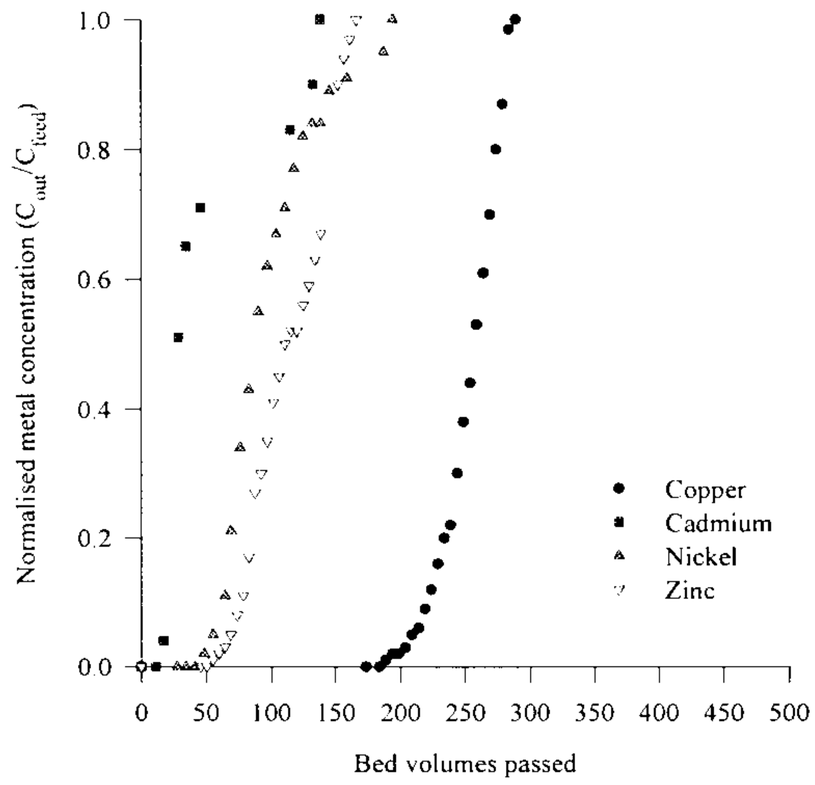

Experimental Parameters

Target metal	C_f mM	Bed height cm	Bed volume ml	Flow rate $l\ hr^{-1}\ m^{-2}$	specific usage g/1000l	service capacity mmol g^{-1}	EBCT min
Cu^{2+}	0.4	2.85	1.8	17	3157	0.13	10
Cd^{2+}	0.6	2.5	1.6	17.3	29.5k	0.02	8.7
Ni^{2+}	1.0	2.8	1.8	23.6	4274	0.23	7.2
Zn^{2+}	0.8	2.8	1.8	15.7	4643	0.17	10.7

Figure 5.14. Mini-column breakthrough curves for *L. Hyperborea* (single metal).

The pressure drop across the columns was found to vary with the flow rate and with the ionic composition of the effluent. There was a noticeable increase in the pressure drop across the algal-columns during regeneration of the metal-laden biosorbent bed. There was also an increase in the average pressure drop across the column during the course of metal loading of the algal bed. This increase in pressure drop across the algal bed may be linked to osmotic fluctuations within the algal column due to conversion of the biomass from the protonated to the metal form.

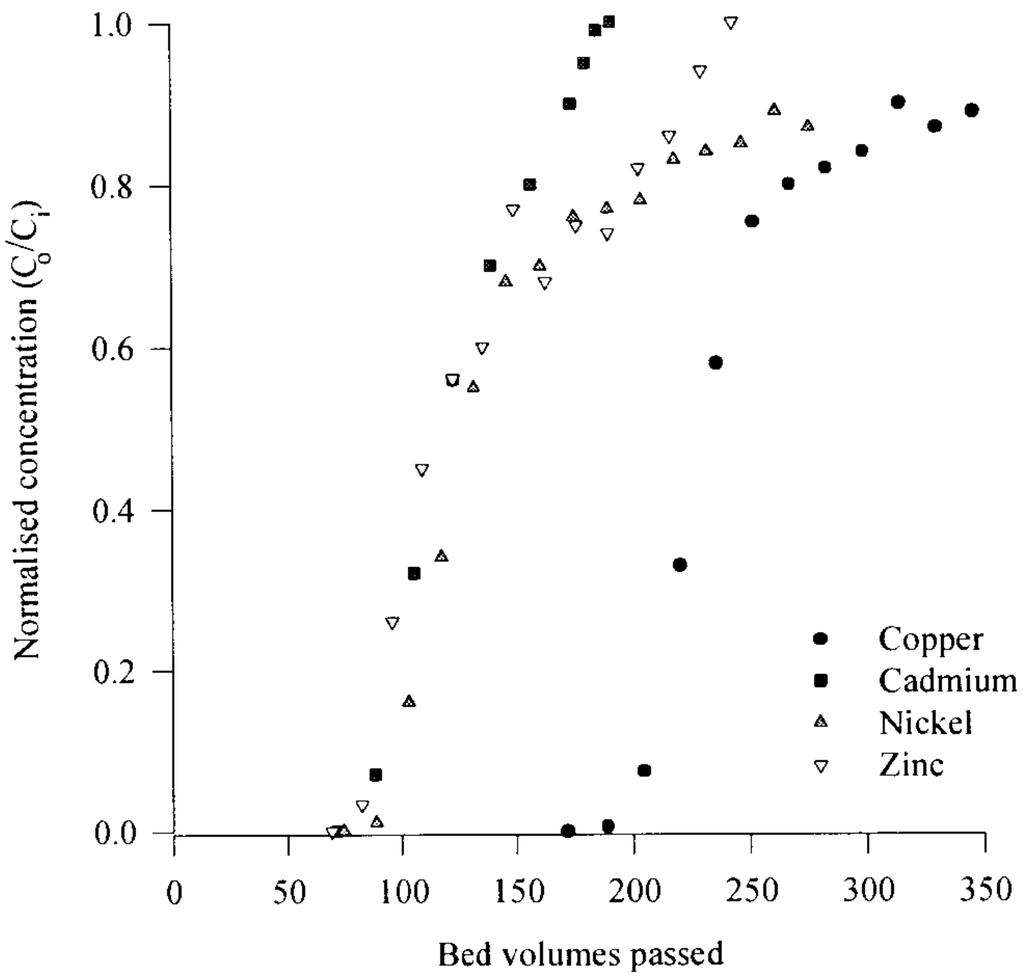

Experimental Parameters

Target metal	C_f mM	Bed height cm	Bed volume ml	Flow rate $l\,hr^{-1}\,m^{-2}$	specific usage g/1000l	service capacity mmol g^{-1}	EBCT min
Cu^{2+}	0.9	3.3	4.0	61.3	2130	0.42	3.2
Cd^{2+}	1.0	3.3	4.0	55.7	4498	0.22	3.6
Ni^{2+}	1.1	3.3	4.0	47.0	3834	0.29	4.2
Zn^{2+}	0.9	3.3	4.0	43.5	4990	0.18	4.6

Figure 5.15. Mini-column breakthrough curves for DLF (single metal).

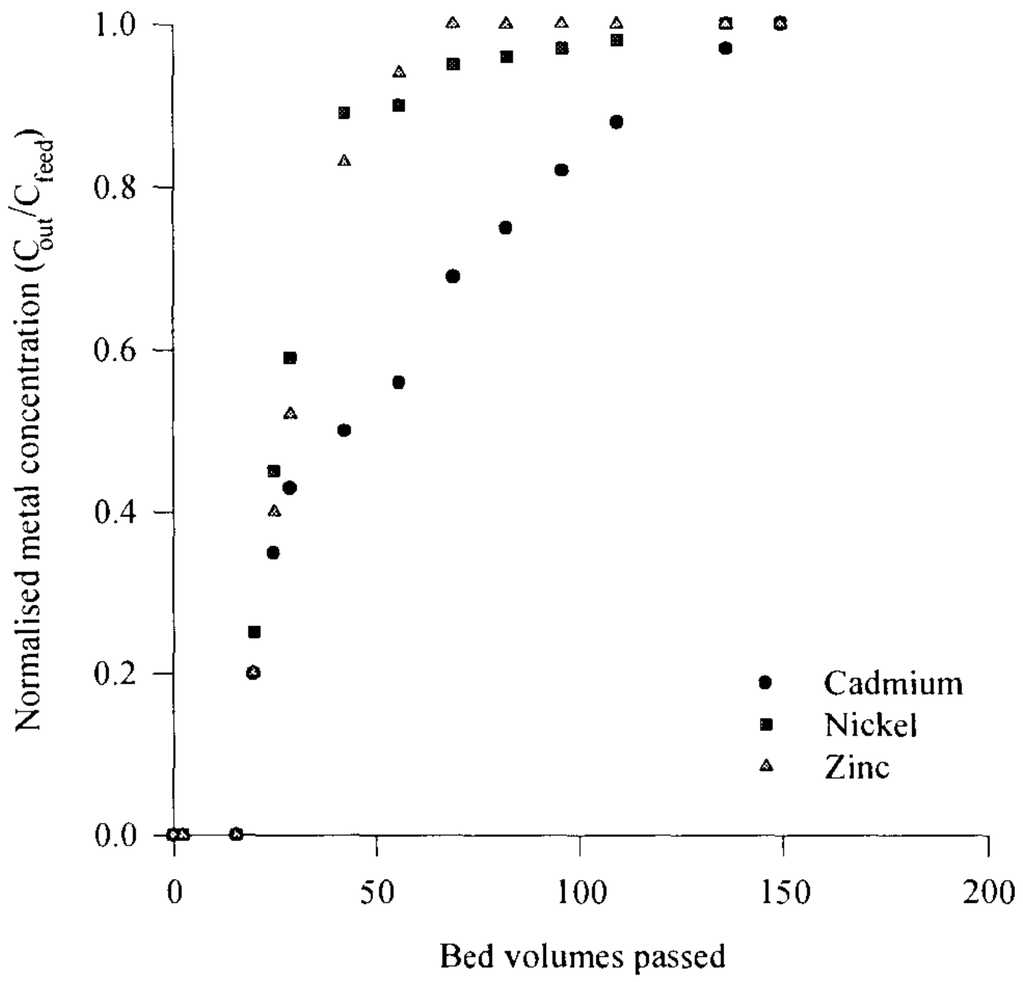

Experimental Parameters

Target metal	C_f mM	Bed height cm	Bed volume ml	Flow rate $l\ hr^{-1}\ m^{-2}$	Specific usage g/1000l	Service capacity mmol g^{-1}	EBCT min
All	0.9	3.3	4.0	43.5	26 kg	0.09	4.6

Figure 5.16. Mini-column breakthrough curves for DLF (multi-metal).

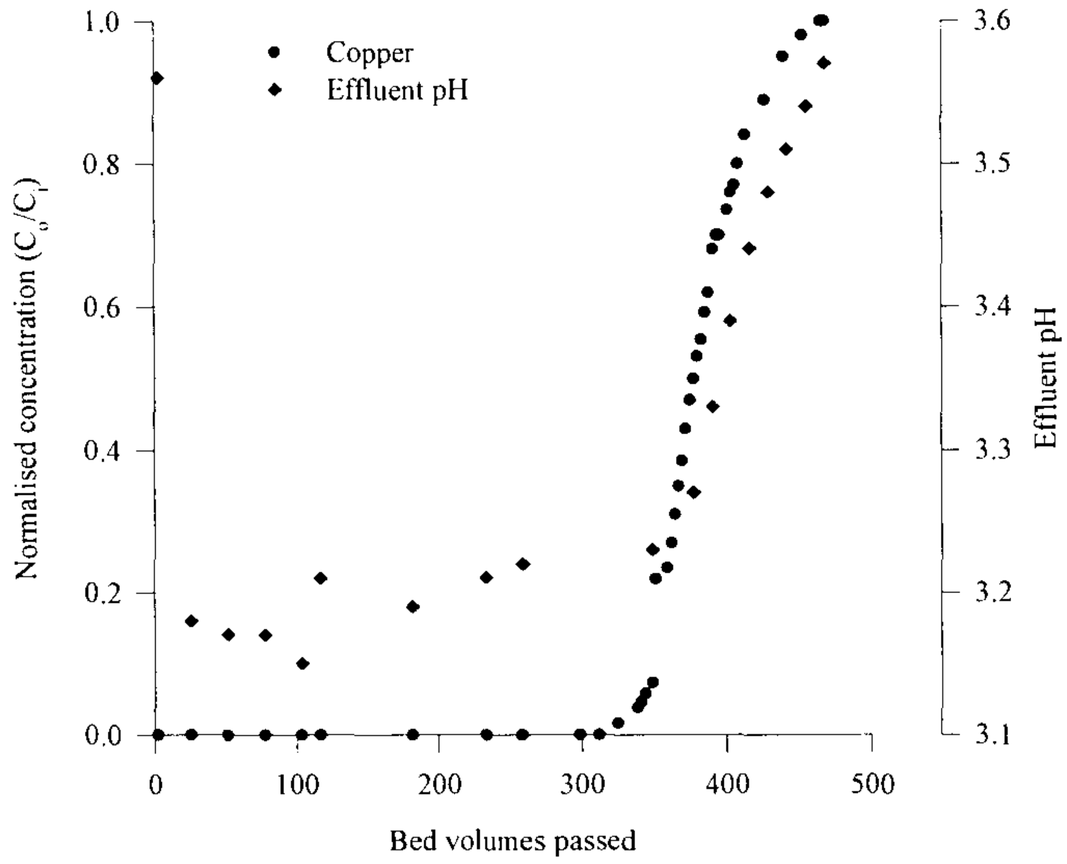

Experimental Parameters

Target metal	C_f, mM	Bed height, cm	Bed volume, ml	Flow rate $l\,hr^{-1}\,m^{-2}$	Solution pH
Cu^{2+}	0.5	8.1	6.35	42	4

Figure 5.17. pH and copper breakthrough curves for DAN.

Native and processed seaweed based biosorbents show good service capacities. These capacities are dependent on the empty bed contact time. The specific usage of algal biosorbents is influenced by the liquid residence time. Increase in bed depth results in reduction of sorbent usage and increase in service capacity. Monitoring the effluent pH provides a good indication of the breakthrough of metal ions.

Testing of algal fixed-bed columns against real industrial plating solutions

In order to test the performance of algae-based biosorbents (native and dealginate) against real plating effluent streams, preliminary sorption screening tests were carried out to identify target solutions. The aircraft plating shop has a large number of rinse water solutions containing various metals at different concentrations. Simulant synthetic solutions were used to identify rinse water solutions against which to test algal biosorbents. A representative sample of results for AN and DAN obtained during the screening tests are depicted in Table 5.2. Apart from the chromium bearing

solutions, the majority of the synthetic solutions were adequately treated by both native as well as dealginate algal biosorbents. Algal biosorbents showed good sorption capacity for the nickel plating rinse waters which represent a combined rinse water from two plating baths ($NiCl_2$ and $Ni(SO_3NH_2)_2$). The low sorption affinity displayed by algal biosorbents towards chromium bearing solutions may be explained by the low pH of the rinse waters due to the presence of sulfuric and boric acid. The weakly-acidic surface functional groups present in algae are only partially dissociated around pH 3 (see chapters 2 and 3). Also, hydrolysis of chromium (III) ions[15] results in a range of species in solution including non-ionic $CrOHSO_4$ and $Cr(OH)_2(SO_4)_2$ which probably show little interaction with the negative surface of the algal particles.

Solution	pH	AN	DAN
		Metal uptake, mmol g^{-1}	Metal uptake, mmol g^{-1}
1 mM $CdCl_2$	4.6	1	0.65
1 mM $CoCl_2$	4.6	0.6	0.6
1 mM $CuSO_4$	4.6	1.1	0.7
1 mM $CuSO_4$ 0.65 mM H_2SO_4	3	0.5	0.4
1 mM $NiCl_2$	4	0.65	0.4
0.5 mM $Ni(SO_3NH_2)_2$ 0.5 mM $NiCl_2$ 0.5 mM H_3BO_3	6	0.8	0.6
1 mM $ZnCl_2$	4.6	0.8	0.5
1 mM $ZnCl_2$ 2 mM NH_4Cl 5 mM KCl	4.8	0.7	0.5
0.5 mM $Cr_2(SO_4)_3$ 0.01 mM H_2SO_4	3.6	0.15	0.1
1 mM CrO3 0.01 mM H_2SO_4	3	0.1	0.05
0.95 mM CrO_3 0.025 mM $Cr_2(SO_4)_3$ 0.01 mM H_2SO_4	3.1	0.1	0.06

Table 5.2. Comparison of sorption behavior by AN and DAN for simulant metal-plating solutions.

The performance of the seaweed based biosorbents against the real industrial nickel plating bath rinse waters was rather encouraging. A comparison of the algal biosorbents versus an oxidized activated carbon and two commercially available ion exchange resins provides clear evidence of the potential of algal biosorbents relative

to other conventional ion exchange sorbent materials (see Fig. 5.18.). The algae-based biosorbents (native and dealginate) treated similar volumes of metal-bearing effluent compared with the oxidized active carbon 207C (OII). Interestingly, the algal sorbents displayed a similar sorption capacity for nickel from the rinse waters compared with Purolite's S930 (iminodiacetic resin) on a dry weight basis (see Table 5.3. for properties of S930 and S950 used for this comparison). The number of bed volumes treated are slightly lower for the biosorbents compared with the S930 resin (see Fig. 5.18.). The biosorbents possess a lower bulk density in comparison with the ion exchange resins. This property is responsible for the lower number of bed volumes of nickel solution treated. The dry weight capacity for nickel (for service cycle capacities see Table 5.4.) is considerably greater for the algal sorbents in comparison with the oxidized active carbon and comparable with the S930 resin.

Resin	Purolite S930	Purolite S950
Functional group	Iminodiacetic	Aminomethylene phosphate
Capacity (Na^+ form), eq/l	0.94	1.2
Operating pH range	2 - 11	2 - 11
Particle size, mm	0.3 - 1.2	0.3 - 1.2
Moisture retention, %	45-50	60-65

Table 5.3. Characteristic data of conventional ion exchange resins.

The cadmium stripping bath solution contained significant amounts of ammonium nitrate. The ammonium ion complexes the cadmium ions in solution. The algal biosorbents were unable to break the cadmium-ammonium complex and therefore, cadmium breakthrough was seen to occur almost instantaneously following commencement of the service cycle (not shown here). Previous regeneration experiments of cadmium-laden biosorbents with ammonium chloride have shown 80% elution of the bound metal. It is clear that the cadmium-ammonium complex is not preferred by the metal-binding sites within the algal sorbents. Purolite's S930 ion

exchange resin was also unable to break the cadmium-ammonium complex and displayed similarly low sorption capacity for the cadmium stripping bath rinse waters. The identical behavior of algal biosorbents compared with the chelating ion exchange resin S930 strongly indicates similar surface reactions are responsible for metal sorption. The possibility of algal biosorbents coordinating metal ions by chelation seems likely.

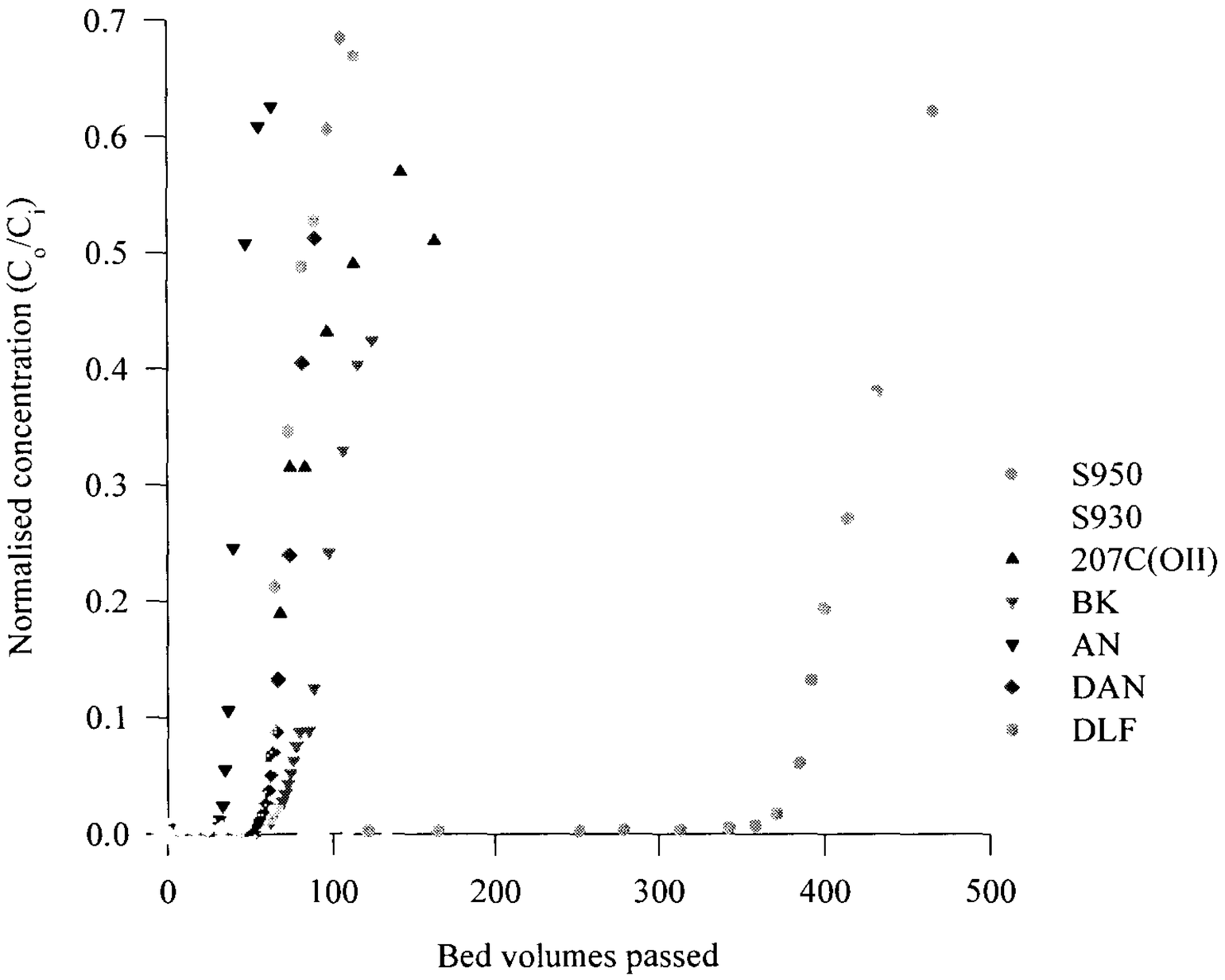

Experimental Parameters

Target metal	C_f, mM	Bed height, cm	Bed volume, ml	EBCT min	Solution pH
Ni^{2+}	0.8	5	4	10	4

Figure 5.18. Breakthrough profiles of various sorbents for nickel plating solution.

Sorbent	Equilibrium sorption capacity mmol g^{-1}	10% breakthrough capacity mmol g^{-1}
	Nickel	Nickel plating bath
BK	0.5	0.2 (85 BV)
AN	0.5	0.15 (36 BV)
DAN	0.5	0.2 (65 BV)
DLF	0.4	0.22 (60 BV)
207C OII	0.26	0.08 (60 BV)
S930	n.a.	0.21 (155 BV)
S950	n.a.	0.48 (385 BV)

Table 5.4. Nickel breakthrough and equilibrium sorption capacities of various sorbents.

Cross-flow microfiltration

The nickel membrane was quickly fouled during filtration of the algal slurry resulting in a significant reduction in the permeate flux (see Fig. 5.19.). The permeate flux fell from an optimistic 400 l m^{-2} h^{-1} to around 8 l m^{-2} h^{-1} for a transmembrane pressure of 0.275 barG over the four hour period. The membrane was back flushed with compressed air to remove any fouling material in order to improve the permeate flux. A higher initial permeate flux of 820 l m^{-2} h^{-1} was obtained, however, once again membrane fouling reduced the flux to less than 10 l m^{-2} h^{-1} after 2h of operation (see Fig. 5.19.).

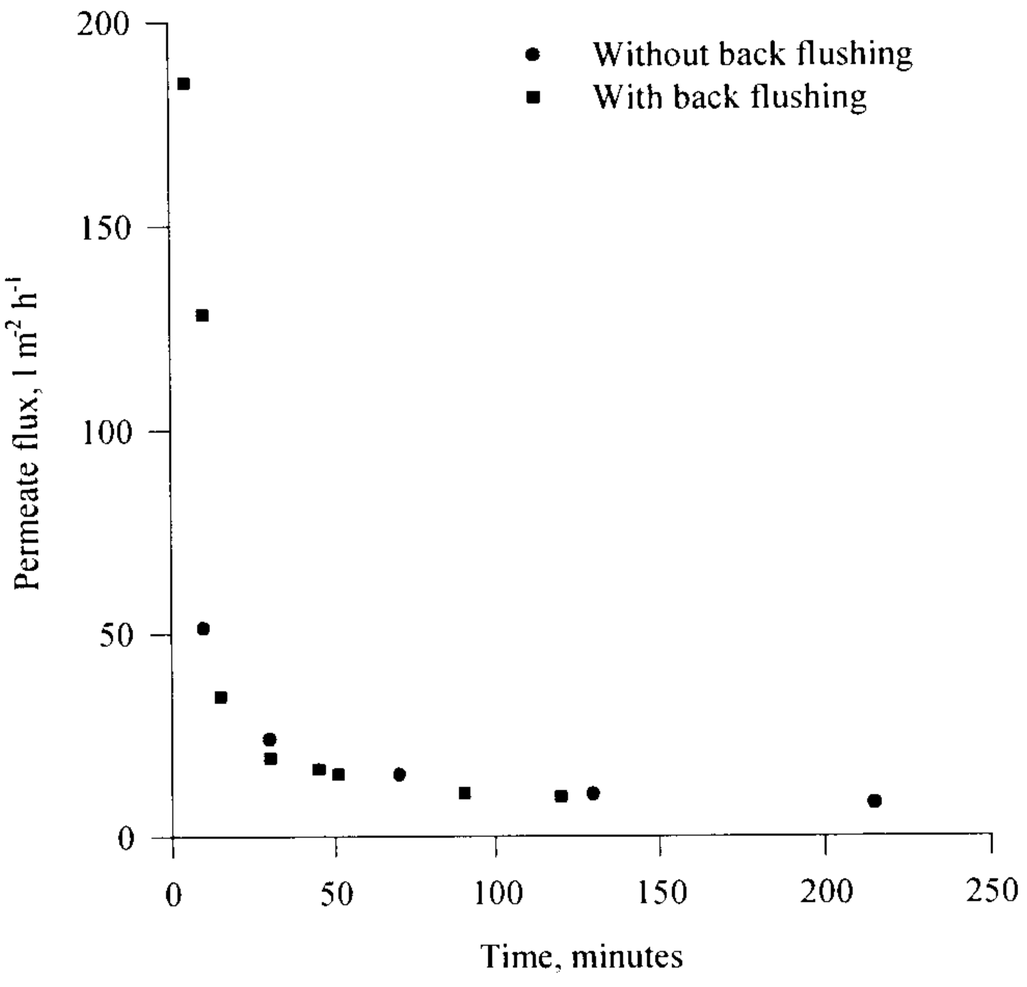

Figure 5.19. Permeate flux for cross-flow microfiltration of DLF slurry.

Preliminary trials with the MF-BIOSORB process were not successful in providing an adequate permeate flux. Problems associated with membrane fouling and concentration polarization must be overcome if this technology is to realize its potential and be considered as a viable option. Other types of surface filters (including ceramic filters) should be studied in the future. The nickel membrane used in the microfiltration process had sharp edges around the filter pores which in all probability were responsible for cutting-up the algal particles thereby affecting filter blocking. It is necessary to further investigate the effect of higher transmembrane pressures on the permeate flux. Pressures in excess of 2 barG have been used in some applications[16]. Microfilters are very durable and can sustain pressures as high as 7 bar (100 psi). Also, use of higher concentrations of biosorbent particles in the slurry may reduce membrane fouling and concentration polarization by a scrubbing action. This has been experienced with combined activated carbon adsorption and micro-filtration processes[16]. Modification of the biosorbent particles (crosslinking or physical entrapment) to improve their physical strength may also help in improving the

separation during cross-flow microfiltration. Other techniques include using electrical force fields and ultrasonics to overcome the problem of membrane fouling.

Disposal of spent algal biomass

It is clear from the present study that algae-based biosorbents disintegrate following several sorption/desorption cycles and therefore at some stage they must be disposed off in a suitable manner. One possible route for the disposal could involve ashing the residue material by incineration followed by land filling the ash.

Protonated native algal material show a relatively low ash content value of between 0.5-1.5% by weight (see Table 5.5.). The high ash content of the unwashed algal material is due to the presence of high amounts of calcium and other metal ions within the algal cell walls. These metal ions are sequestered from the marine environment in which the algae grow. The high ash content of dealginate biosorbents is slightly surprising considering that prewashing of the residue with dilute mineral acid had been carried out. Residual metallic ions such as calcium and magnesium ions may still be retained within the processed seaweed residue which may be exchanged during the metal biosorption process. Repeated washing of the processed material should reduce the ash content value of the processed residue even further. It is quite likely that as a consequence of several heavy metal sorption/elution cycles, the ash content of the protonated biomass will be reduced so that disposal by incineration would significantly reduce the volume of material requiring final disposal.

The high calorific value of algae could result in an auto-thermal incineration process, however, this line of inquiry must be explored further as there is insufficient information to make an informed decision. In particular, drying of protonated washed algal particles may be accomplished by utilizing waste heat from the incineration step. Drying of algal biomass may be necessary to reduce transportation costs if final users like small plating shops are potential customers.

Species	Ash content (wt/wt %)		
	Untreated Material	Protonated Material	Gross Cal. Value Dry Basis (kcal kg^{-1})
AN	23.7	1.1	3591
BK	18.9	0.6	2598
LH	22.4	1.5	n/a
DAN	24.5	10.2	n/a
DLF	22.4	8.8	n/a

Table 5.5. Analysis of seaweed ash content.

There is considerable scope to carry out a detailed feasibility study exploring the economics of algal biosorbents in waste water treatment as part of the broader concept of sustainable renewable treatment technologies for the future.

Section 5.4. Conclusions

The breakthrough profiles of heavy metal ions are self sharpening and attain constant pattern provided the algal bed height is greater than 5 cm. Flow rate of effluent solution strongly influences the shape of the breakthrough profile. Empty bed contact times approaching 6 minutes are recommended for treating metal-bearing effluents using algal beds. This ensures optimum usage of the sorbent sorption capacity. The calculated mass transfer zone height is found to vary with effluent flow rate.

Repeated cycles of copper sorption/elution indicates reduction in the service capacity of the algal bed. This reduction in service capacity is most pronounced after the first sorption/elution cycle. Some of the metal sorption sites within the algae may covalently bind copper ions to the algal surface. These binding sites may resist regeneration during the elution cycle and therefore lower the service capacity of the sorbent bed.

Dealginate seaweed residue samples display good breakthrough capacities for nickel removal from industrial aircraft plating rinse waters. The performance of algal-based sorbents compare favorably in comparison with a chelating iminodiacetic resin and an oxidized active carbon. The chelating organic exchanger shows similar sorption behavior compared with the marine algal biosorbents. The possibility of metal biosorption by weakly-acidic chelating surface functional groups in algae cannot be ruled out.

The low ash content of protonated algal biosorbents and the high calorific value of biomass favors the possibility of incineration of the used biosorbent material once its useful commercial life comes to an end.

Section 5.5. References

1. Helfferich, F. 1995, Ion Exchange, Dover Publications Inc., New York.
2. Slater, M. J. 1991, Principles of ion exchange technology, Butterworth-Heinemann Ltd., Oxford, UK.
3. Michaels, A. S. 1952, Ind. Eng. Chem., vol. 44, no. 8, 1922.
4. Jefferson, C. P. 1972, Am. Inst. Chem. Eng. J., vol. 18, no. 2, 409.
5. Raghavan, N. S. and Ruthven, D. M. 1983, Am. Inst. Chem. Eng. J., vol. 18, no. 6, 922
6. Peel, R. G. and Benedek, A. 1981, Can. J. Chem. Eng., vol. 59, no. 6, 688.
7. Trujillo, E. M., Jeffers, T. H., Ferguson, D. and Stevenson, H. Q. 1991, Environ. Sci. Technol., vol. 25, no. 9, 1559.
8. Volesky, B. and Prasetyo, I. 1994, Biotechnol. Bioeng., vol. 43, no. 11, 1010.
9. Kratochvil, D., Volesky, B. and Demopoulos, G. 1997, Water Research, vol. 31, no. 9, 2327.
10. Tan, H. K. S. and Spinner, I. H. 1994, Can. J. Chem. Eng., vol. 72, no. 2, 330.
11. Kratochvil, D., Fourest, E. and Volesky, B. 1995, Biotechnology Letters, vol. 17, no. 7, 777.
12. Matheickal, J. T. and Yu, Q. 1996, Wat. Sci. Tech., vol. 34, no. 9, 1.
13. Matheickal, J. T., Yu, Q. and Feltham, J. 1997, Environ. Tech., vol. 18, no. 1, 25.
14 Brower, J. B., Ryan, R. L. and Pazirandeh, M. 1997, Environ. Sci. Technol., vol. 31, no. 10, 2910.
15. Kratochvil, D., Pimentel, P. F. and Volesky, B. 1998, Environ. Sci. Technol., vol. 32, no. 18, 2693.
16. Pirbazari, M., Badriyha, B.N. and Gavindran, V. 1992, J. AWWA, December issue, 95.

General Conclusions

"I know not what I may appear to the world, but to myself I seem to have been only like a boy playing on the sea-shore, and diverting myself in now and then finding a smoother pebble or a prettier shell than ordinary, whilst the greater ocean of truth lay all undiscovered before me."

(Sir Issac Newton 1642-1727)

Chapter 6

General Conclusions

This chapter provides an overview of the conclusions that may be drawn from the current study. Also, areas that require further development and may form the basis of future investigations are highlighted.

Section 6.1. Conclusions

Brown marine algae show considerable swelling upon rewetting. The water regain is thought to be associated with the algin content of the species. In addition, the higher guluronic acid content of *L. hyperborea* is possibly responsible for this species displaying higher swelling compared with other algae despite its lower overall algin content.

Quantification of the ion exchange capacity of algal biosorbents was carried out using potentiometric titrations. The reactivity of the algal surface towards metal ions in near-neutral aqueous solutions is attributed to weakly-acidic surface functional groups e.g. carboxylic as well as phenolic-type groups. The higher algin containing algae e.g. *Durvillea potatorum* displays the highest concentration of reactive sites compared with the other native algal varieties. Dealginate seaweed residues show similar surface reactivity, however, the concentration of metal binding sites is quantitatively less. The acid-dissociation constant values extracted from the titration curves closely match those of free alginic acid samples indicating similar reactive functional sites.

Chemical modification of reactive sites in algae using methanolic/HCl confirms the strong affinity of metal ions with carboxylate groups present in the biosorbents. Subsequent reduction in metal biosorption following esterification of carboxyl groups in both native and dealginate seaweed samples is clear evidence of the role of cellular polysaccharides e.g. alginic acid in heavy metal biosorption. Any sulfated polysaccharides present in marine algae are solubilised during algal washing and

pretreatment and hence are not thought to play a dominant role in subsequent metal sorption. This has been confirmed by the absence of characteristic (S=O) vibrational bands from FT-IR spectra of algae.

All marine algal species evaluated in the current study sequester metal ions following the selectivity series $Cu^{2+}>Cd^{2+}>Ni^{2+}>Zn^{2+}$. The equilibrium sorption capacity for copper ions is always higher in comparison with that of nickel and zinc ions for the same algal species. Copper ions are thought to engage in chelation-type surface reactions in addition to simple ion exchange with protons of weakly acidic surface functional groups. Nickel and zinc ions most likely undergo simple ion exchange reactions as well as electrostatic interactions with the negatively charged algal surface as verified by zeta-potential measurements.

The pH-dependence of the metal biosorption phenomenon provides further evidence of the significance of ion exchange type surface reactions during algae-metal interactions. Stoichiometric release of protons during metal biosorption has been observed and suggests a bidentate binding mechanism between metal ions in solution and protons on the algal surface. Lower metal biosorption capacity at reduced solution pH is due to protonation of weakly-acidic metal binding sites in algae. Competitive interactions between Na^{+} and Ni^{2+} or Zn^{2+} ions for surface functional groups occurs at high background ionic strength.

Representation of the equilibrium biosorption process using a surface complex formation model indicates that around 40% of the copper binding sites in native marine algae undergo chelation-type surface reactions. Two different types of surface reactions must be considered in order to represent the interactions of copper ions with the algal surface. Nickel and zinc ions do not undergo similar chelation reactions. Covalently bound copper ions are not easily released from the biomass by reduction in solution pH. *L. hyperborea* displays predominantly ion exchange type surface reactions which suggests that the proportion of mannuronic/guluronic acid residues in algae plays an important role in determining the extent of chelation-type interactions between metal ions and the algal surface.

The metal biosorption process is reversible. Inorganic mineral acids are capable of eluting previously sequestered metal ions. However, degradation of the cellular polysaccharides due to hydrolysis reactions result in reduced potential for multiple reuse. Nickel and zinc ions may be eluted using less aggressive eluants including acidified ammonium chloride and sodium chloride solutions. Covalently bound copper and cadmium ions may be eluted by strong complexing agents including Na_2EDTA or strong acids capable of breaking the covalent bonds.

The rate of metal biosorption is limited by diffusional resistance to transport of metal ions within the algal particles. Steric hindrance and specific interactions of metal ions with functional groups within the cellular matrix of algal particles significantly limits the rate of metal biosorption. For smaller particles, where the effective path length for ion migration is reduced, the biosorption rates are significantly increased.

Metal sorption under dynamic conditions of continuous operation were studied employing a fixed bed flow-through sorption column. As expected, the optimal lowest sorbent usage rate was found to be in the region of low flow rates (loadings) when the sorbent material was properly contacted and the dynamic bed mass transfer "front" was relatively short. Biosorption breakthrough curves for single metal solutions as well as synthetic metal plating solutions have shown promising potential. The algal biosorbents display constant pattern breakthrough curves which are self sharpening and indicate favorable equilibrium between metal ions and the metal biosorption sites. Pressure drop across the columns is less than 1barg for all biosorbents studied (aspect ratio H/D~10) and therefore quite acceptable. Average specific biosorbent usage values are around 400-450 g 1000 l^{-1} of solution treated (C_f 0.5 mM, pH4). *Durvillea potatorum* is the most successful algal biosorbent capable of treating around 300 BV of 0.5 mM copper solution, 180 BV of (0.5 mM) nickel solution and 125 BV of (0.5 mM) zinc solution. Processed dealginate based biosorbents have shown excellent metal sorption characteristics in column mode. Around 100 BV of metal bearing solution was successfully treated. DAN is capable of treating over 300 BV of 0.5 mM copper solution with no breakthrough. Over

several sorption/desorption cycles however, the biosorbent particles display textural changes due to solubilisation of cellular material and reduction in service capacity due to incomplete regeneration.

The effluent pH exiting the biosorbent column follows the breakthrough profile for the heavy metal ion. Release of protons from within the algal bed as a consequence of metal removal from solution results in a steady reduced effluent pH. This low solution pH increases as the metal ion breakthrough occurs during exhaustion of the algal bed and may have potential as a means of process control.

Both native and dealginate seaweed residues may be successfully employed in the treatment of nickel plating rinse waters. Their performance is comparable to conventional organic iminodiacetic chelating resins and oxidized active carbons which possess similar reactive sites for metal sorption. The lower wet bulk density of algal biosorbents results in relatively less volume of nickel plating effluent treated compared with organic ion exchange resins. However, on a dry weight basis, the biosorbents are more evenly matched.

Section 6.2. Future work

The past three years have been spent studying the feasibility of metal sorption by algal based biosorbents. It is clear from the work, that the materials have tremendous potential for removal of toxic metals from near neutral aqueous solutions. The high metal sorption capacity of native and dealginate seaweeds coupled with their relatively inexpensive cost suggests that these materials could be competitive adsorbents in the water treatment market.

The design and operation of a water treatment process based on algal biosorbents is still however, quite some way off. Several lines of inquiry require follow-up work to be carried out. These are discussed in the following section.

The algal biosorbents do not possess the structural rigidity that is a prerequisite of any water treatment process based on the use of fixed-bed column-type technology. A look at other treatment technologies including large batch-type contact vessels where waste water is contacted with the sorbent material followed by some kind of sorbent separation system needs to be evaluated. Obviously, the feasibility of such a process flow-sheet has to be compared in cost terms versus conventional water treatment processes based on precipitation or treatment using ion exchange resins.

Hydrodynamic operating conditions of an algal fixed-bed column must be evaluated on a scale significantly larger than the mini-columns used during the current study. The column performance over several sorption/desorption cycles at varying flow rates must be carried out. Possible bacterial growth on the algal bed as well as problems associated with the characteristic smell of seaweed must be addressed before the materials may be considered in any water treatment process.

Preliminary studies aimed at regenerating the metal laden algal biomass have shown promise. Further detailed investigations need to be carried out. Sorbent regenerability is critical as this will prolong the usability of the biosorbent employed for water treatment and help to increase the economic viability of a treatment process based on algae. The number of treatment cycles before the biosorbent is discarded is an important parameter determining the overall economics of the process. In addition to biosorbent reuse, a life cycle assessment on the biosorbents must be carried out. This study must be able to successfully answer the question "What will be the method employed regarding final disposal of the spent biosorbent material?" The calorific value of algal material suggests that auto-thermal incineration may be a possible route.

Appendix 1

Section 1

An electric field in the electrolyte solution results in transferrence of ions (i) in the direction of the current and is proportional to the gradient of the electric potential (φ), the concentration (C_i) and the electrochemical valence (z_i) of the species:

$$J_i = -u_i z_i C_i \, grad\varphi$$

u_i, the proportionality factor is the electrochemical mobility term and is given by the Nernst-Einstien equation:

$$u_i = \frac{D_i F}{RT}$$

In solutions with concentration gradients, electric transferrence of ions is superimposed on thermal diffusion and is given by the Nernst-Planck equation:

$$J_i = -D_i\left[\frac{\partial q_i}{\partial r} + z_i q_i \frac{F}{RT}\frac{\partial \phi}{\partial r}\right]$$

Thus for the co-ion E, the Nernst-Planck equation may be written as:

$$J_E = -D_E\left[\frac{\partial q_E}{\partial r} + z_E q_E \frac{F}{RT}\frac{\partial \phi}{\partial r}\right] = 0$$

$$\frac{\partial q_E}{\partial r} = z_E q_E \frac{F}{RT}\frac{\partial \phi}{\partial r}$$

$$\frac{1}{z_E q_E}\frac{\partial q_E}{\partial r} = \frac{F}{RT}\frac{\partial \phi}{\partial r}$$

$$\frac{1}{z_E{}^2 q_E}\frac{\partial\left(q_H + z_B q_B\right)}{\partial r} = \frac{F}{RT}\frac{\partial\phi}{\partial r}$$

$$\frac{1}{z_E\left(q_H + z_B q_B\right)}\frac{\partial\left(q_H + z_B q_B\right)}{\partial r} = \frac{F}{RT}\frac{\partial\phi}{\partial r}$$

$$J_B = -D_B\left\{\frac{\partial q_B}{\partial r} + z_B q_B\frac{F}{RT}\frac{\partial\phi}{\partial r}\right\}$$

$$J_B = -D_B\left\{\frac{\partial q_B}{\partial r} + \frac{z_B q_B}{z_E\left(q_H + z_B q_B\right)}\frac{\partial\left(q_H + z_B q_B\right)}{\partial r}\right\}$$

$$J_H = -D_H\left\{\frac{\partial q_H}{\partial r} + q_H\frac{F}{RT}\frac{\partial\phi}{\partial r}\right\}$$

$$J_H = -D_H\left\{\frac{\partial q_H}{\partial r} + \frac{q_H}{z_E\left(q_H + z_B q_B\right)}\frac{\partial\left(q_H + z_B q_B\right)}{\partial r}\right\}$$

$$-D_H\left[\frac{\partial_H}{\partial r} + \frac{q_H}{z_E\left(q_H + z_B q_B\right)}\frac{\partial\left(q_H + z_B q_B\right)}{\partial r}\right] = z_B D_B\left[\frac{\partial q_B}{\partial r} + \frac{z_B q_B}{z_E\left(q_H + z_B q_B\right)}\frac{\partial\left(q_H + z_B q_B\right)}{\partial r}\right]$$

$$\frac{\partial\left(q_H + z_B q_B\right)}{\partial r} = X$$

$$-D_H\frac{\partial q_H}{\partial r} - \frac{D_H q_H}{z_E\left(q_H + z_B q_B\right)}\frac{\partial X}{\partial r} = z_B D_B\frac{\partial q_B}{\partial r} + \frac{z_B D_B z_B q_B}{z_E\left(q_H + z_B q_B\right)}\frac{\partial X}{\partial r}$$

$$-\frac{\partial X}{\partial r}\left\{\frac{D_H q_H}{z_E\left(q_H + z_B q_B\right)} + \frac{z_B D_B z_B q_B}{z_E\left(q_H + z_B q_B\right)}\right\} = z_B D_B\frac{\partial q_B}{\partial r} + D_H\frac{\partial q_H}{\partial r}$$

$$\frac{\partial X}{\partial r} = \frac{\partial q_H}{\partial r} + z_B \frac{\partial q_B}{\partial r}$$

$$\frac{1}{z_B}\left(\frac{\partial X}{\partial r} - \frac{\partial q_H}{\partial r}\right) = \frac{\partial q_B}{\partial r}$$

$$-\frac{\partial X}{\partial r}\left\{\frac{D_H q_H}{z_E\left(q_H + z_B q_B\right)} + \frac{z_B D_B z_B q_B}{z_E\left(q_H + z_B q_B\right)}\right\} = D_B\left(\frac{\partial X}{\partial r} - \frac{\partial q_H}{\partial r}\right) + D_H \frac{\partial q_H}{\partial r}$$

$$-\frac{\partial X}{\partial r}\left\{\frac{D_H q_H}{z_E\left(q_H + z_B q_B\right)} + \frac{z_B D_B z_B q_B}{z_E\left(q_H + z_B q_B\right)}\right\} - D_B\left(\frac{\partial X}{\partial r}\right) = \frac{\partial q_H}{\partial r}\left[D_H - D_B\right]$$

$$-\frac{\partial X}{\partial r}\left\{\frac{D_H q_H}{z_E\left(q_H + z_B q_B\right)} + \frac{z_B D_B z_B q_B}{z_E\left(q_H + z_B q_B\right)} + D_B\right\} = \frac{\partial q_H}{\partial r}\left[D_H - D_B\right]$$

$$J_H = -D_H\left[\frac{\partial q_H}{\partial r} + \frac{q_H}{z_E\left(q_H + z_B q_B\right)} \frac{\partial\left(q_H + z_B q_B\right)}{\partial r}\right]$$

$$-\frac{\partial X}{\partial r}\left[\frac{D_H q_H + z_B D_B z_B q_B + D_B\left(z_E\left(q_H + z_B q_B\right)\right)}{z_E\left(q_H + z_B q_B\right)}\right] = \frac{\partial q_H}{\partial r}\left[D_H - D_B\right]$$

$$J_B = -D_B\left\{\frac{\partial q_B}{\partial_r} + \frac{Z_B q_B}{Z_E\left(q_H + Z_B q_B\right)} \frac{\partial\left(q_H + Z_B q_B\right)}{\partial r}\right\}$$

$$J_H = -D_H\left\{\frac{\partial q_H}{\partial_r} + \frac{q_H}{Z_E\left(q_H + Z_B q_B\right)} \frac{\partial\left(q_H + Z_B q_B\right)}{\partial r}\right\}$$

$$-\frac{\partial X}{\partial r}\left[\frac{D_H q_H + z_B D_B z_B q_B + D_B\left(z_E\left(q_H + z_B q_B\right)\right)}{z_E\left(q_H + z_B q_B\right)}\right] = \frac{\partial q_H}{\partial r}\left[D_H - D_B\right]$$

$$\frac{\partial X}{\partial r} = \frac{z_E\left[q_H + z_B q_B\right]}{\left[D_H q_H + z_B D_B z_B q_B + D_B z_E q_H + D_B z_E z_B q_B\right]}\left[D_E - D_H\right]\frac{\partial q_H}{\partial r}$$

$$J_H = -D_H\left[\frac{D_B z_B q_B\left(z_B + z_E\right) + q_H\left(D_H + D_B z_E\right) + q_H\left(D_B - D_H\right)}{D_B z_B q_B\left(z_B + z_E\right) + q_H\left(D_H + D_B z_E\right)}\right]\frac{\partial q_H}{\partial r}$$

$$J_H = -D_H\left[\frac{D_B z_B q_B\left(z_B + z_E\right) + q_H D_B\left(1 + z_E\right)}{D_B z_B q_B\left(z_B + z_E\right) + q_H\left(D_H + D_B z_E\right)}\right]\frac{\partial q_H}{\partial r}$$

$$J_H = -D_H\left[\frac{U_B\left(z_B + z_E\right) + U_H\left(1 + z_E\right)}{U_B\left(z_B + z_E\right) + U_H\left(\alpha + z_E\right)}\right]\frac{\partial q_H}{\partial r} \qquad (9)$$

$$-\frac{\partial X}{\partial r}\left\{\frac{D_H q_H}{z_E\left(q_H + z_B q_B\right)} + \frac{z_B D_B z_B q_B}{z_E\left(q_H + z_B q_B\right)} + D_H\right\} = \frac{\partial q_B}{\partial r}\left[z_B D_B - z_B D_H\right]$$

$$J_B = -D_B\left[\frac{\partial q_B}{\partial r} + \frac{z_B q_B}{z_E\left(q_H + z_B q_B\right)}\frac{\partial\left(q_H + z_B q_B\right)}{\partial r}\right]$$

$$J_B = -D_B\left[\frac{q_H\left[1 + z_E\right] + z_B q_B\left[z_E + z_B\right]}{q_H\left[1 + z_E\right] + q_B z_B\left[\frac{z_B}{\alpha} + z_E\right]}\right]\frac{\partial q_B}{\partial r}$$

$$J_B = -D_B\left[\frac{U_H\left(1 + z_E\right) + U_B\left[Z_E + Z_B\right]}{U_H\left[1 + z_E\right] + U_B\left[\frac{z_B}{\alpha} + z_E\right]}\right]\frac{\partial q_B}{\partial r}$$

$$J_B = -\alpha D_B\left[\frac{U_H\left(1 + z_E\right) + U_B\left[Z_E + Z_B\right]}{\alpha U_H\left[1 + z_E\right] + U_B\left[z_B + \alpha z_E\right]}\right]\frac{\partial q_B}{\partial r} \qquad (10)$$

Section 2

$$q_H + z_B q_B = z_E q_E$$

$$U \equiv \frac{zq}{Q}$$

$$J_H + z_B J_B = z_E J_E \approx 0 \qquad \delta \le r \le r_o$$

$$J_H = -D_H \left[\frac{\left(z_E + z_B\right)U_B + \left(1 + z_E\right)U_H}{\left(z_E + z_B\right)U_B + \left(\alpha + z_E\right)U_H} \right] \frac{\partial q_H}{\partial r}$$

$$J_B = -D_B \alpha \left[\frac{\left(z_E + z_B\right)U_B + \left(1 + z_E\right)U_H}{\left(\alpha z_E + z_B\right)U_B + \left(1 + z_E\right)\alpha U_H} \right] \frac{\partial q_B}{\partial r}$$

$$0 = \frac{1}{\left(z_E + z_B\right)U_B + \left(\alpha + z_E\right)U_H} \frac{\partial q_H}{\partial r} + \frac{1}{\left(\alpha z_E + z_B\right)U_B + \left(1 + z_E\right)\alpha U_H} \frac{\partial z_B q_B}{\partial r}$$

$$\left[\alpha z_E U_B + z_B U_B + \alpha U_H + z_E \alpha U_H\right] \frac{\partial U_H}{\partial r} + \left[z_E U_B + z_B U_B + \alpha U_H + z_E U_H\right] = 0$$

$$z_E \left(U_H + U_B\right) \frac{\partial}{\partial r}\left[U_B + \alpha U_H\right] + \left(z_B U_B + \alpha U_H\right) \frac{\partial}{\partial r}\left[U_H + U_B\right] = 0$$

$$z_E \frac{1}{\left(z_B U_B + \alpha U_H\right)} \frac{\partial}{\partial r}\left[U_B + \alpha U_H\right] + \frac{1}{\left(U_H + U_B\right)} \frac{\partial}{\partial r}\left[U_H + U_B\right] = 0$$

Substituting $U_H = uU_B$

$$\frac{z_E}{\left(z_B + u\alpha\right)U_B} \frac{\partial}{\partial r}\left[U_B(1 + \alpha u)\right] + \frac{1}{(1 + u)U_B} \frac{\partial}{\partial r}\left[U_B(1 + u)\right] = 0$$

$$\frac{z_E}{\left(z_B+u\alpha\right)U_B}\left[\left(\frac{\partial U_B}{\partial r}\right)(1+\alpha u)+U_B\alpha\frac{\partial u}{\partial r}\right]+\frac{1}{(1+u)U_B}\left[\left(\frac{\partial U_B}{\partial r}\right)(1+u)+U_B\frac{\partial u}{\partial r}\right]=0$$

$$(1+\alpha u)\left[\frac{z_E}{z_B+u\alpha}\right]\frac{\partial \ln U_B}{\partial r}+\frac{\alpha z_E}{\left(z_B+u\alpha\right)}\frac{\partial u}{\partial r}+\left(\frac{1}{1+u}\right)\frac{\partial \ln U_B}{\partial r}(1+u)+\frac{1}{1+u}\frac{\partial u}{\partial r}=0$$

$$\left[\frac{(1+\alpha u)z_E}{\left(z_B+u\alpha\right)}+1\right]\frac{\partial \ln U_B}{\partial r}+\left[\left(\frac{\alpha z_E}{z_B+u\alpha}\right)+\frac{1}{1+u}\right]\frac{\partial u}{\partial r}=0$$

$$\frac{\partial \ln U_B}{\partial r}+\left[\frac{\left(\frac{\alpha z_E}{z_B+u\alpha}\right)+\left(\frac{1}{1+u}\right)}{\frac{(1+\alpha u)z_E}{z_B+u\alpha}+1}\right]\frac{\partial u}{\partial r}=0$$

The second term $\left[\frac{\left(\frac{\alpha z_E}{z_B+u\alpha}\right)+\left(\frac{1}{1+u}\right)}{\frac{(1+\alpha u)z_E}{z_B+u\alpha}+1}\right]$ may be written as:

$$\frac{1}{(1+u)}\left[\frac{\left(z_E+1\right)\alpha u+\left(\alpha z_E+z_B\right)}{\alpha\left(z_E+1\right)u+\left(z_E+z_B\right)}\right]$$

Using partial fractions:

$$\frac{A}{1+u}+\frac{B}{au+b}\text{ where }a=\alpha\left(z_E+1\right)\text{ and }b=\left(z_E+z_B\right)$$

$$A[au+b]+B[1+u]=\alpha\left(z_E+1\right)u+\left(\alpha z_E+z_B\right)$$

$$Aau+Ab+B+Bu=au+c$$

Solving for A:

$$A = \frac{a-c}{a-b}$$

and solving for B:

$$B = a\left[\frac{c-b}{a-b}\right]$$

$$\frac{\partial \ln U_B}{\partial r} + \left[\frac{A}{1+u} + \frac{B}{au+b}\right]\frac{\partial u}{\partial r} = 0$$

$$\ln U_B + A\ln(1+u) + \left(\frac{B}{a}\right)\ln(au+b) = \text{constant}$$

Using the boundary condition (14): $U_B=U_{Bo}$, $u=0$ @ $r_\delta=1$

$$\text{constant} = \ln U_{Bo} + A\ln(1) + \left(\frac{B}{a}\right)\ln\left(0+\frac{b}{a}\right)$$

Hence:

$$\ln\left(\frac{U_B}{U_{Bo}}\right) + A\ln(1+u) + \frac{B}{a}\ln\left(\frac{au+b}{b}\right) = 0$$

let $G \equiv \left(\frac{a}{b}\right)$

$$A = \frac{a-c}{a-b} = \frac{\alpha\left(z_E+1\right)-\left(\alpha z_E+z_B\right)}{\alpha\left(z_E+1\right)-\left(z_E+z_B\right)}$$

$$\frac{1}{A} = 1 + \left[\frac{z_E(\alpha - 1)}{\alpha - z_B} \right] = 1 + S$$

$$\frac{B}{a} = \frac{c-b}{a-b} = \frac{z_E(\alpha - 1)}{\alpha z_E(\alpha - 1) + (\alpha - z_B)}$$

$$\frac{B}{a} = \frac{S}{S+1}$$

Hence:

$$\ln\left(\frac{U_B}{U_{Bo}}\right) + \frac{1}{1+S}\ln(1+u) + \frac{S}{S+1}\ln(Gu+1) = 0$$

$$(1+u)(Gu+1)^S = \left(\frac{U_{Bo}}{U_B}\right)^{1+S}$$

Since $u = \dfrac{U_H}{U_B}$

$$(U_B + U_A)(GU_H + U_B)S = (U_{Bo})^{1+S} \qquad (18)$$

Section 3

$$-\frac{J_H}{D_H}-\frac{z_B J_B}{D_B}=\frac{-J_H D_B - z_B J_B D_H}{\left(D_H D_B\right)}$$

$$-\frac{J_H}{D_H}-\frac{z_B J_B}{D_B}=-J_H\frac{\left(D_B - D_H\right)}{D_H D_B}$$

$$J_H=-D_H\left[\frac{\partial q_H}{\partial r}+\frac{q_H}{z_E\left(q_H+z_B q_B\right)}\frac{\partial\left(z_E q_E\right)}{\partial r}\right]$$

$$J_B=-D_B\left[\frac{\partial q_B}{\partial r}+\frac{z_B q_B}{z_E\left(z_E q_E\right)}\frac{\partial\left(z_E q_E\right)}{\partial r}\right]$$

$$\frac{\partial q_H}{\partial r}+\frac{q_H}{z_E\left(q_H+z_B q_B\right)}\frac{\partial\left(q_H+z_B q_B\right)}{\partial r}+z_B\left[\frac{\partial q_B}{\partial r}+\frac{z_B q_B}{z_E\left(q_H+z_B q_B\right)}\frac{\partial\left(q_H+z_B q_B\right)}{\partial r}\right]$$

$$=\left(\frac{D_B - D_H}{D_B D_H}\right)z_B J_B$$

$$\frac{Q}{r_o}\frac{\partial U_H}{\partial \rho}+\frac{QU_H}{r_o z_E\left(U_H+U_B\right)}\frac{\partial U_E}{\partial \rho}+\frac{z_B Q}{r_o}\left[\frac{1}{z_B}\frac{\partial U_B}{\partial \rho}+\frac{U_B}{z_E U_E}\frac{\partial U_E}{\partial \rho}\right]=\frac{\left(D_B - D_H\right)}{D_B D_H}z_B J_B$$

$$\frac{Q}{r_o}\left[\frac{\partial U_H}{\partial \rho}+\frac{\partial U_B}{\partial \rho}\right]+\frac{Q}{r_o z_E}\left\{\frac{U_H}{U_E}+\frac{z_B U_B}{U_E}\right\}\frac{\partial U_E}{\partial \rho}=\left[\frac{D_B - D_H}{D_B D_H}\right]z_B J_B$$

$$\frac{Q}{r_o}\frac{\partial U_E}{\partial \rho}+\frac{Q}{r_o z_E}\left[\frac{U_H+z_B U_B}{U_E}\right]\frac{\partial U_E}{\partial \rho}=\frac{D_B - D_H}{D_B D_H}z_B J_B$$

$$\frac{Q}{r_o}\left\{1+\frac{U_H+z_BU_B}{z_EU_E}\right\}\frac{\partial U_E}{\partial \rho}=\left\{\frac{D_B-D_H}{D_BD_H}\right\}z_BJ_B$$

$$\frac{Q}{r_o}\left\{1+\left(\frac{U_H+z_BU_B}{z_EU_E}\right)\right\}\frac{\partial U_E}{\partial \rho}=\frac{1-\alpha}{D_H}z_BJ_B$$

$$\frac{QD_H}{z_Br_o(1-\alpha)}\left\{1+\left[\frac{U_H+z_BU_B}{z_EU_E}\right]\right\}\frac{\partial U_E}{\partial \rho}=J_B$$

$$U_E\left[GU_H+U_E-U_H\right]^S=UB_o{}^{(1+S)}$$

$$U_E\left[U_H(G-1)+U_E\right]^S=UB_o{}^{(1+S)}$$

$$U_E^{\frac{1}{S}}\left[U_H(G-1)+U_E\right]=U_{Bo}{}^{\frac{(1+S)}{S}}$$

$$U_H(G-1)+U_E=\frac{U_{Bo}{}^{\frac{(1+S)}{S}}}{U_E{}^{\frac{1}{S}}}$$

$$U_H(G-1)=\left[\frac{U_{Bo}{}^{1+S}}{U_E}\right]^{\frac{1}{S}}-U_E$$

$$U_H=\frac{\left\{\left[\frac{U_{Bo}{}^{1+S}}{U_E}\right]^{\frac{1}{S}}-U_E\right\}}{[G-1]}$$

$$\left[U_H+U_B\right]\left[GU_H+U_B\right]^S=U_{Bo}^{1+S}$$

$$U_E\left[G\left[U_E-U_B\right]+U_B\right]^S=U_{Bo}^{1+S}$$

$$U_E^{\frac{1}{S}}\left[G\left[U_E - U_B\right] + U_B\right] = U_{Bo}^{\frac{1+S}{S}}$$

$$GU_E + U_B[1-G] = \left[\frac{U_{Bo}^{1+S}}{U_E}\right]^{\frac{1}{S}}$$

$$U_B = \frac{\left\{\left[\frac{U_{Bo}^{1+S}}{U_E}\right]^{\frac{1}{S}} - GU_E\right\}}{[1-G]}$$

$$U_E z_E + z_B U_B + U_H \equiv U_E z_E + \frac{z_B}{1-G}\left\{\left(\frac{U_{Bo}^{1+S}}{U_E}\right)^{\frac{1}{S}} - GU_E\right\} - \frac{1}{1-G}\left\{\left(\frac{U_{Bo}^{1+S}}{U_E}\right)^{\frac{1}{S}} - U_E\right\}$$

$$U_E z_E + U_B z_B + U_H \equiv \frac{1}{1-G}\left\{U_E z_E(1-G) + z_B\left\{\left(\frac{U_{Bo}^{1+S}}{U_E}\right)^{\frac{1}{S}} - GU_E\right\} - \left\{\left(\frac{U_{Bo}^{1+S}}{U_E}\right)^{\frac{1}{S}} - U_E\right\}\right\}$$

$$U_E Z_E + U_B Z_B + U_H \equiv \frac{1}{1-G}\left\{U_E\left(z_E+1\right) - U_E G\left(z_E + z_B\right) + \left(\frac{U_{Bo}^{1+S}}{U_E}\right)^{\frac{1}{S}}\left(z_B - 1\right)\right\}$$

$$\left(\frac{U_E Z_E + U_B Z_B + U_H}{U_E Z_E}\right) \equiv \frac{1}{1-G}\left\{\frac{\left(z_E+1\right)}{z_E} - G\left(\frac{z_E + z_B}{z_E}\right) + \left(\frac{U_{Bo}}{U_E}\right)^{\frac{1+S}{S}}\left(\frac{z_B - 1}{z_E}\right)\right\}$$

$$J_B = \frac{D_H Q}{z_B(1-\alpha)(1-G)r_o}\left\{\left(\frac{z_B - 1}{z_E}\right)\left(\frac{U_{Bo}}{u_E}\right)^{\frac{1+S}{S}} - G\left(\frac{z_B - z_E}{z_E}\right) + \left(\frac{z_E + 1}{z_E}\right)\right\}\frac{\partial U_E}{\partial \rho}$$

Substituting into Fick's second law and using a pseudo-steady state assumption, (19) is obtained:

$$\frac{\partial q_B}{\partial t} = \overline{D}\nabla^2 q_B = \overline{D}\frac{1}{\rho^2}\frac{\partial}{\partial \rho}\left(\rho^2 \frac{\partial q_B}{\partial \rho}\right) \qquad \text{(Fick's second law)}$$

at pseudo-steady state, $\frac{\partial q_B}{\partial t} = 0$

$$\frac{\partial}{\partial \rho}\left[\rho^2\left\{\left(z_B - 1\right)\left(\frac{U_{Bo}}{U_E}\right)^{\frac{1+S}{S}} - G\left(z_B + z_E\right) + \left(1 + z_E\right)\right\}\frac{\partial U_E}{\partial \rho}\right] = 0\,; \qquad \rho_\delta \le \rho \le 1 \quad (19)$$

Section 4

Solution of the partial differential equation (19) was achieved using the boundary conditions (12)-(17) and (20):

$$\frac{\partial}{\partial\rho}\left[\rho^2\left\{\left(z_B-1\right)\left(\frac{U_{Bo}}{U_E}\right)^{\frac{1+S}{S}}-G\left(z_B+z_E\right)+\left(1+z_E\right)\right\}\frac{\partial U_E}{\partial\rho}\right]=0\,;\qquad \rho_\delta\le\rho\le 1$$

$$\rho_2\left\{\left(z_B-1\right)\left(\frac{U_{Bo}}{U_E}\right)^{\frac{1+S}{S}}-G\left(z_B+z_E\right)+\left(1+z_E\right)\right\}\frac{\partial U_E}{\partial\rho}=C_1$$

$$\int\left(z_B-1\right)\left(\frac{U_{Bo}}{U_E}\right)^{\left(\frac{1+S}{S}\right)}\partial U_E-\int\left[G\left(z_B+z_E\right)-\left(1+z_E\right)\right]\partial U_E=\int\frac{C_1}{\rho^2}\partial\rho$$

$$\left(z_B-1\right)U_{Bo}^{\frac{1+S}{S}}\int U_E^{-\frac{1+S}{S}}\partial U_E-\left[G\left(z_B+z_E\right)-\left(1+z_E\right)\right]\int\partial U_E=-\int\frac{C_1}{\rho^2}\partial\rho$$

$$-S\left(z_B-1\right)\left(\frac{U_{Bo}^{1+S}}{U_E}\right)^{\frac{1}{S}}-\left\{G\left(z_B+z_E\right)-\left(1+z_E\right)\right\}U_E=-\frac{C_1}{\rho}+C_2$$

$$q_H=z_Eq_E=q_\delta\,;\qquad \text{at } r=\delta\equiv\rho_\delta \qquad (15)$$

$$q_B=0,\ \text{i.e. } U_B=0 \qquad (16)$$

$$\left(U_H+U_B\right)\left(GU_H+U_B\right)^S=U_{Bo}^{1+S}\,;\qquad \rho_\delta\le\rho\le 1 \qquad (18)$$

$$U_H\left[GU_H\right]S=U_{Bo}^{1+S}$$

$$U_H=U_{E\delta}$$

$$G^{S}U_{H}^{1+S} = U_{Bo}^{1+S}$$

$$U_{E_\delta} G^{\frac{S}{1+S}} = U_{Bo}$$

$$U_{E\delta} = U_{Bo}G^{-\left(\frac{S}{1+S}\right)}; \quad \rho=\rho_\delta \qquad (20)$$

$$\rho=1; \quad U_H + U_B = U_E$$

$$U_H=0$$

$$U_E = U_{Bo} = \frac{q_B z_B}{Q} = U_E$$

$$\rho = \rho_\delta ; \qquad U_E = U_{Bo}G^{\frac{-S}{1+S}}$$

$$-S(z_B-1)\left(\frac{U_{Bo}^{1+S}}{U_{Bo}}\right)^{\frac{1}{S}} - \left\{G(z_B+z_E)-(1+z_E)\right\}U_{Bo} = -C_1 + C_2$$

$$-S(z_B-1)U_{Bo} - \left\{G(z_B+z_E)-(1+z_E)\right\}U_{Bo} = -C_1 + C_2$$

$$-S(z_B-1)\left(\frac{U_{Bo}^{\frac{1+S}{S}}}{\left[U_{Bo}G^{-\frac{S}{1+S}}\right]^{\frac{1}{S}}}\right) - \left\{G(z_B+z_E)-(1+z_E)\right\}U_{Bo}G^{-\frac{S}{1+S}} = -\frac{C_1}{\rho_\delta} + C_2$$

$$-S(z_B-1)\left[\frac{U_{Bo}}{G^{-\frac{1}{1+S}}}\right] - \left\{G(z_B+z_E)-(1+z_E)\right\}U_{Bo}G^{-\frac{S}{1+S}} = -\frac{C_1}{\rho_\delta} + C_2$$

$$-S\left(z_B-1\right)U_{Bo}G^{\frac{1}{1+S}}-\left\{G\left(z_B+z_E\right)-\left(1+z_E\right)\right\}U_{Bo}G^{-\frac{S}{1+S}}=-\frac{C_1}{\rho_\delta}+C_2$$

$$S\left(z_B-1\right)U_{Bo}+\left\{G\left(z_B+z_E\right)-\left(1+z_E\right)\right\}U_{Bo}=C_1-C_2$$

$$-S\left(z_B-1\right)U_{Bo}G^{\frac{1}{1+S}}-\left\{G\left(z_B+z_E\right)-\left(1+z_E\right)\right\}U_{Bo}G^{-\frac{S}{1+S}}=-\frac{C_1}{\rho_\delta}+C_2$$

$$S\left(z_B-1\right)U_{Bo}\left[1-G^{\frac{1}{1+S}}\right]+\left\{G\left(z_B+z_E\right)-\left(1+z_E\right)\right\}\left[U_{Bo}\right]\left[1-G^{-\frac{S}{1+S}}\right]=C_1\left[1-\frac{1}{\rho_\delta}\right]$$

$$\rho_\delta\left[\frac{U_{Bo}S\left(z_B-1\right)\left(1-G^{\frac{1}{1+S}}\right)+U_{Bo}\left\{G\left(z_B+z_E\right)-\left(1+z_E\right)\right\}\left\{1-G^{-\frac{S}{1+S}}\right\}}{\left(\rho_\delta-1\right)}\right]=C_1$$

$$\frac{\partial U_E}{\partial\rho}=C_1\frac{1}{\rho^2\left\{\left(z_B-1\right)\left(\frac{U_{Bo}}{U_E}\right)^{\frac{1+S}{S}}-G\left(z_B+z_E\right)+\left(1+z_E\right)\right\}}$$

$$\frac{\partial U_E}{\partial\rho}=\frac{U_{Bo}S\left(z_B-1\right)\left(1-G^{\frac{1}{1+S}}\right)+U_{Bo}\left\{G\left(z_B+z_E\right)-\left(1+z_E\right)\right\}\left(1-G^{-\frac{S}{1+S}}\right)}{\rho\left(\rho-1\right)\left\{\left(z_B-1\right)\left(\frac{U_{Bo}}{U_E}\right)^{\frac{1+S}{S}}-G\left(z_B+z_E\right)+\left(1+z_E\right)\right\}}$$

$$J_H=-D_H\left[\frac{\left(z_E+z_B\right)U_B+\left(1+z_E\right)U_H}{\left(z_E+z_B\right)U_B+\left(\alpha+z_E\right)U_H}\right]\frac{\partial q_H}{\partial r}$$

Using the initial conditions:

$$U_H + U_B = U_E$$

$$U_B = 0;\ \rho = \rho_\delta$$

$$U_H = U_E = U_{Bo} G^{-\frac{S}{1+S}},\ \rho = \rho_\delta$$

$$J_H = -D_H \left[\frac{1+z_E}{\alpha + z_E}\right] \frac{\partial q_H}{\partial r}$$

$$\frac{q_H}{Q} = U_H; \qquad \frac{\partial q_H}{\partial r} = \frac{Q \partial U_H}{\partial r}$$

$$J_H = -D_H \left[\frac{1+z_E}{\alpha + z_E}\right] \frac{Q \partial U_H}{r_o \partial \rho}$$

$$\frac{\partial U_H}{\partial \rho} = \frac{\partial U_E}{\partial \rho}$$

$$J_H = -\frac{D_H Q}{r_o} \left[\frac{1+z_E}{\alpha + z_E}\right] \frac{\partial U_H}{\partial \rho}$$

$$\frac{d\delta}{dt} = \frac{D_{Na}}{r_o} \left[\frac{1+z_E}{\alpha + z_E}\right] \frac{\partial U_H}{\partial \rho}$$

$$\frac{d\rho}{dt} = \frac{D_H}{r_o^2} \left[\frac{1+z_E}{\alpha + z_E}\right] \frac{\partial U_H}{\partial \rho}$$

$$\rho(\rho-1)\frac{d\rho}{dt}=\left[\frac{1+z_E}{\alpha+z_E}\right]\left\{\frac{U_{Bo}S(z_B-1)\left(1-G^{\frac{1}{1+S}}\right)+U_{Bo}\left\{G(z_B+z_E)-(1+z_E)\right\}\left[1-G^{-\frac{S}{1+S}}\right]}{(z_B-1)\left(\frac{U_{Bo}}{U_E}\right)^{\frac{1+S}{S}}-G(z_B+z_E)+(1+z_E)}\right\}\frac{D_{Na}}{r_o^2}$$

$$\left(\frac{U_{Bo}}{U_E}\right)^{\frac{1+S}{S}}=G$$

$$\rho(\rho-1)\frac{d\rho}{dt}=\left[\frac{1+z_E}{\alpha+z_E}\right]\left\{\frac{S(z_B-1)\left(1-G^{\frac{1}{1+S}}\right)+\left\{G(z_B+z_E)-(1+z_E)\right\}\left[1-G^{-\frac{S}{1+S}}\right]}{(z_B-1)G-G(z_B+z_E)+(1+z_E)}\right\}\frac{U_{Bo}D_H}{r_o^2}$$

$$2\rho^3-3\rho^2+1=\left\{\frac{S(z_B-1)\left(1-G^{\frac{1}{1+S}}\right)+\left\{G(z_B+z_E)-(1+z_E)\right\}\left[1-G^{-\frac{S}{1+S}}\right]}{z_E(1-\alpha)(1-G)}\right\}\frac{6\alpha U_{Bo}D_B}{r_o^2}t \quad (21)$$

Appendix 2

The constant pattern type breakthrough curve can be predicted in terms of the length of the algal bed occupied by the counterion wave at any given time. Theoretically, the wave occupies the entire length of the bed, however, it is often effectively contained in a short section of the algal bed. The averaged concentration of metal ions contained in this short section of the bed zone can be calculated by integrating the area above the breakthrough curve (see Fig. A.2.1.).

$$\overline{q_z} = \left(\frac{L}{V_z}\right)\int_{t_B}^{t_T}(C_F - C)dt \qquad (1)$$

The metal ions contained within the interstitial spaces of the algal bed are ignored.

The maximum concentration of ions that could be achieved by the algal bed is simply:

$$Q = \left(\frac{L}{V_z}\right)\int_{t_B}^{t_T} C_F dt \qquad (2)$$

Hence:

$$\frac{\overline{q_z}}{Q} = \frac{\int_{t_B}^{t_T}(C_F - C)dt}{C_F(t_T - t_B)} = 1 - f_E \qquad (3)$$

The time needed to achieve this average uptake of metal ions within the zone is given by:

$$\overline{q_z} = \frac{LC_F t_F}{V_Z} \qquad (4)$$

Hence:

$$t_F = (1 - f_E)(t_T - t_B) \qquad (5)$$

Taking into account the time to form the exchange zone at entry,

$$\frac{V_z}{V_B} = \frac{(t_T - t_B)}{(t_T - t_F)} = \frac{z_E}{z} = \frac{(t_T - t_B)}{[t_T - (1 - f_E)(t_T - t_B)]} \qquad (6)$$

from which equation z_E, the exchange zone height (see Fig. A.2.1.) can be calculated using the breakthrough curve.

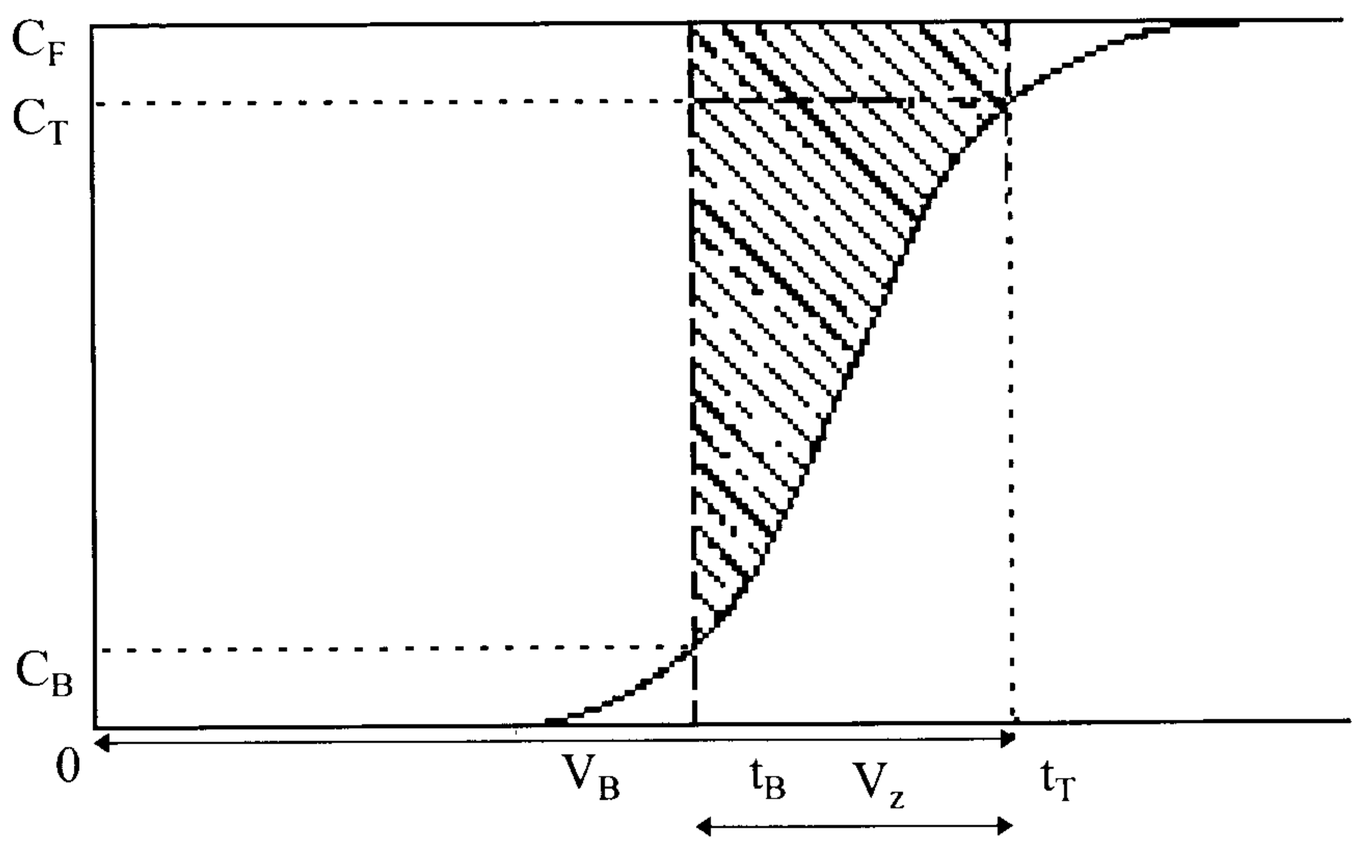

Figure A.2.1. Exchange zone on breakthrough curve.

List of Publications

1. Malik, D. J., Streat, M. and Greig, J. 1999, Characterisation and evaluation of seaweed based sorbents for treating toxic metal bearing solutions. Trans. IChemE, 77, Part B, 227.
2. Malik, D. J. and Streat, M. 1997, Sorption of metals from aqueous media using seaweed based biosorbents, 1997 IChemE Research Event, Newcastle-upon-Tyne.
3. Streat, M., Tai, M. H., Saha, B. and Malik, D. J. 1998, Development of advanced ion exchange materials and methods for the removal of toxic metals from metallurgical waste effluents. Brite Euram report (six months, 01/05/98 - 31/10/98), Contract No. BRPR-CT96-0158, project no. BE95-2169.
4. Streat, M., Tai, M. H., Saha, B. and Malik, D. J. 1998, Development of advanced ion exchange materials and methods for the removal of toxic metals from metallurgical waste effluents. Brite Euram report (six months, 01/11/97 - 30/04/98), Contract No. BRPR-CT96-0158, project no. BE95-2169.
5. Streat, M., Tai, M. H., Saha, B. and Malik, D. J. 1997, Development of advanced ion exchange materials and methods for the removal of toxic metals from metallurgical waste effluents. Brite Euram report (six months, 01/04/97 - 30/09/97), Contract No. BRPR-CT96-0158, project no. BE95-2169.
6. Streat, M., Tai, M. H., Saha, B. and Malik, D. J. 1996, Development of advanced ion exchange materials and methods for the removal of toxic metals from metallurgical waste effluents. Brite Euram report (six months, 01/05/96 - 30/09/96), Contract No. BRPR-CT96-0158, project no. BE95-2169.